



**6TH INTERNATIONAL SCIENTIFIC
CONFERENCE**

**“RESEARCH FOR ENVIRONMENT
AND CIVIL ENGINEERING
DEVELOPMENT 17”**

PROCEEDINGS

“CIVIL ENGINEERING 17”

VOLUME 6

International Scientific Conference
“Research for Environment and Civil Engineering Development 17”
and Proceedings
“CIVIL ENGINEERING 17”

The 6th International Scientific Conference "Research for Environment and Civil Engineering Development 17" held on November 2 - 3, 2017 is a continuation of a well-established tradition of organizing scientific conferences every second year, thus providing regular publication of scientific articles. In Conference the scientists and civil engineering professionals are presenting their reports at four conference sections. Alongside with the scientists and civil engineering professionals from the Latvia University of Life Sciences and Technologies and Riga Technical University, scientists from the universities of Lithuania, Estonia, Russia, Poland, Ukraine, and Belarus have made a great contribution to the conference. The main research directions represented at the conference are: Building and Renovation, Construction Materials and Structures, Environment and Environmental Engineering, Landscape Architecture, Industrial Energy Efficiency, Water Resources Engineering, Land Management and Geodesy and Real Estate Valuation and Market. Aim of the conference is scientific discussions, exchange of information on the latest research topics and new cooperation possibilities in the future.

The conference's "Research for Environment and Civil Engineering Development 17" and proceedings "CIVIL ENGINEERING 17" international scientific committee is represented by experts and academic staff from Latvia, Lithuania, Estonia, Poland, Russia, Ukraine, Bulgaria and Norway.

The 6th International Scientific Conference "Research for Environment and Civil Engineering Development 17" is events where researchers from different scientific fields are welcome to share, discuss and get new ideas about the scientific topics of their interest. This is an opportunity for everyone to generate new ideas and work forwards joint projects in the future. Proceedings "CIVIL ENGINEERING 17" are source where accumulate that's scientific idea's.

Nowadays research fields of environment and civil engineering involve different other scientific branches covering building construction, architectural, environmental sciences, land management and geodesy and landscape planning.

The conference is open to educators and researchers in the fields of civil engineering, building construction, renovation, environment engineering, architecture and landscape architecture, land management and geodesy, real estate valuation and market.

It is important to note that scientific papers from the previous International Scientific Conference "CIVIL ENGINEERING 13" Proceedings were included in the SCOPUS, EBSCO Central & Eastern European Academic Source, AGRIS, CAB ABSTRACTS databases. These conference proceedings also will be sent for submission for SCOPUS, AGRIS, CAB Abstracts and EBSCO Academic Search Complete databases.

Dr.sc.ing., assoc.professor Armands Celms

Chairperson of conference committees:

Vivita Pukite, associate professor, Dr.oec., Latvia University of Life Sciences and Technologies, Latvia

ORGANIZING COMMITTEE

Chairperson:

Vivita Pukite, associate professor, Dr.oec., Latvia University of Life Sciences and Technologies, Latvia

Members:

Anda Jankava, professor, Dr.oec., Latvia University of Life Sciences and Technologies, Latvia

Inga Grinfelde, assistant professor, Mg.sc.ing., Latvia University of Life Sciences and Technologies, Latvia

Jānis Kreilis, associate professor, Dr.sc.ing. Latvia University of Life Sciences and Technologies, Latvia

Sandra Gusta, associate professor, Dr.oec., Latvia University of Life Sciences and Technologies, Latvia

Una Iļe, assistant professor, Dr.arch., Latvia University of Life Sciences and Technologies, Latvia

ISSN 2255-8861 (online)



Latvia University
of Life Sciences
and Technologies



VBF

6TH INTERNATIONAL SCIENTIFIC CONFERENCE
“RESEARCH FOR ENVIRONMENT AND
CIVIL ENGINEERING DEVELOPMENT 17”

PROCEEDINGS

“CIVIL ENGINEERING 17”

VOLUME 6

Jelgava, 2017

CIVIL ENGINEERING 17

6th International Scientific Conference “Research for Environment and Civil Engineering Development 17”
Proceedings, Vol. 6

Jelgava, Latvia University of Life Sciences and Technologies, 2017, 132 pages

ISSN 2255-8861 (online)

DOI: 10.22616/CE.2017

SCIENTIFIC COMMITTEE

Chairperson:

Armands Celms, associate professor, Dr.sc.ing., Latvia University of Life Sciences and Technologies, Latvia

Members:

Aldis Grekis, Dr.sc.ing., Riga Technical University, Latvia

Anatolijs Borodinecs, professor, Dr.sc.ing., Riga Technical University, Latvia

Anda Jankava, professor, Dr.oec., Latvia University of Life Sciences and Technologies, Latvia

Andris Chate, professor, Dr.sc.ing., Riga Technical University, Latvia

Andris Steinerts, associate professor Emeritus, Dr.sc.ing., Latvia University of Life Sciences and Technologies, Latvia

Anna Ramata, assistant professor, Dr.sc.ing., Riga Technical University, Latvia

Arturs Lesinskis, professor, Dr.sc.ing., Latvia University of Life Sciences and Technologies, Latvia

Audrius Aleknavicius, professor, Dr., Aleksandras Stulginskis University, Lithuania

Aurelia Rudzianskaite, researcher, Dr., Aleksandras Stulginskis University, Lithuania

Bruno Kirulis, assistant professor, Dr.sc.ing., Latvia University of Life Sciences and Technologies, Latvia

Daiga Zigmunde, professor, Dr.arch., Latvia University of Life Sciences and Technologies, Latvia

Dmitrijs Serdjuks, professor, Dr.sc.ing., Riga Technical University, Latvia

Donatas Rekus, associated Professor, Dr., Kaunas University of Technology, Lithuania

Genadijs Sahmenko, Dr.sc.ing., Riga Technical University, Latvia

Guntis Andersons, associate professor Emeritus, Dr.sc.ing., Latvia University of Life Sciences and Technologies, Latvia

Harri Lille, associate professor Emeritus, Cand.Sc. in Physics and Mathematics, Estonian University of Life Sciences, Estonia

Hendrik Voll, Dr.sc.ing., Tallin Technology University, Estonia

Ihor Trevoho, professor, Dr.hab.ing., Lviv Polytechnic National University, Ukraine

Janis Kaminskis, associate professor, Dr.sc.ing., Riga Technical University, Latvia

Janis Kreilis, associate professor, Dr.sc.ing., Latvia University of Life Sciences and Technologies, Latvia

Janis Zvirgzds, associate professor, Dr.sc.ing., Riga Technical University, Latvia

Juris Skujans, professor, Dr.sc.ing., Latvia University of Life Sciences and Technologies, Latvia

Karsten Jorgensen, professor, Dr.Scient., Norwegian University of Life Sciences, Norway

Lilita Ozola, professor, Dr.sc.ing., Latvia University of Life Sciences and Technologies, Latvia

Lybimir Lazov, professor, PhD, D.h.c., Technical University Gabrovo, Bulgaria

Maciej Orzechowski, eng., Dr., Wroclaw University of Environmental and Life Sciences, Poland

Martti – Jaan Miljan, professor, Dr., Estonian University of Life Sciences, Estonia

Mihkel Kiviste, associate professor, Dr.sc.ing., Estonian University of Life Sciences, Estonia

Reinis Ziemeļnieks, associate professor, Dr.sc.ing., Latvia University of Life Sciences and Technologies, Latvia

Stojan Kravanja, professor, dr., University of Maribor, Slovenia

Uldis Gross, associate professor, Dr. phys. Latvia University of Life Sciences and Technologies, Latvia

Uldis Lencis, Dr.sc.ing., Riga Technical University, Latvia

Ulvis Skadins, associate professor, Dr.sc.ing., Latvia University of Life Sciences and Technologies, Latvia

Vilda Grybauskiene, associate professor, Dr., Aleksandras Stulginskis University, Lithuania

Vivita Pukite, associate professor, Dr.oec., Latvia University of Life Sciences and Technologies, Latvia

EDITORS

Editor of language

Inese Ozola, Dr.philol.

Technical editor

Vita Cintina, Mg.sc.ing.

CONTENTS

MATERIALS AND STRUCTURES	6
Agata Włóka, Kamil Pawłowski CRITICAL BUCKLING TIME OF COMPRESSED STEEL BARS CONSIDERING HIGH TEMPERATURE CREEP.....	6
Raimondas Sadzevicius, Tatjana Sankauskiene, Rytis Skominas, Vincas Gurskis, Dainius Ramukevicius DURABILITY OF CONCRETE COVERING LAYER OF REINFORCED CONCRETE SLABS FOR EARTH DAM SLOPE PROTECTION	12
Vincas Gurskis, Rytis Skominas, Giedrius Sakalinskas EVALUATION OF SURFACE MATERIALS FOR PAVEMENTS AND FOOTPATHS	19
Kamil Pawłowski, Agata Włóka INFLUENCE OF STEEL IMPACT STRENGTH ON THE MAINTENANCE AND OPERATION OF CIVIL ENGINEERING STRUCTURES	25
Ramune Lebedeva, Vilma Vaicekauskiene INFLUENCE OF THE BALTIC SEA WATER ON KLAIPEDA SEAPORT HYDROTECHNICAL STRUCTURES.....	32
Stojan Kravanja MIXED-INTEGER NON-LINEAR PROGRAMMING IN CIVIL ENGINEERING	42
Janis Kreilis, Edgars Zeltins REUSE OF STEEL STRUCTURAL ELEMENTS WITH BOLTED CONNECTIONS... ..	48
Sharif E. Guseynov, Jekaterina V. Aleksejeva, Ruslans Aleksejevs, Uldis Zaimis THEORETICAL BASIS AND EXPERIMENTAL MEANS OF THE HYDROPHILIC NANOSTRUCTURE FORMATION PROCESS ON THE TITANIUM SURFACE BY DIRECT LASER IRRADIATION.....	54
LAND MANAGEMENT AND GEODESY	64
Armands Celms, Ilona Reķe, Jānis Kaminskis COMMON STUDIES OF NATIONAL HEIGHT SYSTEM IN LATVIA AND LITHUANIA	64
Dainora Jankauskienė, Marija Eidukevičiūtė, Vitalijus Volkovas GEODETIC AND GEOTECHNICAL MEANS OF SEA BREAKWATERS' MONITORING SYSTEM.....	70
Lina Kukliene, Dainora Jankauskiene, Indrius Kuklys, Birutė Ruzgiene REQUIREMENTS FOR AERIAL MAPPING USING UAV-PHOTOGRAMMETRY TECHNOLOGY: BALTIC SEA COAST MEASUREMENT	77

Roman Peresoliak UKRAINIAN CADASTRAL EXCHANGE FILE EVOLUTION PATH AND ITS FEATURES	84
Natalja Liba, Kaupo Kokamägi, Ina Järve IMPACT OF VARIOUS VEGETATION TYPES ON MOBILE LASER SCANNING ELEVATION ACCURACY	93
WATER RESOURCES ENGINEERING	100
Georgij Kiselov, Vladimir Jemeljanov, Janis Ievinsh ASSESSMENT OF IMPROVING THE EFFICIENCY OF FIRE EXTINGUISHING BY USING SURFACE ACTIVE AGENTS	100
ENVIRONMENTAL ENGINEERING	110
Mārtiņš Ruduks, Arturs Lešinskis TEST REFERENCE YEAR OF RIGA, LATVIA	110
BUILDING AND RENOVATION	118
Andris Kreslins, Visvaldis Vrublevskis, Anna Ramata HEAT SUPPLY SYSTEMS OF RENOVATED RESIDENTIAL BUILDINGS	118
Martti-Jaan Miljan, Rain Allikmäe, Andres Jürgenson, Matis Miljan, Jaan Miljan HYGROTHERMAL BEHAVIOUR OF THE TIMBER-FRAMED SAUNA WITH STRAW-BALE WALLS	124

MATERIALS AND STRUCTURES

DOI: 10.22616/CE.2017.001

Critical Buckling Time of Compressed Steel Bars Considering High Temperature Creep

Agata Włóka, Kamil Pawłowski, *Wrocław University of Environmental and Life Sciences*

Abstract. Steel structures are sensitive to the risks associated with elevated temperatures, especially in the range of fire temperatures. This applies in particular to slender compressed elements such as columns, truss rods etc. These hazards are not only related to the deterioration of the mechanical properties of steel at elevated temperatures, increased deformations and stresses, but they may also cause short-term high temperature creep, which can lead to rapid loss of stability of compressed elements in a short time, with stresses significantly lower than Euler's critical stresses. Thus, for safety reasons it is important to know the time for which the structure will retain its load capacity. This paper presents the results of calculation of the critical time, after which the total loss of stability of the axially compressed prismatic steel bar occurs. Calculations were made with the use of the initial imperfection method, taking into account experimentally determined relationship between creep strain and time, in the form of $\varepsilon_c = f(\sigma, t) = k\sigma^n t$. The results of theoretical calculations were compared with the creep times obtained in the experimental creep tests of axially compressed steel members at elevated temperatures. Laboratory short-term creep tests were performed in the Instron/Satec KN 600 universal testing machine equipped with a furnace for high-temperature testing type SF-16 2230, that enables testing at temperatures up to 1200°C. This paper presents only a part of the research and analyses conducted for ordinary structural steel, at 700°C.

Keywords: fire temperatures, structural steel, structural stability, short-time creep

Introduction

The load capacity of steel structures at elevated temperatures, especially at the fire temperature ranges, depends on many factors. These include a significant decrease in the strength of steel, accompanied by a rise in temperature, lowered elasticity modulus and the associated decrease in stiffness of the elements, or the increase in stress resulting from the thermal expansion of the elements. Another factor that must be taken into account when bearing capacity of steel structures is determined at elevated temperatures is creep, which is significantly accelerated by high temperature. This applies in particular to slender construction elements that work under compressive loads, such as columns or compressed bars of trusses. Accelerated creep may cause such elements to rapidly lose stability at loads much lower than would be expected from the theoretical value of Euler's critical load. This problem is ignored both in the European standards EUROCODE 3 and US AISC, which can lead to significant errors in the design of compressed steel elements subjected to fire [4].

Creep may be defined briefly as an increase in deformation of the element as a function of time under constant load. The creep phenomenon occurs at any temperature and even at small values of loads. However, at temperatures of fire, creep becomes

particularly important, and it may determine the load capacity of the designed structural elements [2].

The dependence of the strain increase over time is usually presented in the form of the so-called creep curve [2, 3, 5]. The idealised creep curve is shown in Figure 1.

There are three characteristic ranges on this curve. The first range – primary creep – begins at the time of occurrence of the initial strain associated with the load applied to the element. This stage is characterized by the decrease in creep rate as a function of time. Creep rate decreases until the minimum value is reached. Upon reaching the minimum creep rate the second range begins – the so-called secondary creep or steady-state creep. The value of creep rate in this stage is constant. The third range – tertiary creep – is characterised by an increasing creep rate, leading to the failure of the element in a relatively short time.

Practical applications often use the power relationship between the minimum creep rate during the second stage and stress in a cross section of the element [1].

$$\dot{\varepsilon}_{c,min} = f(\sigma) = k\sigma^n$$

Parameters k and n of the above equation should be determined by experimental investigations.

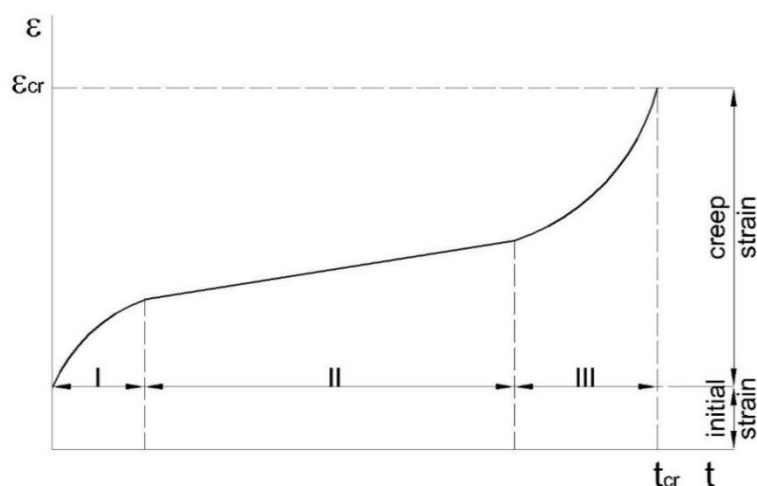


Fig. 1. Idealised creep curve

In this paper the authors attempted to theoretically predict the critical time of the loss of stability of the axially compressed steel element due to creep. Time prediction of the loss of stability was based on the method of initial imperfections. For the application of this method, it was necessary to determine the parameters of the power creep law for the investigated steel. Parameters of the creep law were determined based on the laboratory tensile creep tests at an elevated temperature. The results of the predictions were compared with the experimental data, collected during laboratory buckling creep tests.

Materials and methods

The tests were conducted on samples of ordinary structural S235JR steel. The chemical composition of the steel is provided in Table 1. The chemical composition was determined using a BAIRD-DV4 optical emission spectrometer. The tests and analyses presented in this paper were conducted at a temperature of 700°C.

TABLE 1

Chemical composition of the S235JR steel

Element	Content [%]
C	0.13
Mn	0.58
Si	0.19
P	0.02
S	0.03
Cr	0.04
Ni	0.10
Mo	0.02
V	0.00
Cu	0.21
Ti	0.00

The laboratory tests consisted of two series of tests.

The first series included steel creep tests at elevated temperatures. During these tests, samples were subjected to constant tensile stresses of different values. The aim of the study was to determine the relationship between the creep rate determined in the second stage of creep and the stresses in the cross section of the sample. The analyses were carried out on samples of a round cross section with a diameter of 10 mm, made in accordance with the recommendations of PN-EN ISO 6892-1: 2010 [6]. The data collected during the tensile creep tests were used to determine the parameters of the power creep law, which was necessary to calculate the critical buckling times, using initial imperfections method.

The second series of tests was a study of the effect of creep at elevated temperatures on the buckling of steel elements subjected to compressive loads of different values. Test specimens were made in the form of prismatic bars with a rectangular cross-section of 12 x 30 mm and a length of 500 mm. Support types of the specimens during the tests were hinged on both ends.

Both series of tests were performed in the SATEC / Instron KN600 universal testing machine. An SF-16 2230 high temperature furnace was used to heat the samples. The temperature of the samples placed inside the furnace was controlled by a cRIO-9076 controller equipped with an NI 9211 thermocouple module and a K-type thermocouple. Horizontal displacements in the buckling tests were measured using a Soltron ACR 100 LVTD sensor. The measuring site is shown in Figure 2

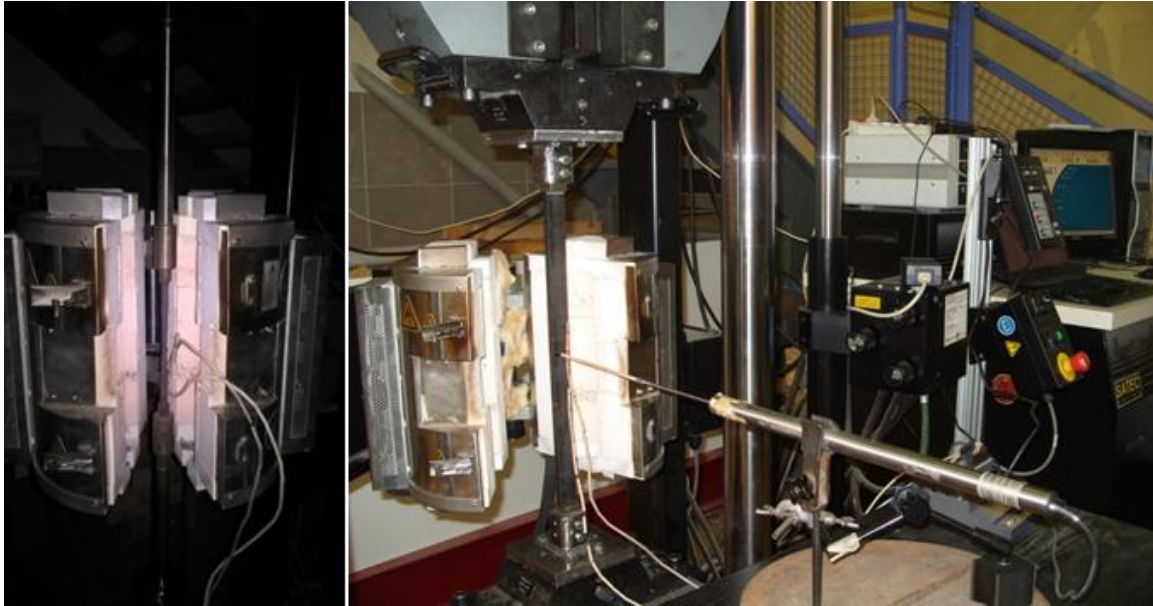


Fig. 2. Test site: left for testing tensile creep, right for buckling tests

Results of the tensile creep tests

As a result of the tests, the creep curves shown in Figure 3 were obtained. For each creep curve, the minimum creep rate in the second stage was determined. Then the relationship between the minimum creep rate and the tensile stress (Fig. 4) in

the form of the function $\dot{\epsilon}_c = f(\sigma) = k\sigma^n$ was determined. For S235JR steel at a temperature of 700°C the k value was $4.65 \cdot 10^{-13}$ [MPa⁻ⁿ·s⁻¹], while n was 4.83. A detailed discussion of the results is given in the paper [9].

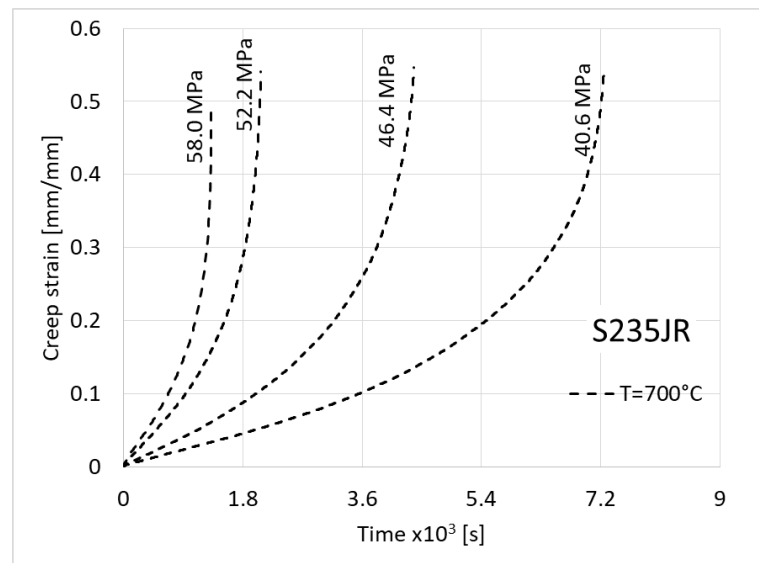


Fig. 3. Creep curves of S235JR steel at the temperature of 700°C

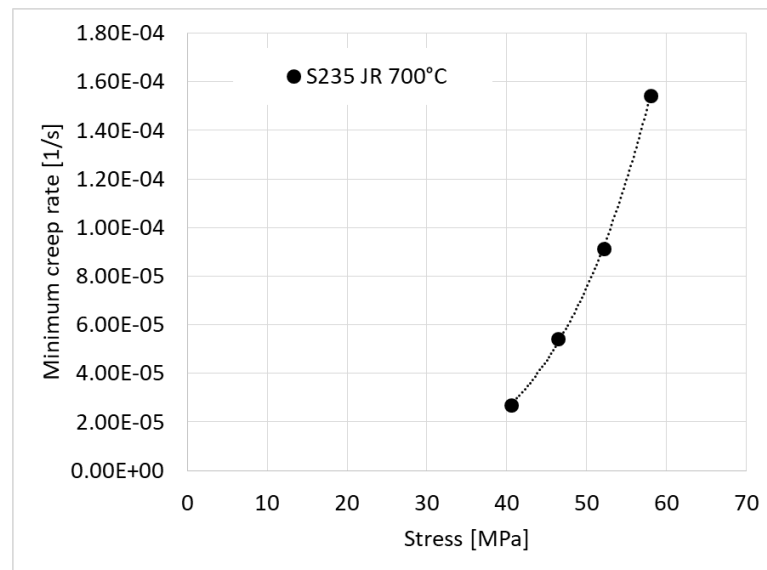


Fig. 4. Relationship between minimum creep rate and tensile stress for S235JR steel at 700 ° C

Results of the investigations on the impact of creep on the buckling of steel elements

As a result of the tests on the influence of creep on the buckling of axially compressed steel elements, the relationship between the buckling magnitude – the displacement perpendicular to the axis of the test piece in the middle of its length – and the time of load

of the test specimens were determined. Sample relationships obtained during the tests are shown in Fig. 5. For S235JR steel at 700°C, the time after which the total loss of stability of the tested elements occurred ranged from 2 to 3 hours, depending on the magnitude of the load applied to the sample. A wider discussion of the results of the research has been provided in the paper [8].

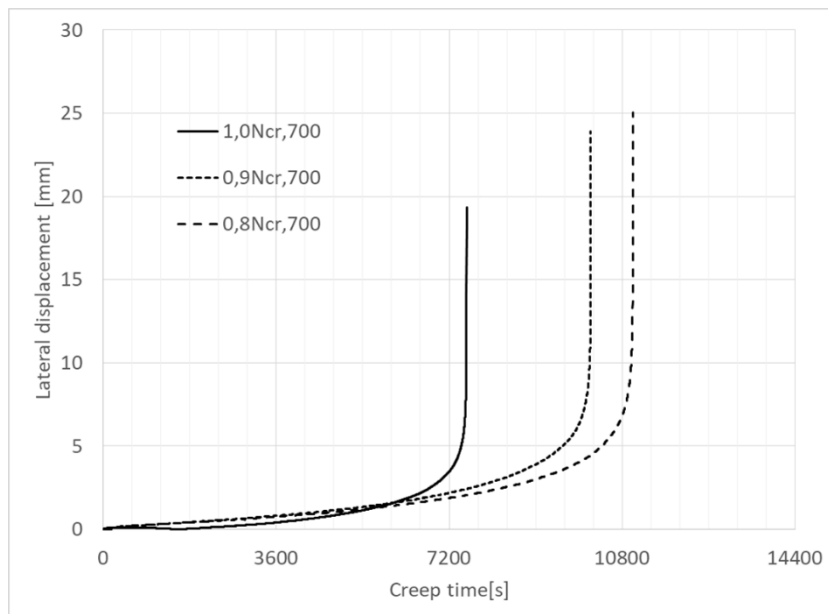


Fig. 5. Sample relationship between lateral buckling displacement and creep time, S235JR steel at the temperature of 700°C

Theoretical Findings

In this paper the authors attempted to theoretically determine the time after which the loss of stability of the axially compressed steel bar operating at elevated temperature occurs. For this purpose, the initial

imperfection method described in the work [7] was used. This method is based on the assumption that the rod before the load is pre-bent – has an initial imperfection of value v_0 (Fig. 6.)

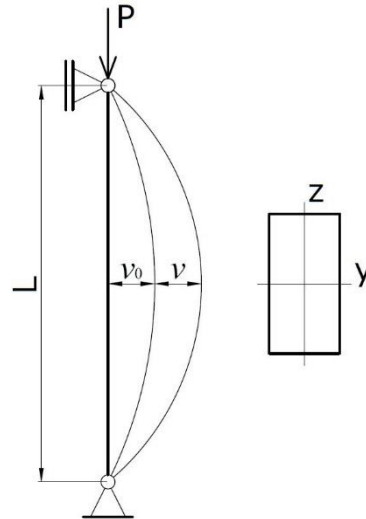


Fig. 6. Buckling of axially loaded compression member

The analyses presented in this paper assume the value of the initial imperfection:

$$v_0 = 0.01 \sin \frac{\pi x}{l}$$

When force P is applied, the deflection of the element increases by the value v . Since the axis of the bent element does not coincide with the axis of action of force P , an additional bending moment of value

$$M = P(v_0 + v)$$

is generated in the element, and the stresses in any of the cross-sectional levels are

$$\sigma = \frac{P}{A} - \frac{My}{J}$$

The equation above demonstrates that the normal stresses in the different cross-sectional levels will vary, and consequently, that the plastic strains caused by creep will not be constant at the different cross-sectional levels. In this study the value of plastic strains caused by creep is determined from the equation:

$$\varepsilon_c = f(\sigma, t) = tk\sigma^n$$

assuming, based on previous research, $k = 4.65 \cdot 10^{-13}$ [$\text{MPa}^{-n} \cdot \text{s}^{-1}$] and $n = 5$.

Knowing the increase in strains in the individual levels of the cross section, which will cause creep after time t from the initial load, the curvature increment of the analyzed element can be determined, and thus also increase in the deflection Δv caused by creep. By repeating the calculations for the increasing time t , the relationship between the increase of the deflection of the element and the time may be determined, as well as the critical time, after which the loss of stability of the bar occurs. The sample results of the calculation and the method of determining the predicted critical time are presented in Figure 7.

As can be seen in Figure 7, the relationship between the theoretically predicted lateral deflection of the element and the creep time is similar to that obtained in laboratory tests, which is shown in Figure 5. Also, the magnitude of the critical buckling time obtained is similar for both methods.

Figure 8 presents the theoretical calculations of the critical buckling times and their comparison with the times obtained in laboratory tests. In both cases, the time after which the complete loss of stability of the analyzed element occurs decreases with the increase of normal stress in the cross section due to force P applied at time $t = 0$. However, the theoretical values obtained for critical times are significantly lower than those determined experimentally.

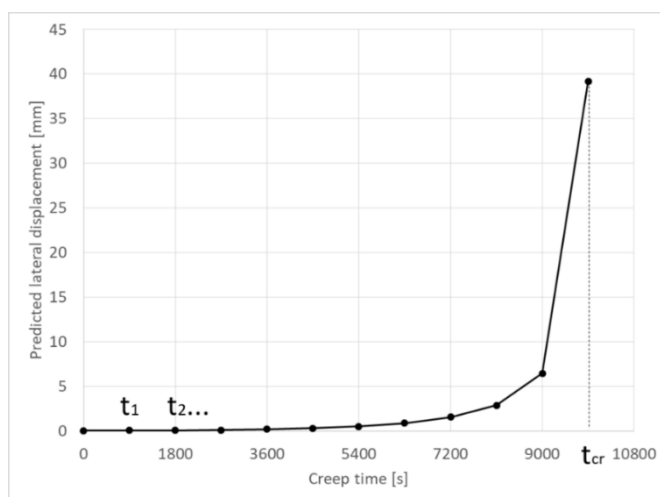


Fig. 7. Dependence between the predicted lateral displacement and creep time

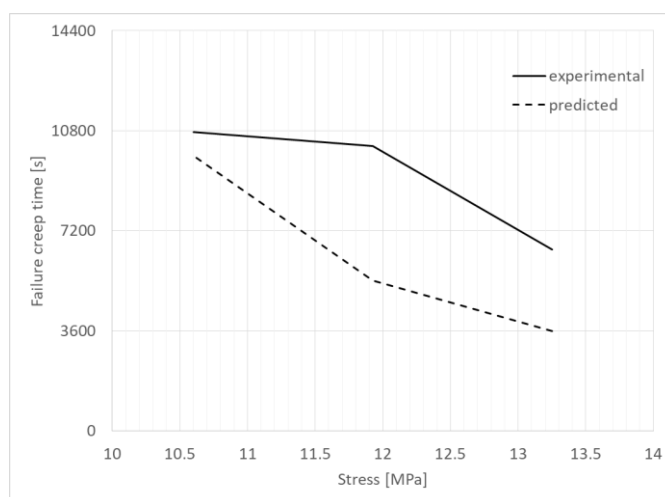


Fig. 8. Dependence between the predicted and experimental creep time and stress in the cross section of the element

Conclusions

The initial imperfections method allows us to predict the critical time, after which the loss of stability due to creep of the axially compressed steel member will occur. In order to use this method, it is necessary to know the values of the power creep law parameters. In the event if they are not known, their values should be determined experimentally. The nature of the critical time changes as a function of the

normal stress in a cross section is the same for the time calculated theoretically and the time determined in the laboratory. This time decreases as the compressive stress increases. However, there are significant differences between the theoretically predicted and experimentally determined times. This means that the initial imperfection method requires more careful analysis and modification.

References

- [1] **Беляев, Н. М.** *Сопротивление материалов*. Москва: Наука, 1965, 856 p.
- [2] **Blake, A.** *Handbook of mechanics, materials and structures*. United States: John Wiley and Sons, 1985, 729 p.
- [3] **Hoff, N.J.** (Editor) *Creep in structures*. Berlin: Springer-Verlag, 1962, 374p.
- [4] **Morovat, M.A., Engelhardt, M.D., Helwig, T.A., and Taleff, E.M.** Experimental examination of creep buckling of steel columns in fire. *In Structural Stability Research Council Annual Stability Conference 2016, SSRC 2016*. Structural Stability Research Council 2016 (SSRC). pp. 248-261.
- [5] **Nabarro, F.R.N., de Villiers, H.L.** *Physics of creep and creep-resistant alloys*. United Kingdom: Taylor and Francis Ltd 1995, 350p.
- [6] PN-ISO 6892-1:2016-09. *Metallic materials - Tensile testing - Part 1: Method of test at room temperature*.
- [7] **Вольмир, А.С.** *Устойчивость упругих систем*. Москва: Наука, 1963, 879 p.
- [8] **Włóka, A., Pawłowski, K., Świerzeko, R.** Impact of high temperature creep on the buckling of axially compressed steel members. *IOP Conference Series: Materials Science and Engineering*, Volume 245, pp. 1-6. doi:10.1088/1757-899X/245/3/032052
- [9] **Włóka, A., Pawłowski, K., Świerzeko, R.** Investigation of high temperature creep of structural steel. *7th International Conference on Safety and Durability of Structures ICOSADOS: proceedings, UTAD, Portugal; 2016*, p. 1-8

Durability of Concrete Covering Layer of Reinforced Concrete Slabs for Earth Dam Slope Protection

Raimondas Sadzevicius, Tatjana Sankauskiene, Rytis Skominas, Vincas Gurskis, Dainius Ramukevicius, *Aleksandras Stulginskis University, Lithuania*

Abstract. In Lithuania there are over 1000 ponds constructed and 620 have been evaluated as potentially dangerous hydraulic structures. Our water-retaining infrastructure deteriorates under environmental impacts, therefore the ageing of building materials causes a greater probability of deterioration and even failure. Durability of hydraulic structures depends on maintenance circumstances, surveillance, timely repair of structures or rehabilitations. Prognosis of the deterioration speed and durability of slabs is the main problem in each pond. The durability of concrete slabs covering layer can be evaluated by time (T_{layer}), which equals the time to expose reinforcement of a reinforced concrete structure. Based on the results of the field investigation, the modelling of durability of reinforced concrete slabs for earth dam slope protection was performed. Regularities of concrete compression strength of reinforced concrete slabs for earth dam slope protection under the influence of freezing–thawing cycles and other environmental factors were established. Using the developed durability evaluation method of reinforced concrete slabs for earth dam slope protection, the remaining service life of the construction till the probable beginning ($T_{5\%}$) or end of its deterioration ($T_{50\%}$) may be calculated. It is also possible to determine the time (T_{layer}), during which the reinforcement of the reinforced concrete construction is uncovered/exposed. Using the estimated constant of degradation in designing of reinforced concrete slabs for earth dam slope protection for using them at changing water level, there is a possibility to choose concrete of such strength, that the reinforcement of the construction would not be exposed during the intended period of usage.

Keywords: Durability of concrete, earth dams, slope protection, concrete slabs, lifetime of covering layer

Introduction

Concrete durability has been defined by the American Concrete Institute (ACI) as its resistance to weathering action, chemical attack, abrasion and other degradation processes. The primary factor determining durability is a good-quality concrete with low porosity i.e. low permeability [23]. The other advantages of durable concrete include resistance to alkali-silica reaction and sulfates, increased corrosion protection, and reduced heat of hydration [1].

Every reinforced concrete construction degrades with time, but the degradation of reinforced concrete slabs for earth dam slope protection (hereinafter – slabs) occurs particularly often. Due to environmental impacts [15] (weathering action, chemical attack, alkalinity (alkali-silica reaction (ASR)), carbonation (alkali-carbonate reaction (ACR)), freezing and thawing (F-T) cycles and abrasive effects of waterborne silt, sand, gravel, rocks, ice, and etc.) some deterioration of the slabs occurs, which influences negatively not only some slabs, but after their failure danger arises for the whole slope not being protected, thus affecting the reliability, durability and safety of the water-retaining infrastructure in general.

The design service life of slabs is 30 years, but many slabs of hydraulic structures on Lithuania hydroschemes are older than 30 years, therefore the ageing of building materials creates a greater probability of deterioration and even failure. If

dangerous defects and deteriorations are not repaired in time, a huge technical and ecological loss may occur. From the economic point of view the execution of new slope protection is more expensive, therefore the preservation of the present reinforced concrete slabs and performing restoration and/or reconstruction at the right time is a more preferable measure.

The analysis of the methods for evaluation of the durability of usable reinforced concrete structures influenced by environmental factors [19] shows, that the technical state, the bearing capacity and the durability of reinforced concrete constructions of hydraulic structures are mostly influenced by aggressive humid environmental impacts (the most potentially destructive weathering factor is (F-T) cycles while the concrete is wet). Different types of suspected frost related damage to concrete structures in hydro power plants are identified and categorized in the thesis [18]. A number of mechanisms affecting the material performance during freeze-thaw are reviewed in the thesis [17]. In the European standards [4] three different methods (Slab-Test, CIF-method and Cube test) are mentioned for the estimation of the freeze-thaw resistance of concrete with regard to internal structural damage. European, Lithuanian and Russian standards [5], [6], [12], [14] are used for the evaluation of frost related damage to concrete structures too.

Durability related deterioration is referred to as materials-related distress (MRD). The deterioration processes are caused by the freezing of water and

subsequent expansion in the paste, the aggregate particles, and forming erosion, development of pittings in the covering layer of slabs (Fig.1).



Fig. 1. Pittings and deteriorated concrete covering layer of slabs

A few investigations have attempted to establish a relation between porosity, strength, and durability-related properties. In [3] a non-linear relationship between compressive strength and density was observed. In general, as expected, compressive strength increased with density. Due to the relatively high porosity of the interfacial zone compared to other regions, it becomes a weak link in the concrete structure. As a result, concrete strength and durability-related properties to a considerable extent are dictated by the properties of the interface region. In order to improve concrete durability, it is essential to improve strength and durability of the interfacial region [20].

The prediction of nonair-entrained concrete service life in cases of deterioration due to freezing and thawing is described in [2].

The purpose of these investigations based on the field research is to establish the actual quantities of compression strength of concrete used in the slabs and to evaluate (F-T) cycles impact on the change of concrete properties and the durability of the concrete cover of slabs.

Methods of field investigations and laboratory tests

Using the field investigations and laboratory tests (standard methods) the main physical – mechanical properties of slabs – their concrete compression strength and water absorbability were determined and statistically evaluated. These properties are necessary for the evaluation of changes in concrete properties under frost impact, for the calculations of the constant of deterioration and the parameters of the durability of structures.

The compression strength of functioning concrete hydraulic structures was evaluated by the non-destructive method [10] and testing the samples of

irregular shape [22]. The concrete compression strength of samples is evaluated by an ordinary compression test. For this purpose hydraulic or lever compression machines are used in accordance with the standard requirements. The concrete compression strength of the samples of irregular shape was calculated into concrete compressive strength of standard cubes of 100×100×100 mm. Such an evaluation was accomplished by means of the proposed formulae and corresponding coefficients.

From the statistically evaluated research results of the slabs' concrete compression strength and water absorbability the rates of concrete resistance to frost were calculated. We used a new, nonstandard concrete frost resistance mark determination method, developed by the researchers of Aleksandras Stulginskis University (former Lithuanian University of Agriculture), where this property is approximately evaluated by concrete compression strength and water absorbability.

Knowing the compression strength f_c of the concrete [8], [9], [10], [11] water absorbability by mass W_m [7] and allowed or forecasted loss of the concrete strength Δf_c , it is possible to estimate laboratory (F-T) cycles number n_{50} [14]:

$$n_{50} = c \cdot \Delta f_c^{-d} \quad (1)$$

where

n_{50} – numbers of laboratory (F-T) cycles freezing samples until $-55 \pm 2^\circ \text{C}$ by [14],

Δf_c – concrete strength loss in % due the influence of (F-T) cycles, calculated by [12],

c, d – coefficients found in the tables made by the researchers of Aleksandras Stulginskis University.

Regarding concrete frost resistance, mark F shows the number of (F-T) cycles n_F when samples are frozen under a temperature of $-18 \pm 2^\circ \text{C}$, so the number of standard (F-T) cycles is calculated

according to the formula developed by the researchers of Aleksandras Stulginskis University:

$$n_{F_c} = 34.848 \cdot n_{50}^{0.6157} \quad (2)$$

Function determination coefficient $R^2 = 0.9947$.

Evaluating the impact of (F-T) cycles on the change of investigated slabs concrete physical–mechanical properties the frost resistant parameters $F_5\%$ and $F_{50}\%$ were used.

According to the [12], the beginning of deterioration was fixed by the number of cycles, when from freezing, the sample surface up to 5 % of sample mass (frost resistance index $F_{5\%}$) deteriorates. From the first observed deterioration symptoms till absolute deterioration of the surface some time passes.

According to the construction regulations [16] the deterioration end was fixed by a number of cycles $F_{50}\%$ where the concrete compression strength of the 25–30 mm thick outer (cover) concrete layer shrinks twice, i.e. to 50 % of the estimated strength during the research.

Natural frost cycles, by means of corrective coefficients (chosen according to the graph elaborated by the researchers of Aleksandras Stulginskis University), were recounted into the laboratory (F-T) cycles and further recalculated to the parameters of structures durability – probable

deterioration times $T_5\%$ (the probable deterioration start time) or $T_{50}\%$ (the probable deterioration end time).

Dependences established between the field investigations concrete physical – mechanical properties and calculated parameters of structures durability $T_5\%$, $T_{50}\%$, T_{layer} were examined by correlation analysis. Formulae of dependences were established, correlation coefficients calculated and their reliability evaluated.

Results

During the period of 2008–2014 we investigated concrete compression strength (mean value) and water absorbability of the slab samples made from coarse grained cement without additives. In total, 12 Lithuania’s earth dams were chosen for investigations. Using the research results of the 7 dams’ slabs concrete compression strengths f_c and water absorbability W_m and formulae (1, 2), concrete frost resistance parameters $F_5\%$ and $F_{50}\%$ were calculated, which were further used to determine the durability probable deterioration times $T_5\%$ and $T_{50}\%$, presented in Table 1.

For a practical use proposed dependences equations are presented in Fig. 2.

TABLE 1
Research Results of Concrete Compression Strength f_c , Water Absorbability W_m and Calculated Concrete Frost Resistance Parameters $F_5\%$, $F_{50}\%$ and Durability Parameters $T_5\%$, $T_{50}\%$ [Source: construction by authors]

No.	Name of dam	f_c , MPa W_m , %	$F_5\%$, cycles	$F_{50}\%$, cycles	$T_5\%$, years	$T_{50}\%$, years
1	2	3	4	5	6	7
1	Krokialaukis	27.6±1.2 4.54±0.28	171,8	1029,0	34,4	205,8
		28.9±1.4 4.24±0.21	192.1	1219.9	38.4	244.0
2	Anulynas	6.2±0.7 11.3±0.8	30.6	81.9	6.11	16.4
		3.4±0.1 15.5±0.2	22.7	54.1	4.53	10.8
		3.7±0.1 14.2±0.1	23.5	56.4	4.7	11.3
		3.9±0.1 13.7±0.2	24.9	60.7	4.98	12.1
		4.4±0.3 13.0±0.2	25.6	62.9	5.11	12.6
		4.7±0.3 12.5±0.1	26.4	65.8	5.27	13.2
		5.3±0.1 11.8±0.6	28.5	72.8	5.71	14.6
		6.2±0.1 10.5±0.1	31.5	86.1	6.29	17.2
		7.4±0.23 9.52±0.22	37.0	108.8	7.41	21.8
		8.8±0.1 8.64±0.14	45.1	134.3	9.02	26.9

TABLE 1 CONTINUED

No.	Name of dam	f_c , MPa W_m , %	$F_{5\%}$, cycles	$F_{50\%}$, cycles	$T_{5\%}$, years	$T_{50\%}$, years
3	Kazlai	6.3±0.6 12.6±0.3	27.9	71.6	5.57	14.3
4	Jūrė	7.1±0.4 14.6±0.2	26.8	68.2	5.35	13.6
		14.8±1.1 6.85±0.12	56.4	189.8	11.3	38.0
5	Marijampolė	6.0±0.9 12.8±0.4	27.2	69.0	5.44	13.8
6	Anulynas	20.6±1.5 9.54±0.32	76.4	301.7	15.3	60.3
		15.5±1.0 11.7±0.9	57.3	195.2	11.5	39.0
		15.6±2.1 10.0±1.4	57.3	195.2	11.5	39.0
7	Kaulakiai I	20.9±1.6 8.79±0.28	83.2	335.6	16.6	67.1
		15.0±2.2 9.23±0.70	56.4	189.8	11.3	38.0
		14.0±1.6 12.5±1.8	54.65	179.27	10.9	35.9

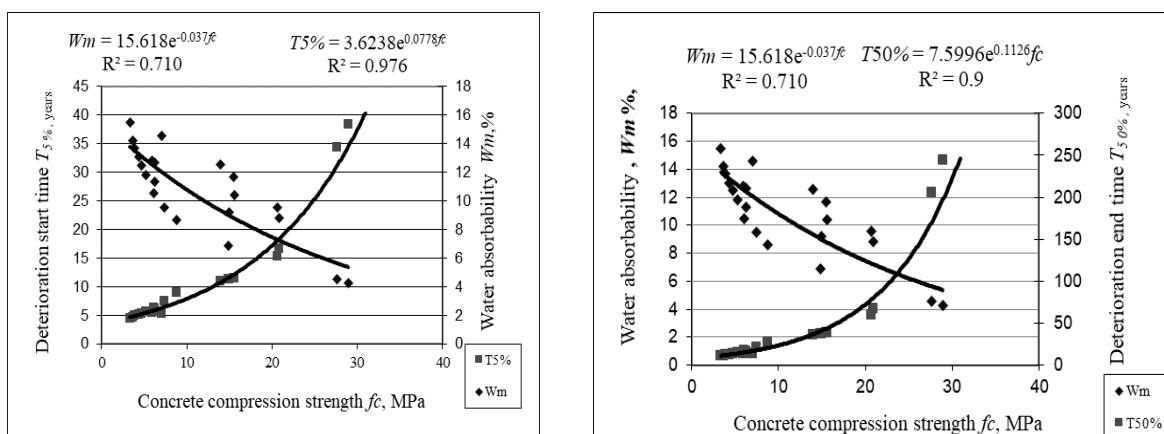


Fig. 2. Equations dependences of slabs concrete compression strength f_c , water absorbability by mass W_m , and probable deterioration times $T_{5\%}$ and $T_{50\%}$

Functional reliability of concrete compression strength f_c , water absorbability by mass W_m , and probable deterioration times $T_{5\%}$ and $T_{50\%}$ of slabs checked by double correlation. It was found that the dependence strength ranges from very strong (when $r_{xy} > 0.9$) to strong (when r_{xy} from 0.7 to 0.9). Calculated correlation coefficients are reliable, their importance level $p < 0.05$. Estimated determination coefficients R^2 range from 0.9 to 0.976, so it's true to say that researched strength and water absorbability parameters from 90.0 to 97.6% influence investigated durability parameters (the other part – influence of other parameters).

Using the proposed equations dependences, a calculation can be made for how many years are left for structure's use till probable deterioration starts ($T_{5\%}$) or ends ($T_{50\%}$).

These equations may be used for the evaluation of the state and durability of used reinforced concrete

slabs by the probable deterioration time. In calculations by the formulae one needs to know the values of the concrete compression strength f_c , water absorbability W_m and the size of concrete strength loss Δf_c because of frost impact.

By means of the proposed method reinforced concrete slabs durability parameters ($T_{5\%}$ and $T_{50\%}$) of 7 Lithuania's earth dam were calculated. It was found, that the structure at $f_c = 28.9 \pm 1.4$ MPa (one of the biggest in the researched structures) and at $W_m = 4.24\%$, influenced of 5 laboratory frost cycles during the year, can be used till probable deterioration start $T_{5\%} = 38.4$ years and till probable deterioration end $T_{50\%} = 244.0$ years. Under $f_c = 3.4 \pm 0.1$ MPa (one of the smallest researched structures) and $W_m = 15.5\%$ such slab could be used accordingly: $T_{5\%} = 4.53$ years and $T_{50\%} = 10.8$ years.

It was noticed during the expedition, that all the investigated surfaces of earth dam slopes slabs in the

zone of changing water level are more or less deteriorated in the form of pitting. There are several reasons of forming pitting, but the main is—erosion of concrete by influence of (F-T) cycles.

The surface of the structures on the changing water level zone is in contact with ice, swimming solids or sediments (especially gravel) abrasive impact. After establishing the most affecting impact in the separate ponds, there is a need to explore the reasons for pitting occurrence in a more detailed way.

Other reasons of concrete erosion presented in the sources of scientific literature, for instance, cavitation, are less frequently described with regard to the structures researched, because in the researched ponds, water flow pulsation speeds are small (< 2m/s).

The research results of 12 dams slabs’ concrete compression strength f_c and pitting depth are presented in the Table 2.

TABLE 2

Research Results of Dams Age, Concrete Compression Strength f_c and Pitting Depth
[Source: construction by authors]

No.	Name of dam	Age of structure, years	Concrete compression strength f_c , MPa	Pitting depth, mm
1	2	3	4	5
1	Angiriai	22	7.9±0.6	33.8
			9.0±0.7	23.9
2	Antanavas HP	47	8.2±0.9	36.3
			6.4±0.40	44.1
			6.0±0.4	43.6
3	Anulynas	24	15.5±1.0	9.4
4	Babtai I	31	8.3±0.7	36.9
			10.6±1.1	23.4
5	Gailiušiai	29	9.1±0.4	30.7
6	Graužė III	23	7.3±0.4	44.7
			8.2±0.8	29.9
		22	7.6±0.6	37.4
			6.2±0.3	45.3
7	Jūrė	23	9.8±0.5	20.4
		26	7.1±0.4	38.6
8	Kaulakiai I	25	14.0±1.6	11.5
9	Kazlai	13	7.6±0.4	22.6
		11	6.3±0.6	44.9
10	Kruostas HP	49	7.2±0.6	53.2
			9.5±0.4	46.7
			5.5±0.2	62.5
11	Marijampolė	20	6.0±0.9	55.3
12	Pilvė -Vabalkšnis	13	6.7±0.3	36.6
		13	7.1±0.6	28.0
		11	4.2±0.1	41.9
		11	4.4±0.0	50.6

According to the analysis of 12 earth dams’ slopes protection with reinforced concrete slabs testing results, the surfaces of structures made of weak concrete were damaged much more. The top speed of pitting deepening was established in slabs made of weak concrete ($f_c = 4.2\div 6.3$ MPa) at Pilvė–Vabalkšnis, Kazlai dams. The average deepening speed of a pitting was 4.6 mm and 4.1 mm per year in the structures of Pilvė – Vabalkšnis and Kazlai respectively.

The average deepening speed of pitting in the structures made of concrete with average compression strength $f_c = 15.5$ MPa (at Anulynas dam) was the smallest – only 0.4 mm per year.

The deepening speed of a pitting v (constant of degradation) – in relation to the average compression strength of slabs’ concrete f_c may be expressed by equation

$$v = 45.813 \cdot f_c^{-1.723} \quad (3)$$

Where:

v – average deepening speed of pitting in structures, mm per year,

f_c – average compression strength of concrete, MPa.

Determination coefficient of the function $R^2 = 0.6747$.

Using the formula (3), the time (T_{layer}) can be estimated through which pitting will reach a dangerous depth for the structure. This depth is to be equal to the thickness of the covering layer of the structure's concrete (according to the former design standards, it had to be no smaller than 30 mm, and due to the currently used design norms it must be 40 mm).

Time (T_{layer}), during which reinforcement of the reinforced concrete slab will be exposed, depending on concrete compression strength f_c may be expressed by

$$T_{40\text{mm}\text{layer}} = 7.7187 \cdot f_c - 26.852 \quad (4)$$

where

$T_{40\text{mm}\text{layer}}$ – functioning period of a 40 mm thick covering layer of the structure expressed in years,

f_c – average compression strength of concrete, MPa.

Determination coefficient of the function $R^2 = 0.7956$.

Similar dependences equation, $T_{\text{ap.sl.}} = 7.5465 f_c - 42.859$, is created using the data of research on the retaining walls and shaft culverts and presented in work [16].

Durability time (T_{layer}), which was calculated using the constant of degradation and concrete compression strength, shows that in structures, manufactured in Lithuania from weak concrete ($f_c = 4.4$ MPa), when the concrete covering layer is 40 mm thick, reinforcement had to be exposed accordingly after 8.7 years of use. In structures, manufactured from stronger concrete ($f_c = 15.5$ MPa) it will be exposed accordingly after 102.4 years of use.

Using dependences (3) and (4) for designed earth dam slabs, which are used on changing water level, the concrete of appropriate strength can be chosen, so that reinforcement of these structures will not be exposed during a foreseen time.

For example, we calculated, that a 40 mm covering concrete layer of slab (under changing water level) would collapse just after 100 years, if it was made from concrete, the compression strength of which was 16.4 MPa.

Empirical dependences (3) and (4) may be used for the tentative evaluation of properties of coarse-grained cement, without additives concrete, during the evaluation of used earth dam slopes slabs condition.

Concrete compression strength f_c and parameters of structures durability $T_{40\text{mm}\text{layer}}$, during which reinforcement of reinforced concrete slab will be exposed, reliability of the functional dependences was checked by double correlation. It was found that the dependences are strong ($r_{xy} = 0.9$). Calculated correlation coefficients are reliable, their importance level $p < 0.05$. The established determination coefficient $R^2 = 0.7956$, therefore it can be stated that the examined strength parameters influence the investigated parameters of durability by 79.6%, other part belongs to the influence of less important parameters.

We did not calculate the effect of corrosion on the overall durability of slabs in our paper. Researcher [13] has investigated marine structures and found that “for a given concrete structure in a given environment, the overall durability requirement is based on the specification of a given service period before the probability for onset of corrosion exceeds a certain upper level, and for this level, a probability of 10% was adopted for marine structures. In order to calculate the probability of corrosion, durability analyses are carried out, and this provides the basis for selecting proper combinations of concrete quality and cover thickness. An increased concrete cover also would significantly affect the probability of corrosion. While a nominal cover of 70 mm for Portland cement concrete would give a service period of about 30 years, increased cover of up to 90 and 120 mm would increase the service period by up to more than 60 and more than 120 years, respectively”. These results conform to our research of thickness covering concrete layer of slabs.

Conclusions

1. The method for durability evaluation of reinforced concrete slabs for earth dam slope protection has been developed. By means of the method, knowing the values of a structure's concrete strength, water absorbability and allowed concrete strength loss due to frost action, the main parameters of slabs durability can be calculated – the probable deterioration start time $T_5\%$ (covering layer strength f_c loss under the frost influence by 5%) and the probable deterioration end time $T_{50\%}$ (covering layer strength f_c loss under the frost influence by 50%).
2. Durability of slabs covering layer can be evaluated by time (T_{layer}), which equals the reinforcement exposure of the reinforced concrete structure.
3. Using durability parameter (T_{layer}), it was calculated, that 40 mm covering concrete layer of slab would collapse just after 100 years, if it was made from concrete, the compression strength of which was 16.4 MPa.

References

1. **Ayub, T., Shafiq, N., Khan, S.U.** Durability of Concrete with Different Mineral Admixtures: A Review. World Academy of Science, Engineering and Technology. *International Journal of Civil, Environmental, Structural, Construction and Architectural Engineering*, 2013, Vol:7, No:8.
2. **Bryant, L. M., Mlakar, P.F.** Predicting concrete service life in cases of deterioration due to freezing and thawing. *Technical Report REMR-CS-35*, U.S. Army engineer waterways experiment station, Vicksburg, MS. (1991).
3. **Brunauer, S.** The Structure of Hardened Portland Cement and Concrete. *Proceedings of the 8th Conference on the Silicate Industry*. Budapest, Hungary, June 9-12, pp. 205-230, as reported by Massazza (1996).
4. **CEN/TR 15177:2006.** Testing the freeze-thaw resistance of concrete. Internal structural damage.
5. **CEN/TR 12390-9.** Testing hardened concrete - Part 9: Freeze-thaw resistance – Scaling.
6. **CDF Test** - Test method for the freeze-thaw resistance of concrete - tests with sodium chloride solution (CDF), *RILEM Recommendation TC 117-FDC: 'Freeze-thaw and de-icing resistance of concrete'*, *Mater. Struct.* 29. (1996). P. 523-528.
7. **EN 12390-8: 2009** Testing hardened concrete - Part 8: Depth of penetration of water under pressure.
8. **EN 12390-3: 2009** Testing hardened concrete - Part 3: Compressive strength of test specimens. Testing hardened concrete - Part 7: Density of hardened concrete.
9. **EN 12504-1: 2009** Testing concrete in structures - Part 1: Cored specimens - Taking, examining and testing in compression.
10. **EN 12504-2: 2012** Testing concrete in structures - Part 2: Non-destructive testing - Determination of rebound number.
11. **EN 13791:2007** Assessment of in-situ compressive strength in structures and precast concrete components.
12. **LST 1428.19:2016** Concrete - Test methods - Part 19: Determination of frost resistance to one-sided freezing and thawing.
13. **Gjørsv, Odd E.** Durability design and quality assurance of major concrete infrastructure. *Advances in Concrete Construction*. 2013, Vol. 1, No. 1. p. 45-63.
14. **GOST 10060-87.** Concretes. Methods of frost resistance determination. *Standart USSR*. Moscow, Gosstroy USSR, 1987. 14 p.
15. **Massazza, F.** Action of Environmental Conditions. *RILEM REPORT 11: Interfacial Transition Zone in Concrete*. London, England, U.K.: J. C. Maso, ed. E&FN SPON, First Edition, 1996. p. 132-149.
16. **Рекомендации** по обеспечению надежности и долговечности железобетонных конструкций промышленных зданий и сооружений при их реконструкции и восстановлении. Москва: Стройиздат, 1990, 176 с.
17. **Rønning, T.F.** *Freeze-Thaw Resistance of Concrete – Effect of Curing Condition, Moisture Exchange and Materials*. PhD Thesis, NTNU Trondheim – Norwegian University of Science and Technology, Technology, 2001. 414 p.
18. **Rosenqvist M.** *Frost-induced deterioration of concrete in hydraulic structures. Interactions between water absorption, leaching and frost action*. Ph.D. thesis. Lund University, Lund 2016. 98 p.
19. **Šadzevičius, R.** *Modelling and Analysis of Environmental Impact on Reinforced Concrete Slabs for Earth Dam Slope Protection*. Ph.D. thesis. Kaunas: Lithuanian University of Agriculture, 2005. 125 p.
20. **Tarun, R. Naik.** Concrete durability as influenced by density and/or porosity. *Presented and Published at the Cement and Concrete Institute of Mexico Symposium "World of Concrete - Mexico"*. Guadalajara, Mexico, June 4-7, 1997. Report No. CBU-1997-27.
21. **Vaišvila, K.A., Lindišas, L., Šadzevičius, R.** The research of deterioration of reinforced concrete structures functioning in the alternative level of water engineering constructions. *In: Vandens ūkio inžinerija: mokslo darbai*. LŽŪU, Lietuvos vandens ūkio inst., 2001, vol. 18 (40), p.47–52.
22. **Вайшвила, К.А., Микуцкис, Ф.** Оценка прочности бетона на сжатие при испытании образцов неправильной формы. *Civil Engineering '05: International Scientific Conference Proceedings*: Jelgava, 2005, P. 12-20.
23. **Zhang, S. P., Zong, L.** Evaluation of Relationship between Water Absorption and Durability of Concrete Materials. *Advances in Materials Science and Engineering*, 2014. Article ID 650373, 8 pages, 2014. doi:10.1155/2014/650373

Evaluation of Surface Materials for Pavements and Footpaths

Vincas Gurskis, Rytis Skominas, Giedrius Sakalinskas, *Aleksandras Stulginskis University, Lithuania*

Abstract. Scientific studies, standards and regulations regarding the requirements for design, construction, exploitation and maintenance of pavements and footpaths were analysed during the research. The main problems which appear during the construction and exploitation of these engineering structures were also studied. Estimating the most optimal surface material for pavements and footpaths, the most popular materials (asphalt, site-cast concrete, concrete slabs, concrete blocks, clinker blocks, stone blocks and gravel) were analysed. Evaluating different surface materials, the parameters were taken from a survey. In this survey the designers of pavements and footpaths as well as constructors participated. The public opinion was also taken into account. For the estimation of optimal surface material multicriteria analysis software Visual Promethee was used. The analysis shows that the most optimal surface material for pavements and footpaths is concrete blocks.

Keywords: pavement, footpath, surface material.

Introduction

Pavements and footpaths are very important engineering structures in communication nets for walkability [3]. According to Tim Massart [5] walking and cycling are green transport modes which will get more attention in the future. Therefore, during the development of an infrastructure it is necessary that pavements and footpaths get more attention. N. Stevens and P. Salmon [7] offer that footpath design efforts should consider the overall foot-path system and the intertwined functional purposes of providing safety and a sense of place. Urban planning needs new ways to interpret built environments as not only technical systems, but often poorly understood (and designed) socio-spatial systems. This cooperative effort between Human Factors and Urban Planning disciplines should be allowed for new insights into the development of more pedestrian orientated footpath environments.

Unfortunately, in some Eastern Europe countries pavements and footpaths are not being repaired or reconstructed due to lack of finances, there are not enough money for making new pavements and footpaths. Lithuania has the same problems too. One of the possibilities to prevent defects is to create a special application on smartphone for reporting defects. The user can enter in detail any defect or remark with GPS coordinates, a picture, and some comments. City authorities using this method will have a lot of valuable data at their disposal to make informed decisions for footway modifications and maintenance [5].

According to the Italian researchers [2] it is necessary to record the flow of people, and afterwards, according to this data it is possible to estimate problematic places, to select priorities for reconstruction of pavements and footpaths.

Unfortunately, in Lithuania, like in some others EU countries, there are no rules regarding the construction of pavements and footpaths. In Lithuania

the pavements and footpaths are designed according to the following recommendations: "Pedestrian and bicycle path design guidelines" [6]. Of course, the new designed or reconstructed pavements and footpaths must meet the requirements for people with disabilities listed in the document "Technical Construction Regulation STR 2.03.01:2001 Structure and territories. Requirements for people with special needs". This social group is particularly sensitive in terms of using improperly constructed pavements and footpaths. According to the World Health Organization [10] 253 million people live with vision impairment: 36 million are blind and 217 million have moderate to severe vision impairment. Therefore, when constructing new or reconstructing old pavements and footpaths it is necessary that they meet the requirements for these people.

In Lithuania's regulations there are only basic requirements for pavements and footpaths: a cross slope 0.5...3 %, longitudinal slope $\leq 4\%$ (in special places $\leq 8\%$), the width for 1 person ≥ 1 m, the width for 1 person with disabilities ≥ 1.2 m, the height ≥ 2.25 m [6]. Unfortunately, the pavements and footpaths constructed during the Soviet period did not meet these requirements (Fig. 1). The poor technical state of pavements and footpaths constructed during that period was affected by many factors: low quality base and subbase (too thin of layers, inadequate density of compacted layers, inappropriate slopes, not suitably embedded kerbs, too low frost resistance of surface materials.

The pavements and footpaths are constructed similarly to the roads: removal of vegetative layer, if necessary the subgrade formation, subbase layer (resistant for freezing – thawing) formation, base layer formation and surface layer construction. In the last layer, builders (including municipalities) who are constructing new or reconstructing old pavements and footpaths have a problem as to which surface

material to select. The surface material must be durable, aesthetic and simply exploited. Therefore, it is necessary to compare different materials. It is possible to find studies about the effect of walking sounds from different walked-on materials on

people’s soundscape [1], [4]. However, the studies about other properties are insufficient. Thus, the aim of this work was to estimate the most optimal surface material for pavements and footpaths.



Fig. 1. Pavement constructed during the Soviet period

Methodology

As a research object seven most popular surface materials used for pavements and footpaths were chosen: asphalt, site-cast concrete, concrete slabs, concrete blocks, clinker blocks, stone blocks and gravel. All these materials have different properties and it is hard to estimate which material is the best. Therefore, multi-criteria analysis was selected for the evaluation of the materials.

For multi-criteria analysis data were gathered from the specialist survey whose participants were the employees from the Lithuanian Road Administration under the Ministry of Transport and Communications, State Territorial Planning and Construction Inspectorate under the Ministry of Environment, Departments of Architecture and Urbanism of Municipalities, heads of construction, designers and technical supervisors. The questionnaire was anonymous. Ten criteria were selected for the evaluation of surface materials: durability, versatility, aesthetics, resistance to mechanical or chemical attack, possibility to repair and reconstruct, exploitation costs, labour mechanization level, safety in use, variety of colours and shapes as well as supply. All criteria were evaluated on a 10 points system: 10 – excellent, 1 – very poor. If a questionnaire was filled in a perfunctory manner, with mistakes or partly they were denied.

The public opinion about surface materials of pavements and footpaths was also taken into account. For this purpose, a second survey was conducted. In this survey there were two main questions: which surface material is the best and which criterion is the most important.

The main factor for the surface material selection is cost. Cost is the main criterion in public procurement. Therefore, the municipalities are constrained to choose the least expensive variants (with the least expensive surface materials of pavements and footpaths). To evaluate this criterion an economic calculation for construction was done using the SES 2004 software. During the calculations the construction cost of 100 m² surface material with first layer (without kerbs) was estimated including all taxes valid in Lithuania.

Another very important criterion is durability. This criterion depends on many factors: material characteristics, exploitation, environmental impact, etc. Durability can be described by lifetime. The lifetime in this research was estimated according to the date given in the “Technical Construction Regulation STR 1.12.05:2002 Usage and lifetime of the structure” document.

For multi-criteria analysis the software Visual Promethee was selected. Visual Promethee is multi-criteria decision aid software. It includes many approaches, models and methods to handle decision or evaluation problems where multiple evaluation criteria have to be taken into account. Three main methods in the Visual Promethee software are used: Multi-criteria Table, Aggregation and Weighted Sum and Outranking Methods [11].

Analysing the data with Visual Promethee software, three tests were performed: with equal criteria and with dominant criterion. Cost and aesthetics were selected as the dominant criteria. They had two times higher of a score than others.

Test results

According to the specialists’ opinion (Table 1) the most durable and resistant to environmental impact surface material for pavements and footpaths is stone blocks and the weakest material is gravel, which has the shortest lifetime before repair. The most versatile material is asphalt and it can be used almost in all cases, while the gravel has a reverse evaluation – it is suitable in only some cases. Specialists think that the most aesthetic material and which has the widest variety of colours, is clinker blocks and gravel was evaluated as the worst material. According to the possibility to be repaired and reconstructed, concrete blocks got the highest evaluation due to the possibility to replace separate blocks having defects. The site-cast concrete received the lowest evaluation due to the complicated repair technology of concrete.

Exploitation costs are the highest in gravel pavements and footpaths and the lowest in pavements and footpaths with stone block surface material. The fastest construction process is associated with using asphalt due to the labour mechanization level, while the longest construction process is associated with using stone blocks due to the high amount of manual labour and the irregular form of blocks. Regarding one essential requirement “Safe in use” the specialists think that the safest surface material is asphalt and the least safe stone blocks due to the possibility to slip or stumble. Gravel got the highest evaluation in terms of supply due to the large number of quarries in Lithuania. The stone blocks as a non-natural resource of Lithuania received the lowest evaluation.

TABLE 1

Specialists survey results

Surface material	Durability	Versatility	Aesthetics	Resistance	Possibility to repair and reconstruct	Exploitation costs	Labour mechanization level	Safety in use	Variety of colours and shapes	Supply
Asphalt	8.09	9.32	7.03	7.65	7.09	7.74	8.71	8.29	3.00	7.35
Site-cast concrete	6.24	7.59	6.09	6.41	<u>5.76</u>	6.76	7.18	7.41	3.97	8.29
Concrete slabs	6.88	7.15	7.18	6.65	8.00	7.26	6.29	6.88	5.94	7.91
Concrete blocks	8.06	7.97	8.59	8.00	8.53	7.74	6.56	7.53	8.35	7.94
Clinker blocks	8.24	7.76	9.41	7.88	8.21	7.56	6.35	6.82	8.85	5.82
Stone blocks	9.26	6.15	9.24	9.21	8.09	8.15	<u>6.09</u>	<u>6.47</u>	6.59	<u>5.38</u>
Gravel	<u>4.82</u>	<u>4.82</u>	<u>3.88</u>	<u>4.65</u>	8.38	<u>5.38</u>	8.12	7.00	<u>2.18</u>	9.47

According to public opinion (Fig. 2) the top 3 surface materials for pavements and footpaths are concrete blocks (37.3 %), clinker blocks (23.5 %) and stone blocks (23.5 %). The most undesirable surface

material is gravel (0.01 %). Therefore, it can be stated that people mostly like durable and aesthetic materials.

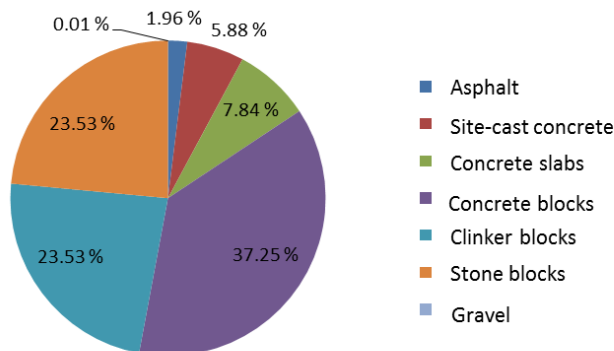


Fig. 2. Requested surface materials for pavements and footpaths according to public opinion

Evaluating second part of the public survey it is seen that the main criteria of surface materials are aesthetics (41 %) and durability (21.6 %). The cost criterion reached only the fourth place (9.8 %) and

safety in use and possibility to repair and reconstruct are not considered to be significant criteria (2 %) (Fig. 3).

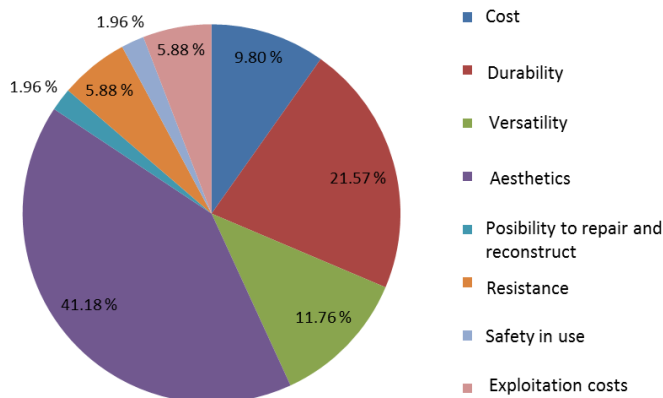


Fig. 3. Main criteria of surface materials for pavements and footpaths according to public opinion

According to economic calculations (Table 2) the most expensive pavements and footpaths are those made from stone blocks and clinker blocks, while the

cheapest – gravel. The difference between the most expensive and cheapest structures is more than 12 times.

TABLE 2

Economic calculations

Parameter	Surface material						
	Asphalt	Site-cast concrete	Concrete slabs	Concrete blocks	Clinker blocks	Stone blocks	Gravel
Construction cost of 100 m ² surface material with first layer (without kerbs), in Euros	2430.4	3627.2	1879.8	2369.5	4604.9	5055.4	417.6
Cost difference for the least expensive material (gravel), %	5.8	8.7	4.5	5.7	11.0	12.1	–

This distribution of cost was influenced by several factors. The supply is one of the main indicators - gravel is so cheap and stone blocks are so expensive compared with the other materials. The high mechanization level in construction reduces the cost, for example in constructing asphalt or gravel pavements or footpaths. The high level of manual labour increases the cost.

According to the lifetime estimated by the “Technical Construction Regulation STR 1.12.05:2002 Usage and lifetime of the structure”, the most durable material for pavements and footpaths is site-cast concrete (lifetime 40 years), followed by stone blocks (lifetime 30 years), concrete and clinker blocks (lifetime 20 years), asphalt and concrete slabs (lifetime 15 years) and the weakest materials – gravel (lifetime 10 years).

The multi-criteria analysis, using equal scores for the criteria (Fig. 4 a), shows that the optimal choice for pavements and footpaths is concrete blocks and the worst – gravel. The analysis with dominant criterion (cost) (Fig. 4 b) results in the same answer – the best surface material is concrete blocks. The last on the list also is gravel, but in this test the gap between the last and next to last (asphalt) is considerably smaller. The analysis regarding the dominant criterion (aesthetics) (Fig. 4 c) shows that the best material is concrete blocks and the worst – gravel. In the second and third place as in the test using equal scores for criteria are clinker blocks and stone blocks. The test regarding the dominant criterion (cost) shows that concrete slabs and clinker blocks are in the second and third place.

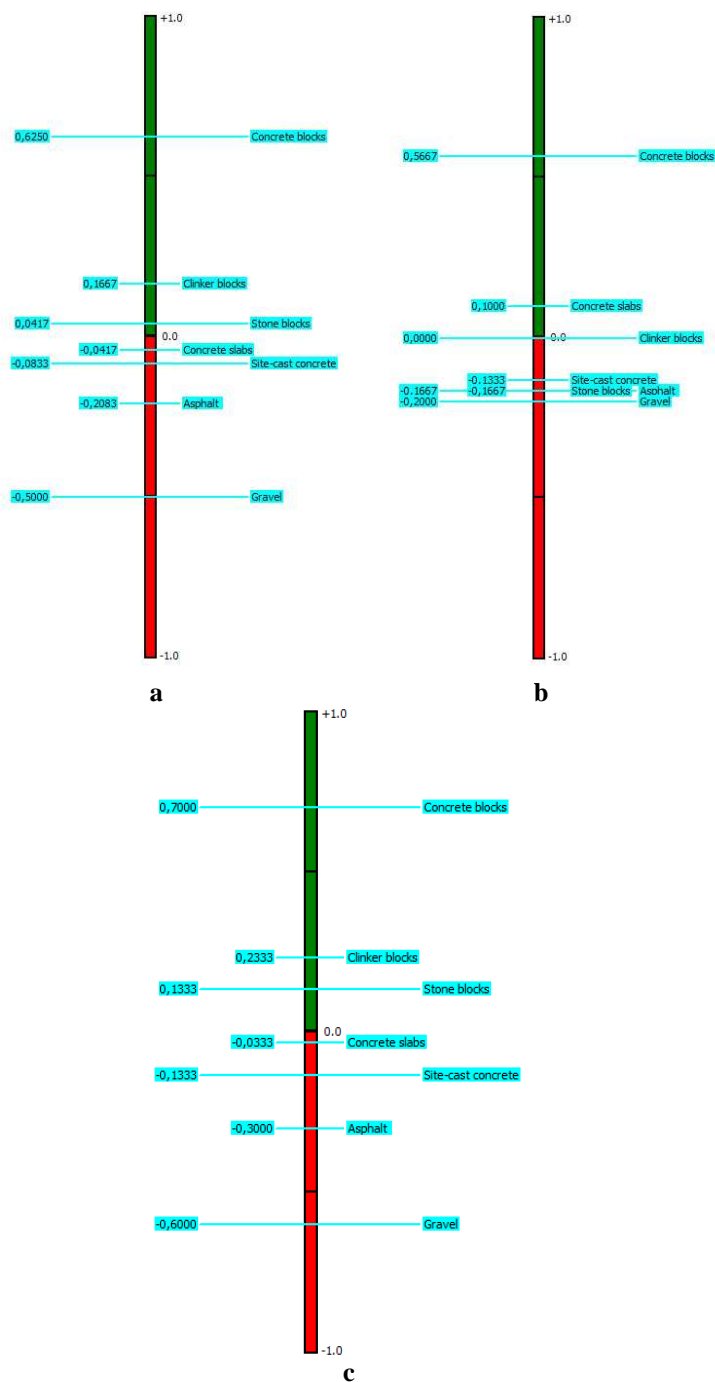


Fig. 4. Multi-criteria analysis results (a – equal criteria test, b – dominant criterion (cost) test, c – dominant criterion (aesthetics) test)

Conclusions

- The majority of pavements and footpaths, which were constructed in the Soviet period, did not meet the modern day requirements. Therefore, it is not safe to use them.
- According to the public survey it is estimated that the main criteria for pavements and footpaths surface material are aesthetics (41 %) and durability (22 %). The materials which are in greatest demand are: concrete blocks (37 %), stone blocks (24 %) and clinker blocks (24 %).
- Economic calculations show that the costs of construction of pavements or footpaths differ 12 times. The most expensive pavements or footpaths are those from/with stone blocks (50.55 €/m²) and the least expensive are gravel pavements and footpaths (4.18 €/m²).
- According to multi-criteria analysis it is estimated that the optimal variant is pavements and footpaths with concrete blocks surface material. The worst choice is gravel.

References

1. **Aletta, F., Kanga, J., Astolfi, A., Fuda S.** Differences in soundscape appreciation of walking sounds from different footpath materials in urban parks. *Sustainable Cities and Society*, Vol. 27, November 2016, p. 367–376.
2. **Corazza, M. V., Di Mascio, P.** How to make traffic calming more walking friendly: directions to increase intersections performances for pedestrians. In: *The Extra Workshop ICTCT e Safe Non-motorised Traffic*. Planning, Evaluation, Behavioural, Legal and Institutional Issues, Vancouver. [online 20.04.2017] http://www.ictct.org/migrated_2014/ictct_document_nr_175_Corazza.pdf.
3. **Cruisea, S. M., Huntera, R. F., Keea, F., Donnellyc, M., Ellisa, G., Tully, M. A.** A comparison of road- and footpath-based walkability indices and their associations with active travel. *Journal of Transport & Health* Vol.6, September 2017, p. 119-127.
4. **Fuda, S., Aletta, F., Kang, J., Astolfi, A.** Sound Perception of Different Materials for the Footpaths of Urban Parks. *Energy Procedia*, Vol.78, November 2015, p. 13 – 18
5. **Massart T.** Footway evaluation. *Transportation Research Procedia*, Vol. 14, 2016, p. 2449 – 2457.
6. Pedestrian and bicycle path design guidelines, 2012 (in Lithuanian).
7. **Stevens, N., Salmon, P.** Safe places for pedestrians: Using cognitive work analysis to consider the relationships between the engineering and urban design of footpaths. *Accident Analysis & Prevention*, Vol. 72, November 2014, p. 257-266.
8. Technical Construction Regulation STR 1.12.05:2002 Usage and lifetime of the structure. (in Lithuanian).
9. Technical Construction Regulation. STR 2.03.01:2001 Structure and territories. Requirements for people with special needs.
10. Vision impairment and blindness. World health organization, 2017 [online 15.03.2017] <http://www.who.int/mediacentre/factsheets/fs282/en/>.
11. Visual Promethee [online 05.01.2018] <http://www.promethee-gaia.net/features.html>

Influence of Steel Impact Strength on the Maintenance and Operation of Civil Engineering Structures

Kamil Pawłowski, Agata Włóka, *Wroclaw University of Environmental and Life Sciences*

Abstract. Steel structures are extremely susceptible to all material defects that may occur in the bearing elements. Material defects may result in local weakening or accumulations of stress that lead to the emergence of fractures and the propagation of cracks, which, in turn, may cause structural damage. The capability of steel to resist to cold cracking is referred to as impact strength. It is particularly important due to the course of disasters that may occur as a result of such a fracture. They are extremely rapid and thus may have very serious consequences as they do not leave sufficient time for evacuation. The paper discusses the analysis of historical steels in terms of the impact strength of steel used in bridge structures for a period exceeding a hundred years and the attempt to determine the influence of fatigue on the impact strength of steel. In order to determine this correlation, samples were collected from the truss structures of the main girders of bridge spans. Samples were collected from two sites on the structure: the lower chords of the main girders in the mid-span of the girder and from the support zone. Previously, the bridge steel had been subjected to tests of tensile strength, chemical composition and an initial test of impact strength of steel was conducted at a temperature of -20°C ; 0°C and $+20^{\circ}\text{C}$. The results were presented in papers [3]. The current article provides a much wider scope of tests, both in terms of the number of analysed samples and the differences in temperature. A total of 30 samples were tested at temperatures of -60°C , -40°C , -20°C , 0°C and 20°C . The tests confirmed the initial hypothesis that fatigue influences the impact strength of steel. We have also succeeded in developing an impact strength curve for historical steels, which is different from that presented in the subject literature.

Keywords: impact strength, steel, bridges, fatigue load.

Introduction

Steel is currently widely used as a construction material in various types of structures, starting from residential buildings to industrial and transport structures. Both the steel manufacturing technology itself and the ways to use steel for erecting construction facilities have been developing for centuries. Various technological problems related to the application of steel were encountered. They included, among others, the influence of increased temperature on steel bearing capacity, sensitivity to dynamic loads, fatigue-related problems and brittle fractures. Many of these issues were successfully solved to a sufficient extent. However, new questions arise with the development of technology and the simultaneous ageing of existing structures. The authors of this paper decided to handle the issue related to the simultaneous occurrence of the influence of fatigue load of construction steel and the impact strength of steel, pursuant to the hypothesis of accumulating damages [1], [4]. The analysed steel

was obtained from the structure of a railroad bridge that has been in operation for more than 100 years. A bridge, as a structure subjected to regular loads, is the perfect type of structure to be selected for the analysis of the accumulation of such influences. Historical steel, manufactured at the end of the 19th century, is a very valuable research material, as it may provide an answer to the question of how to deal with historical structures in the event if it is necessary to repair or reinforce them. The paper presents the results of impact strength tests for samples collected from parts of the structure where the lowest and the highest fatigue-related influences occurred. The results of impact strength tests conducted at temperatures from -60°C to $+20^{\circ}\text{C}$ are presented. The results presented herein are a continuation of the research published in the paper [3], expanded by further temperatures of the steel work of fracture tests and the number of analysed samples.

Characteristics of the analysed object



Fig. 1. A view of the railroad bridge at km 25.414 of line No. 30 Łuków- Lublin

The span of the bridge from which samples were collected for the analysis is located on the Łuków-Lublin line No. 30, at km 25.414 (Fig. 1). The structure was erected at the end of the 19th century, as part of the Łuków-Lublin railroad. The railway line was apparently constructed by the Russians and was of strategic importance for the Russian armed forces during World War I.

The object is a single-span steel structure based on simply supported beam design. The design is shown in Figure 2. The main girders of the object are two

trusses of a theoretical span of 22.36 m, with railroad tracks placed on beams of the bottom chord of the truss, which is a Pratt truss with parallel chords. Crossbars are placed at approx. 2.8 m. The height of the trusses is 3.05m. The spacing between the main girders is 5.25m. Two sidebars with 1.83m axial spacing are connected to the crossbars, stiffened with a vertical bracing in the middle of the truss span and horizontal bracings on the plane of the top and bottom chords.

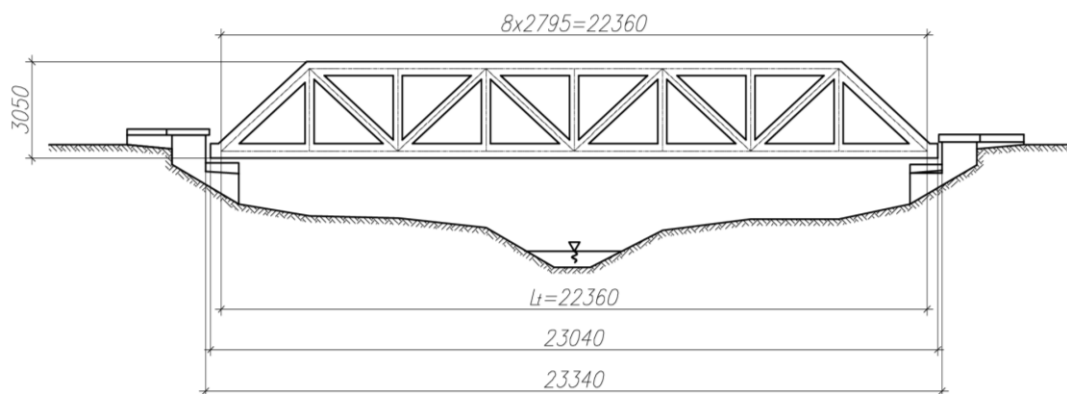


Fig. 2. Diagram of the bridge

The samples for analysis were collected from these elements of the bridge that were subjected to fatigue load to the lowest and highest extent during the operation of the bridge. Due to the static scheme of the simply supported beam, this was the zone in the middle of the span and at the supporting pillar. The

samples of the highest fatigue load were collected from the sheet metal of the bottom chord of the truss, from the element marked as number 3 in Figure 3. The samples of the lowest fatigue load were cut from element number 1, shown in Figure 3.

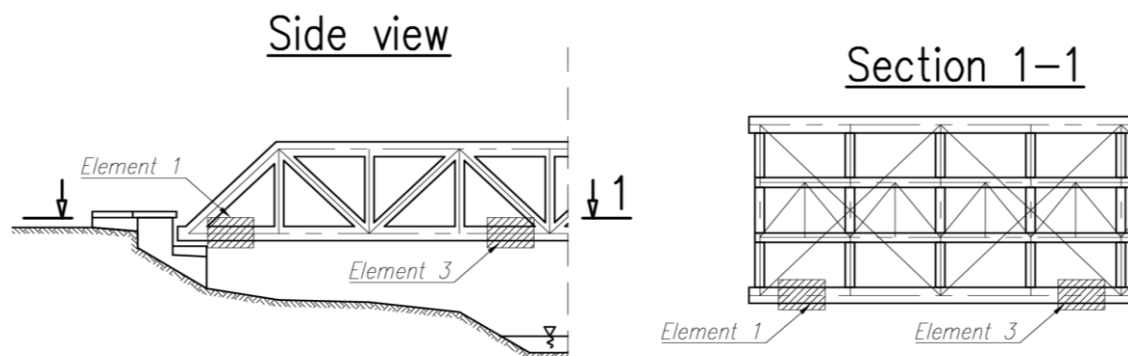


Fig. 3. Locations of elements from which samples were cut out for analysis

The authors' previously conducted tests, the results of which were published in paper [3], included the results of the analysis of basic mechanical properties of the analysed steel, chemical composition analysis and preliminary impact strength tests at temperatures ranging from -20°C to $+20^{\circ}\text{C}$. These results allowed us to determine the type of steel from which the bridge was constructed and confirmed the initial hypothesis concerning the influence of fatigue load on steel impact strength. Due to that, the authors decided to conduct further research and to expand the temperature range of impact strength tests. This refers mainly to temperatures below zero, which are much worse for the properties of construction steel.

Research methodology

Impact strength, which may be defined as the resistance of the material to fractures caused by impact, is also a measure of brittleness. This means that the more brittle the material, the lower its impact strength [2]. Both in the construction industry and in other fields of technology, certain minimal values of impact strength have been set for specific types of steel, depending on the stress of the structural element.

Impact strength tests are conducted in compliance with the PN-EN ISO 148-1 standard [6], on samples with notches of a standardised shape and dimensions,

supported on both ends (Figure 4). The standard foresees two types of samples, with V and U shaped notches. The analysed samples should have a square cross-section of the dimensions $8 \times 8 \text{mm}$. Impact strength tests are performed with the use of equipment that enables one to apply a high force in a short time, usually called impact hammers. The most commonly used device is the Charpy hammer.

Sections of material from which test samples are then collected should be cut cold using a moulder or cutter. At the same time, attention should be paid to local overheating of the sample or potential cold compression of the material that might negatively affect the impact strength test. For example, the sample may be cut using an acetylene burner, but adequate excess should be then foreseen, which will then be removed while cutting a normalised dimension sample. The number of samples is specified by the aforementioned standard [6]. Samples should be completely chip processed only in specific cases one edge may be left unprocessed. The notch on the sample is created by milling, drilling or cutting. The notch surface should be free from any cracks or fractures. All dimensions of the notch, such as its depth, edge opening angle, or the radius of the rounding of notch bottom are precisely defined in the reference standard [6] as they have a considerable influence on the obtained results.

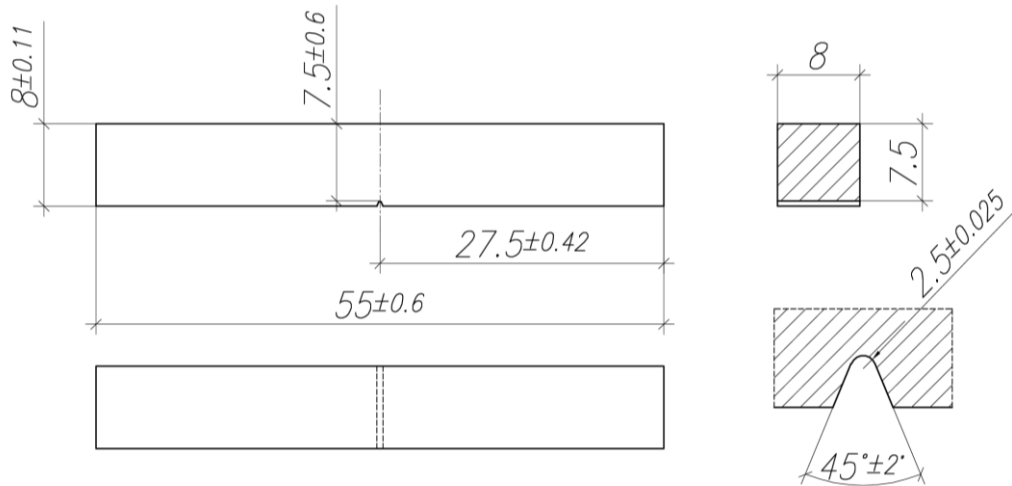


Fig. 4. Sample for Charpy impact strength testing

Results of steel impact strength tests

Steel impact strength tests were ordered to be conducted at a specialist laboratory at the Batory Steel Works in Chorzow. The test was conducted with the use of a Charpy hammer. The results of the work of fracture for the steel samples collected from the element subject to low fatigue load are presented in Table 1 and in the diagram in Figure 5. The analysis of the results mentioned above demonstrates that although the analysed steel should not be characterised by high fatigue use, its work of fracture is very low. This is even more important as the bridge structure is exposed to very low working

temperatures, even below -30°C . The obtained results disqualify this steel as a construction material. The 27J value that has to be met in order to consider the steel as construction material is achieved only at the temperature of 0°C for the analysed element. Thus, pursuant to the binding reference standards, this steel should be classified as J0. However, considering that the presented work of fracture values are characteristic values, after statistical processing of the results it might turn out that this steel may be classified as JR steel, i.e. such steel, for which the impact energy requirement is met at $+20^{\circ}\text{C}$.

Results of work of fracture tests for samples collected from element 1

TABLE 1

Temperature	Element 1				
	-60°C	-40°C	-20°C	0°C	20°C
Work of fracture	[J]	[J]	[J]	[J]	[J]
Sample 1	3	7	31	34	44
Sample 2	4	5	14	36	39
Sample 3	4	6	10	28	36
Average	3.63	5.94	16.31	32.48	39.53
Population standard deviation = $\sqrt{\frac{\sum(x-\bar{x})^2}{n}}$	0.47	0.82	9.10	3.40	3.30
Sample standard deviation = $\sqrt{\frac{\sum(x-\bar{x})^2}{(n-1)}}$	0.6	1.0	11.2	4.2	4.0
Square deviation = $\sum(x-\bar{x})^2$	0.67	2.00	248.67	34.67	32.67

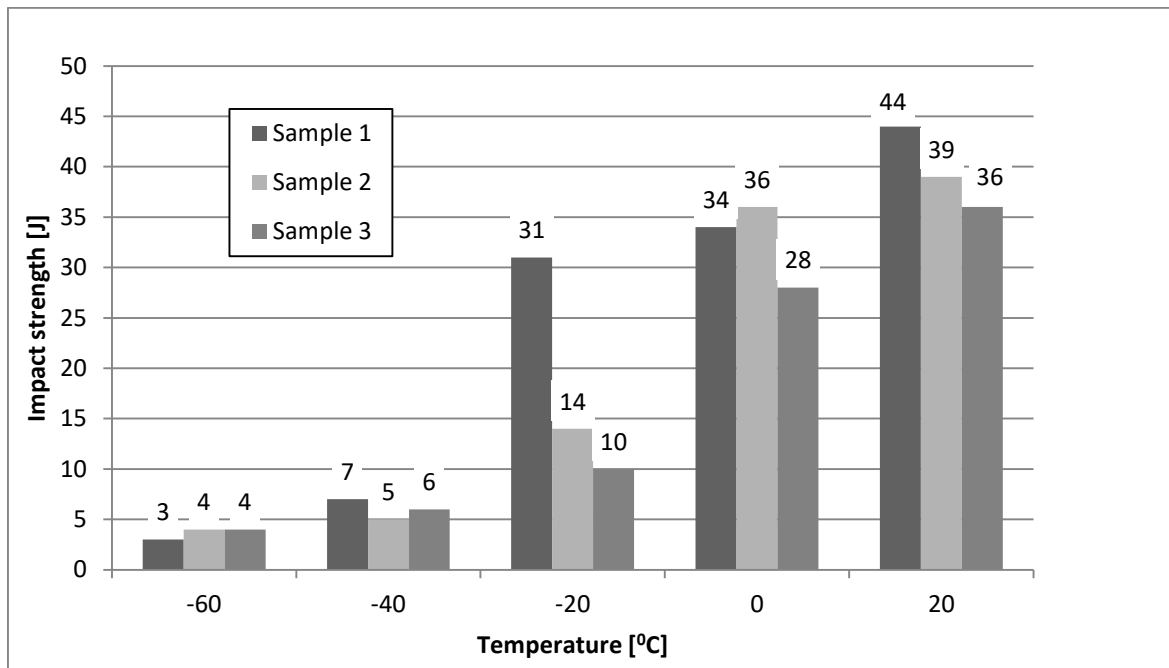


Fig. 5. Diagram illustrating the relation between the work of fracture KV and temperature

Table 2 and Figure 6 show the analogical test results for the samples collected from the element, where the fatigue load was significant, i.e. from the element of the bottom chord of the truss in the middle of its span. One may easily notice that the values of fracture work are much lower than those of element 1. For this element, only at +20°C the fracture work

for V-notch sample exceeds 27J. However, this increase is very significant in comparison to the other obtained results, and one may expect that it is caused by a material anomaly at the location from which samples were collected. In this case, steel cannot be considered as safe to be used in the structure of a bridge, either.

TABLE 2

Results of fracture work tests for samples collected from element 3

Temperature	Element 3				
	-60°C	-40°C	-20°C	0°C	20°C
Work of fracture	[J]	[J]	[J]	[J]	[J]
Sample 1	3	4	18	24	60
Sample 2	3	4	4	12	86
Sample 3	3	5	6	14	54
Average	3.00	4.31	7.56	15.92	65.32
Population standard deviation = $\sqrt{\frac{\sum(x-\bar{x})^2}{n}}$	0.00	0.47	6.18	5.25	13.89
Sample standard deviation = $\sqrt{\frac{\sum(x-\bar{x})^2}{(n-1)}}$	0.0	0.6	7.6	6.4	17.0
Square deviation = $\sum(x-\bar{x})^2$	0.00	0.67	114.67	82.67	578.67

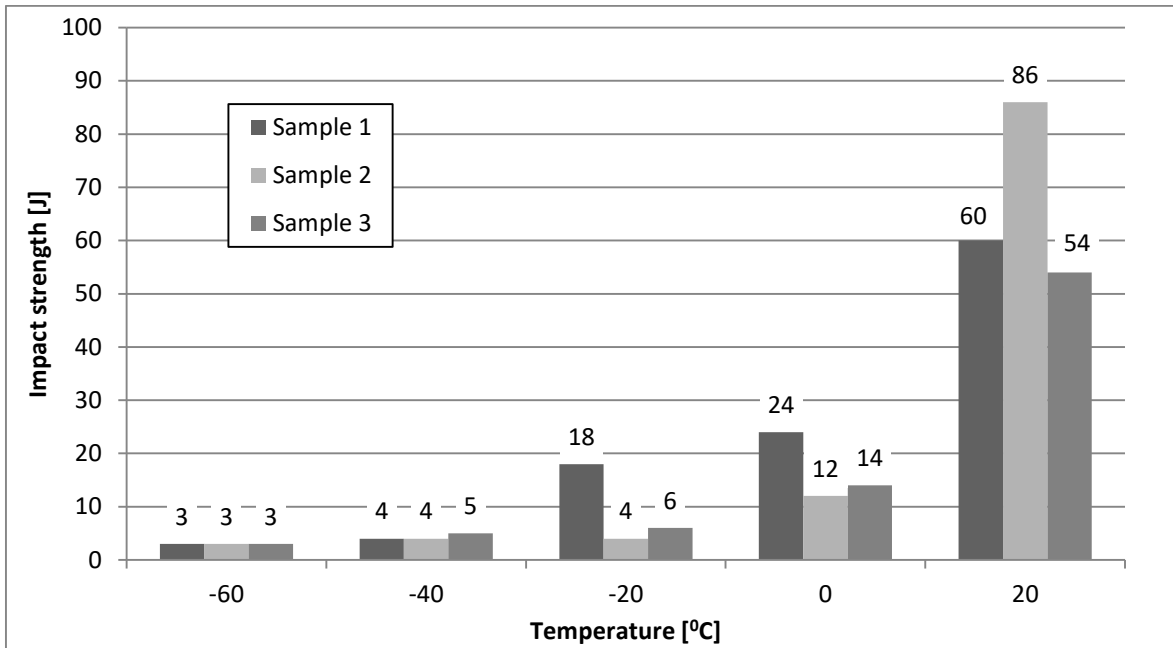


Fig. 6. Diagram illustrating the relation between the work of fracture KV and temperature for samples subjected to fatigue.

The comparison of results is shown in the diagram in Figure 7. The lines reflect the so-called impact strength curves of steel. These curves may be compared to those discussed in the literature. As far as their shape is concerned, it is similar to that of curves presented in other sources [6]. However, it differs by the fact that it does not become flat within

the temperature range below -20°C , as it may have been expected according to the existing state of knowledge, but the fracture work values continue to decrease to -40°C . The work of the fracture values for steel subjected to fatigue are considerably lower than those obtained for steel not subjected to fatigue.

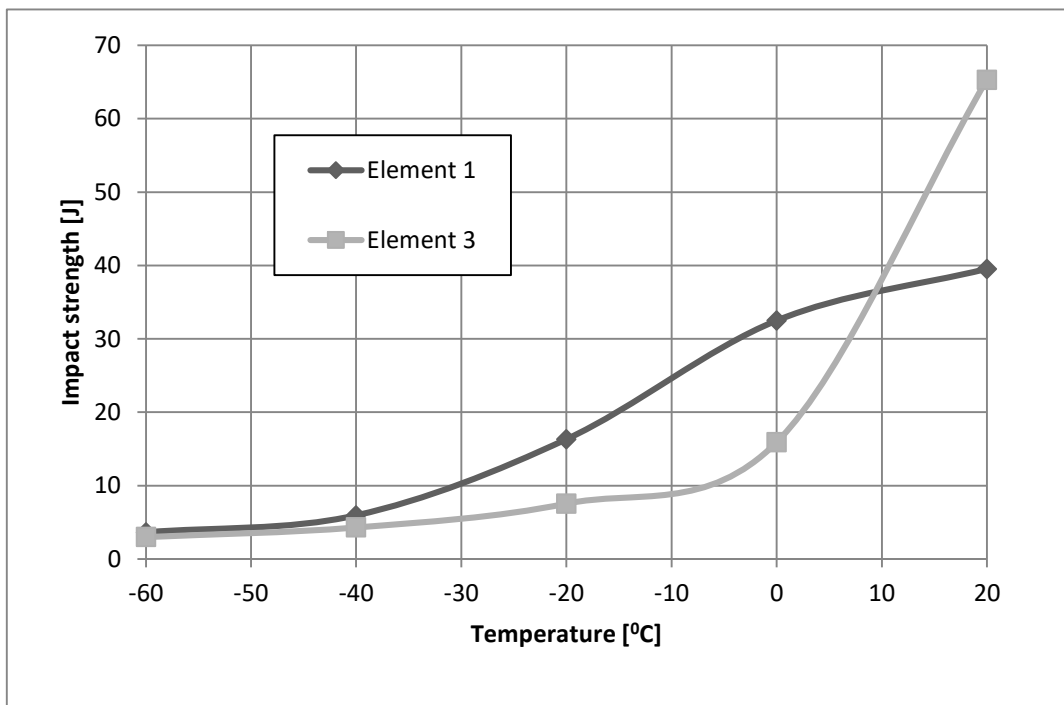


Fig. 7. Steel impact strength curves for samples subjected and not subjected to fatigue.

Conclusions

The analysis of the results presented in this paper demonstrates that the work of structure of historical steels at low temperatures does not meet the requirements defined for today's construction steel. The work of fracture should be no less than 27J. The authors managed to confirm the hypothesis that elements subjected to higher load are characterised by a lower work of fracture at low temperatures, due to

fatigue. Historical types of steel are very brittle, consequently the structures made from such steel are even more prone to sudden failures. This applies in particular to such objects as bridges, which are additionally exposed to the effects of material fatigue. It was also observed that the lowering in the yield strength of steel resulting from fatigue also influences the decrease in the value of the work of fracture KV.

References

1. **Augustyn J., Śledziewski E.** *Awarie konstrukcji stalowych*. Warszawa: Arkady, 1976, 210 p.
2. **Gosowski, B., Kubica, E.** . *Badania laboratoryjne z konstrukcji metalowych*. Wrocław: Oficyna Wydawnicza, 2007, p.33-41
3. **Pawlowski, K., Włóka, A.** Influence of impact strength of steel on the repair and usage possibilities of civil engineering structures. *7th International Conference on Safety and Durability of Structures ICOSADOS 2016*. May 10 - 12, 2016, UTAD, Portugal
4. **Rykaluk, K.** *Pęknięcia w konstrukcjach stalowych*. Wrocław: DWE, 2000. 231 p.
5. **Wyrzykowski, J.W., Pelszakow, E. , Sieniawski, J.** *Odształcenia i pękanie metali*. Warszawa: WNT, 1999, 404 p.
6. **PN-EN ISO 148-1:2017-02** Metale - Próba udarności sposobem Charpy'ego -- Część 1: Metoda badania

Influence of the Baltic Sea water on Klaipeda seaport hydrotechnical structures

Ramune Lebedeva, Vilma Vaicekauskiene, VGTU, Department of Structural Engineering and Klaipeda State University of Applied Sciences

Abstract. Hydrotechnical constructions in Klaipeda Seaport are constantly affected by the Baltic Sea environment (humidity, temperature changes, freezing and thawing effects, etc.). Hydrotechnical concrete is negatively affected by the Baltic Sea water, consisting of certain amounts of salts, highly repetitive moistening and drying (sorption and desorption) processes. Hydrotechnical concrete is characterized by capillary porosity, which is typical of Klaipeda Seaport hydrotechnical structures - quays, because they constantly rise in sea water at different levels of the surface. The aim of the study was to determine the influence of mineral additives on the type of gum, regulating sorbent parameters. The experimental results obtained will provide an opportunity to predict the durability of hydraulic concrete according to its sorption characteristics and damage to corrosion.

Keywords: The Baltic Sea water, hydrotechnical structures, hydrotechnical concrete, active mineral additives, durability.

Introduction

Baltic Sea water is affected by reinforced concrete structures used in the seafront of Klaipeda Seaport (quays, piers), on the banks of the coastal rivers and on the Curonian Spit. The current state of these hydrotechnical structures shows that during their operation in Klaipeda Seaport the waters there are damaging, especially on the surface, and big money is spent on repairing the hydrotechnical engineering structures. This study explores the conditions of exploitation of hydrotechnical reinforced concrete structures under the influence of the Baltic Sea water, researching the effect of the Baltic Sea water on the decomposition of concrete

and investigates active mineral additives to be used to modify cement mixtures, making them resistant to the impact of Baltic Sea water [2]. Demolition of concrete surfaces and corrosion of reinforcement, which occur due to the wetting of concrete with salt water in the Baltic Sea and temperature fluctuations, are typical phenomena in reinforced concrete constructions of hydraulic structures in the Baltic Sea [14], [20]. The results of the research carried out can be applied to the preparation and improvement of the regulatory standards for construction of reinforced concrete structures in the Baltic Sea [12], [23], [27].



Fig. 1. Klaipeda Seaport Hydrotechnical Building, Constituent Constructions, Corrosion of Hydrotechnical Concrete

Hydrotechnical concrete is a conglomerate structure material characterized by capillary porosity. The hydrophilic concrete capillary moistening through pores is caused by the penetration of Baltic Sea water into the capillaries by which it rises to the top of the reinforced concrete structure [13], [21], [3]. The height level that the Baltic Sea water is able to reach through capillaries depends on the diameter of capillaries in the concrete. Capillary moistening is

typical of Klaipeda Seaport's hydrotechnical constructions - berths, piers, moles, because they are constantly exposed to the Baltic Sea water, at different surface levels [10]. Due to the diffusion process, sea water moves from the moist concrete surface to a damp surface because of its specific chemical composition, causing certain corrosion processes in the cement stone [14], [17], [25].

The aquatorium of Klaipeda Seaport, according to its climatic conditions belongs to the western climate region of Lithuania [9]. A steady rise in the ocean level, changes in rainfall and stronger wind gusts cause more and more extreme natural phenomena - storms in the area of Klaipeda Seaport. Studies in the territory of Lithuania on air temperature, rainfall, and

water level changes show that the climate has changed since 1971 and it negatively affects the hydraulic concrete. As the amount of precipitation increases and the Baltic Sea level rises, the water level in Klaipeda Seaport may rise to 0.5-1.0 m, which will affect the hydraulic concrete used in Klaipeda Seaport [8].

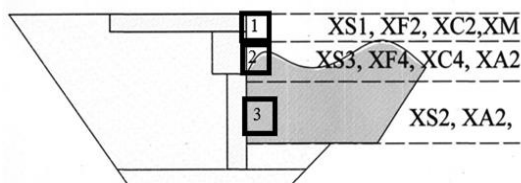


Fig. 2. Zones of operation of hydrotechnical concrete

Taking into account the deteriorating factors of concrete during the operation period, three different zones of operation of hydrotechnical concrete presented in Figure 2 can be distinguished:

- the first one above water level in which the concrete is not impregnated by the capillary absorption of Baltic Sea water is classified as XS1, XF2, XC2 environmental impact classes, where hydrocarbon concrete carbonization occurs, the corrosion of the reinforcement and the surface degradation due to the freezing and thawing cycles;

- the second is in the zone of water level where concrete is permanently dipped in sea water and cyclically exposed to possible negative temperatures (the surface being in the air) – thus classified as XS3, XF4, XC4, XA2 environmental impact classes, in which the hydrotechnical concrete must be resistant to the freezing and thawing cycles together with salts, have low conductivity to chlorides due to corrosion of reinforcement, must be resistant to the carbonization process and chemicals such as resistant to chlorides, sulphates and other compounds in the waters of the Baltic Sea;

- the third zone under water where the concrete is continuously in the Baltic Sea and is chemically exposed to the Baltic Sea water and corrosion of the reinforcement due to the intensive chloride diffusion processes in concrete is classified as XS2, XA2 environmental impact classes, in which the hydraulic concrete is to be resistant to sulphate corrosion and low conductivity for chlorides [6].

Hydrotechnical concrete is negatively affected by the Baltic Sea water, which consists of certain amounts of salts. It is also affected by repeated moistening and drying (sorption) processes. The effect of these factors is determined by the physical and chemical concrete corrosion [17], [32]. Hydrotechnical concrete structures must be resistant to the effects of moisture, penetration of sea water into further layers of concrete and corrosion caused by it. Hydrotechnical concrete, exploited by the impact of the Baltic Sea water is subjected to one of

the most important types of corrosion - carbonisation, which depends on CO₂ diffusion in concrete and CO₂ reactivity with concrete hydration products. The main factors determining the carbonisation rate are the amount of binders in concrete, the ratio of water and binder in concrete, the degree of the hydration of cement, CO₂ and relative humidity in concrete [19], [26], [27]

Mineral additives are used to modify concrete composition by improving the technological properties of the mixtures and the properties and durability of hardened concrete. Mineral additives in the concrete mix increase water impermeability and resistance to aggressive environmental influences [15], [16], [13]. Many sources of literature show that granular blast furnace slag, which is required by the European Standard LST EN 197-1, increase Portland cement's resistance to the effect of the marine environment [5]. The studies of some authors discuss the effect of coal ash on improving concrete properties by optimizing the composition of concrete by replacing the corresponding cement content with coal ash [2], [8], [13], [21]. Scientists have found that there is no optimum amount of ash that we can apply to all concrete mixtures, depending not only on the ash itself, but also on the composition and requirements of cement stone and concrete. Summarizing the results of some researchers, the optimum amount of lacquer ash rises up to 25% [13].

Many scientific papers point to the positive influence of SiO₂ micro dust as an active mineral additive to concrete: it modifies the microstructure of concrete, makes it more homogeneous, reduces the number of large pores, reduces water vapour permeability and increases the strength of concrete, especially using plastics. Researchers have confirmed that SiO₂ micro dust as an active mineral additive increases the compressive strength and durability of concrete, improves its microstructure, thereby increasing the resistance of concrete to aggressive environments [4].

Used materials

Portland cement CEM I 42.5N, slag Portland cement - CEM II / A-S 42.5N, limestone Portland cement - CEM II / A-LL 42.5N and slag cement - CEM III / B 32.5N were used in the research. In assessing the properties of these Portland cements, it has been observed that slag cement is less active during the first days of curing. After analyzing the composition of the cement, the amount of mineral additives added to the composition is as follows: Portland cement CEM I 42.5N - 0% slag amount, clinker content from 95% to 100%, slag cement - CEM II / AS 42.5N is 6 to 20% CEM II / A-LL 42.5N contains from 6 to 20% of the amount of slag, the amount of clinker from 80% to 94%, the addition of blast furnace slag in slag cement CEM III / B (from 80 to 94%), the addition of blast furnace slag to slag cement CEM III / B 32.5N is about 80% and the limestone content is up to 20%. ([17]). Different amounts of slag were chosen, or concrete with no added mineral content has no strict requirements for the composition of the cement: C_3S and $C_3A + C_4AF$ quantities are not customizable, and the amount of C_3A in clinker can sometimes reach 8% or more. The FLUXER GT3 superplasticizer was used, which was modified by the new generation of polycarboxylate and synthetic air-containing Adhesive Centrament Air 202, 0/4 mm fraction sand, granite 2/8 and 11/16 fractional rubble, and modified for composition modifications to water and / cement ratio, and in several compositions the type and percentage of cement was changed. Salt water corresponding to the chemical composition of the Baltic Sea water was used in the study.

Methodology of investigation

Concrete cubes (100 x 100 x 100 mm) were formed for the investigation of water resistance of the

Baltic Sea from the hydraulic concrete. After hardening (28 days) of concrete, samples were cut in half. Concrete samples were tested to measure the viability of the samples in the presence of saline solution in accordance with the chemical composition of the Baltic Sea. The prepared samples of hydrotechnical concrete were weighed on a scale, placed in an oven, and dried at 100 ° C, after a day, the samples were tested by immersing the samples half-way in the solution, measuring the capillary absorption for the first hour every 15 minutes, then every 4h, 8h, then every one day, 2 days, 7 and 14 days. After 14 days of the test of concrete in a Baltic Sea water solution, capillary immersed measurements were taken, samples of hydrotechnical concrete were completely immersed in a solution which corresponds to the chemical composition of the Baltic Sea water (all completely cut cubes) and washed for 2 days. After 2 days of immersion of the concrete samples, these samples were dipped in one side in the chemical composition of the Baltic Sea water and the methodology was repeated again from the beginning. The results of the test were estimated to 0.01 g. The results of the study are presented in Figures 4-15. The capillary absorption of the solution of the chemical composition of the Baltic Sea into the hydrothermal concrete is calculated according to the formula given in the standard:

$$W_m = \frac{m_d - m_s}{m_s} \times 100; \quad (1)$$

where:

W_m – water absorption of concrete sample, %;

m_d – mass of the impregnated sample, kg;

m_s – initial sample mass, kg;

The following equipment was used for testing: weighing scales with a weighing accuracy of 0.1 g, a plastic bath, a thermometer, a stopwatch, a cloth.

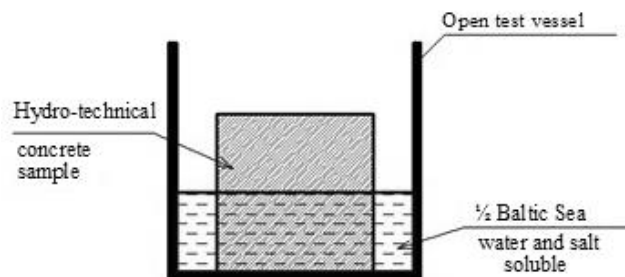


Fig. 3. Sorption Test Scheme

TABLE 1

Components of hydrotechnical concrete used for research on the impact of granular blast furnace slag and rock formations

Mixture label	BS0	BS1	BS2	BS3	BS4	BL1
Slag, %	0	17	35	49	70	17*
CEM I 42.5 N, kg	433	-	216	129	-	-
CEM II A/S 42.5 N	-	433	-	-	-	-
CEM III/B 32.5 N-H(SR)	-	-	216	303	433	-
CEM II A/LL 42.5 N	-	-	-	-	-	433
Granite rubble 2/8, kg	411	411	411	411	411	411
Granite chip 11/16, kg	615	615	615	615	615	615
Sand 0/4, kg	754	754	754	754	754	754
Water, kg	142	142	142	142	142	142
Plasticisers, kg	3.5	3.5	3.5	3.5	3.5	3.5
Airborne supplement, kg	0.26	0.26	0.26	0.26	0.26	0.26
V/C	0.33	0.33	0.33	0.33	0.33	0.33
V/R	0.33	0.33	0.33	0.33	0.33	0.33

17* - was not slag, but limestone cement.

Six composites of the hydrotechnical concrete mixture were formed, which are presented in Table 2. The hydrotechnical concrete constituents were

formed with different three cements, which differ in composition from the mineral additive, its percentage and the amount of different cement.

TABLE 2

Hydrocarbon Structural hydrocarbon concrete used for research on the influence of coal combustion ash

Mixture label	BV0	BV1	BV2	BV3	BV4
Ash, %	0	17	35	49	70
Cement CEM I 42.5 N, kg	433	359	281	221	131
Mineral additive, (of ashes) kg	0	74	152	212	303
Granite rubble 2/8, kg	411	411	411	411	411
Granite chip 11/16, kg	615	615	615	615	615
Sand 0/4, kg	754	754	754	754	754
Water, kg	142	142	142	142	142
Plasticizers, kg	3.5	3.5	3.5	3.5	3.5
Airborne supplement, kg	0.26	0.26	0.26	0.26	0.26
V/C	0.33	0.40	0.51	0.64	1.08
V/R	0.33	0.33	0.33	0.33	0.33

Five compounds of the hydraulic concrete mix were formulated, which are presented in Table 3. These hydrotechnical concrete compounds were formed with 2 different cements, which differ in composition from the mineral additive, by its percentage (0% and 17%). In addition, another mineral additive was introduced: ash, its content ranged from 0% to 70%, v/c ratio was maintained at

0.33, and all other parameters remained unchanged from the initial composition of the concrete mix. Different fillers were used to carry out the evaluation of the filler, or forecasting in hydraulic concrete. It has been determined that the properties of concrete depend on the filler, its structure, which influence the durability properties of concrete.

TABLE 3

The composition of hydrotechnical concrete used for investigations of SiO₂ micro dust

Mixture label	BVSi 0	BVSi 1	BVSi 3	BVSi 4	BVSi 5
SiO ₂ , %	0	2	4	6	7
Cement CEM I 42.5 N, kg	433	359	345	338	330
Ash, %	17	17	17	17	17
SiO ₂ , kg	0	9	17	26	35
Granite rubble 2/8, kg	411	411	411	411	411
Granite chip 11/16, kg	615	615	615	615	615
Sand 0/4, kg	754	754	754	754	754
Water, kg	142	142	142	142	142
Plasticisers, kg	3.5	3.5	3.5	3.5	3.5
Airborne supplement, kg	0.26	0.26	0.26	0.26	0.26
V/C	0.33	0.33	0.33	0.33	0.33
V/R	0.33	0.33	0.33	0.33	0.33

Results of the analysis

In Figure 4, the samples of hydrotechnical concrete were formed with CEM I 42.5N, CEM II A / S 42.5N and CEM III / B 32.5 N different types of cements containing 0%, 17%, 70% granular blast furnace slag additives. These samples with 0%, 17%, and 70% granular blast furnace slag additives were dipped in a saline solution corresponding to the chemical composition of the Baltic Sea water, the

composition of which is given in Tables 1, 2 and 3. The results of sorption in a saline solution of the Baltic Sea with different granular blast furnace slag additives carried out in accordance with the presented method are presented in an impregnated condition state, in a dried state and in a soaked state (4, 5 and 6).

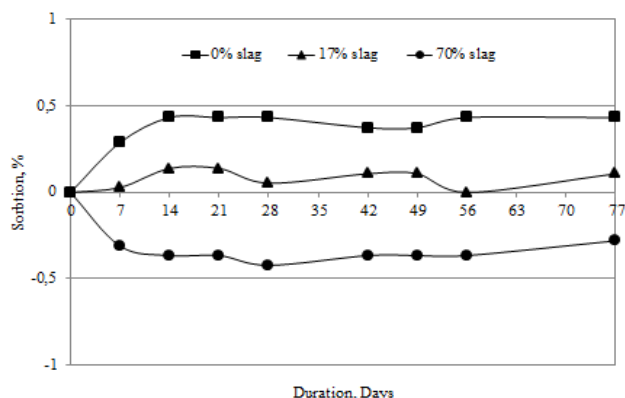


Fig. 4. Testing results of sorption of oversized hydrotechnical concrete with different amounts of slag in cement

In Figure 4, samples were dipped half-way in the water saline solution of the Baltic Sea and left in it for 7 days and the sorption parameters were measured accordingly for 7 days. From Figure 4 it can be seen that the absorption of concrete or solution drying (sorption and desorption) intensively takes up to 14 days and the subsequent monitoring of these processes did not show any changes, therefore further sorption and desorption tests were carried out for up to 14 days. Figure 4 shows the hydrotechnical samples with different types of cements, different amounts of granular blast furnace slag, after 28 days of hardening. The obtained results showed that the

hydrotechnical concrete samples were composed of CEM I type cement containing 0% granular blast furnace slag, the sorption process was carried out, i.e. the salinity of the salt solution increased to 0.5%. Concrete samples with 17% granular blast furnace slag, i.e. the speed of the CEM II A / S type cement sorption process was equal to the rate of the desorption process and the solution absorbed up to 0.2%.

Concrete samples with 70% granular blast furnace slag, i.e. The CEM III / B type cement mortar is up to -0.4%, which means the sample has dried over it.

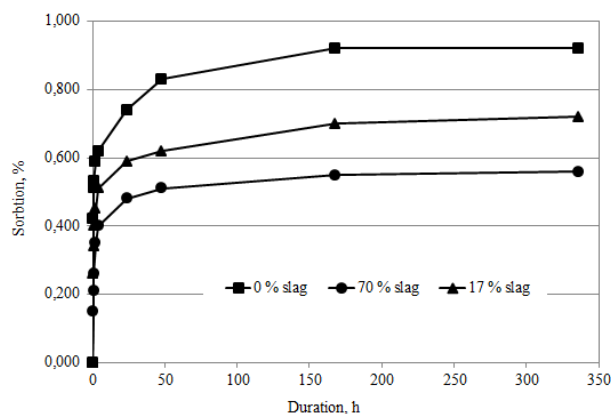


Fig. 5. Results of sorption tests of dried hydrotechnical concrete with different levels of blast furnace slag in cement

In Figure 5, the results of the solidification sorption tests of dried, hydrotechnical concrete samples with different amounts of blast furnace slag after 28 days are presented. The non-slag-free

specimens absorbed most of the Baltic Sea water saline solution and kept it in equilibrium after for approximately one week. Cements with 17% and 70% blast furnace slag are characterized by lower

sorption - with a 0% blast furnace slag additive up to 0.7% and from 70% to 0.58%. It can be concluded that a higher amount of blast furnace slag reduces the hydrophobic concrete sorption.

In Figure 6, the results of the hardening sorption tests of impregnated hydrotechnical samples with different amounts of blast furnace slag after 28 days are presented. In this case, desorption processes

occur, i.e. evaporation of the salt solution from concrete samples. In the non-slag cement, the lowest desorption is observed, in the 17% blast furnace slag containing cement, and 70% in the blast furnace slag cement being the highest. The desorption processes in concrete reduce the amount of water or salt solution and increase its resistance to freezing and thawing effects in wet conditions.

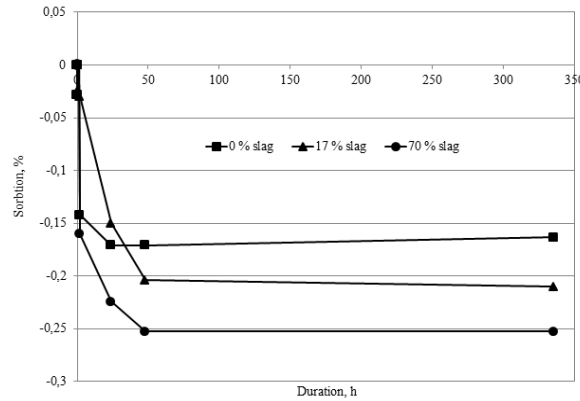


Fig. 6. Results of sorption tests of impregnated hydrotechnical concrete with different amounts of slag in cement.

More detailed sorption tests were carried out with 0%, 17%, 35%, 49% and 70% granular blast furnace slag content in cement constituents. Sorption tests

were also performed on samples of hydrotechnical concrete in an oiled, impregnated and dried state; the results of the tests are presented in Figures 7, 8 and 9.

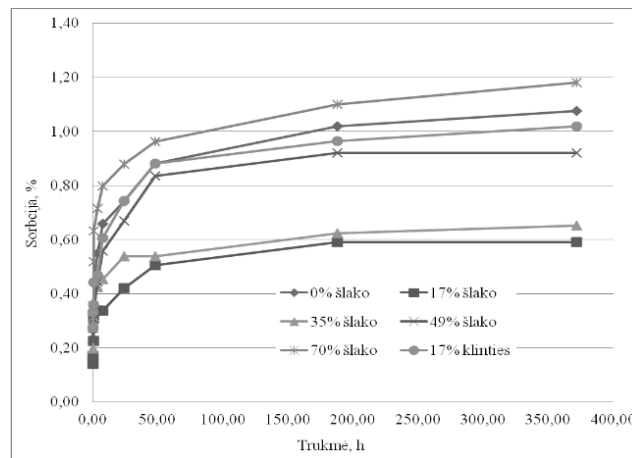


Fig. 7. Results of testing of air dried hydrotechnical concrete with different granular blast furnace slag, lime content in cement

The sorption test presented in Figure 7 shows that samples of hydrocarbon concrete with a 17% slag additive in cement have the lowest water absorption of saline solution of the Baltic Sea. After increasing the amount of granular blast furnace slag, water absorption increases with 49% granular blast furnace

slag additive almost equal to water absorption without granular blast furnace slag additives, but with 70% granular blast furnace slag additive exceeds water absorption in concrete without granular blast furnace slag additives.

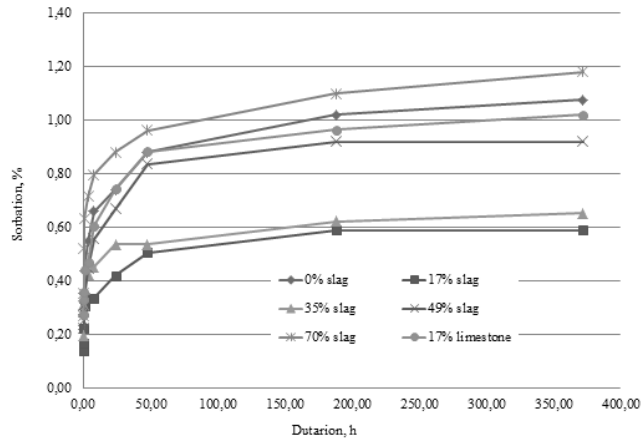


Fig. 8. Results of tests of dried hydrotechnical concrete with different granular blast furnace slag, lime content in cement (sorption)

Figure 8 shows the results of hydrotechnical concrete with different amounts of granular blast furnace slag (0%, 17%, 35%, 49%, 70%) and lime 17% after 28 days of hardening sorption tests in a dry state. The results, which are analogous to the results found in the air dried state, show that the samples with 17% granular blast furnace slag have the lowest sorption, while the maximum sorption is observed in

the samples without granular blast furnace slag additives. Samples with a 17% clay additive have a high sorption, which is almost equivalent to the sorption of samples of 70% granular blast furnace slag additives. The high sorption values of the samples show a low resistance to freezing and thawing of such concrete in a wet state.

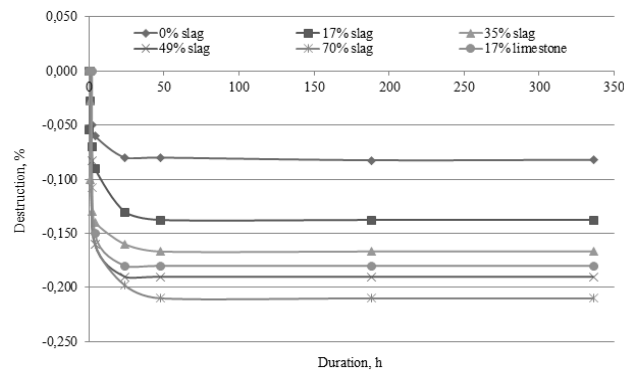


Fig. 9. Test results of impregnated hydrotechnical concrete with different granular blast furnace slag, lime content in cement (desorption)

The results of sorption of impregnated hydrocarbon concrete samples and desorption test results with different amounts of granular blast furnace slag (0%, 17%, 35%, 49%, 70%) and 17% of rock content after 28 days of hardening sorption and desorption results are shown in Fig.9. From the

results presented in Figure 9, we can see that the highest desorption is observed in concrete samples with 70% granular blast furnace slag, which is characterized by the highest sorption, and the lowest desorption is observed in samples with the granular blast furnace slag additive.

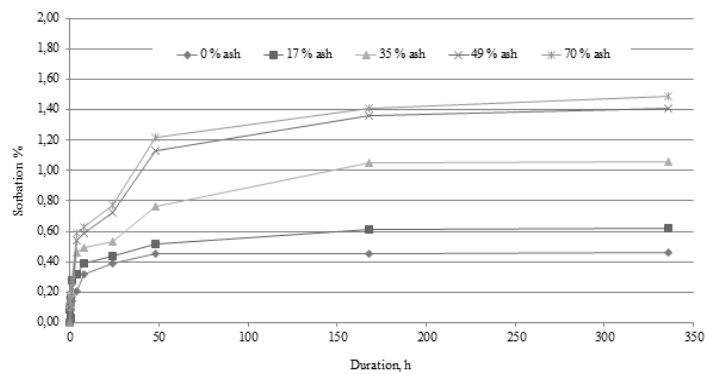


Fig. 10. Results of the sorption tests for oversized hydrotechnical concrete with ash (0%, 17%, 35%, 49% and 70%)

Figure 10 shows the results of testing hydrotechnical concrete samples with different fly ash (0%, 17%, 35%, 49% and 70%) after 28 days of hardening sorption tests. As can be seen from the results presented in Figure 10, the sorption of concrete raises with the increase of the amount of the

fly ash, especially when it exceeds 17%. It can be concluded that the volatile ash additive increases the sorption of concrete, i.e. water absorption and thus reduces the resistance of concrete to the effects of freezing and thawing in a wet state.

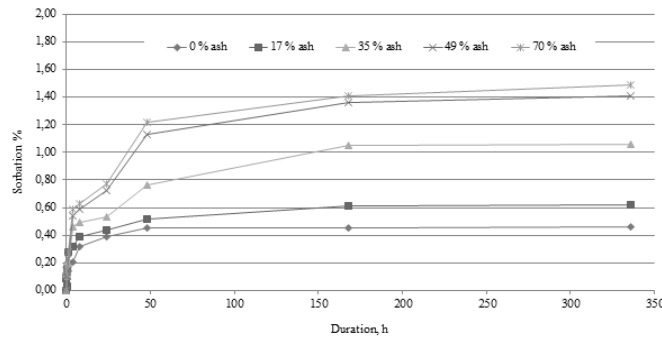


Fig. 11. Results of the sorption tests of dried hydrotechnical concrete with ash (0%, 17%, 35%, 49% and 70%)

Fig. 11 shows the results of a similar sorption test for dried hydrotechnical concrete samples with different fly ash content that increases the amount of

concrete sorption by increasing the volumetric ash content.

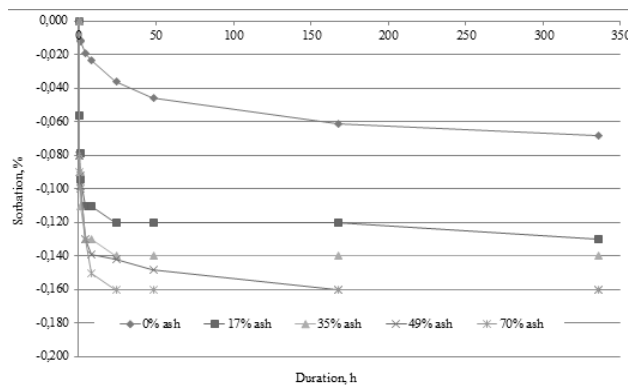


Fig. 12. Results of tests of the impregnated hydrotechnical concrete with different ash content

Figure 12 shows the results of the absorption of the impregnated hydrotechnical concrete with different fly ash content (0%, 17%, 35%, 49% and 70%) in the impregnated state. The results of the

research show that the highest desorption is observed in samples with 70% volatile ash content, while the lowest desorption is the samples without fly ash.

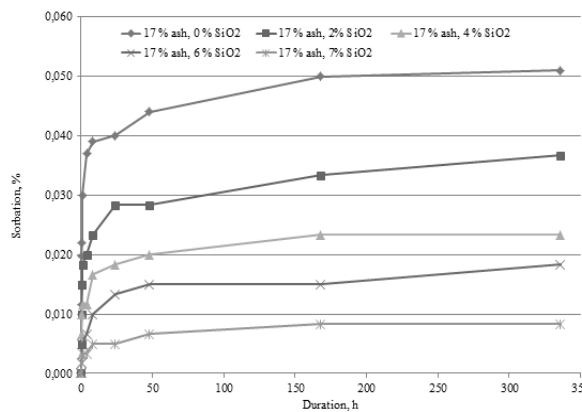


Fig. 13. Air-dried hydrotechnical concrete with 17% ash and different SiO2 test results

Figure 13 shows the results of a 28-day solidification sorption test for air dried hydrotechnical concrete with 17% volatile ash and with different amounts of SiO₂ micro dusts (0%, 2%, 4%, 6%, and 7%). The results obtained in Figure 13 show that with an increase in SiO₂ content of micro

dust up to 7% of the weight of the cement, the concrete sorption value decreases steadily. By changing the 7% cement SiO₂ micro-drops, the value of sorption in concrete can be reduced from 0.05% to 0.08%, i.e., about 5 times.

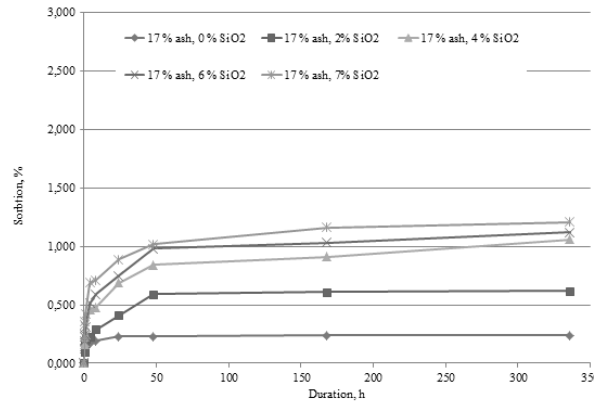


Fig. 14. Results of tests of the dried hydrotechnical concrete with 17% ash and different SiO₂ content

Figure 14 shows that by increasing the amount of SiO₂ microscopic materials in the cement, the concrete sorption value decreases to 7%, and it

decreases by approximately 5 times in the 7% SiO₂ micro dust.

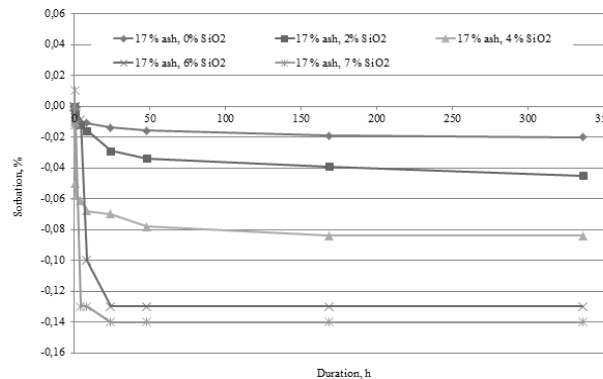


Fig. 15. Impregnated hydrotechnical concrete with 17% ash and different SiO₂ test results

Figure 15 shows the results of the sorption tests for impregnated hydraulic concrete samples with a 17% volatile ash additive and with different amounts of SiO₂ micro dusts (0%, 2%, 4%, 6% and 7%). It can be seen from the results that the highest desorption of hydrocarbon concrete samples is characterized by a 7% SiO₂ micro dust additive, and the lowest desorption is typical of samples without the addition of SiO₂ micro dust.

Findings of the research

1. Visual inspection of hydrotechnical structures in Klaipeda Seaport area showed that surface decomposition of concrete is taking place, due to the operational impact of the Baltic Sea water, the processes of the Baltic Sea water sorption, which cause concrete corrosion.

2. The amounts of salts present in the Baltic Sea water, to which reinforced concrete constructions are

exposed, affect the durability of the hydrotechnical concrete.

3. The impact of the Baltic Sea water is best offset by the addition of cement containing 17% to 70% and 5% SiO₂ micro dust.

4. Concrete with a slag additive from 17% to 49%, replacing part of the cement, has a 43-53% lower sorption. Concrete with a 17% slag cement substitute absorbs at least the salt of the chemical composition of the Baltic Sea, and absorbs 70% of the slag additive similarly to cement without a mineral additive.

5. According to the concrete sorption - desorption parameters, it is possible to determine the durability of concrete during operation in the Baltic Sea environment. The results of concrete sorption - desorption and mass loss resistance to BJA - show that the sorption rate of concrete used in such environment should not exceed 0.8% after 2 weeks.

References

1. *LST 1428.18:1997 Betonas. Bandyto metodai. Vandens įgeriamumo nustatymas.*
2. **Martyneitis, M.** *Mineralinės rišamosios medžiagos.* Kaunas: KPI, 1974. 294 p.
3. **Wunderlich, W. O.** *Hydraulic structures: probabilistic approaches to maintenance.* ASCE. 2005. 646 p.
4. **Skominas R.** *Aplinkos poveikio sukeltų pažeidimų įtaka hidrotechnikos statinių patikimumui ir remonto ilgaamžiškumui.* Akademija. 109p., 2008.
5. **LST EN 197-1: 2011 Cementas. Idalis. Įprastinių cementų sudėtis, techniniai reikalavimai ir atitikties kriterijai.** *Europos standartizacijos komitetas.*
6. **LST EN 206:2013. Betonas. 1 dalis. Techniniai reikalavimai, savybės, gamyba ir atitiktis.** *Europos standartizacijos komitetas.*
7. **Wu, R. K., Zhang, D., Song, M. J.** Properties of polymer-modified cement mortar using pre- enveloping method. *Cement and concrete research.* 2002. Vol. 32 Iss. 3, 425-429 p.
8. **Galvonaite ir kt.** *Geografija.* 2012. T. 48. Nr. 2. P. 97-107. Lietuvos mokslų akademija, 2012.
9. **Bukantis A.** *Lietuvos klimatas.* Vilnius: VU leidykla. 1994. p.188.
10. **Lebedeva R., Skripkiūnas G.** Требования ропейского стандарта к гидротехническому бетону, эксплуатируемому в морской среде, *Проблемы современного бетона и железобетона.* 2013. 5: 99-110
11. **Mehta, P. K., Monteiro, P.** *Concrete - Structure, Properties and Materials,* 2nd edh, Prentice-Hall, Englewood Cliffs, New Jersey, 1993.
12. **Vektorius B., Vilkas V.** *Betono tvarumas.* Monografija. KTU. 2006. – 156 p.
13. **Skripkiūnas G.** *Statybinių konglomeratų struktūra ir savybės.* Vadovėlis. KTU. Vitae Litera. 2007. p. 344.
14. **Батраков, В. Г.** *Модифицированные бетоны /В.Г. Батраков. – М.: Стройиздат, 1990. - 15 с.*
15. **Соловьев, В. И.** *Эффективные модифицированные бетоны /В.И. Соловьев, Р.Б. Ергешев. - Алматы: КазГосИНТИ, 2000. – 11 с.*
16. **Гурский, В. А.** *Антикоррозионная защита бетонных и железобетонных конструкций // Материалы международной научно-практической конференции «Защита от коррозии в строительстве и народном хозяйстве» 17-19 мая 2005 г. Москва.*
17. **Читайшвили Т. Г., Джалагония М. Г.** *Защита бетонной отделки от коррозии при капиллярном переносе/ Транспортное строительство. 1988.-№1.- С.23-24.*
18. **Алексеев, С. Н. , Иванов, Ф. М. Модры С., Шисль П.** *Долговечность железобетона в агрессивных средах.* М.: Стройиздат- 1990. - 316 с.
19. **Алексеев Ю. С. Н., Розенталь Н. К.** *Коррозионная стойкость железобетонных конструкций в агрессивной промышленной среде.* М.: Стройиздат, 1976. -205 с.
20. **Розенталь Н. К., Алексеев С. Н.** *Кинетика карбонизации бетона // Бетон и железобетон. 1969,- №4.*
21. **Галимуллин Р. Г.** *К вопросу механизма и кинетики адсорбции /Тр. КХТИ им. Кирова. Вып. 39,- 1968.- Вып. 43.- 1969.*
22. **Енишерлова С. Г., Ратинов В. Б.** *Исследование механизма и кинетики коррозии бетона и железобетона / Сб. тр. Башниипромстроя. -Вып. 7.- 1966.*
23. **Минас А. И.** *Коррозия бетона и некоторых строительных материалов в условиях службы на засоленных грунтах в сухом климате // Труды конференции «Коррозия бетона и меры борьбы с ней».- М. Изв. АН СССР.-1954.*
24. **Мишутин В. А.** *Долговечность судостроительных бетонов и корпусов плавучих железобетонных доков, эксплуатируемых в морях с различными климатическими условиями.- ЦНИИ «Румб».- 1986.- 123 с.*
25. **Москвин В. М.** *Бетон для морских гидротехнических сооружений.* М.: Машстройиздат, 1949.
26. **Москвин В. М.** *Влияние обрастаний и бактериальной жизни на бетон гидротехнических сооружений.* Сб. ст. НИИ по стр. Минмашстроя, М., 1949.-№1.
27. **Москвин В. М., Иванов Ф. М., Алексеев С. Н., Гузев Е. А.** *Коррозия бетона и железобетона. Методы их защиты.- М.:Стройиздат, 1980.-536 с.*
28. **Москвин В. М., Якуб Т. Ю., Васильева Т. А. и др.** *О диффузионной проницаемости цементного камня // Бетон и железобетон.- 1969,- № 4.- С. 1113.*

Mixed-integer Non-linear Programming in Civil Engineering

Stojan Kravanja, *Faculty of Civil Engineering, Transportation Engineering and Architecture,
University of Maribor, Maribor, Slovenia*

Abstract. The paper discusses the Mixed-Integer Non-linear Programming (MINLP) of problems in civil engineering. The MINLP enables the optimization of continuous parameters simultaneously with discrete alternatives. While continuous parameters are in structural optimization structural costs, masses, loads, stresses, resistances and deflections, as well as the discrete alternatives are in most cases defined as different topologies, standard sizes and materials. The continuous parameters are in the models expressed by continuous variables, whilst the discrete alternatives by discrete (0-1) variables. The MINLP optimization of a structure is usually a comprehensive and highly non-linear calculation process. The MINLP approach requires that a structure is generated as an MINLP superstructure including a number of structure alternatives. One of them is the optimal one. For each optimization problem/structure, an MINLP optimization model of the structure must be developed, where the cost or mass objective function of the structure is subjected to structural analysis and dimensioning equality/inequality constraints. The Modified Outer-Approximation/Equality-Relaxation algorithm and a three-phase MINLP strategy are applied. Three numerical examples, i.e. the MINLP optimization of a cantilever beam, composite floor and high-pressure penstock are presented at the end of the paper.

Keywords: civil engineering, structures, optimization, mixed-integer non-linear programming, MINLP

Introduction

The study handles the Mixed-Integer Non-Linear Programming (MINLP) of problems in civil engineering. The MINLP enables the optimization of discrete alternatives simultaneously with continuous parameters. It performs the discrete optimization of a number of structural elements (topology), standard dimension optimization (sizes), material optimization (grades) and rounded dimension optimization (dimensions are rounded explicitly on ten millimeters or round centimeters) simultaneously with the continuous optimization of a structure self-manufacturing costs/mass, internal forces, resistances and deflections. For this reason, the MINLP optimization approach requires that a structure is generated as an MINLP superstructure, which comprises a number of structural alternatives, defined as a combination between various structural elements,

discrete dimensions, materials and rounded dimensions. One of the defined structure alternatives is during the MINLP optimization process found as the optimal one.

For the MINLP optimization, an MINLP optimization model of a structure must be developed, see below the general model formulation MINLP-G. The model includes the structure cost or mass objective function obj , and structural analysis and dimensioning constraints $q(x,y) \leq 0$. The latter are determined according to the known principles/rules of the mechanics and standards (Eurocodes). In order to perform the simultaneous continuous and discrete optimizations, continuous variables x and discrete (0-1) variables y are defined. In MINLP, at least one of the constraints or the objective function is nonlinear.

$$\begin{aligned} \min \quad & obj = f(x, y) \\ \text{subjected to} \quad & q(x, y) \leq 0 \\ & x \in R \\ & y \in \{0,1\} \end{aligned} \quad (\text{MINLP-G})$$

A number of algorithms were developed in the last three decades for the solution of MINLP problems: the GBD method by Benders [1] and Geoffrion [2]; the NBB method by Beale [3], and Gupta and Ravindran [4]; the OA algorithm by Duran and Grossmann [5]; the FT method by Mawengkang and Murtagh [6]; the SLDP method by Olsen and Vanderplaats [7], and Bremicker et al. [8]; the LP/NLP BB method by Quesada and Grossmann [9]; and the ECP method by Westerlund and Pettersson

[10]. The OA extension, the Outer-Approximation/Equality Relaxation (OA/ER) algorithm, was later invented by Kocis and Grossmann [11] in order to calculate (non)linear equality constraints. Further extension, the Modified OA/ER algorithm was afterwards introduced in order to solve non-convex problems, see Kravanja and Grossmann [12]. This algorithm was adapted and applied in structural optimization by Kravanja et al. [13-15].

For fast calculations of problems, various multilevel MINLP strategies were developed. The strategies perform the optimization of sub-levels rather than the whole problem. Consequently, a lower number of discrete decisions and variables are used in each sub-level when compared to the entire problem. A three-phase MINLP optimization is proposed for structural optimization. The calculation begins with the continuous optimization. The first result is used as a starting point for the further second step, where the discrete optimization of material grades is executed (standard and rounded dimensions are still continuous). After the optimal grades are obtained, the overall discrete material, standard and rounded dimension optimization of a structure is calculated. In this way, the convergence is significantly accelerated. A more detailed information about the multilevel strategies are found in references [16, 17].

A number of problems in the area of structural optimization were solved with the presented MINLP approach: e.g. hydraulic steel gates for dams and hydro-power plants by Kravanja et al. [15, 16], steel and aluminum trusses by Šilih et al. [18], timber truss structures by Šilih et al. [19, 20], multi-storey steel frame buildings by Klanšek et al. [21], single-storey industrial steel buildings by Kravanja and Žula [22] and Kravanja et al. [23], composite I-beam structures from concrete and steel by Kravanja and Šilih [24], Klanšek and Kravanja [25, 26], Žula et al. [27] and Kravanja et al. [28] as well as timber-concrete

composite floors by Jelušič and Kravanja [29]. A recent research work is also referred in the field of MINLP optimization of project schedules by Klanšek [30] and Cajzek and Klanšek [31].

Three numerical examples are introduced in the paper in order to show the capabilities of the presented MINLP approach, i.e. the small optimization problem of a cantilever beam, the medium optimization problem of a composite floor and the large optimization problem of a high-pressure penstock. GAMS (General Algebraic Modelling System) by Brooke et al. [32] is used for modelling the optimization models. The MINLP optimizations are calculated by the computer program MIPSYN, the extension of PROSYN [12] and TOP [33]. GAMS/CONOPT4 (Generalized reduced-gradient method) [34] and GAMS/CPLEX 12.7 (Branch and Bound method) [35] solvers are used.

MINLP optimization of a cantilever beam (small problem)

The first example shows the MINLP optimization of a 3.50 m long laminated timber cantilever beam. The beam supports the self-weight, the uniformly distributed permanent load of 10 kN/m (g) and the uniformly distributed variable imposed load of 15 kN/m (q), see Figure 1. Laminated timber GL24h is considered.

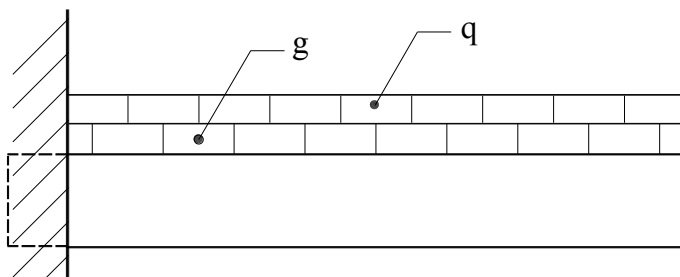


Fig. 1. Cantilever timber beam

The task of the optimization is to calculate the minimal self-manufacturing (material and labor) costs and discrete dimensions of the beam. The optimization model of the cantilever beam is developed. The superstructure of the beam comprises a number of alternatives of even values for the beam height and width. A simple economic objective function is defined. The unit price of the laminated timber considered is 600 EUR/m³ and of the impregnation 125 EUR/m³. The dimensioning constraints (e.g. shear, bending, the lateral-torsional buckling and deflections) are determined according to Eurocode 5 [36].

The minimal self-manufacturing costs of the timber beam yields 446.60 EUR. The obtained discrete dimensions comprise the beam width of 22 cm and the beam height of 80 cm.

MINLP optimization of a composite floor (medium problem)

The second example presents the MINLP optimization of a 21 m long composite floor. A concrete slab and welded steel I beams are composed together with shear connectors. The composite floor supports the self-weight and the uniformly distributed imposed load of 5 kN/m².

The main task to be achieved performing this example, is to find the minimal production costs, material grades and standard dimensions of the composite floor. The superstructure of the floor includes a number of discrete alternatives of steel grades, concrete strengths, reinforcing steel meshes and thicknesses of steel plates. The optimization model of the composite floor defines a cost objective function. The unit prices considered are shown in

Table 1. The dimensioning constraints (shear, bending, the shear buckling and deflections) are determined in accordance with Eurocode 4 [37].

TABLE 1

Unit prices		
Structural steel S 235-S 355	1.1-1.2	EUR/kg
Reinforcing steel S 400	1.3	EUR/kg
Concrete C 25/30-C 50/60	100-125	EUR/m ³
Sheet plate cutting	7.5	EUR/m ¹
Welding	10	EUR/m ¹
Anti-corrosion resistant painting (R30)	25	EUR/m ²
Paneling	10	EUR/m ²

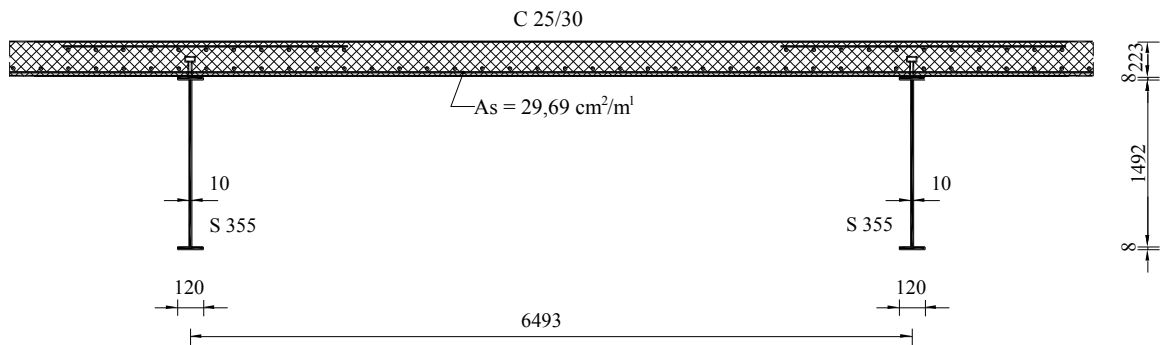


Fig. 2. Optimal composite floor

The minimal production costs of 86.11 EUR/m² are gained in the 3rd MINLP iteration. All necessary material grades/strengths and standard dimensions are also calculated, see Figure 2.

MINLP optimization of a high-pressure penstock (large problem)

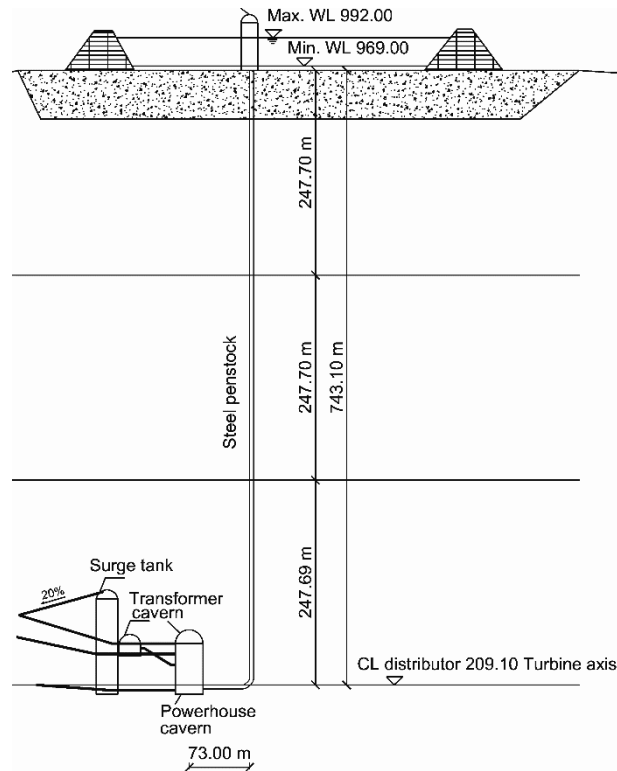


Fig. 3. The vertical variant of the steel penstock Kozjak

The third example shows the optimization of the high-pressure steel penstock for the pumped storage hydroelectric power plant Kozjak, planned to be constructed 15 km far from the city of Maribor, Slovenia. The power plant includes already constructed water reservoir of 3 million m³. 2400 m long steel penstock will be constructed with the water head of 700 m.

The preliminary calculations and the design for the power plant Kozjak were made by IBE Ljubljana in 2011 [38] (the inclined penstock variants) and in 2012 [39] (the vertical penstock). Variants of the penstock were afterwards optimized, see Kravanja [40, 41].

TABLE 2

Optimized longitudinal sections of the vertical penstock Kozjak

x m	Sect	p _{in} m	p _{ex} m	D m	t mm	L _{sect} m	Steel Σ mass kg			
0.00	1	949.20	782.90	3.20	55	81.00	S 690 pipe: 357 617 stiffeners: 23 443 total: 381 060			
81.00	2	883.00	733.90		49	54.00		S 460 pipe: 212 011 stiffeners: 14 723 total: 226 734		
135.00	3	817.60	679.90		46	54.00			S 355 pipe: 198 847 stiffeners: 14 089 total: 212 936	
189.00	4	752.10	625.90		42	54.00				S 235 pipe: 181 332 stiffeners: 13 913 total: 195 245
243.00	5	686.70	571.90		39	36.66			S 160 pipe: 114 206 stiffeners: 9 031 total: 123 237	
Lower part:							1 139 212			
279.66	6	642.20	535.20	3.40	61	54.00	S 460 pipe: 281 154 stiffeners: 12 419 total: 293 573			
333.66	7	576.70	481.20		55	54.00		S 355 pipe: 253 060 stiffeners: 12 047 total: 265 107		
387.66	8	511.30	427.20		49	54.00			S 235 pipe: 225 062 stiffeners: 11 252 total: 236 314	
441.66	9	445.80	373.20		43	54.00				S 160 pipe: 197 160 stiffeners: 11 044 total: 208 204
495.66	10	380.40	319.20		35	31.70			S 100 pipe: 93 988 stiffeners: 6 293 total: 100 281	
Middle part:							1 103 479			
527.36	11	341.90	287.50	3.60	45	54.00	S 355 pipe: 218 436 stiffeners: 10 490 total: 228 926			
581.36	12	276.50	233.50		35	54.00		S 235 pipe: 169 428 stiffeners: 10 150 total: 179 578		
635.36	13	211.00	179.50		28	54.00			S 160 pipe: 135 282 stiffeners: 8 774 total: 144 056	
689.36	14	145.60	125.50		20	54.00				S 100 pipe: 96 417 stiffeners: 8 214 total: 104 631
743.36	15	78.10	69.50		12	31.70				
775.06	16	39.80	37.80		10	9.00				S 30 pipe: 8 900 stiffeners: 1 016 total: 9 916
Upper part:							705 206			
Steel penstock total:							2 947 897			

The optimization model of the penstock includes the mass objective function of the longitudinal steel sections. The dimensioning constraints for the stability of the penstock are defined in accordance with C.E.C.T. Recommendations [42] including the internal and external water pressure load cases. The dynamic effect of the water hammer is taken into consideration, too.

The structure of the special vertical variant consisting of the 784.06 m long and 743.10 m deep penstock is presented in Figure 3. The presented variant in this paper comprises the steel pipe with stiffener rings, designed from three different steel grades: S 355, S 460 and S 690. While the upper part of the penstock which is loaded with minimal water pressure is designed from mild steel S 355, the lower part loaded with a maximal pressure is proposed to be constructed from high-strength steel S 690. High-strength steel S 460 is used for the middle pipe part. (In)equality constraints for the stability of the pipe between two rings, for the stability of stiffener rings and for checking the elastic behavior of the steel material are included in the model. The internal diameters D of the pipe vary from 3.2 to 4.0 m and the pipe longitudinal sections L_{sect} from 9.0 to 81.0 m. While the maximal internal water pressure p_{in} is 94.92 bars, the maximal external water pressure p_{ex} is 78.29 bars.

The minimal penstock mass of 2947.90 tons is calculated including the pipe thicknesses t from 10 to 61 mm, see Table 2.

Summary

The study discusses the Mixed-Integer Non-linear Programming (MINLP) of problems in civil engineering. The MINLP performs the optimization of discrete alternatives simultaneously with continuous parameters of structures.

For each optimization problem/structure, a special MINLP superstructure is generated, constructed from various structure alternatives. The task of the optimization is to find a feasible and optimal structure within all alternatives. An extra MINLP optimization model is developed for each structure in GAMS (General Algebraic Modelling System) environment. In the model, the cost or mass objective function of a structure is defined, constrained to structural analysis and dimensioning constraints. The Modified Outer-Approximation/Equality-Relaxation (the Modified OA/ER) algorithm, the three-phase MINLP optimization strategy and the computer program MIPSYN are used for the optimization.

Three numerical examples, i.e. the MINLP optimization of a timber cantilever beam, concrete-steel composite floor and high-pressure steel penstock are presented at the chapters of the paper. It is proven that the MINLP optimization successfully solves large-scale non-linear and discrete optimization problems of structures in civil engineering.

Acknowledgements

The author is grateful for the support of funds from the Slovenian Research Agency (program P2-0129).

References

1. **Benders, J.F.** Partitioning Procedures for Solving Mixed-variables Programming Problems. *Numer. Math.*, 1962, No. 4, p. 238-252.
2. **Geoffrion, A.M.** Generalized Benders Decomposition. *J. Optim. Theory Appl.*, 1972, No. 10(4), p. 237-260.
3. **Beale, E.M.L.** Integer Programming. *In: The State of the Art in Numerical Analysis*, Academic Press, London, 1977, p. 409-448.
4. **Gupta, O.K., Ravindran, A.** Branch and bound experiments in convex nonlinear integer programming. *Management Science*, 1985, No. 31(12), p. 1533-1546.
5. **Duran, M.A., Grossmann, I.E.** An Outer-Approximation Algorithm for a Class of Mixed-Integer Nonlinear Programs. *Math. Prog.*, 1986, No. 36, p. 307-339.
6. **Mawengkang, H., Murtagh, B.A.** Solving Nonlinear Integer Programs with Large-Scale Optimization Software, *Ann. Oper. Res.*, 1986, No. 5, p. 425-437.
7. **Olsen, G.R., Vanderplaats, G.N.** Method for Nonlinear Optimization with Discrete Design Variables. *AIAA J*, 1989, No. 27(11), p. 1584-1589.
8. **Bremicker, M., Papalambros, P.Y., Loh, H.T.** Solution of Mixed-Discrete Structural Optimization Problems with a New Sequential Linearization Method. *Comput. Struct.*, 1990, No. 37(4), p. 451-461.
9. **Quesada, I., Grossmann, I.E.** An LP/NLP Based Branch and Bound Algorithm for Convex MINLP Optimization Problems. *Computers Chem. Engng.*, 1992, No. 16, p. 937-947.
10. **Westerlund, T., Pettersson, F.** An extended cutting plane method for solving convex MINLP problems. *In: European Symposium on Computer Aided Process Engineering-5, Supplement to Computers Chem. Engng.*, Bled, Slovenia, 1995, p. 131-136.
11. **Kocis, G.R., Grossmann, I.E.** Relaxation Strategy for the Structural Optimization of Process Flowsheets, *Ind. Engng. Chem. Res.*, 1987, No. 26, p. 1869-1880.
12. **Kravanja, Z., Grossmann, I.E.** New Developments and Capabilities in PROSYN - An Automated Topology and Parameter Process Synthesizer. *Computers Chem. Engng.*, 1994, No. 18(11/12), p. 1097-1114.
13. **Kravanja, S., Kravanja, Z., Bedenik, B.S.** The MINLP optimization approach to structural synthesis. Part I: A general view on simultaneous topology and parameter optimization. *International Journal for Numerical Methods in Engineering*, 1998, No. 43, p. 263-292.
14. **Kravanja, S., Kravanja, Z., Bedenik, B.S.** The MINLP optimization approach to structural synthesis. Part II: Simultaneous topology, parameter and standard dimension optimization by the use of the Linked two-phase MINLP strategy. *International Journal for Numerical Methods in Engineering*, 1998, No. 43, p. 293-328.
15. **Kravanja S, Kravanja, Z., Bedenik, B.S.** The MINLP optimization approach to structural synthesis, Part III: Synthesis of roller and sliding hydraulic steel gate structures. *International Journal for Numerical Methods in Engineering*, 1998, No. 43, p. 329-364.

16. Kravanja, S., Soršak, A., Kravanja, Z. Efficient multilevel MINLP strategies for solving large combinatorial problems in engineering. *Optimization and engineering*, 2003, No. 1/2, p. 97-151.
17. Kravanja, S., Šilih, S., Kravanja, Z. The multilevel MINLP optimization approach to structural synthesis: the simultaneous topology, material, standard and rounded dimension optimization. *Advances in engineering software*, 2005, No. 36(9), p. 568-583.
18. Šilih, S., Žula, T., Kravanja, Z., Kravanja, S. MINLP optimization of mechanical structures. *American journal of applied sciences*, 2008, No 5(1), p. 48-54.
19. Šilih, S., Premrov, M., Kravanja, S. Optimum design of plane timber trusses considering joint flexibility. *Engineering structures*, 2005, No. 27(1), p. 145-154.
20. Šilih, S., Kravanja, S., Premrov, M. Shape and discrete sizing optimization of timber trusses by considering of joint flexibility. *Advances in engineering software*, 2010, No. 41(2), p. 286-294.
21. Klanšek, U., Žula, T., Kravanja, Z., Kravanja, S. MINLP optimization of steel frames. *Advanced steel construction*, 2007, No. 3(3), p. 689-705.
22. Kravanja, S., Žula, T. Cost optimization of industrial steel building structures. *Advances in engineering software*, 2010, No. 41(3), p. 442-450.
23. Kravanja, S., Turkalj, G., Šilih, S., Žula, T. Optimal design of single-story steel building structures based on parametric MINLP optimization. *Journal of Constructional Steel Research*, 2013, No. 81, p. 86-103.
24. Kravanja, S., Šilih, S. Optimization based comparison between composite I beams and composite trusses. *Journal of Constructional Steel Research*, 2003, No. 59(5), p. 609-625.
25. Klanšek, U., Kravanja, S. Cost estimation, optimization and competitiveness of different composite floor systems. Part 1, Self-manufacturing cost estimation of composite and steel structures. *Journal of Constructional Steel Research*, 2006, No. 62(5), p. 434-448.
26. Klanšek, U., Kravanja, S. Cost estimation, optimization and competitiveness of different composite floor systems. Part 2, Optimization based competitiveness between the composite I beams, channel-section and hollow-section trusses. *Journal of Constructional Steel Research*, 2006, No. 62(5), p. 449-462.
27. Žula, T., Kravanja, S., Klanšek, U. MINLP optimization of a composite I beam floor system. *Steel and composite structures*, 2016, No. 22(5), p. 1163-1186.
28. Kravanja, S., Žula, T., Klanšek, U. Multi-parametric MINLP optimization study of a composite I beam floor system. *Engineering structures*, 2017, No. 130, p. 316-335.
29. Jelušič, P., Kravanja, S. Optimal design of timber-concrete composite floors based on the multi-parametric MINLP optimization. *Composite structures*, 2017, No. 179, p. 285-293.
30. Klanšek, U. Mixed-integer nonlinear programming model for nonlinear discrete optimization of project schedules under restricted costs. *Journal of construction engineering and management*, 2016, No. 142(3), p. 1-13.
31. Cajzek, R., Klanšek, U. Mixed-integer nonlinear programming based optimal time scheduling of construction projects under nonconvex costs. *Tehnički vjesnik : znanstveno-stručni časopis tehničkih fakulteta Sveučilišta u Osijeku*, 2016, No. 23(1), p. 9-18.
32. Brooke, A., Kendrick, D. and Meeraus, A., *GAMS - A User's Guide*, Scientific Press, Redwood City, CA, 1988.
33. Kravanja, S., Kravanja, Z., Bedenik, B.S., Faith, S. Simultaneous Topology and Parameter Optimization of Mechanical Structures, *In: Proceedings of the First European Conference on Numerical Methods in Engineering*, Elsevier, Amsterdam, 1992, p. 487-495.
34. Drudd, A.S. CONOPT – A Large-Scale GRG Code, *ORSA J. Comput.*, 1994, No. 6, p. 207-216.
35. CPLEX User Notes, ILOG inc.
36. Eurocode 5. Design of timber structures, European Committee for Standardization, Brussels, 2004.
37. Eurocode 4. Design of composite steel and concrete structures – Part 1-1: General rules and rules for buildings, European Committee for Standardization, Brussels, 2004.
38. Močnik, I., Kimovec, J. Penstock dimensioning, 3. civil construction design, Penstock, Kozjak PSP, IBE Ljubljana, 2011.
39. Močnik, I. Technical Report, 3. civil construction design, 3/18 Penstock – cavern type, Kozjak PSP, IBE Ljubljana, 2012.
40. Kravanja, S. Optimization of steel penstock in a bored tunnel, *In: High performance and optimum design of structures and materials, 2014 International Conference on High performance and optimum design of structures and materials, HPSM/OPTI 2014, WIT transactions on the built environment vol. 137*, WIT Press, Southampton, 2014, p. 337-345.
41. Kravanja, S. The optimization of penstock with the recommendations for the design of steel liner and the collaboration of the rock, Variant the vertical penstock, The recommendations for the dimensioning and optimization of steel penstock, Kozjak PSP, Faculty of Civil Engineering, University of Maribor, 2012.
42. C.E.C.T. Recommendations for the design, manufacture and erection of steel penstocks of welded construction for hydro electric installations, European Committee for boilermaking and kindred steel structures, Prepared by the »Penstock« Section, 1979.

Reuse of Steel Structural Elements with Bolted Connections

Janis Kreilis, Edgars Zeltins, *Latvia University of Agriculture*

Abstract. New economy concept – a circular economy as an alternative to the traditional linear economy is an important topic today. Steel structural elements have excellent circular economy credentials in comparison with other building products. Reuse of steel elements offers greater advantages than recycling because the energy, used to remelt the element, is saved. Today numerous studies are being carried out and problems regarding the reuse of steel elements have been identified. The aim of the experimental part of this research is to determine the behaviour of reused structural elements with renewed bolted joints (beam to column) under cyclic and ultimate loading. For this purpose bolts of different classes and sizes were used. Special attention was paid to discovering the changing of connection properties due to residual plastic deformations and strain hardening of joint components. Test results were compared with those produced by the equivalent T-stub method (hand calculation method) and FEM software programme and the analysis of the results are presented.

Keywords: circular economy concept, moment resisting connections, test results, theoretical modelling.

Introduction

Steel is a very widely used material in construction, although its production is very energy intensive. Reduction of energy consumption always is an important issue. There are several ways to achieve this goal. First, it can be achieved by increasing the efficiency or utilization rate. Besides, the recycling of steel at the end of the life of a structure also saves energy, reduces the quantity of natural raw materials and it can be produced into a functionally equivalent product. Reuse of steel elements offers even greater advantages than recycling because the energy used to remelt the element is saved. This leads to a new economy concept – a circular economy as an alternative to the traditional linear economy. Nevertheless, there are many barriers, that hamper the using of the given benefits – technical, logistical problems, cost implications, steel recertification etc. The background of making and exploitation conditions of steel elements, loading type (static, dynamic, cyclic) and level are also very important.

Now problems regarding the reuse of steel elements are identified and numerous studies have been carried out, however the studies devoted to the behaviour of reused steel elements subjected to considerable loads, particularly with bolted joints are insufficient. In this article test results with specimens modelling beam-to-column moment connections are presented. For this purpose, the experimental and theoretical study, described in [1], was continued.

Initially, three series of steel specimens were made and tested once. Most of the test results showed a failure of tensioned bolts with insignificant plastic deformations of connection members - end plates and column flanges. In continuation a lot of tests were performed with these specimens with new bolts to discover the behaviour of connecting components in the case of cyclic and ultimate loading. Numerical analysis, using the so called component method,

adopted in EC 1993-1-8 [2] was carried out and FEM software method was used to evaluate and compare the obtained results.

The aim of this research is to discover the changing of joint properties, if steel elements are reused, and assess the influence of these changes in comparison with the expected theoretical results. The main objectives are: to acquire the relationships by performing the tests, to assess the stiffnesses of the connections, to determine the load bearing capacity and to give some recommendations and suggestions for further research.

Experimental research

The test specimens for modelling the behaviour of beam-to-column bolted connections were made from wide flange beams HE 140 B – as columns and double-sided I beams IPE 180. End-plates were welded to the beams. Properties of welding metal are compatible with parent metal S235JR.

All column-beam models can be divided into three series (Fig.1). Each series consists of equivalent specimens to obtain more reliable test results. It should be noted that series I and series II differ only regarding the location of the bolt rows. Series III specimens have an additional bolt row at the extended part of end plate and column. The effective throat thickness was adopted 4 mm for all welds made during fabrication of specimens. To increase the column web resistance in compression and tension, double sided stiffeners were provided. All materials purchased from producers had adequate certificates for production.

Initial tests [1] with hexagon bolts M12, class 8.8U SB resulted with bolts failure and small plastic deformations of connecting parts (end plates and column flanges). Ignoring these deformations, the specimens were reused and the test programme was expanded for further research. For one part of the

specimens – higher strength bolts M12, class 10.9 HV with adequate nuts and washers were used. For another part of the specimens – bolts M12 were replaced with bolts M16, class 8.8 SB and class 10.9

HV. Cyclic loading was performed with reloading up to 50-60% to study the behaviour of the specimens under short time variable actions. Finally, ultimate loading was performed.

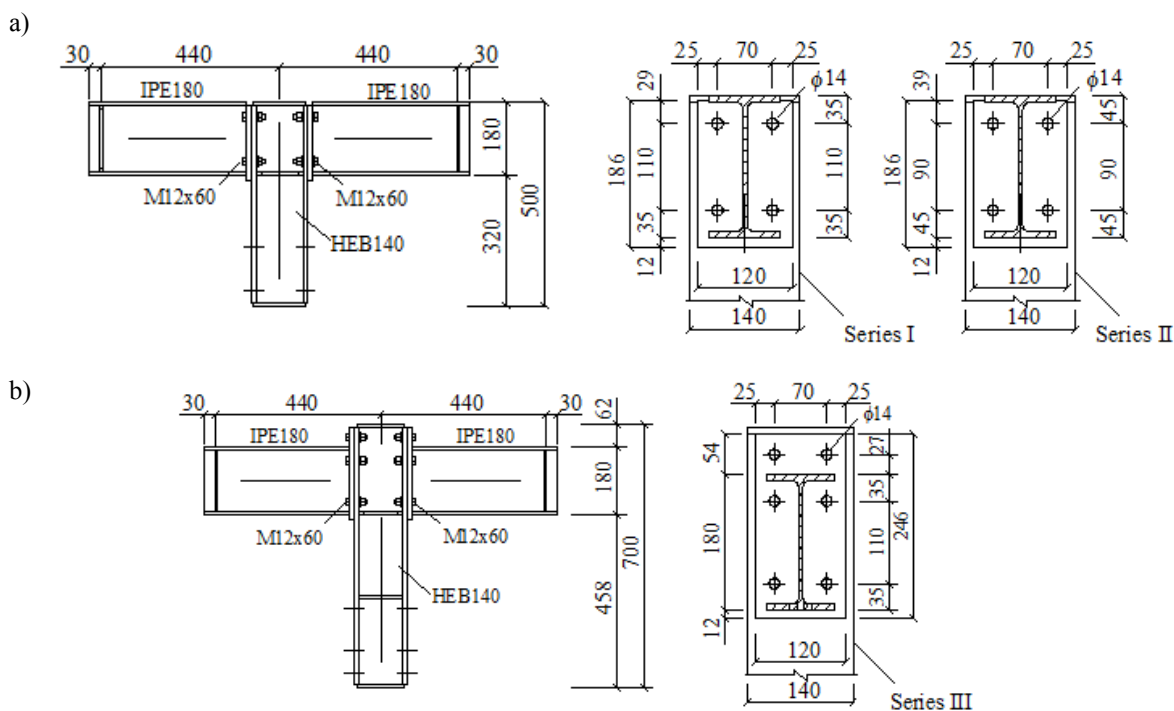


Fig. 1. Drawings of specimens for experimental (initial) tests: a - series I, series II; b - series III

Bolt torque value for tightening (for a non-slip resistant connection) was calculated according to EN 1090-2:2008 [3]. It is stated that the design tension resistance of the bolt:

$$F_{t,Rd} = f_{yd} A_s$$

and bolt design preload:

$$F_{p,Cd} = 0,7 f_{ub} A_s / \gamma_{M7}$$

Torque reference value for bolt tightening

$$M_r = k_m d F_{p,Cd}$$

where $\gamma_{M2} = 1,25$;

$\gamma_{M7} = 1,1$;

$f_{yd} = f_{yb} / \gamma_{M2}$;

$k_m = 0,2$ – for typical steel.

If preload is required only for execution purposes, then the level of preload can be specified in the National Annex, or $\sim 50\%$ $F_{p,Cd}$. Then the calculated torque value $M_{r(non\ slip)}$ when there is no slip resistance (Table 1):

TABLE 1

Preload of bolts according to EN 1090-2:2008

Bolt	Bolt class	A_s mm ²	$F_{t,Rd}$ kN	$M_{r(non\ slip)}$ N m
M12	8.8	84.3	43.2	51.5
M12	10.9	84.3	60.7	64.4
M16	8.8	157	80.4	127.9
M16	10.9	157	113	175.8

This torque value was provided by torque wrench tool. The tightening of bolts was restored after each reloading.

Prepared specimens and loading performance is shown in Fig.2. The tests were carried out using the hydraulic equipment Zwick-Roell and software programme TestXpertII. To define the upper value of the cyclic loading (up to the plastic limit) the results

of the first tests were taken into account. To exclude the initial slip of joining members, the preload of 5 kN was applied. As it was noted, tests with bolts M12 class 8.8 SB showed the weakness of these bolts (see the dotted curves 1 in Fig.3 a, Fig.4 a, Fig.5 a). Nonlinear deformations were caused mainly due to the plastic elongations of the bolts.

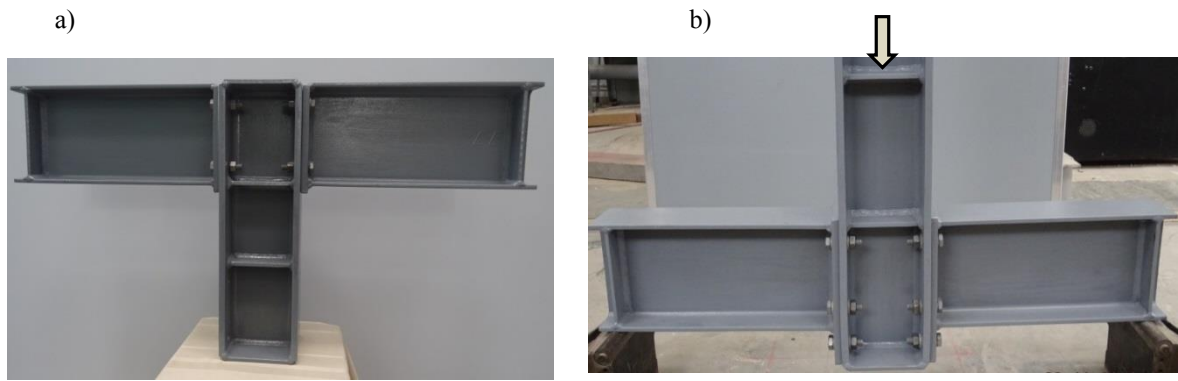


Fig. 2. Column-beam specimens (a) and loading performance during the tests (b)

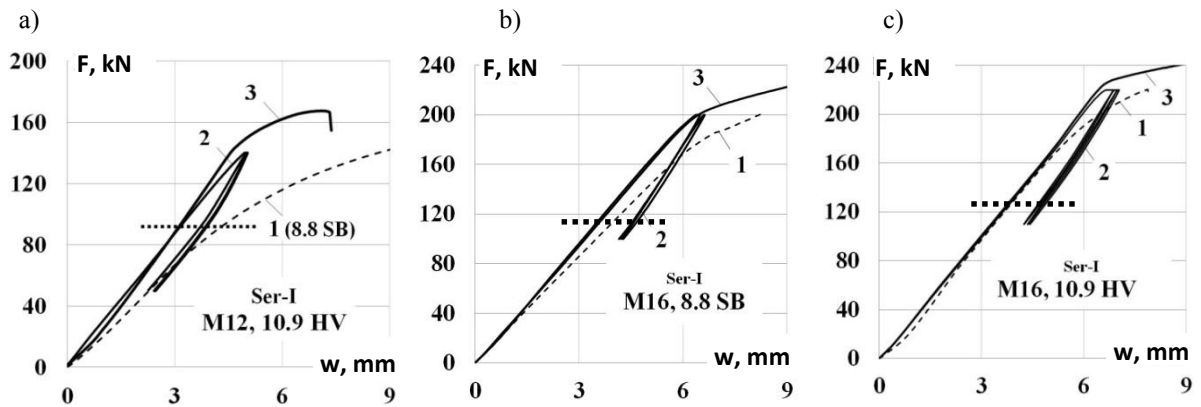


Fig. 3. Test results: specimens of Series I under static and cyclic loading (F – loading; w – displacement)

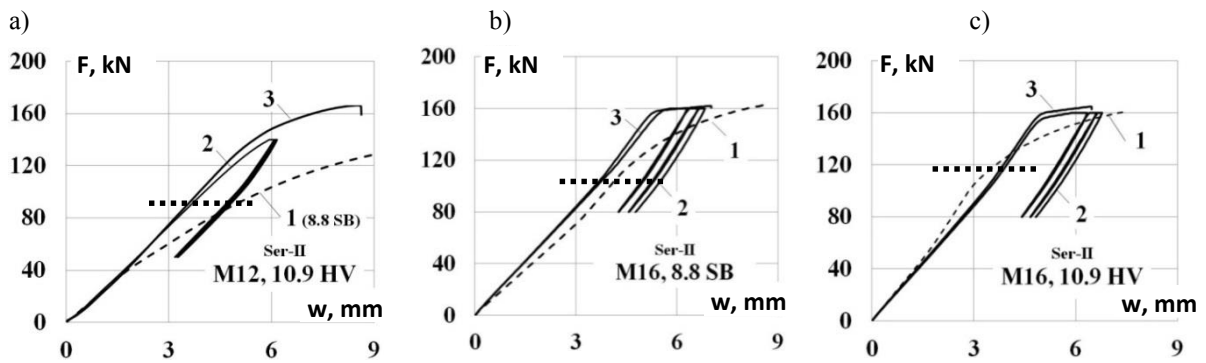


Fig. 4. Test results: specimens of Series II under static and cyclic loading (F – loading; w – displacement)

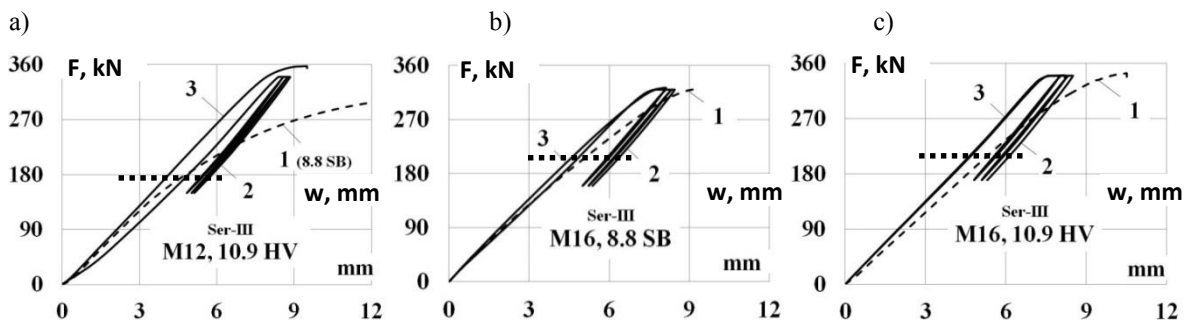


Fig. 5. Test results: specimens of Series III under static and cyclic loading (F – loading; w – displacement)

- Test results with bolts M12 class 10.9 HV instead of the bolts M12 class 8.8 SB:
 - stabilization of deformations can be observed after 3-5 times of cyclic loading (see curves 2);
 - ultimate loading (see curves 3) leads to failure of bolts M12; in case of series III specimens, considerable deformations of the extended parts of the end plates were fixed;
 - the tests for identical samples showed practically equal graphs;
 - comparing the effectiveness of bolts M12 class 10.9 for series I, II and III the distance effect can be assessed between the rows and the number of bolts in joining. Reducing the distance between the bolt rows (only 10 mm for each row) leads to increasing of the ductility and decreasing of stiffness (see Fig.3 a and Fig.4 a). On the contrary – the increase of the load capacity of joining was obtained by an additional bolt row in the extended part of the end plate (Fig.5 a).
- Test results with bolts M16 SB class 8.8 and M16 HV class 10.9 instead of the bolts M12 (Fig.3 b,c; Fig.4 b,c; Fig.5 b,c):
 - the dotted curves 1 show first loading results using bolts M16. It serves as an attempt to determine the real plastic stage of the joining and for the cyclic load level acceptance;
 - obviously the bolts M16 are useful for the specimens of series I. Ultimate loading (see curves 3) shows elastic-plastic stage behaviour without brittle collapsing;

- due to the plastic deformations of the end plates and the column flanges the joinings of II and III series become ductile. In this case increasing the bolt size does not increase the load capacity of joining; particularly it is visible in test results with specimens of series II. The cyclic loading and ultimate loading (see curves 2 and 3) show plastic stage behaviour without reserves of load bearing capacity;

- comparing the curves of first loading and last loading (until constant plastic deformations) the strain hardening effect is visible. It should be applied to all components of the joint, but especially on behaviour of the end plates and column flanges. As a result - the yielding stress of the steel increases and stiffness of the joining changes. Many studies have been devoted to the effects of strain hardening under the cyclic loading [5], [6], but they are insufficient regarding reused structural elements.

Theoretical modelling

Numerical analysis, using the component method, adopted in EC 1993-1-8 [2] was used. The behaviour of the components have been studied considering that the joint can be sub-divided. One of the main components is the equivalent T-stub in tension modelling column flange and beam end-plate in bending. For theoretical analysis the MathCad programme is used to calculate tensioned equivalent T-stub flange resistances and perform the necessary checks. The results are given in Table 2.

TABLE 2

Calculated T-stub flange resistances

Series	Diameter of the Bolt		Bolt class	Column flange			Beam end-plate	
				F _{t1Rd,c} (Mode 1)	F _{t2Rd,c} (Mode 2)	F _{t3Rd,c} (Mode 3)	F _{t1Rd,ep} (Mode 1)	F _{t2Rd,ep} (Mode 2)
1	2	3	4	5	6	7	8	
I	M12	8.8	244.5	102.2	<u>97.1</u>	212.2	<u>92.0</u>	
		10.9	244.5	115.1	121.4	211.7	<u>103.2</u>	
	M16	8.8	263.4	146.8	180.9	226.1	<u>131.1</u>	
		10.9	263.4	170.9	226.1	227.2	<u>152.2</u>	
II	M12	8.8	244.5	98.1	<u>97.1</u>	200.8	<u>89.5</u>	
		10.9	244.5	111.0	121.4	200.8	<u>100.8</u>	
II	M16	8.8	263.4	142.7	180.9	213.4	<u>128.4</u>	
		10.9	263.4	166.8	226.1	213.8	<u>149.5</u>	
III	M12	row1	8.8	244.5	100.0	97.1	113.1	<u>73.7</u>
				233.4	<u>94.8</u>	97.1	215.4	<u>92.7</u>
		row2	10.9	244.5	113.0	121.4	113.1	<u>87.2</u>
				233.4	107.8	121.4	215.4	<u>104.0</u>
	M16	row1	8.8	263.4	144.7	180.9	122.1	120.2
				251.4	139.5	180.9	228.4	<u>86.5*</u>
		row2	10.9	263.4	168.8	226.1	122.1	145.3
				251.4	163.6	226.1	228.4	<u>84.6*</u>

* - classified as beam flange collapse in compression

Following the conditions given in [2], [4] the design tension resistances of T-stub flange are

obtained for each bolt row separately. Significant impact on the results is created by the location of bolt

rows and stiffening of column web and flanges. Practically the method is based on the correct determination of the effective length of yielding line, named as circular or non circular pattern, i.e., designer need to choose the correct values of l_{eff} from Tables 6.4 – 6.6 [2].

Theoretically it is obvious, that the value of the resistance of the end plate in bending is the main

limiting factor. Actually, mode 2 (bolt failure with yielding of the flange of T-stub) prevailed in tests.

Plastic moment resistances of the bolt rows were calculated from the lesser values of tension resistances. Considering double-sided beam-to-column joint configuration (Fig.1), the corresponding loads which mark the limit state are as shown in Table 3:

TABLE 3

Moment resistances and corresponding loads

Series	Bolt size	Moment resistances of bolted joints $M_{pl,Rd}$, kNm		Corresponding loading F_{Ed} , kN		Stiffness S_j kNm/rad	Stiffness S_{eksp} kNm/rad
		Bolt class 8.8	Bolt class 10.9	Bolt class 8.8	Bolt class 10.9		
I	M12	15.5	17.4	83.8	94.0	3705	2212
	M16	20.8	23.2	112.4	125.4	4620	2395
II	M12	14.7	16.7	79.5	90.3	3120	1910
	M16	20.0	21.9	108.4	118.4	3820	2064
III	M12	28.7	32.8	155.1	177.3	10110	3075
	M16	36.6	36.7	197.8	198.4	12340	3075

For comparing and verification of given results, the IDEA StatiCa Connection software programme (the programme uses component-based finite element model) was used. All the results obtained are comparable and the software programme discovered 6 – 10 % reserves of load capacity due to a more accurate modelling of the interaction of the joining elements.

Results and discussion

Test results with reused specimens under cyclic and ultimate loading show significant deviations from the expected theoretical volumes obtained for initial (first) loading conditions. As it can be seen in Figures 3, 4 and 5, reusing the specimens with renewed bolts lead to the changing of connection properties. The rotational stiffness values and design resistances of connections should be analysed.

Accordingly to the initial properties of the specimens, the boundary limits of stiffnesses are $S_{j,rig} = 50400$ kNm/rad – if the rigid connection, and $S_{j,pin} = 3150$ kNm/rad – if pinned connection, i.e., actually the models should be classified as semi-rigid (Table 3).

In addition to the experimental curves F-w, moment-rotation curves M- ϕ were determined from which the stiffness calculation is possible. Only the linear part of the curves from the last (ultimate) loading was taken into account. Numerical values of the stiffnesses S_{eksp} are shown in Table 3. Comparing the results with those from the initial conditions (S_j), it should be concluded, that all the reused specimens have become more ductile and the connections can be classified as pinned. This should be explained by the changing of the initial conditions.

As noted before, the plate elements of the connections (end plates, column flanges) due to small residual plastic deformations and strain hardening

changed the interaction of joining elements. Therefore, the moment-rotation curves (linear part of them) reflect mainly the resistance of alone tensioned bolts until the full contact between the plates is restored. Following this, in the case of reusing the steel joining elements, it is important to take into consideration the contact conditions between the plate surfaces.

Assessing the strength of the model joint, the resistances are lesser than the moment resistance of the beam cross section (39.1 kNm), therefore the joint is classified as partial-strength joint.

The load bearing capacity of the reused specimens (see horizontal dotted lines in Fig.3, Fig.4 and Fig.5) is much higher than the expected design resistances. Along with the above reasons it can be noted that significant reserves may be caused also from the inadequacy of steel element properties (according to the Certificate of quality and quantity). For example - tensile strength f_u of bolts class 8.8 SB actually is declared up to 908 MPa and the resistance of steel S235JR plates actually is up to 304 MPa (yield strength).

Increasing of the load bearing capacity of joints by using the bolt class 10.9 HV instead of class 8.8 SB should be assessed in conjunction with more brittle failure of bolts class 10.9 HV (in case of extreme loading). In this context, the use of more plastic bolts 8.8 SB increases the safety of joining and the whole structure.

Conclusions

In case of reusing of steel structural elements with bolted connections particular attention should be paid to the contact conditions between the joined elements. Due to incomplete surface contact the joining may become much more ductile.

The analysis of the given test results show, that

the moment resisting connection with semi-rigid stiffness due to insignificant plastic deformations and strain hardening during the previous (initial) tests can be changed to pinned joining. Following this, the behaviour of the entire construction should be evaluated.

Significant reserves of the load bearing capacity discovered by the results of testing (30-40% in comparing with theoretical) show an influence of many factors, including inadequacy of steel element

properties (according to the Certificate of quality and quantity). Using a professional software programme confirms this conclusion.

Acknowledgements

The authors are very thankful to the company CSK Steel Ltd for providing the specimens for the tests and computer software for calculations.

References

1. **Zeltniš, E., Kreilis, J.** Test results and theoretical study of moment resisting connections. In: *Proceedings of the 7th International conference on Safety and Durability of Structures (ICOSADOS 2016)*, Vila Real, Portugal, May 10 - 12, 2016/ University of Trás-os-Montes e Alto Douro. Vila Real: UTAD, 2016.
2. **EN 1993-1-8:2005.** Eurocode 3: Design of steel structures - Part 1-8: Design of joints. European Committee for Standardization.
3. **EN 1090-2:2008.** Execution of Steel Structures and Aluminium Structures – Part 2: Technical Requirements for Steel Structures.
4. **Joints in Steel Construction.** Moment-Resisting Joints to Eurocode 3. *Publication P398*. The Steel Construction Institute and The British Constructional Steelwork Association, 2013., 163 p.
5. **Budaházy V., Dunai L.** (2017). Experimental study on cyclic plastic behaviour of steel joint components. *Proceedings of Eurosteel 2017* (Special Issue) Vol 1, Issue 2-3, p. 590-608 (DOI: 10.1002/cepa.98)
6. **Zeinoddini-Meimand V., Ghassemieh M., et.al.** Finite Element Analysis of Flush End Plate Moment Connections under Cyclic Loading. *International Scholarly and Scientific Research & Innovation*, Vol.8, No1, 2014, p. 96-104.

Theoretical Basis and Experimental Means of the Hydrophilic Nanostructure Formation Process on the Titanium Surface by Direct Laser Irradiation

Sharif E. Guseynov^{1,2,3}, Jekaterina V. Aleksejeva¹, Ruslans Aleksejevs⁴, Uldis Zaimis^{1,2}, ¹Liepaja University, Institute of Fundamental Science and Innovative Technologies, ²Liepaja University, Faculty of Science and Engineering, ³"Entelgine" Research & Advisory Company, Ltd., ⁴Lomonosov Moscow State University, Faculty of Mechanics and Mathematics, Department of Mathematics

Abstract. One of the most promising ways of periodic and/or nonperiodic nanostructure formation on implants' material surface, particularly on a titanium surface, providing the implants with the desired adhesive and wettability properties, is direct laser nanostructuring which uses only a laser beam with no atomic-force microscope's ancillary needle or masks in order to form surface nanorelief. In the present paper, the model of a nanostructure formation on a solid surface by microsecond laser pulses melting the material is described. It is shown that the typical size of the surface nanostructure formed depends on the laser wavelength, pulse energy, pulse repetition rate, and pulse duration. Within the present study a series of six experiments devoted to direct laser nanostructuring of titanium and copper surfaces was carried out. Besides, the effects of nanoroughness on the contact and sliding angles on hydrophilic surfaces were studied theoretically and experimentally.

Keywords: nanoroughness of surface, contact angle, nanostructured hydrophilic surface, laser irradiation

Introduction

At the present time nanostructures are given additional attention for being an extremely promising object regarding its application in different fields of science, technology and medicine. Surface nanostructuring leads to the improvement of nanotribological [1], thermalphysic and thermodynamic [2], electron-emission [3] properties of materials, promotes the increase of implants' biocompatibility ([4], [5], [6]) as well as leads to the desired alteration of adhesive properties ([7], [8], [9]) and wettability ([10], [11]). One of the most promising ways of periodic and/or nonperiodic nanostructure formation on implants' material surface, particularly on a titanium surface, providing the implants with the desired adhesive and wettability properties, is direct laser nanostructuring (see [12], [13] and respective references given in these) which uses only a laser beam with no atomic-force microscope's ancillary needle or masks in order to form a surface nanorelief. The advantage of this method consists in its simplicity and flexibility: (a) the use of a single laser beam of a small size allows one to achieve a high locality of exposure corresponding to the size (100x100 micrometer) of a separate laser spot; (b) the use of a software-programmable laser beam scanning on the implants' material surface with a high irradiation pulse repetition frequency allows to nanostructure

sufficiently large surface areas within almost arbitrary boundaries with high spatial resolution.

This study, which to a certain extent is a continuation of the research [14], is devoted to the formation of a hydrophilic nanostructure on the surface of a ball-shaped titanium head of a human hip joint endoprosthesis using direct laser nanostructuring. The necessity of hydrophilicity property of the implant surface is due to the fact that the state of the surface of titanium implants plays a decisive role in cell-cell adhesion, because the interaction between a biological environment (hard and soft tissues, blood, body fluids and serum, etc.) and the implant occurs on its surface, and the biological response from the living tissue depends on a variety of surface properties, such as chemical composition, purity, texture and topography, surface energy, corrosion resistance, and the tendency to denaturalization of the surrounding proteins. In this work, following the work [15], we will consider that a partially hydrophilic or hydrophobic surface with respect to any fluid is such a solid surface that for it the fluid gives a finite contact angle: if the contact angle θ between a drop of the liquid and the solid surface varies within the interval $\left(0, \frac{\pi}{2}\right)$, then this

surface is called hydrophilic; if $\theta \in \left(\frac{\pi}{2}, \frac{5 \cdot \pi}{6}\right]$, then

the surface is called hydrophobic; if $\theta \in \left(\frac{5 \cdot \pi}{6}, \pi\right]$,

then the surface is classified as ultrahydrophobic; with $\theta=0$ and $\theta=\pi$ we have correspondingly complete wettability and complete nonwettability of the surface.

Scientific basis: mathematical models and design formulas

Surface energy, surface tension and surface forces near the phase interfaces

Within representation of continuous medium, while analyzing two-phase systems, phase boundaries are interpreted as geometric surfaces. However, real phase boundaries are thin transition layers of a rather complicated structure. Molecules which form the transition layer interact with the molecules of both adjacent phases, that is why the properties of a transition layer differ from the properties of a substance in the phases. This is the reason why during the interpretation of the phase boundaries some phenomenological properties appear. A correct description of microsurface forces lies in the foundation of surface tension's and capillarity's interpretation both in the old approach of Clairaut and Laplace and in the new approach of Bakker ([16], [17], [18]), which is based on introducing the pressure tensor in the interphase area. The description of microsurface forces should begin with the definition of interphase energy on the surface of the phase boundary of phases solid-liquid (and also of the phases of liquid-liquid, liquid-gas, solid-solid) and proceed with the definition of surface forces in the interphase area. It is known [19] that if both phases are fluid (liquid-liquid, liquid-gas), then their phase boundary can be stretched or it can shrink not affecting the thermodynamic equilibrium; if one phase is solid and the other is liquid or gaseous, then the surface of their phase boundary can experience only elastic deformations, however some degree of freedom appears if the liquid is able to slide on the sufficiently smooth solid material (for example, when mercury slides down a glass; water slides on a paraffin surface; blood or body fluids slide down a burnished surface of a titanium implant, etc.); if both phases are solid, then the behaviour of the phase boundary is similar to the case solid-liquid, however the implementation of a real phase contact is possible only with atomic smoothness or requires plastic deformation, or prior to melting, or evaporation and

condensation with subsequent crystallization. Only in the case when both phases are fluid, a direct measurement of the phase boundary tension is possible. In the case, when both phases are solid, a direct measurement of the phase boundary tension is achievable with some approximation if and only if in some temperature region the yield point is lowered. In the case, when one phase is solid and the other is gaseous, a direct measurement of the phase boundary tension is impossible. The main mistakes made while measuring the surface energy in the process of the formation of a new surface are: (a) omission of an irreversible part of a fracture work, which turns into heat or energy residual deformations; (b) omission of the fact that fresh (that is, just created) surfaces are in nonequilibrium state with higher energy – they appear to be covered by charge with density of up to $3.5 \cdot 10^{-4} C \cdot m^{-2}$, that consumes part of the fracture work. The special state of fresh surfaces is expressed not only by increased energy, but also by a higher chemical activity. Relaxation down to an equilibrium state usually occurs for about ten minutes due to the electron emission and surface conduction.

Formation of a new phase boundary is connected with the consumption of work in order to move a part of molecules from the phases to the surface layer. In isothermal conditions the work of formation of the phase surface's element dF is equal to the increment of Helmholtz energy dU_F of the surface: $dU_F = \sigma \cdot dF$, where σ is the specific Helmholtz energy of the phase boundary, which decreases as the temperature increases and at critical temperature $T_{c.t.}$ achieves the approximate value of zero (in steam-and-liquid systems $\sigma = 0$, and the difference between the phases disappears). The values of σ for the surface of a solid body on a border with a liquid are not identical to the corresponding coefficients of surface tension ([20]). Accurate theoretical formulas for the calculation of liquids' surface tension coefficient do not exist. The main methodological difficulty of calculation of the surface tension is the problem of ensuring solid surface purity, when it is in contact with a liquid, as well as the purity of the liquid. There are some methods of experimental calculation among which the most popular are [21]: the maximum gas bubble pressure method; capillary rise method; method of ring lifting; electromagnetic measurement methods; the drop weight method; hanging drop method; lying bubble or drop method. The simplest experimental method of determining the empirical dependence of the phase boundary's specific

Helmholtz energy on the temperature is the following relation obtained from the theory of corresponding

states ([22]): $\sigma = \sigma_0 \cdot \left(1 - \frac{T}{T_{c.t.}}\right)^{\frac{11}{9}}$, where σ_0 is

determined by the experiments carried out with one constant value of temperature. This formula has shown itself well working for liquids with homonuclear molecules, however it can be approximatively used also for the majority of other liquids. For calculations of water's σ it is recommended to use the following interpolation

$$\text{formula: } \sigma = 0.235 \left(1 - \frac{T}{T_{c.t.}}\right)^{1.256} \left(1 - 0.625 \frac{T_{c.t.} - T}{T_{c.t.}}\right).$$

Wetting process

In the introduction we mentioned (following the work [15] the contact angle of wetting θ between a solid surface and a tangent to the phase boundary gas-liquid. From the minimality condition of the surface's Helmholtz energy ([23], [24]) one can obtain the following relation known as Young's law:

$$\theta = \arccosine\left(\frac{\sigma_{solid, gas} - \sigma_{solid, liquid}}{\sigma}\right). \text{ It is important to}$$

note that the contact angle is very sensitive to such difficult-to-control factors as roughness of a solid surface or presence of foreign impurity on the solid surface or in the liquid, particularly if this impurity is surface-active, which, concentrating on the thermodynamic phase boundary, cause surface tension lowering: for instance, R-OH alcohols; R-COH aldehydes; R-COOH carboxylic acids; CH₃-, C₂H₅-, C₁₇H₃₅-, etc. hydrocarbon radicals; COH and COOH functional groups; oleic acid C₁₇H₃₃COOH; stearic acid sodium C₁₇H₃₅COONa; etc. The increase in the roughness of the solid surface increases its wettability, that is, it decreases the value of θ . For some solid bodies participating in the phase solid-liquid in a certain interval of temperature, a dependence of the contact angle θ on the temperature is held [25]. As it is shown in [25], almost always an increase in temperature on a hydrophilic surface leads to the improvement of wettability, that is, to diminution of the angle θ , but on hydrophobic surfaces – to the worsening of wettability, that is, to the increase of the angle θ . Also it is important to note (especially regarding the implants) that the contact angle of wetting θ depends also on hysteresis of wetting– on the direction of wetting a solid body surface by a

liquid, that is, on the fact, whether the liquid is flowing on the surface or down from it.

The phase separation surface's equilibrium and axisymmetric equilibrium separation surfaces of phases

If the liquid rests relative to the coordinate system related to Earth, then in hydromechanics this rest is called absolute rest; if the liquid rests relative to the coordinate system which moves with uniform acceleration relative to Earth, then this rest is called relative rest. For both absolute rest and relative rest Euler's equations in the vector form hold:

$$\vec{F} - \frac{1}{\rho} \cdot \nabla p = 0, \text{ where } \vec{F} \text{ is mass forces density}$$

vector, which, in the case of relative rest, includes inertial forces; ρ is liquid density; p is liquid pressure. Due to the fact that mass forces have potential in the majority of cases, one can write $\vec{F} = -\nabla\Phi$, where Φ is a force function.

Consequently, Euler's equation turns into equation

$$\nabla\Phi + \frac{1}{\rho} \cdot \nabla p = 0, \text{ whose general integral for the cases,}$$

when $\rho = \rho(p)$, is the formula $\Phi + \Upsilon = const$,

called the equation of hydrostatics, where $\Upsilon = \int \frac{dp}{\rho}$

denotes pressure function. It should be noted that, if the liquid is a heavy compressible liquid, then out of all mass forces only the gravitational force affects it, so the general integral looks like $\Phi = g \cdot z + const$, where z denotes the coordinate which is counted vertically up. For a heavy compressible liquid the general integral of Euler's equation has the form

$$z + \frac{p}{g \cdot \rho} = const, \text{ and this formula represents}$$

hydrostatic distribution of pressure. When a gas-liquid system is in the equilibrium state, then in each contacting phase, firstly, the equations of hydrostatics hold and, secondly, for every point on the phase boundary defined by a position vector \vec{r} Laplace formula $p_1 - p_2 = 2 \cdot \sigma \cdot H(\vec{r})$ is true, which means

that on the boundary between two fluid phases the surface tension causes a pressure jump in the contacting phases, which is proportional to the average curvature H of the phase boundary. From these two relations (equation of hydrostatics and Laplace formula) one can deduce the main differential equation of hydrostatic equilibrium, whose general integral

$$2 \cdot \sigma \cdot H(\vec{r}) = (\rho_{liquid} - \rho_{gas}) \cdot \Phi(\vec{r}) + const \text{ determines}$$

the shape of the phase boundary. In the most practically important axial-symmetric problems on liquid there are: a homogeneous gravitational field with intensity g , directed along the vertical axis OZ ; centrifugal force field caused by a uniform rotation of the gas-liquid system around the same axis OZ with an angular velocity ω . In this case, the potential of mass forces has the form $\Phi = g \cdot z - \frac{1}{2} \cdot \omega^2 \cdot d^2$, where $d = \sqrt{x^2 + y^2}$ is the distance to the rotation axis. When the system rests, the potential of mass forces is determined by the formula $\Phi = g \cdot z$, but the main equation of hydrostatic equilibrium has the expression:

$$2 \cdot \sigma \cdot H(z) = \delta \cdot g \cdot (\rho_{liquid} - \rho_{gas}) \cdot z + 2 \cdot \sigma \cdot H(0),$$

where the term $2 \cdot \sigma \cdot H(0)$ represents the pressure jump on some "zero" level; $\delta = +1$ in the case, when the vertical axis OZ is pointed up (and the gravitational field is pointed down), and $\delta = -1$ in the case, when the vertical axis OZ is pointed down. For a resting system with a characteristic size $L_{ch.d.}$ it is possible to use the main equation of hydrostatic equilibrium in order to obtain the scale of gravitational forces $f_{grav} \sim g \cdot (\rho_{liquid} - \rho_{gas}) \cdot L_{ch.d.}$ and

the scale of surface tension forces $f_{s.t.} \sim \frac{\sigma}{L_{ch.d.}}$. Then

Bond number Bo , which is the criterion of similarity in hydrodynamics and determines the relation between external forces (usually, gravity) and surface tension forces has the following form:

$$Bo = \frac{f_{grav}}{f_{s.t.}} = g \cdot (\rho_{liquid} - \rho_{gas}) \cdot \frac{L_{ch.d.}^2}{\sigma}. \text{ The condition}$$

$Bo = 1$ determines linear size of the region, where the gravitational forces and surface tension forces are

equal: $L_{lin.d.} = \sqrt{\frac{\sigma}{g \cdot (\rho_{liquid} - \rho_{gas})}}$. The quantity $L_{lin.d.}$ is

called the capillary constant. For the majority of liquids with $p \ll p_{c.t.}$ ($p_{c.t.}$ is critical pressure), that is, on Earth conditions, the value of capillary constant varies within $1 \div 3 \text{ mm}$. Obviously, if one divides the equation of hydrostatic equilibrium

$2 \cdot \sigma \cdot H(z) = \delta \cdot g \cdot (\rho_{liquid} - \rho_{gas}) \cdot z + 2 \cdot \sigma \cdot H(0)$ by the quantity $\sqrt{\sigma \cdot g \cdot (\rho_{liquid} - \rho_{gas})}$, then it turns into the

following dimensionless form: $2 \cdot \tilde{H}(\tilde{z}) = \delta \cdot \tilde{z} + C$,

where $\tilde{H} = L_{lin.d.} \cdot H$, $\tilde{z} = \frac{z}{L_{lin.d.}}$, $C = 2 \cdot H(0) \cdot L_{lin.d.}$.

Melting process

At sufficient energy density, duration and order of a laser pulse melting of solid body's surface occurs – in our case, of a ball-shaped titanium head of a human hip joint endoprosthesis. When the laser pulse irradiation stops, the process of cooling the processed surface starts and is carried out by the means of heat removal deep into the solid phase and subsequent solidification of the surface layer. It is supposed that the power of laser irradiation is such that the phase transition solid-liquid occurs. Then, with appropriate approximation, temperature fields in the liquid $T_{liquid}(x, t)$ and solid $T_{solid}(x, t)$ phases can be described by the following boundary value problem ([13], [26], [27]):

$$\frac{\partial T_{liquid}(x, t)}{\partial t} = a_{liquid} \cdot \frac{\partial^2 T_{liquid}(x, t)}{\partial x^2}, \quad 0 < x < y(t), \quad (1)$$

$$\frac{\partial T_{solid}(x, t)}{\partial t} = a_{solid} \cdot \frac{\partial^2 T_{solid}(x, t)}{\partial x^2}, \quad y(t) < x < \infty, \quad (2)$$

$$T_{solid}(x, t)|_{t=0} = T_{solid}(x, t)|_{x=\infty} = T_0, \quad (3)$$

$$\frac{\partial Q(t)}{\partial t} + \lambda_{liquid} \cdot \frac{\partial T_{liquid}(x, t)}{\partial x} \Big|_{x=0} = 0, \quad (4)$$

$$T_{liquid}(x, t)|_{x=y(t)} = T_{solid}(x, t)|_{x=y(t)} = T_1, \quad (5)$$

$$\lambda_{liquid} \cdot \frac{\partial T_{liquid}(x,t)}{\partial x} \Big|_{x=y(t)} = H \cdot \rho \cdot y'(t) + \lambda_{solid} \cdot \frac{\partial T_{solid}(x,t)}{\partial x} \Big|_{x=y(t)} \quad (6)$$

where $y(t)$ is the moving boundary of the phase transition; $Q(t)$ is the absorbed energy per surface unit for the time $t \ll \tau$, here τ denotes the duration of a laser pulse; $a = \frac{\lambda}{c \cdot \rho}$ is thermal diffusivity, where λ , c and ρ denote correspondingly thermal conductivity, specific heat and density of a metal ($a_{solid}, \lambda_{solid}, c_{solid}, \rho_{solid}$) or liquid ($a_{liquid}, \lambda_{liquid}, c_{liquid}, \rho_{liquid}$); T_0 and T_1 denote

correspondingly the initial temperature of the solid body and the temperature of the phase transition; H is the latent melting heat, which is absorbed on the moving phase boundary. Supposing that the temperature of the metal surface processed by laser pulse achieves phase transition point during the time $t_0 \ll \tau$ and the temperature of the liquid phase varies slightly during the further process $t_0 < t < \tau$, we can replace the boundary condition (4) by the following more simple condition:

$$T_{liquid}(x,t) \Big|_{x=0} = T_2 = T_{liquid}(x,\tau) \Big|_{x=0} > T_1, \quad (7)$$

where T_2 is a temperature of molten metal on the surface that can be defined by the heat balance equation.

Combining (1)-(3), (5) and (7) we can write that

$$T_2 = T_1 + \frac{\operatorname{erf}\left(\frac{\beta}{\sqrt{2 \cdot a_{liquid}}}\right)}{2 \cdot c_{liquid} \cdot \rho \cdot \sqrt{a_{liquid}} \cdot \left(1 - e^{-\frac{\beta^2}{2 \cdot a_{liquid}}}\right) \cdot \operatorname{erfc}\left(\frac{\beta}{\sqrt{2 \cdot a_{solid}}}\right)} \times \left\{ \left(\sqrt{\frac{\pi}{\tau}} \cdot Q(\tau) - \sqrt{2 \cdot \pi} \cdot H \cdot \rho_{solid} \cdot \beta \right) \cdot \operatorname{erfc}\left(\frac{\beta}{\sqrt{2 \cdot a_{solid}}}\right) - 2 \cdot c_{solid} \cdot \rho_{solid} \cdot (T_1 - T_0) \right\}, \quad (8)$$

where $\operatorname{erf}(\omega) = \frac{2}{\sqrt{\pi}} \cdot \int_0^\omega e^{-\xi^2} d\xi$ is the Gauss error function; $\operatorname{erfc}(\omega) = 1 - \operatorname{erf}(\omega)$ is the complementary

error function; the parameter β can be found from the following transcendental equation:

$$\frac{2 \cdot \sqrt{\frac{a}{\pi}} \cdot c \cdot \rho \cdot (T_1 - T_0)}{\operatorname{erfc}\left(\frac{\beta}{\sqrt{2 \cdot a}}\right)} = \sqrt{2} \cdot H \cdot \rho \cdot \beta \cdot \left(e^{-\frac{\beta^2}{2 \cdot a}} - 2 \right) + \frac{Q(\tau)}{\tau}, \quad (9)$$

$$Q(\tau) = H \cdot \rho \cdot y(\tau) + \int_0^{y(\tau)} c_{solid} \cdot \rho_{solid} \cdot (T_1 - T_0) dx + \int_0^{y(\tau)} c_{liquid} \cdot \rho \cdot (T_{liquid} - T_1) dx + \int_{y(\tau)}^\infty c_{solid} \cdot \rho_{solid} \cdot (T_{solid} - T_0) dx. \quad (10)$$

The formulas (8)-(10) allow us to calculate the melting depth of different solid materials irradiated by laser pulses of various duration and energy. As it has already been mentioned above, under the influence of laser irradiation high temperature stress occurs in the metals. The deformation process in these

conditions is followed by residual deformation, whose appearance is related to nonelastic effects and reorganization of crystal's defect structure. Stress' relaxation can have a heterogeneous character due to the formation of new structure zones called relaxation zones [32] in the old excited structure. Depending on

the state of the system, on the conditions of external influence, on the degree of process development it may occur that relaxation zones can be centers of a new phase, groups of dislocations and disclinations, microcracks, clusters of atoms and vacancies forming clusters, micropore, dislocation loops, etc. One can imagine the deforming as three simultaneously coexistent phases: relaxation field determined by the

parameter $\varphi_{i,j}(r,t)$, stress field $\sigma_{i,j}(r,t)$ corresponding to external load and relaxation zones with concentration $n(r,t)$. Temporary dependence $\varphi_{i,j}(r,t)$, $\sigma_{i,j}(r,t)$ and $n(r,t)$ is defined by the following system of nonlinear differential equations:

$$\begin{cases} \dot{\varphi}_{i,j} = -\kappa \cdot \varphi_{i,j} + g_1 \cdot n; \\ \dot{n} = -\gamma \cdot n + \frac{\varphi_{i,j} \cdot \sigma_{i,j}}{g_2}; \\ \dot{\sigma}_{i,j} = \nu \cdot (\sigma_{i,k} - \sigma_0) - g_3 \cdot \varphi_{i,j} \cdot n, \end{cases} \quad (11)$$

where parameters κ , γ , ν , g_i ($i = \overline{1,3}$) are material constant; quantity σ_0 is determined by the applied external loads and corresponds to the residual stress set as the result of relaxation.

In the system (11) the term $-\kappa \cdot \varphi_{i,k}$ is the decay of the relaxation process; the term $-\gamma \cdot n$ describes disintegration of the formed relaxation zones; the term $\nu \cdot (\sigma_{i,k} - \sigma_0)$ describes the stress relaxation in linear approximation, when their interference is absent; the term $g_1 \cdot n$ is related to the relaxation field generation due to the formation of relaxation zones; the term $\frac{\varphi_{i,k} \cdot \sigma_{i,k}}{g_2}$ takes into account the influence of

the relaxation field $\varphi_{i,j}(r,t)$ and stress field $\sigma_{i,j}(r,t)$ on the generation of relaxation zones; the term $g_3 \cdot \varphi_{i,j} \cdot n$ is caused by the influence of the relaxation field and the relaxation zones on the speed of stress relaxation. As the speed of alteration of the relaxation field is much lower than the speed of the processes atomic relaxation described by the constants γ and ν , in (7) one can use adiabatic elimination of variables. Taking into account possible spatial fluctuations whose role grows as the temperature and external loads increase, we get the following kinetic equation for the relaxation parameter:

$$\varphi_{i,j} = D \cdot \Delta \varphi_{i,j} + \frac{g_1}{g_2 \cdot \gamma} \cdot \left\{ \left(\sigma_0 - \frac{g_2 \cdot \gamma}{g_1} \cdot \kappa \right) \cdot \varphi_{i,j} - \frac{g_3 \cdot \sigma_0}{g_2 \cdot \gamma \cdot \nu} \cdot \varphi_{i,j}^3 \right\}, \quad (12)$$

where D is the diffusion coefficient of atoms in a warmed-up zone.

If we take into account the diffusion's dispersion, then equation (12) will turn into the well-known Ginzburg-Landau generalized equation ([33], [34]).

For $\sigma_0 < \sigma_c = \frac{g_2 \cdot \gamma}{g_1} \cdot \kappa$ equation (12) has one stable solution $\varphi_{i,j}(r,t) = 0$; if exceeding of the critical value $\sigma_0 > \sigma_c$ occurs, new coherent states of the system are realized with spatial periodicity, whose

period can be calculated using the formula

$$P = \frac{\sigma_0 - \sigma_c}{2 \cdot \pi \cdot \sigma_0} \cdot \sqrt{\frac{3 \cdot D}{8 \cdot \nu}}.$$

Using the kinetic equation from the theory of surface nucleation ([2], [28], [29], [30]) as well as the variational principle for the main laws of thermal conduction, one can obtain ([31]) the following closed formula for the characteristic size-radius of a crystalline phase nucleus in a supercooled liquid:

$$r(t) = \nu_0 \cdot d \cdot e^{-\frac{U}{k \cdot T_1}} \cdot \frac{k \cdot T_1^2}{U \cdot \varepsilon} \cdot \left(\frac{h}{U+h} - e^{-\frac{U \cdot \varepsilon \cdot t}{k \cdot T_1^2}} + \frac{U}{U+h} \cdot e^{-\frac{(U+h) \cdot \varepsilon \cdot t}{k \cdot T_1^2}} \right), \quad (13)$$

where ν_0 is the Debye oscillation frequency of atoms in a supercooled liquid; U is the activation energy for atom movement; $k \cdot T$ is thermal energy; d is the characteristic size for a single atom; h is the heat of the phase transformation for one atom; ε is the average speed of melt cooling. Using the formula (13) one can precisely estimate the characteristic size-radius of a crystalline phase nucleus, that is, the size of nanostructures appearing on the surface of the processing solid body, while it is melting under laser pulse irradiation.

Experimental facilities, experiments and results

Experimental facilities

Within the present study we have carried out a series of six experiments devoted to direct laser nanostructuring of titanium (Ti) and copper (Cu) surface. All the processed samples had the same sizes: $L \times W \times H = 5 \times 3 \times 0.1 \text{ mm}$. The surfaces of the samples had 14th surface finish class. The samples were placed in a laser facility chamber Nd³⁺:YAG crystal and were irradiated in a motionless laser beam. For a detailed analysis of the irradiated samples' profiles we used a desktop scanning electron microscope TM3030 with low vacuum regime, which allows us to carry out the experiments without sample preparation and to investigate samples without prior metal deposition; controlled by a simple and understandable interface with the functions of automatic focus, contrast and brightness setting; equipped with two detectors – of secondary and reflected electrons, – owing to which it is possible to get comprehensive information about the surface of the investigated samples. The laser facility Nd³⁺:YAG crystal, which was used in order to carry out a series of experiments devoted to direct laser nanostructuring of surfaces of 4 titanium and 2 copper samples, has the following capabilities: laser wavelength: 532 nm; maximum pulse energy: 0.15 J; pulse repetition rate: 10 Hz; initial pulse duration: 5÷9 ns; pulse duration: 5÷400 μs . After repeated irradiation with one beam of microsecond Nd³⁺:YAG crystal-laser formation of nanosized structures on the copper and titanium surfaces was observed. Laser irradiation intensity was maximal in the center of the irradiation spot and was going down closer to its periphery. After repeated pulse action on one surface patch, a deep crater appeared in the spot's center. However, on the periphery, where the laser irradiation intensity was lower, one could observe only some surface melting. Using SEM-analysis (that is, using

scanning electron microscopy with X-ray spectrometry microanalysis) no submicrometer structures were detected in the central high-intensity part of the spot. However, formation of nanorelief was detected in the peripheral part of the irradiation zone. For all six samples we detected roughness of a characteristic size along the surface on the surface in the peripheral low-intensity region of the spot as well as small-scale roughness in the form of saliences put over the surface. A round shape of the obtained nanoreliefs implies the surface being molten by the laser irradiation and subsequent crystallization with the formation of the above mentioned submicrometer structures. Taking into account the possibility of slight material melting, we can consider a surface under thermal flow of pulsed laser irradiation that provokes the solid-liquid phase transition.

Experiment 1

In this experiment copper foil was taken as a sample, and for its laser processing the following characteristics of microsecond laser facility Nd³⁺:YAG crystal were chosen: laser wavelength (LW): 532 nm; pulse energy (PE): 0.14 J; pulse repetition rate (PRR): 10 Hz; pulse duration (PD): 130 μs . The results of a single pulse action on this sample are shown in Fig.1. The obtained nanostructured surface has a good hydrophilic property with an average interfacial contact angle $\theta_{\text{average}} \approx 51^\circ$, where water was used as the liquid.

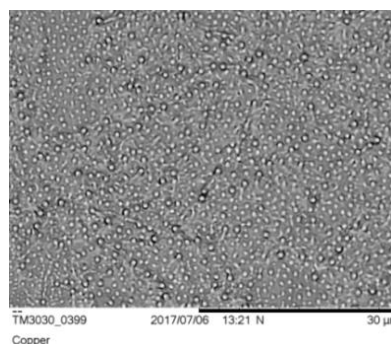


Fig. 1. Nanostructured copper surface (one-time processing) with an average contact angle of 51° (good hydrophilic property). Nd³⁺:YAG crystal-laser's features: LW=532 nm; PE=0.14 J; PRR=10 Hz; PD=130 μs .

Experiment 2

In this experiment copper foil was again taken as a sample, and for its laser processing the following characteristics of the microsecond laser facility Nd³⁺:YAG crystal were chosen: LW=532 nm; PE=0.14 J; PRR=10 Hz; PD=130 μs . The results of a twofold pulse action on this sample are shown in

Fig.2. The obtained nanostructured surface has a much worse hydrophilic property (more exactly, has a hydrophobic property) with an average interfacial contact angle $\theta_{average} \approx 115^\circ$, where water was used as the liquid.

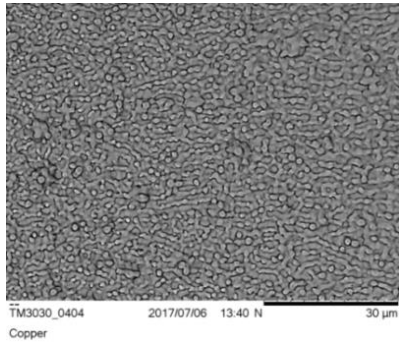


Fig. 2. Nanostructured copper surface (twofold processing) with an average contact angle of 115° (hydrophobic property). Nd³⁺:YAG crystal-laser's features: LW=532 nm; PRR=10 Hz; PD=130 µs.

Experiment 3

In this experiment titanium foil was taken as a sample, and for its laser processing the following characteristics of the microsecond laser facility Nd³⁺:YAG crystal were chosen: LW=532 nm; PE=0.15 J; PRR=10 Hz; PD=100 µs. The results of a single pulse action on this sample are shown in Fig.3. The obtained nanostructured surface has a very good hydrophilic property with an average interfacial contact angle $\theta_{average} \approx 28^\circ$, where both water and physiological solution NaCl 0.9% were used as the liquid.

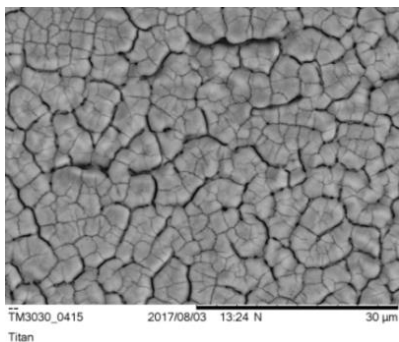


Fig. 3. Nanostructured titanium surface (one-time processing) with an average contact angle of 28° (very good hydrophilic property). Nd³⁺:YAG crystal-laser's features: LW=532 nm; PE=0.15 J; PRR=10 Hz; PD=100 µs.

Experiment 4

In this experiment titanium foil was again taken as a sample, and for its laser processing the following characteristics of the microsecond laser facility

Nd³⁺:YAG crystal were chosen LW=532 nm; PE=0.15 J; PRR=10 Hz; PD=130 µs. The results of a single pulse action on this sample are shown in Fig.4. The obtained nanostructured surface has a good hydrophilic property with an average interfacial contact angle $\theta_{average} \approx 42^\circ$, however it is slightly worse than in the results of the third experiment. In this experiment both water and physiological solution NaCl 0.9% were used as the liquid.

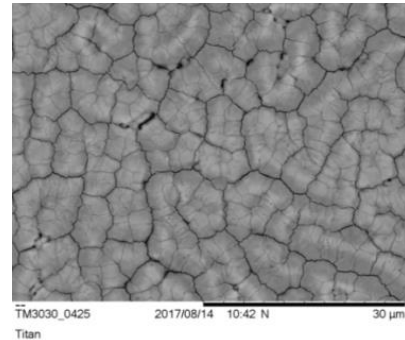


Fig. 4. Nanostructured titanium surface (one-time processing) with an average contact angle of 42° (good hydrophilic property). Nd³⁺:YAG crystal-laser's features: LW=532 nm; PE=0.15 J; PRR=10 Hz; PD=130 µs.

Experiment 5

In this experiment titanium foil was again taken as a sample, and for its laser processing the following characteristics of the microsecond laser facility Nd³⁺:YAG crystal were chosen: LW=532 nm; PE=0.15 J; PRR=10 Hz; PD=85 µs. The processing was implemented by the stripes with the use of a lens for focusing of the laser beam. The results of a single pulse action on this sample are shown in Fig.5. The obtained nanostructured surface has the following hydrophilic property: the liquid (both water and physiological solution NaCl 0.9%) flows only in one direction,

$$\theta_{average} \approx \begin{cases} 66^\circ & \text{on processed strips,} \\ 134^\circ & \text{between processed strips.} \end{cases}$$

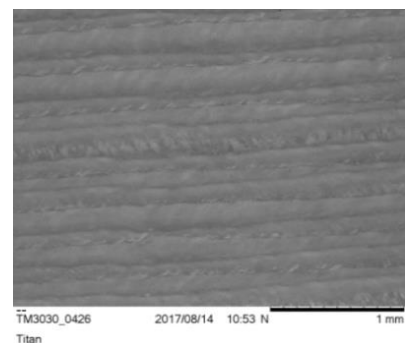


Fig. 5. Nanostructured titanium surface (one-time processing with a lens for focusing of a laser beam) with an average contact

angle of 66° on processed strips: the liquid flows only in one direction. Nd³⁺:YAG crystal-laser's features: LW=532 nm; PE=0.15 J; PRR=10 Hz; PD=85 μ s.

Experiment 6

In this experiment titanium foil was again taken as a sample, and for its laser processing the following characteristics of the microsecond laser facility Nd³⁺:YAG crystal were chosen: LW=532 nm; PE=0.15 J; PRR=10 Hz; PD=300 μ s. The results of a single pulse action on this sample are shown in Fig.6. The obtained nanostructured surface has a very good hydrophilic property with an average interfacial contact angle $\theta_{average} \approx 34^\circ$, where both water and physiological solution NaCl 0.9% were used as the liquid.

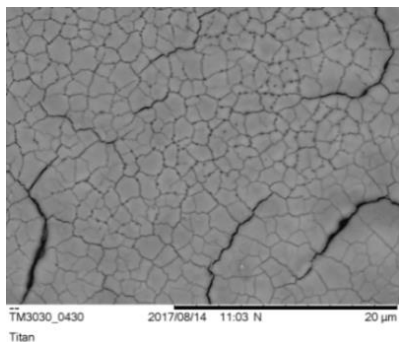


Fig. 6. Nanostructured titanium surface (one-time processing) with an average contact angle of 34° (very good hydrophilic property). Nd³⁺:YAG crystal-laser's features: LW=532 nm; PE=0.15 J; PRR=10 Hz; PD=300 μ s.

Conclusions

In this paper, the theoretical basis of a hydrophilic nanostructure formation process on a titanium surface by direct laser irradiation is described in detail. The design formulas, with the help of which it is possible to determine the shape of the phase interface; to calculate the melting depth of solid material irradiation with laser pulses of various duration and energy; to precisely estimate the characteristic size-radius of a crystalline phase nucleus; etc., are given in closed form. Besides, in this paper, the experimental means and conditions, and the results of a series of six experiments carried out on direct laser nanostructuring of titanium and copper surfaces are described in detail.

Acknowledgements

For the first two co-authors, the present article was elaborated within the framework of the State Research Programme "Next Generation Information and Communication Technologies (NexIT)", Project No. 4.

References

1. Eletsii, A. V., Erkimbaev, A. O., Zitserman, V. Yu., Kobzev, G. A., Trakhtengerts, M. S. Thermophysical Properties of Nanoobjects: Data Classification and Validity Evaluation. *Journal of High Temperature*, 2012, Vol. 50, No. 4, p. 488-495.
2. Cao, G. *Nanostructures and Nanomaterials: Synthesis, Properties, and Applications*. London: Imperial College Press, 2004, xiv+433 p.
3. Bhushan, B., Israelachvili, J. N., Landman, U. Nanotribology: Friction, Wear and Lubrication at the Atomic Scale. *Nature: International Journal of Science*, 1995, Vol. 374, No. 6523, p. 607-616.
4. Hao, L., Lawrence, J. *Laser Surface Treatment of Bio-Implant Materials*. Chichester: John Wiley & Sons, 2005, xix+211 p.
5. Oshida, Y. *Bioscience and Bioengineering of Titanium Materials*. Waltham: Elsevier, 2013, xiv+500 p.
6. Remeeva, E. A., Rozanova, I. B., Elinson, V. M., Sevastianov, V. I. Influence of Biomaterials Surface on Platelets Release ATP in vitro. *International Journal of Artificial Organs*, 2013, Vol. 26, No. 7, p. 634-639.
7. Israelachvili, J. N. *Intermolecular and Surface Forces: With Applications to Colloidal and Biological Systems*. New York: Academic Press, 1992, xxi+450 p.
8. Kendall, K. Adhesion: Molecules and Mechanics. *Journal of Science*, 1994, Vol. 263, No. 5154, p. 1720-1725.
9. Majumder, A., Ghatak, A., Sharma, A. Microfluidic Adhesion Induced by Subsurface Microstructures. *Journal of Science*, 2007, Vol. 318, No. 5848, p. 258-261.
10. Ferrara, M. C., Pilloni, L., Mazzarelli, S., Tapfer, L. Hydrophilic and Optical Properties of Nanostructured Titania Prepared by Solgel Dip Coating. *Journal of Physics D: Applied Physics*, 2010, Vol. 43, No. 9, 95301(37 p.).
11. Rios, P. F., Dodiuk, H., Kenig, S., McCarthy, S., Dotan, A. The Effects of Nanostructure and Composition on the Hydrophobic Properties of Solid Surfaces. *Journal of Adhesion Science and Technology*, 2006, Vol. 20, No. 6, p. 563-587.
12. Khomich, V. Yu., Urlichich, Yu. M., Shmakov, V. A., Tokarev, V. N., Galstyan, A. M., Mikolutskiy, S. I., Malinskiy, T. V., Ganin, D. V. Formation of Submicron Structures on the Surface of Zirconium Dioxide under Illumination of Nanosecond Laser. *Journal of Inorganic Materials: Applied Research*, 2013, Vol. 4, No. 3, p. 201-204.
13. Khasaya, R. R., Khomich, Y. V., Malinskiy, T. V., Mikolutskiy, S. I., Yamshchikov, V. A., Zhelezov, Y. A. Titanium Surface Processing by Nanosecond Laser Radiation. *Letters on Materials*, 2014, Vol. 4, No. 1, p. 45-48.
14. Zaimis, U., Guseynov, Sh. E. Scientifically Substantiated Guidelines for Physico-mathematical Modelling of Laser Surface-treatment of Wear-resistant Implants for Human Joint Replacements. *In: Proceedings of the 11th International Scientific and Practical Conference "Environment. Technology. Resources"*, Vol. 3, 2017, p. 350-356.
15. Adamson, A. W., Gast, A. P. *Physical Chemistry of Surfaces*. New York: John Wiley & Sons, 1997, xxi+784 p.
16. *Современная теория капиллярности: к 100-летию теории капиллярности Гиббса* / под редакцией А.И. Русанова, Ф.Ч. Гудрича. Ленинград: Химия, Ленинградское отделение, 1980, 340 p.
17. Blkerman, J. J. Capillarity before Laplace: Clairaut, Segner, Monge, Young. *Archive for History of Exact Sciences*, 1978, Vol. 18, No. 2, p. 103-122.
18. Bakker, G. *Handbook on Experimental Physics, Vol. 6: Capillarity and Surface Tension*. Leipzig: Akademische Verlagsgesellschaft, 1928, xv+458 p.
19. Churaev, N. V., Derjaguin, B. V., Muller, V. M. *Surface Forces*. Berlin: Springer-Verlag, 1987, 440 p.

20. Гохштейн, А. Я. *Поверхностное натяжение твердых тел и адсорбция*. Москва: Наука, 1976, 400 с.
21. Кикоин, А.К., Кикоин, И.К. *Молекулярная физика*. Москва: Наука, 1976, 480 с.
22. Оно, S., Kondo, S. Molecular Theory of Surface Tension in Liquids. *In: Structure of Liquids. Encyclopaedia of Physics*. Berlin-Heidelberg: Springer-Verlag, 1960, Vol. 3, No. 3, p. 134-280.
23. Лабунцов, Д. А., Ягов В. В. *Гидростатическое равновесие и волновые движения газожидкостных систем*. Москва: Московский энергетический институт, 1977, 72 с.
24. Landau, L. D., Lifshitz, E. M. *Course of Theoretical Physics, Vol. 6: Fluid Mechanics*. Oxford Pergamon Press, 1987, xiii+539 p.
25. Зимон, А. Д. *Адгезия жидкости и смачивания*. Москва: Химия, 1974, 412 с.
26. Khomich, V. Yu., Mikolutskiy, S. I., Shmakov, V. A., Yamschikov, V. A. Model of Nanostructure Formation on Solid Surface Melted by Laser Pulse. *In: Proceedings of the International Conference on Nanomaterials: Application & Properties*, 2012, Vol. 1. No. 4, 04RES01(4 p).
27. Миколуцкий, С. И., Хомич, В. Ю., Ямщиков, В. А., Токарев, В. Н., Шмаков, В. А. Исследование процессов формирования наноструктур на поверхности материалов под действием излучения ArF-лазера. *Успехи прикладной физики*, 2013, Том 1, № 4, с. 548-553.
28. Pomogailo, A. D., Kestelman, V. N. *Metallopolymer Nanocomposites*. Berlin-Heidelberg: Springer-Verlag, 2005, xx+564 p.
29. Deb, P. *Kinetics of Heterogeneous Solid State Processes*. New York: Springer, 2014, vii+49 p.
30. Barret, P. *Kinetics of Heterogeneous Processes*. Paris: Gauthier-Villars, 1973, 574 p.
31. Tokarev, V. N., Shmakov, V. A., Khomich, V. Yu., Khasaya, R. R., Mikolutsky, S. I., Nebogatkin, S. V., Yamschikov, V. A. Review of Methods of Direct Laser Nanostructuring Technological Materials. *In: Proceedings of the 29th International Congress on Applications of Lasers and Electrooptics*, 2010, p. 1257-1265.
32. Khomich, V. Yu., Shmakov, V. A. Formation of Periodic Nanodimensional Structures on the Surface of Solids during Phase and Structural Transformations. *Doklady Physics*, 2012, Vol. 57, No. 9, p. 349-351.
33. Gurtin, M. E. Generalized Ginzburg-Landau and Cahn-Hilliard Equations Based on a Microforce Balance. *Journal of Physics D: Nonlinear Phenomena*, 1996, Vol. 92, No. 3-4, p. 178-192.
34. Hohenberg, P. C., Krekhov, A. P. An Introduction to the Ginzburg-Landau Theory of Phase Transitions and Nonequilibrium Patterns. *Journal of Physics Reports*, 2015, Vol. 572, p. 1-42.

LAND MANAGEMENT AND GEODESY

DOI: 10.22616/CE.2017.009

Common Studies of National Height System in Latvia and Lithuania

Armands Celms¹, Ilona Reķe¹, Jānis Kaminskis², ¹Latvia University of Agriculture, ²Riga Technical University

Abstract. Already after our independence in the nineties of the twentieth century, we used common height system - Baltic Normal height system 1977 (BHS 1977). Latter we have made big job for verification and modernization of our geodetic network in the frames of different international campaigns. There we always cooperating with Nordic countries in frames of Nordic Geodetic Commission (NKG). Also we have had sector programme between Denmark and Baltic countries about modernization of geodetic network. Already in that time we carried out common work in the field of gravity survey, levelling and GNSS observation. As European Union member states – Latvia and Lithuania have changed their national height systems to European Vertical Reference System realizations. Latest product of such efforts, we have freely available latest Nordic quasi-geoid model NKG2015, too. For studies of height network consistency in regional and international level we carry out GNSS observation campaigns and making comparison of the obtained survey results and computed ones from different geoid models, for example LV98, NKG2015, EGG2015 etc. In such way, we are making conclusions about quality of geodetic network and giving recommendation for the future work. The aim of the research is using GNSS measurements gain insight for methodology development of geodetic point height testing. To achieve the aim following tasks were set: 1) perform GNSS measurements of first order levelling network points in Latvia and Lithuania; 2) to do data processing to get station coordinates; 3) to compare point elevations. For GNSS measurements use for height determination it is very significantly to use advanced measuring technologies and verified data processing methodology. RMS errors describe high accuracy of performed measurements.

Keywords: vertical network, GNSS, geoid model, normal height.

Introduction

Already after our independence in the nineties of the twentieth century we used common height system - Baltic Normal height system 1977 (BHS 1977). Latter we have made big job for verification and modernization of our geodetic network in the frames of different international campaigns. First common international campaign for verification of our geodetic network should be mentioned Danish-Baltic sector program, which took place in all three countries [9]. There geodesists from Danish National Land survey – KMS shared their experience and gave recommendations for future works. Besides theoretical studies, there were done practical control measurements on first order levelling lines to control stability of benchmarks. There we always cooperating with Nordic countries in frames of Nordic Geodetic Commission (NKG). Also we have had sector programme between Denmark and Baltic countries about modernization of geodetic network. Already in that time we carried out common work in the field of gravity survey, levelling and GNSS observation. And as a latest product of such efforts we have freely available Nordic quasi-geoid model NKG2015. For studies of height network consistency in regional and international level we carry out GNSS observation campaigns and making comparison of the obtained survey results and computed ones from different geoid models, for example LV98, NKG2015, EGG2015 etc. In such way we can make conclusions

about quality of geodetic network and make recommendation for the future work.

The heights between Baltic states in BHS 1977 were connected in united geodetic network. But since 1st December 2014 in Latvia as a national height system finds the European Vertical Reference System realization in Latvia – Latvian Normal Height System 2000,5 (LHS-2000,5) [1]. Lithuania has changed their national height system to European Vertical Reference System realization in Lithuania – Lithuanian height system LAS07 on January 1st, 2016. Approximately difference between the old (BHS 1977) and new height system (LAS07) in the middle of Lithuania is about 14 cm. Estonia has changed their national height system to European Vertical Reference System realization on January 1st, 2018.

Nowadays the Global Navigation Satellite System (GNSS) offers more and more advantages. To gain insight for methodology development of geodetic point height testing using GNSS measurements authors did measurements of 13 first order levelling network points in the territory of Latvia and 5 first order levelling network points in the territory of Lithuania using GNSS method. This method was chosen because of their simplicity – using global positioning and calculating ellipsoidal coordinates it is possible to see the height difference control in height system datum point and regional main geodetic

points [13]. On points where direct GNSS observations are not possible to do due to satellite invisibility there is still need for precise levelling works [5].

For precise geodetic GNSS measuring, it is necessary to have a precise quasigeoid model. Since 1st December 2014 Latvian specialists have developed a new quasigeoid model LV'14 with 4 cm accuracy [12]. Lithuanian digital geoid model will be improved after completing the first and second order of geodetic vertical network, as well terrestrial gravity measurements. This will enable to derive normal height from ellipsoidal heights determined by GNSS and replace traditional levelling of lower orders [10].

The aim of the research is to gain insight for methodology development of geodetic point height testing using GNSS measurements. To achieve the aim following tasks were set: 1) perform GNSS measurements of first order levelling network in Latvia and Lithuania; 2) to do data processing to get station coordinates; 3) to compare point elevations.

Materials and Methods

Establishment of Latvian National First Order Levelling Network has begun in 2000. Field measurements were finished in 2010 [3]. Geodetic measurements were made by the specialists of the Latvian State Land Service from 2000 till 2005 and Latvian Geospatial Information agency from 2006 till 2010. For the network establishment were used data of geodetic and gravimetric observations. The general requirement for not exceeding RMS error 0.5 mm/km of the measured height differences was followed in the course of establishment of the National First Order Levelling Network [4].

Lithuanian National First Order Network (NGVN) establishment was going on from 1998 till 2007. Contracting authority for network establishment was National Land Service under the Ministry of Agriculture. The network consists of 5 loops in total of precise levelling lines [1].

Connection between Latvian and Lithuanian vertical networks was made in three places so connecting lines and constructing two first order levelling loops. The accuracy of Latvian and Lithuanian united levelling network in first iteration (standard deviation is 0.617 kgal×mm/km) is at the same level as that of the vertical networks of biggest part of other countries participating in UELN project [1]. In 2008 Lithuania has also created two border connection points with Poland so connecting Lithuanian vertical network to European vertical network [11]. Now after national height systems' replacement from BHS 1977 to European Vertical Reference System realisations in Latvia and Lithuania the height connection between Latvia and Lithuania do not work [6].

For height determination traditionally were used precise levelling and nowadays mostly for measurements and height determination we also using GNSS as advanced instrument and new innovative technology. There are many opportunities to do studies on heights and compatibility between selected geodetic points. Very suitable instrument for studies or research on geodetic consistency is homogenous quasi-geoid or geoid model over decided area. On our case we found suitable geoid model LV98 (Fig. 1.) for this purpose. Geoid model LV98 were used in Latvia till December 1st, 2014. In the future we are planning to introduce also NKG2015 geoid for validation and verification of geodetic network [12].

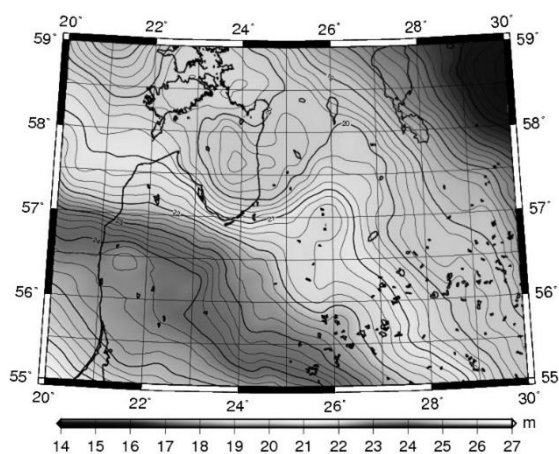


Fig. 1. Geoid model LV98 for territory of Latvia and Lithuania (source: authors' drawing).

As the first work for the GNSS measurements was the national geodetic network point inspection. There were some possible points selected and then visited on site to detect for each point the horizon above point

and possibility to use GNSS methods for its height determination, also the point location conformity to point sketch. On the point were done global positioning real time measurements to detect the

location of satellites above point. The requirement of open area is 20 degrees and for GNSS measurement PDOP should be at least 4 satellites. From the inspected points there were thirteen 1st class levelling network points chosen as an appropriate geodetic point for GNSS measurements – ground marks 1415,

1001, 37, 1155, 1537, 1636, 1676, 1727, 8248 and fundamental marks 1484, 0608, 3389 and 1463. In Lithuania were measured following first order geodetic points: ground marks 44V-988, 74V10308, 63V-01, 52V10013 and 74V10389 (Fig. 2).

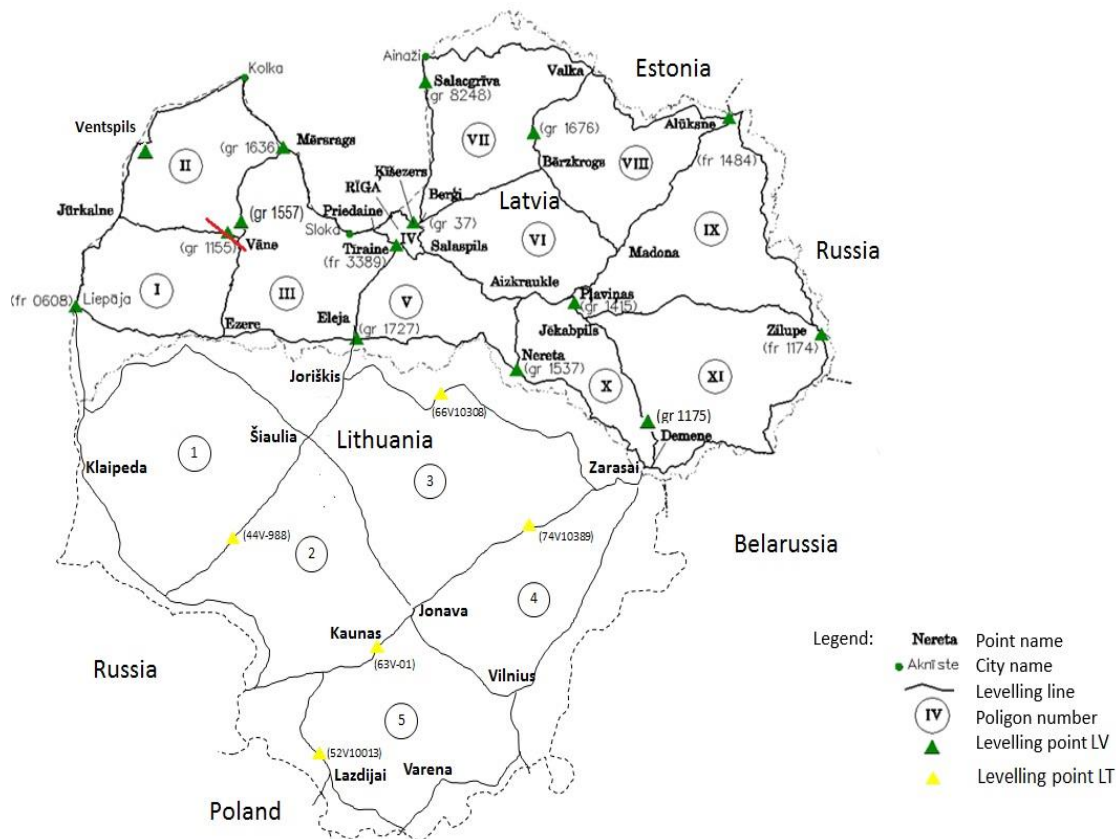


Fig. 2. Performed GNSS measurements in 1st class levelling network of Latvia and Lithuania (source: authors' drawing).

The involved specialists in this project were from Latvian University of Agriculture, Riga Technical University, Latvia University, Aleksandras Stulginskis University, Kaunas Technical University and some private companies from Latvia. The main idea was to perform GNSS measurements on all selected points in the same time using global positioning in post-processing mode so providing avoidance from some errors.

Three years were performed 3 measurement sessions of Latvian first order levelling network – 14th December 2012, 22th November 2013 and 27th November 2014. On June 30th, 2016 were performed 4th session and additionally involved experts from Lithuania. In this session in the same time were measured 13 first order levelling points in Latvia and 5 first order levelling points in Lithuania (Fig. 2.).

In measuring sessions from 2012 – 2014 the GNSS measurement has taken at least 4 hours long in the morning about 10 to 14 o'clock in Latvia Positioning System Base Station (LatPOS) network. LatPos is GNSS continuously operating network of Latvia [6]. On each first class levelling network point

was installed GNSS receiver – Leica, Trimble, Topcon or GeoMax receiver – and 4 hours long collected GNSS data. In 2016 the duration of measurements was 5 hours in early morning about 6 to 11 o'clock in LatPOS network and Lithuania Positioning System Base Station (LitPOS) network.

After measuring for precise data processing and adjustment there were collected data from 3 nearest LatPOS or LitPOS base stations. The data from GNSS receivers and LatPOS/LitPOS stations were used for data adjustment and point height determination [15].

GNSS collected data were processed and analyzed by authors using academic software package Bernese GNSS Software (Version 5.2). There were raised following requirements for data processing: cut off angle – 20 degrees above horizon, precise ephemerides, NGS antenna calibration models, closest vector selection and free network adjustment.

Results and Discussion

For GNSS data processing was used software Bernese GNSS Software version 5.2. Reference

points were selected 9 EPN (EUREF permanent network) stations: BOR1, GLSV, MAR6, ONSA, Riga, LAMA, LAMA, JOEN, PULK, VLNS.

All stations on 30th of June 2016 assigned to Class A. For input data were used satellite ephemerides, the Earth's rotation parameters, ionosphere model and code shift (differential Code Biases (DCB)).

In the first processing step reference stations were converted to the day when the observations were made using the rates of IGB08.vel file. International GNSS Service (IGS) reference surface IGB08 is partial (incomplete) update the previous version IGS08. Several IGS08 station unusable observation failure and other operational reasons. IGB08 goal is to provide a reference surface.

Vectors were generated using automatic baseline creation options OBS-MAX. This option automatically generates vectors after the maximum number of common observation. The first option is calculated on the estimated float solution. Then it is calculated uncertainties. Uncertainty was calculated based on all approaches to the methods offered by the software Bernese v 5.2: after the phase-based Wide-lane (WL) uncertainties (vectors shorter than 200 km), Phase-Based Wide-lane (L5) Ambiguity Resolution (<200 km), after the phase-based Narrow-lane (NL) uncertainties (vectors shorter about 200 km) and quasi-free ionosphere strategies (QIF). Treatment was performed using 3-degree angle. After the uncertainty of estimates is calculated using the final solution "free constraint solution" option. The

minimum amount of constraint solution - define the Geodetic datum of the site coordinates using Network Conditions [8].

Each station is identified by one of the notes in the "e/f/h". This means e - estimated station coordinates (and / or rates are calculated), f - FIXED: Fixed Station with its "a priori" values h - HELMR: Station measured and used to determine the limits of e - ECCEN: Applies the eccentric station.

The next calculations of coordinates and velocity determination of each station or any network restrictions.

It should be noted that the day-long session with the selected item spacing 2 hours, 12 + 1 = 13 parameters. 2017 measurement processing for 2016 used a 1-hour interval.

A priori tropospheric model and global mapping function - DRY GMF is used in conjunction with the "wet" mapping function WET_GMF Computation of the partial derivatives of the troposphere zenith delay parameters (not for the a priori troposphere model). Gradient adjustment model - CHENHER. (Chen and Herring). Relative tropospheric zenith delay is equal to 5 m [7].

At the processing stations may choose station to be excluded from the assessment of the troposphere. This is necessary to choose the relative tropospheric modelling for small networks. Tropospheric parameters are summarized in file and applicate to stations for which data are available in the troposphere

TABLE 1

Station coordinates and evaluation (reference epoch 2016-06-30 12:00:00) (Source: construction by authors)

Station	Name	N [GG.GGGGGG]	E [GG.GGGGGG]	U [m]	RMS error (N)[m]	RMS error (E)[m]	RMS error (U) [m]
37	3700001	57.008253	24.244461	27.753	0.001	0.002	0.003
677	67700001	55.387412	25.056543	150.839	0.002	0.002	0.006
1026	102600001	57.684461	22.317175	24.718	0.001	0.001	0.004
1175	117500001	55.738400	26.679104	175.516	0.001	0.001	0.002
1415	141500001	56.585332	25.778344	98.174	0.001	0.001	0.003
1463	146300001	57.012043	21.390681	35.848	0.001	0.001	0.005
1537	153700001	56.252400	25.216775	101.930	0.001	0.001	0.004
1557	155700001	56.946010	22.602501	104.316	0.001	0.001	0.004
1636	163600001	57.385169	22.972672	27.534	0.001	0.001	0.005
1676	167600001	57.454856	25.421595	78.702	0.001	0.001	0.004
1727	172700001	56.415087	23.696916	55.308	0.001	0.001	0.004
5770	577000001	55.429877	22.628199	137.163	0.001	0.001	0.004
BOR1	12205M002	52.276958	17.073460	124.359	0.000	0.000	0.001
GLSV	12356M001	50.364184	30.496736	226.313	0.000	0.000	0.001
JOEN	10512M001	62.391175	30.096163	113.795	0.000	0.000	0.001
KAUN	KAUN00001	54.877735	24.005481	60.785	0.002	0.002	0.006
LAMA	12209M001	53.892402	20.669945	187.032	0.000	0.000	0.001
MAR6	10405M002	60.595145	17.258530	75.533	0.000	0.000	0.001
ONSA	10402M004	57.395300	11.925521	45.608	0.000	0.000	0.001
PEDE	PEDE00001	57.494531	27.338593	176.513	0.002	0.002	0.008
PULK	12305M001	59.771840	30.327787	101.170	0.000	0.000	0.001
RIGA	12302M002	56.948621	24.058778	34.727	0.000	0.000	0.001
VLNS	10801M001	54.653144	25.298673	240.843	0.000	0.000	0.001
ZILU	ZILU00001	56.370086	28.118101	158.208	0.001	0.001	0.003

Each of the 24 surveyed stations are calculated using tropospheric parameters of Latvian and Lithuanian territory. The points were calculated referencing 9 EPN stations (BOR1, GLSV, JOEN, LAMA, MAR6, ONSA, PULK, RIGA, VLNS) in epoch 30.06.2016. (using velocity file (*.vel) for reference stations). As input data were used code shifting (P1C11606.DCB, P1P21606.DCB), Earth rotation parameters (COD19037.ERP), precise orbits (COD19034.EPH) and ionospheric model (COD19034.ION). The point evaluation of the North and East values is less than 2 mm. Height component average value is approximately 3 mm, and in some points it reaches 6 and 8 mm (677, KAUN and PEDE).

About correct geodetic data there is common ongoing activities within Nordic Geodetic Commission (NKG) for compatible local geoid model all over region. Very essential for good results is to use correct or accurate geodetic data. For modelling also gravity data should be verified or cross validated between different survey campaigns and sources [14]. It is great contribution for new NKG2015 geoid model over region, which was released during gravity field meeting International Symposium on Gravity, Geoid and Height Systems 2016 Thessaloniki, Greece on 19 – 23 September 2016. Also selected GNSS and levelling nodal or reference points from every country are used for control or accuracy estimation from official NKG database. Usually in database countries store the best available geodetic data for research and development of new applications.

Conclusions

For such GNSS measurement project successful organization it is very necessary to do previous preparation and critical situation analysis. Also performing GNSS measurements in the same time in the territory of Latvia and Lithuania the experience of mutual cross-border cooperation is accumulated.

References

1. **Aleksejenko, I., Kaminskis, J., Sakne, J.,** et al. Levelling network Connection Between Latvia and Lithuania. *Environmental Engineering*, Lithuania: Vilnius Gediminas Technical University, 2011, p. 1269-1278.
2. **Celms, A., Bimane I., Reke I.** European Vertical Reference System in Baltic Countries. *Baltic Surveying*, 2014, No. 1 (8), p. 49–55.
3. **Celms, A., Kaminskis, J.** Levelling results of first order line Kolka – Rucava. *Baltic Surveying '05*, 2005, Latvia: Latvia University of Agriculture, p. 165-170.
4. **Celms, A., Kronbergs, M., Cintina, V.** Accuracy Estimation of the Latvia First Order levelling Network. *GEOFORUM*, 2012, No.1, p. 44 – 47.
5. **Celms, A., Kronbergs, M., Cintina V.,** et al. Precision of Latvia Levelling Network Nodal Point Height. *CIVIL ENGINEERING*, 2013, No. 4, p. 310-317.
6. **Celms A., Reke I., Ratkevics A.** European Vertical Reference System Influence in Latvia. *Innovative Materials, Structures and Technologies*, 2015 p. 30-37.
7. **Dach, R., Jean, Y.** Technical Report. (2012) *International GNSS Service*. [online 15.03.2017.]. ftp://igs.org/pub/resource/pubs/2012_techreport.pdf.
8. **Dach, R., Lutz, S., Walser, P.,** et al. Bernese GNSS Software. Version 5.2. Astronomical Institute, University of Bern, 2015.
9. **Ellmann A., Torim A., Abols N.,** et al. Different solutions adopted to modernize the height networks in the Baltic countries. *The importance of Heights Proc. "Geodesy and Surveying in the future"*, March 15–17, 1999, Gavle, Sweden, p. 349–360.
10. **Krikštonis, B., Paršeliūnas, E. K., Viskontas, P.,** et al. Designing issues of the geodetic vertical reference network of Lithuania. *Environmental Engineering*, 2014, p. 1-10.

For GNSS measurement height determination it is very significantly to use advanced measuring technologies and verified data processing methodology. There we can use some knowledge from classical geodetic – astronomical approach that is rather independent method for height network validation.

Performed measurements have a high accuracy which describes RMS errors. Average error value for axis N and E is 0.001 m, but measurement height component average error value is 0.003 m.

The results obtained from GNSS measurements can be used for height system and geoid model conformity assessment in Baltic region. In connection with geoid model significance to geodetic result data precision, it is desirable to perform GNSS measurements of I class levelling networks in Latvia, Lithuania and Estonia. This way it can verify and test geoid model on larger areas thereby getting certainty about geoid model precision. I class geodetic network between Lithuania, Latvia and Estonia are physically levelled or directly connected. We can recommend for near future to use revitalizing method from classical geodesy coming from times before GPS was used. In this, we use digital zenith camera for deflection of vertical (DoV) measurements. It is like to use together knowledge of astronomy and geodesy as independent control for levelling, gravity and ellipsoidal heights from GPS observations. It is very useful to perform DoV observations on many control/nodal points in Lithuania and Latvia, as well in future also in Estonia, especially on islands. It will help to increase accuracy for geoid model on land and on sea. If the geoid model accuracy will increase (to 2 cm) the validity of calculated height values also will increase.

Acknowledgements

The research was supported by project “Strengthening Research Capacity in the Latvia University of Agriculture”.

11. **Krikštaponis, B., Tumeliene, E.** Development of Lithuanian National Geodetic Vertical First Order Network. *Environmental Engineering*, 2011 p. 1362-1369.
12. *Latvijas kvaziģeoīda modelis* (Latvian quasigeoid model) [online 13.11.2017.]. http://map.lgia.gov.lv/index.php?lang=0&cPath=2&txt_id=130
13. **Lazdāns, J., Aleksejenko, I., Kaminskis, J.,** et al. Aktualitāte Latvijas sasaistē ar Eiropas augstumu sistēmu (Current Events Latvia Connecting with European Height System). *Latvia University Scientific conference No.67*, 2009.
14. **Mārdla, S., Āgren, J., Strykowski, G.,** et al. From Discrete Gravity Survey Data to a High-resolution Gravity Field Representation in the Nordic-Baltic Region. *Marine Geodesy*, 2017, 40, p. 416 – 453.
15. **Reiniks, M., Lazdāns, J., Ratkus, B.** Valsts augstuma izejas līmeņa noteikšana (Determination of state height datum level). *Rīga Technical University scientific articles.No.7*, p 7-13.

Geodetic and Geotechnical Means of Sea Breakwaters' Monitoring System

Dainora Jankauskienė^{1,2}, Marija Eidukevičiūtė¹, Vitalijus Volkovas¹, ¹*Kaunas University of Technology*, ²*Klaipėda State University of Applied Science*

Abstract. The Baltic Sea breakwaters are important objects to ensure fluent operation of Klaipėda State Sea Port. To monitor their stability and reliability, the geodetic and geotechnical monitoring techniques were developed and installed along the Southern and Northern Breakwaters of Klaipėda. The monitoring system measures simultaneously points (prisms) set up on stones of the breakwater at specific locations and reinforced tetrapods, the tilting of towers which are located along the breakwaters, as well as observes the displacement in cracks of breakwater's concrete constructions and records the sea level. For these measurements the respective devices are used: electronic tacheometers, two-axial sensors, cracks-gauges and piezometers. The set of the recorded data samples was composed of 10,100 observations and was processed by special software "Settop auscultation". The monitoring shows the stability in breakwaters with no deformations or slumps unobserved. The created monitoring system used for the experiment approves the efficiency of application for continuous observations of the hydro-technical structure.

Key words: monitoring system, measurements of breakwaters, geodetic instruments, sensors, data analysis.

Introduction

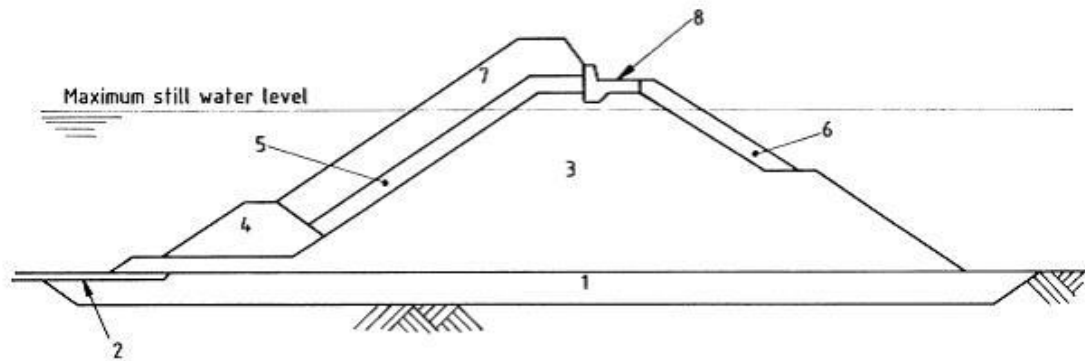
The breakwaters of seaports are of several types and their functions are very important for protection of the coast from negative effect of sea waves and storms. Mostly, main constructions of breakwaters are made of stones and even small damage of such construction can cause painful subsequences. Therefore, a regular control of breakwaters state is necessary to avoid the damage of any types of breakwaters.

The main task was to determine the value of motion frequency of construction elements. The reason of such movements (displacements) can be settlements of breakwaters' foundations, degradation of the breakwaters' constituent elements or storms. The biggest threat that can cause these negative factors is the destruction of objects. Recent modern monitoring systems that provide the possibility of geotechnical and geodetic monitoring now

effectively allows preliminary assessment to track and predict the state of objects in real time.

The general purpose and structure of breakwater

Breakwaters are widely used all over the world, mainly to provide the shelter from wave action. This protection is primarily designed for vessels in port and for port facilities, but sometimes breakwaters are also used to protect valuable habitats that are threatened by the destructive forces of the sea or to protect beaches from erosion. Although the threat is usually caused by wave action, the protection against currents is also important. Additionally, breakwaters can prevent or reduce the siltation of navigation channels. In some cases, breakwaters also accommodate loading facilities for cargo or passengers. The general structure of the breakwater is provided in Fig. 1 with listed elements and their functions.



No.	Element	Function
1	Foundation improvement (if necessary)	Provides embankment stability
2	Scour protection apron	Prevents erosion
3	Core	Provides bulk of structure and reduces wave transmission
4	Toe mound	Supports the main armour
5	Underlayer	Contains the core and provides foundation for armour
6	Rear face armour	Protects core from overtopping waves. Provides wave protection inside harbour
7	Main armour	Provides wave protection
8	Concrete crest structure (with key or cut-off toe)	Provides access and reduces overtopping (Key prevents sliding failure)

Fig. 1. Elements and their functions within typical breakwater (British Standard, 1991)

The object for experimental measurements is Northern and Southern Breakwaters of Klaipeda State Seaport (Fig. 2). General characteristics are the following: the structures are of inclined dams, reinforced by stones, concrete slabs and tetrapods;

Southern Breakwater has the length of 1,374 m, built in 1847-1861, 1900-1908; Northern Breakwater has the length of 733 m, in 1834-1858; both were reconstructed in 2002.



Fig. 2. Location of experimental objects – Northern and Southern Breakwater of Klaipeda State Seaport: a) general view b) Northern zoomed (from Google Earth application)

Monitoring methodology and means

To monitor the parameters and a condition of Klaipėda breakwaters, the system includes the instruments used both for geodetic and geotechnical monitoring of the environment. The geotechnical monitoring uses the means and instruments attributed to geotechnical engineering. According to the definition from (Bucksch H., Dictionary..1997), it is the part of civil engineering involving the interrelationship between the geological environment and the works of man. It has a wide application and various parameters of the building have to be surveyed: the changes in the structures' position (in horizontal/vertical direction), atmospheric condition to evaluate their influence on the structure's characteristics and so on.

In comparison with other monitoring techniques, such as high-definition surveying and remote sensing and geotechnical instrumentation techniques, the geodetic deformation monitoring techniques are based on the ground surface network of points interconnected by angle and/or distance measurements; they measure only the ground surface deformations.

For breakwaters' monitoring in Klaipėda sea port, the function of geodetic monitoring is performed by a tacheometer, an electronic geodetic instrument of the high accuracy. The tacheometer is fixed on the support and mounted inside a special cabin (box) with openings for prevention of the environment actions. The cabin protects the instrument from the snow, rain and vandalism. The electronic tacheometer performs measurements automatically according to an indicated cycle. The night time is recommended for measurements to avoid refraction influence when working in daytime. Before each cycle of measurements, targeting of tacheometer to reference points is done automatically, that is necessary for recalculating coordinates of stations. The accumulator collects data of measurements and transmits to the main server. Points for monitoring are arranged in a spatial mode by prisms. The special program is used for processing of measurements' results.

Geotechnical monitoring includes the usage of such instruments or sensors: tilt sensors, cracks-gauges and piezometer. All these sensors are connected to one network.

Tilt meters are fastened to the tower construction at different height for determination of towers' tilts and directions. Tilts in two perpendicular directions (a , b) (Fig. 3) are calculated according to the formula:

$$z = \frac{l}{\sqrt{\tan^2 \phi + \tan^2 \omega + 1}}$$
$$b = z \cdot \tan \phi$$
$$a = z \cdot \tan \omega$$



Fig. 3. Tilts of tower

The cracks-gauges are located in these places where cracks are the biggest (about 10 mm), when inspecting the breakwaters' construction. The piezometer is arranged besides the tower for observation of the sea level. The instrument is placed in the iron pipe (length – 3 m, width – 15 cm) and sunk into the sea water. The piezometer continually measures the pressure of water. The pipe should be arranged not vertically, but inclined and attached to the stones and bottom.

The software “Settop auscultation” is used for data processing, visualization and report preparation from all sensors. The presentation of measurements' results in graphics (diagrams) and numerical forms are possible (Fig. 5). A warning system is active and information is transmitted immediately, if damages of objects exceed indicated standards. All results of measurements are presented online in real time.

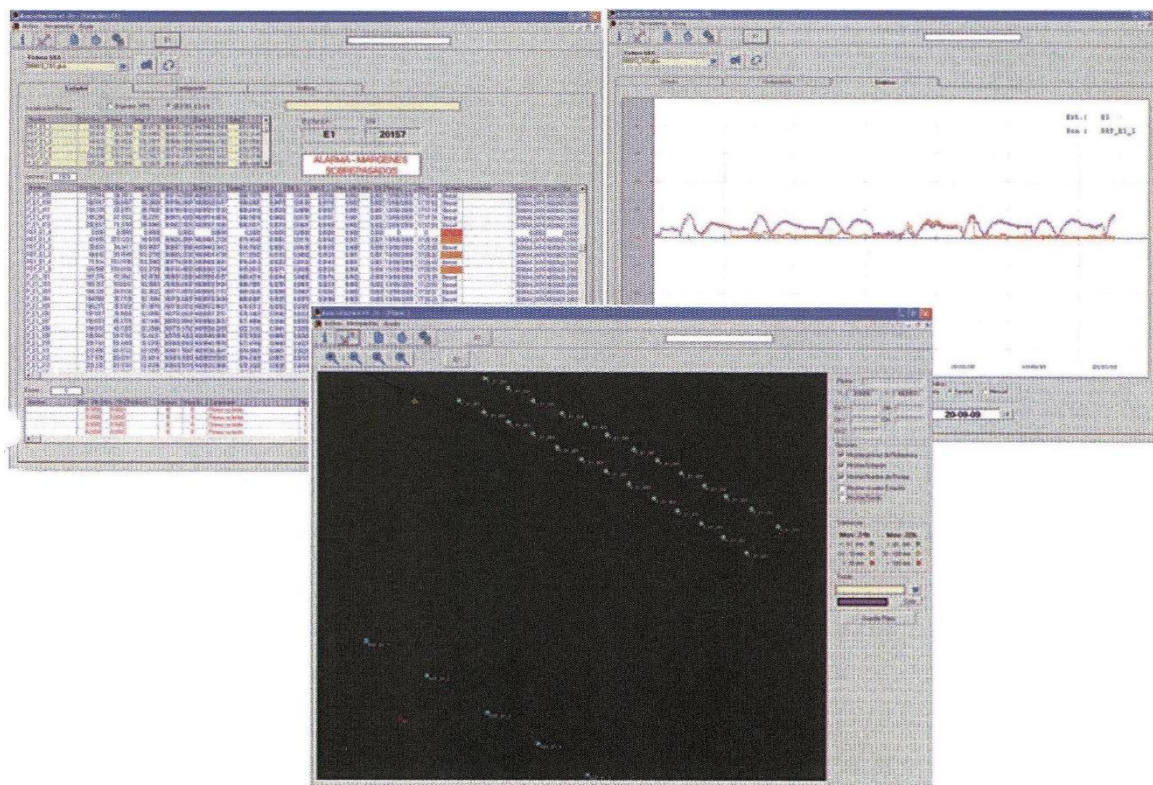


Fig. 4. Fragment of reporting data from “Settop auscultation” software

Description of elements for fixing structural changes and used measuring instruments are presented in Table 1. The shortest distance from the

tacheometer to measuring prisms is 70 m and the longest – 650 m. Instruments are calibrated before measurements.

TABLE 1

Description of monitoring elements and used technical means

No.	Measuring instruments*	Measured elements	Required accuracy	Description
1	Electronic tacheometers “Trimble S8”, data accumulator “Settop M1”, internet connection 3G	Points, arranged on stones and reinforced tetrapods	1.1 mm m (0.5")	Points fixed by prisms are distributed along breakwaters on the side of Curonian Spit: at Northern older part – 9 points with intervals of 50 m, at newest – 8 points with 18-28 m; at Southern – 34 points. Two tacheometers used for measurements were set up on the seaport territory, as well 5 reference points and 2 points of geodetic network (see Figures 5, 7).
2	Two-axial sensors (gauge), “Geosense MEMS Tilt Meter”, data accumulator “Geosense Wi- SOS400 Biaxial”	Tilts of towers	±0.005 mrad	Determination of 4 towers’ tilts at two perpendicular directions (A and B) and directions: 2 – on Southern (sensors at 10 m heights) and 2 – on Northern breakwaters (Figs 6, 7).
3	The cracks-gauge “Geosense VWCM4000”, accumulator “Wi-SOS400 VNode”	Cracks of breakwaters’ concrete constructions	±0.1 % of measured value	Observation of 6 locations on Southern breakwater and 4 – on Northern.
4	The piezometer “Geosense VWP3300”, accumulator “Wi-SOS400 Node”	Sea level changes	1 cm/ 0.1°C	Beside Southern breakwater’s tower.

Monitoring results

The data from the measurement points were recorded once per 24 hours; at night time – on 0.00 hr. 3D positions’ determination and detection of changes (displacements) are results of observations. The piezometer was recording the data at 6.00 hrs.

The analysis of breakwaters’ monitoring (results from 15 measurements’ cycles) was carried out using reported data set:

- daily displacements (in x, y and z directions) of each point (prisms),
- towers tilts at two perpendicular directions,
- changes of cracks,
- sea level differentiations.

Figures 6-9 present the reported data examples from Southern breakwater measurements during a month’s period (2015, 16.08-15.09) showing an example of the reported data.

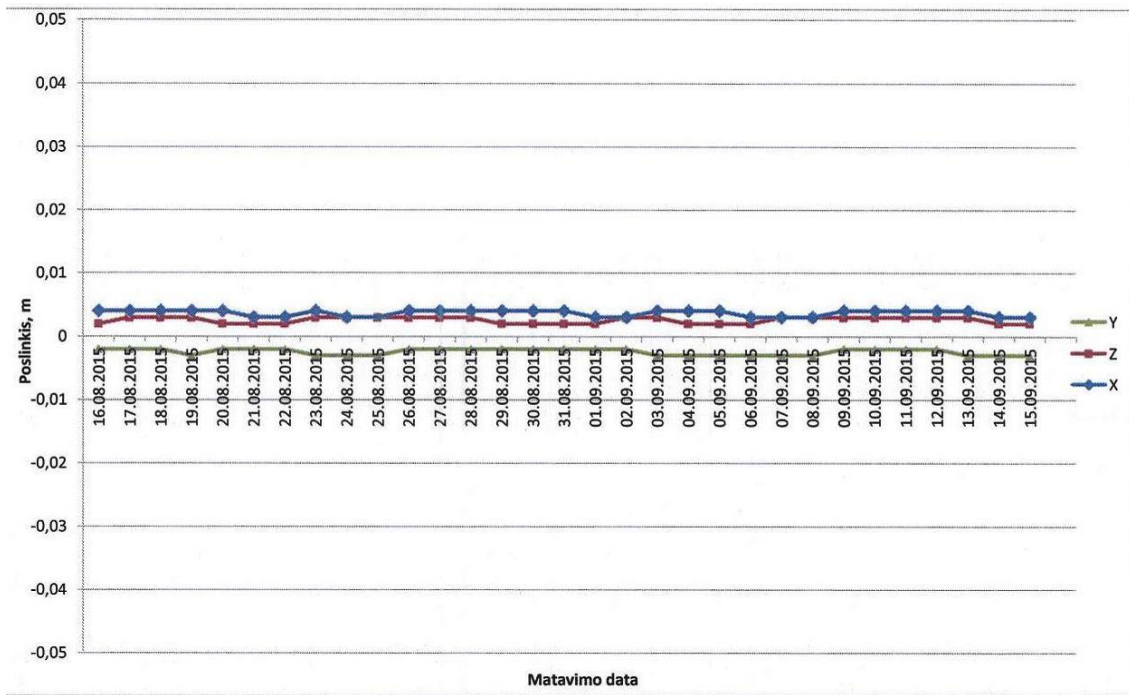


Fig. 5. Diagram of displacements defined from measurement of Southern Breakwater point (prism No.23) during the month: the maximal displacement is in x direction – 4 mm

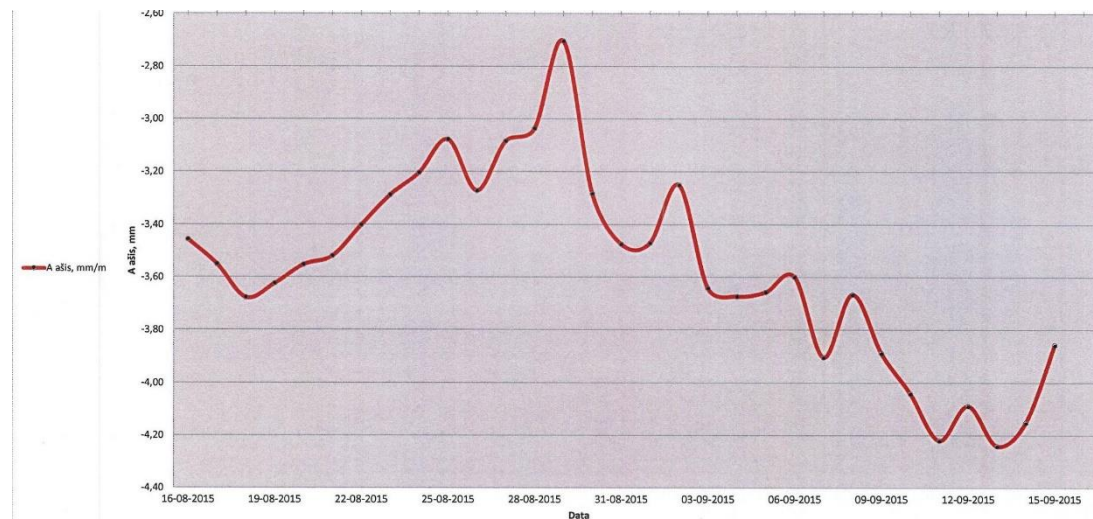


Fig. 6. Diagram of tower tilts at Southern Breakwater’s newest part (A axis, sensor No.676): the maximal tilt – 4.25 mm

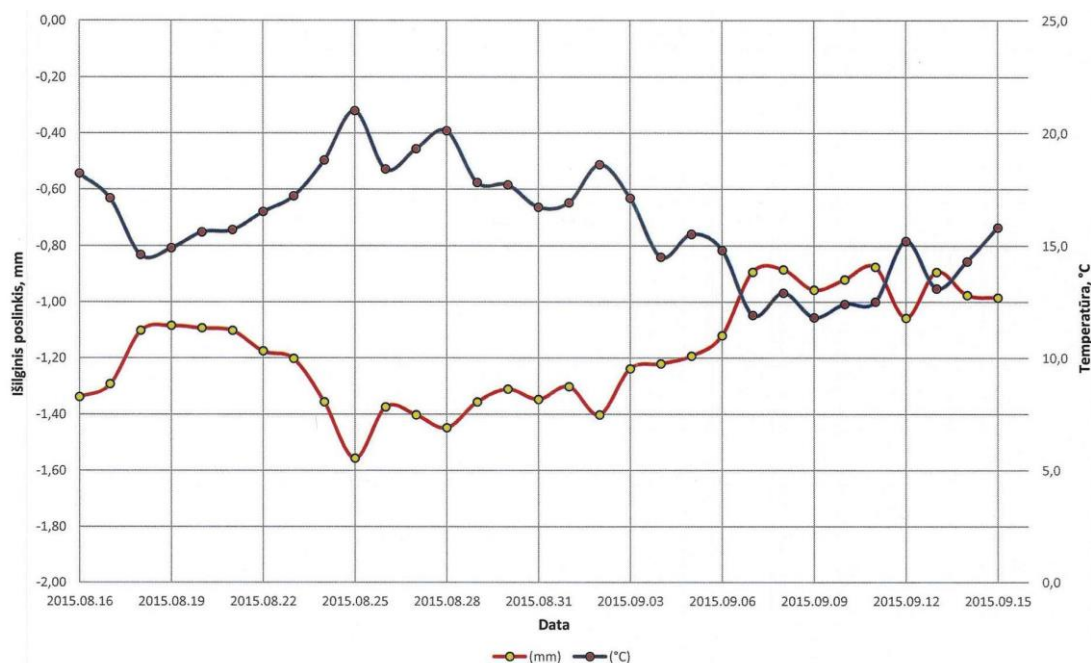


Fig. 7. Diagram of a crack values (Southern Breakwater, 493 m, crack-gauge No 629) and temperature changes

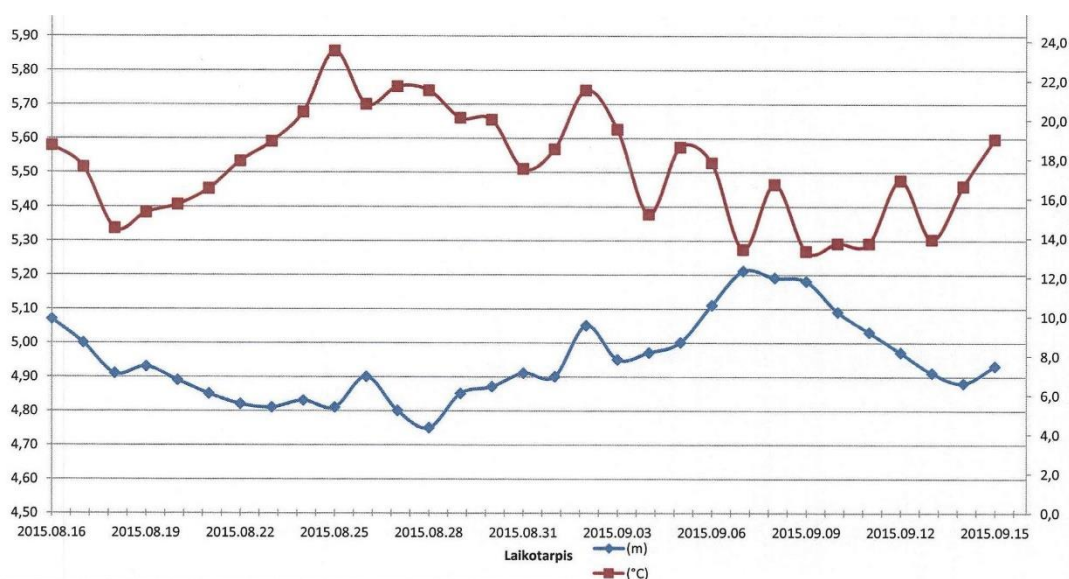


Fig. 8. Diagram of the sea level and temperature changes

Some problems were faced with during experimental measurements:

- Prisms (10 points at Southern and Northern Breakwaters) were broken because of a strong wind, high waves and damaged by people. Some prisms were turned; therefore, instruments could not find a position and perform measurements. Due to this reason it is necessary to change or regulate prisms continuously.
- Damage of the cracks-gauge (2 locations were not fixed).
- Disconnection of power supply (when carrying out the construction work) – a tacheometer was not active for several days.

- A broken antenna of data coupled the device.

Conclusion

The used breakwaters monitoring system which consists of two different types of measurement instruments involves the whole required procedures for breaks prevention and realization of all technical requirements for breakwaters' observation: the detailed recognition of experimental area, the thorough selection of measuring instruments and their installation points, setting up of prisms and an overview of locations for cracks determination; automatic processing of data sets which are continuously generated by sensors.

A huge data set was constructed for the analysis – 10,100 observations; this provided the base for further investigation of deformation assessment, the determination of seasonal influence on breakwaters’ parameters and also allowed to compare the difference of an impact depending on the location of the breakwater. The review of monitoring results shows that the significant changes of breakwaters slopes’ fastening elements (points’ displacements, cracks of chosen locations) were not detected. All measured elements remained stable, any

deformations or slumps were unobserved, but still a further analysis is required.

Breakwaters’ stability extremely depended on meteorological conditions because the wind induced waves and currents, storms, air temperature; moreover, negative actions of humans interrupted measurements’ procedure. Therefore, stability of the measured elements could be temporary and it is recommended that breakwaters’ monitoring should be carried out continuously.

References

1. British Standard-British Standard 6349-7_ 1991, Code of practice for maritime structures, Part 7_ Guide to the design and construction of. BS 6349-7:1991
2. **Bucksch H.** (1997) *Dictionary Geotechnical Engineering*, Springer, 30/3136 – 543210, 1997
3. **Antunes P., Travanca R., Rodrigues H., Melo J., Jara J., Varum H., André P** (2012) *Dynamic Structural Health Monitoring of Slender Structures Using Optical Sensors*. *Sensors* 2012, 12, 6629-6644
4. **Moreau F., Dauteuil O., Bour O., Gavrilenko** (2006) GPS measurements of ground deformation induced by water level variations into a granitic aquifer (French Brittany), *Terra Nova*, 18, 50–54, 2006
5. **Matsuya I., Katamura R., Sato M., Iba M., Kondo H., Kanekawa K., Takahashi M., Hatada T., Nitta Y., Tanii T., Shoji S., Nishitani A., Ohdomari I.** (2010) Measuring Relative - Story Displacement and Local Inclination Angle Using Multiple Position - Sensitive Detectors, *Sensors*, 2010, 10, 9687-9697;
6. **Choudhury M., Rizos C.** (2010) Slow structural deformation monitoring using Locata – a trial at Tumut Pond Dam, *Journal of Applied Geodesy* 4 (2010), 177–187de Gruyter 2010.
7. **Guo J., Zhou M., Wang C., Mei L.** (2012) The application of the model of coordinate S-transformation for stability analysis of datum points in high-precision GPS deformation monitoring networks; *Journal of Applied Geodesy*, Vol.6(2012).

Requirements for Aerial Mapping Using UAV-photogrammetry Technology: Baltic Sea Coast Measurement

Lina Kukliene¹, Dainora Jankauskiene^{1,2}, Indrius Kuklys¹, Birutė Ruzgiene¹, ¹*Klaipėda State University of Applied Sciences*; ²*Kaunas University of Technology*

Abstract. The use of Unmanned Aerial Vehicles (UAVs) with the integrated camera for image capturing, GPNS, the management equipment and specialized software for processing of images has been rapidly expanding for aerial mapping. The quality of cartographic products at the initial stage depends on well-designed technical specifications for photogrammetric mapping and conditions of the project realization. The successful photogrammetric mission and efficiency of the performed photogrammetric processes should be specified by the requirements that meet not only the needs of Lithuania but also those of the European Union. Thus the paper deals with the analysis of the essential requirements for aerial mapping due to the application of the highly advanced UAV-Photogrammetry technology, as well as outlines conditions and parameters that can be used for preparing and specifying the documentation of aerial photogrammetric workflow and realization of a project. The methodology for the determination of mapping costs is developed and the example of efficiency evaluation is presented which is based on the photogrammetric data gained by UAV technology using an experimental object which is mapping of the Baltic Sea coast at Palanga city in Lithuania.

Keywords: Unmanned Aerial Vehicles, aerial mapping, photogrammetric requirements, costs evaluation.

Introduction

The aerial mapping is one of the most advanced methods to obtain information about the surface of the Earth and other objects using photographic images. The quality of images and cartographic products mainly depends on the success of aerial photography mission, qualified guidance of photogrammetric works, and appropriate realization of aerial mapping requirements that meet the needs of Lithuania and preferences of the European Union.

Recently, the interest of application of small planes flying at low altitude, the so-called Unmanned Aerial Vehicles (UAV) in photogrammetric and geodetic environment is rapidly growing in many countries including Lithuania. Unmanned Aerial Vehicle with the integrated digital camera and automatic management of taking photography is an effective platform equipped with UAV-Photogrammetry technology that is used for digital photogrammetric data processing and generation of the aerial mapping products. The UAV platform is also named a Remote Operation Aerial Vehicle (ROAV). The UAV-Photogrammetry technology is increasingly replacing the classical methods applied in geodetic, cadastral, etc. measurements. The main advantages of UAV application are the following: the costs for getting aerial mapping product is not high (decreasing), images are collected fast and in real time, there is also a possibility of taking a photography of the territories where the relief is complicated or it is not possible to reach the object, moreover, the processing of images is fast, and the created cartographic products fulfill the requirements of accuracy.

UAV-Photogrammetry is applied in many fields, for example, for taking images when the leaves of the trees are covering the objects of surface; on the other hand, close-range photogrammetry is used for mapping of the linear objects (network of roads, sea coasts, etc.), and for fixing the position of electricity networks, as well as for measuring the cultural monuments for reconstruction, and, ultimately, for creating the cadastral maps, etc. ([3], [14], [8], [2]).

The orthophoto maps of high accuracy (quality) and three-dimensional surface models are main products generated by the use of aerial photogrammetric technology. The aerial mapping products are presented to consumers in the form of digital maps, and digital terrain or 3D surface models can be processed by the use of GIS applications ([7], [9]).

The goal of the research is to analyze the features and parameters for aerial photography by the use of Unmanned Aerial Vehicle and to outline the main photogrammetric requirements that can be accepted as the basis for preparing the technical specification of aerial mapping project and realization of photogrammetric workflow applying the UAV-Photogrammetry technology.

1. Project specification for aerial mapping applying UAV-Photogrammetry technology

The initial stage of the territory mapping project/technical specification preparation indicates the main objective of the project works and identifies its parts, i.e. project tasks and objects. The detailed data of aerial mapping object should be specified, such as:

width, length, area, dislocation of territory (a scheme is provided in the cartographic material), and features of the relief, etc. For aerial photography on the border area it is mandatory to apply to the relevant authorities in order to obtain all necessary permits. The deadlines for all aerial mapping works have to be foreseen.

Common conditions for aerial photography.

Aerial photography can be executed in good meteorological conditions, i.e. in light wind (when speed is of 1.6-3.3 m/s) and in minimal cloudiness. The calendar time of aerial photography is determined taking into account the specific meteorological conditions of the seasons. The aerial photography is usually performed early in spring until the vegetation has not yet cropped, or, on the other hand, late in autumn, so that the leaves of the trees have not covered the ground surface. Aerial photography of the object on the seaside can be realized in spring before the stormy season begins (preliminary in March) and/ or in the autumn, after the stormy season has ended (e.g. in November). The

time for aerial photography depends on the general conditions of the Earth's surface and the sun's height. It's best to take photographs at noon, when the falling shadows are the shortest. The geometric, visual and informative features of photographic images depend on the technical means of the aerial photography, such as: type of platform and the integrated sensor for photographic imaging, i.e. the properties of the digital camera, and, additionally, on geodetic measurements creating a photogrammetric base network.

1.1. Technical means: UAV, digital cameras

Taking photography of an area is carried out by a camera integrated at Unmanned Aerial Vehicle with the automatic management and control system or at planes that meet the requirements for aerial mission over the territory. Photographic and photogrammetric data are collected in half automatic or automatic manner.

The Unmanned Aerial Vehicles of different type, classification and category can be used as a platform for area photography from low altitude, see Figure 1 ([1], [18], [15]).

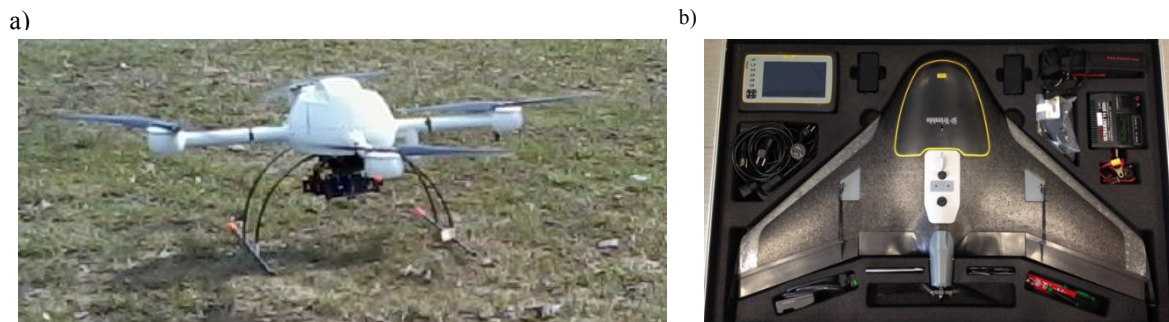


Fig. 1. UAVs used at different projects in Lithuania: a) four-wheel helicopter with mounted camera; b) a set of fixed-wing UAV, model UX5 Trimble

For area photography, the unmanned vehicle flies at low speed (about 50-60 km/h) and the flight height ranges from 30 m to 750 m. The Vehicle can fly at even 12 m/s wind speed, and it can land under complicated conditions ([17], [10]).

For example, the platform of fixed-wing UAV, UX5 Trimble is of low cost and weight platform with foam construction. A wingspan is of 1.0 m and the weight is 2.5 kg. Dimensions of UAV are 100×65×10 cm. The UAV cruise speed is 80 km/h and can fly up to 50 min on low wind and in light rain. A flight range is approx. 60 km, some extra for launching and landing. The maximal communication and control range is up to 5 km. The guidance of UAV platform can be full automatic, semi-manual or manual. The take-off of the platform, flight and landing on the surface can be executed in an automatic or manual mode. The flight planning software allows optimal guidance of the flight.

The main features of digital cameras are as follows: focal length, geometric and radiometric resolution of the sensor, pixel size; features of the

optical system, and formats (saving) of photographs. The sensor's pixel size is an important parameter that defines sensor sensitivity and optical resolution. Radiometric resolution indicates spectral properties, i.e. the saturation (intensity) of the images color is expressed in bits for pixel. The small pixel size determines the light sensitivity and in a diversity of weather conditions affects the quality of the photographs. The camera's optical system must be fixed, i.e. the focal length is constant. A fixed optical system increases the stability of the camera's internal geometry ([6]).

A higher shutter speed should be used to eliminate motion blur. Even at slower flying speeds, a wind gust resulting in a roll or a small change in pitch and longer exposure times can lead to motion blur. Image blur causes the radius of uncertainty in tie point matching to increase by a factor of 4, which has a direct effect on the resulting vertical accuracy in the point cloud and DSM.

The example of camera's features is presented in Table 1. A high-resolution professional camera Sony

NEX-5R with fixed-optics *Voigtlander* lens was used for taking images over the test area, namely the Baltic Sea coast extending along Palanga city.

TABLE 1

Main features of high-resolution professional camera *Sony NEX-5R* with fixed-optics

Features	Sizes	<i>Voigtlander</i> lens
Focal length	15 mm	
APS-C sensor	16.1 Mega pixels	
Full frame size of image	4912×3264 pixels	
Sensor's area	365.04 mm ²	
Size of sensor	23.40×15.60 mm	
Pixel size	4.8×4.8 μm.	
Fixed-optics <i>Voigtlander</i> lens increase the stability of the camera's internal geometry. Small pixel size determines the light sensitivity and sharp images can be acquired.		

Aerial photography should be executed with a digital camera having a sensor's size not less than 12 MP and radiometric resolution – 24 bits.

1.2. Aerial mapping project realization

The photogrammetric network is created for the external orientation of photographic images and for generation of photogrammetric products. For this purpose, geodetic points (targets) are projected and before taking images targets at the area are marked by artificial, background contrasting special marks. After aerial photography, these marks must be clearly visible in photographic imagery. The dimensions of the mark may be 40×40 cm. In order to obtain more precise aerial mapping products, the targets are distributed in a specific order: at the beginning, at the end and at the middle of the flight patch as well as in the areas of complicated relief. The coordinates of the targets are determined by geodetic methods, measured by electronic geodetic instruments, and often by the Global Positioning System (GPNS) using GPS network data. The coordinates of the targets are determined by the GPS method with an accuracy of 5-10 cm ([11]).

The GPS module integrated at UAV allows to determine the geodetic coordinates of each image projection center during the flight, thus reducing the need of geodetic reference points. Taking images over a territory when the vehicle is equipped with GPS and gyroscopic stabilization equipment, the accuracy of the aerial images is about ±10-15 cm. After aerial photography, a catalog of GPS coordinates and projection centers of aerial photographs as well as layout diagrams are provided.

The parameters for aerial photography mission.

Before the aerial photography, the UAV flight height above the surface (Aerial Ground Level (AGL)) during image acquisition is determined and the camera's technical characteristics are evaluated. The flight height depends on the required resolution of the photographic images (the size of the image pixel in the area – GSD (Ground Sample Distance),

the camera sensor's pixel size and focal length ([13], [5]).

The resolution of photographic images describes the accuracy of photogrammetric products and can range from 2.4 cm to 24 cm. The GSD is calculated according to the formula:

$$GSD = p \frac{AGL}{c}, \quad (1)$$

where p is the pixel size of the sensor, μm; AGL – aerial ground level, m; c – camera focal length, mm. For example, if the required resolution of the images is 2.4 cm and the *Sony NEX-5R* camera (see camera's features) is used for taking photographs, the flight height above the surface will be 75 m.

Prior to a flight the camera is turned on, the ISO is determined to auto mode, F-value 4.5, the focus of camera is fixed and shutter speed is regulated depending on the weather conditions, terrain features and desired images overlap.

The flight planner software (e.g. *Aerial Imaging, Trimble*) provides optimal flight performance. After checking the parameters of the UAV, the flight mode is shifted to the automated flying. When UAV achieves the appointed height, the process of taking pictures starts. The software operates not only the UAV, but also is managing camera exposure ranges. Therefore, the image acquisition becomes completely automatic.

The overlapping of photographs is an important parameter for obtaining high quality cartographic products. The best results are obtained when an overlapping is more than 5 photographic images. Taking into account that the UAV system is unstable during the aerial photography the position mostly depends on the wind gusts, so it is recommended that 70-80% of images have to be overlapping.

After the realization of the aerial photography, the basic features of the gained images are presented as follows: original size (pxl.), resolution (dpi), pixel size (μm), frame format (cm), images size in the area (m), radiometric resolution (bit), and memory

capacity (Mb). Photogrammetric and photographic image quality is evaluated.

The processing of photographic images, accuracy and acquired products.

The application of the digital photogrammetric software (e.g. *TBC Photogrammetry Module, Aerial Imaging, Trimble*) allows to transform images into the required coordinate system (the process of exterior orientation), and thus are the orthophoto maps generated and created the three-dimensional model (3D). For more convenient data analysis and visualization, an orthophoto map can be divided into blocks. The generation step (resolution) for the orthophoto is defined. Since the UAV runs at low altitudes, it is recommended to generate an orthophoto map at the step of 10 cm.

The following generalized rule applies for the accuracy evaluation of aerial mapping products, which means that the precision of planimetric coordinates must be twice as high as the GSD, whereas the altitudes must be higher three times. In addition, the *Trimble* Corporation declares the following criteria for assessing the accuracy of UAV-Photogrammetry data, the mean and maximum errors of planimetric coordinates are $1.0 \times \text{GSD}$ and $1.6 \times \text{GSD}$, and elevations of $1.6 \times \text{GSD}$ and $2.5 \times \text{GSD}$. For example, if $\text{GSD} = 2.4 \text{ cm}$, then the mean and maximum errors in the x and y directions are 2.4 cm and 3.8 cm; direction z - 3.8 cm and 6.0 cm.

An orthophoto map, the geometric and radiometric features of which meet the requirements, is presented to the user in the appropriate format (e.g. GEO TIF). Cartographic products can be delivered to

customers by means of interactive maps and three-dimensional models of surface. At the next step, the obtained cartographic digital data is processed and archived by ArcGIS or by another type of software, and the required production is presented for the user in the GIS server or is located on another web site.

2. Costs and effectiveness consideration

Currently, when various technologies for the image acquisition, management and processing are available, it is important to consider the cost-effectiveness of a certain aerial mapping with the UAV application. In general, the price of the product comprises an actual expense plus overheads. Overheads vary greatly regarding the salary structure of administrative services and the amount of taxes to be paid ([4], [16]).

The example of cost strategy is presented and based on the executed UAV flight mission over the Baltic Sea coast at Palanga city and generation of aerial mapping products stages. The territory is photographed with a *Sony NEX-5R* digital camera, equipped into the vehicle *UX5, Trimble*. The length of the patch is about 2 km (approximate area - 43 ha), the size of the pixel in the area (GSD) is 3 cm, and about 400 photographs are received. An orthophoto map was generated by *Aerial Imaging* software and a 3D coastal modeling was performed, see Figure 2.

The area covered by images during the flights is related with height of flight (AGL) and is one of important factors for the UAV mission duration and project cost evaluation ([12]). Table 2 presents the data of imaging area according to the different GSD and flying height (AGL).



Fig. 2. Orthophoto map of the Baltic Sea coast at Palanga city generated by the use of UAV-Photogrammetry technology

TABLE 2

Imaging area depending on GSD and AGL (Sony NEX-5R, UX5 Trimble)

GSD, cm	AGL, m	Image size on ground (imaging area), m
2.4	75.0	117.8×78.3
3.0	93.7	147.3×97.9
5.0	154.2	245.6×163.2
10.0	312.5	491.2×326.4
20.0	625.0	982.4×652.8
24.0	750.0	1178.9×783.4

Before the UAV flight the preparation works as follows: reconnaissance of territory, planning of ground control points (GCP), marking of GCPs on the area, determination of signalized and natural

(features) points' coordinates using geodetic techniques. The efficiency of the preparation works of UAV flight mission is presented in Table 3.

TABLE 3

Time costs for preparation and UAV flight mission

Stages	Efficiency, h
Reconnaissance of territory	1
Ground control points projecting (23 points)	1
Signal preparation and marking (6 points)	1.5
Coordinate determination of GCPs	1
UAV flight mission realization (1 path), 2 executers	1.5
Total	6.0

The performance details of photogrammetric modelling with 400 images (one path) for aerial

triangulation (AT), DEM and digital orthophoto generation (DOM) are listed in Table 4.

TABLE 4

Time duration for images processing

Processes	Operation (400 images)	Time duration, val.	
		Automatic	Manual
AT	Data preparation	-	0.5
	Tie points matching	3	-
	GCP measurement	-	1.5
	Block adjustment	1	-
DEM	Image matching	2	-
	Data filtering	0.5	-
	Post processing	0.5	-
	Editing	-	2
DOM	Orthophoto generation	1.5	-
	Color adjustment	1	-
	Mosaicking	2.5	-
	Editing	-	3
Total		12	7

The generation of mapping production (automated processes) is based on costs per image (0.5 €) plus labor (manual) costs per hour (5 €). Therefore, total cost for processing of 400 images is 235 €, see in Table 4.

Concerning data mentioned above, the aerial photography costs consist of a base cost for preparation works (transportation and overheads as well) plus a charge for the image area and regarding of pixel size (GSD). Table 5 shows the price-list in consideration of mapping area.

TABLE 5

Price-list for aerial mapping

Area, ha	UAV aerial photography cost, EUR		
	GSD 3 cm	GSD 5 cm	GSD 10 cm
Up to 2	570	340	280
2–5	740	400	280
5–10	970	450	400
10–15	1,430	510	570
15–50	2,000	860	680
50–100	3,400	1,400	800

The costs for UAV-Photogrammetry experimental project (one path – area 43 ha, at GSD – 3 cm) realization is EUR 2,000 (see Table 5) and plus cost for image processing, in total – 2.235 €.

The costs variation for UAV-Photogrammetry (aerial mapping) application depends on the calculations of product providers, including special employment as well. Undoubtedly, mapping companies can provide different costs for aerial-imaging by UAV systems and photogrammetric data processing. The estimation of the works (price and time) usually dependent on the skills, experience of employment, equipment available, the amount of salary for the employees, and the cost for administration of the project, etc.

Conclusions

The interest in Unmanned Aerial Vehicle’s great potential for the aerial mapping is growing in many countries including Lithuania. Unmanned Aerial Vehicle in combination with photogrammetry provides low cost, a small area, and prompt data collection used for image processing and demonstrates the modern technology employed for environment imaging. The photogrammetric requirements for aerial mapping project realization are developed, when low-flying (up to 750 m) Unmanned Aerial Vehicles is applied as a platform with integrated camera, flight control system, and GPS for flight mission.

The UAV-Photogrammetry project’s workflow specifications outline the following main data, requirements and parameters:

- location of an object, size of the territory, features of the terrain and project completion dates; the

required accuracy of the aerial mapping products that is specified by the customer (e.g. 10 cm);

- the pixel size in the area (GSD), taking into account the accuracy of the aerial mapping products required;
 - depending on the size of a camera’s sensor and the GSD, the flying height (AGL) of the Unmanaged Aerial Vehicle should be defined;
 - in order to obtain more accurate results of the exterior orientation of images, a photogrammetric network has to be constructed prior to the execution of the aerial photography mission. In the case, when the images exterior orientation does not require high accuracy, it is sufficient to use the coordinates of each image projection center determined by GPS.
 - an aerial photography should be realized by a camera with a stable optical system (fixed focal length and focus is not changed), with a sensor size of at least 12 MP, a radiometric resolution – of 24 bits;
 - overlapping of images is recommended up to 70–80% for acquisition of better results of matching images. In case of larger overlapping (e.g., 90%), an excessive number of photographic images is obtained;
 - aerial mapping products are specified selecting the step which generates orthogonal photographs.
- The cost considerations of the Unmanned Aerial Vehicle application for the purpose of photogrammetry employment at experimental object are presented.

References

1. Černiauskas, E; Bručas, D. 2014. Daugiasraigčių sraigtaspanių naudojimo stebėjimo užduotims atlikti tyrimas. *Aviacijos technologijos* [Aviation technologies], 2(1): 53-58.
2. Eisenbeiss, H. 2009. *UAV photogrammetry*: Dissertation, Federal Institute of Technology (ETH), Institute of Geodesy and Photogrammetry, Zurich, Switzerland, Mitteilungen. 235 p.
3. Haala, N.; Cramer, M.; Weimer, F.; Trittler, M. 2011. Performance Test on UAV-Based Photogrammetric Data Collection, *International Archives of the Photogrammetry, Remote Sensing and Spatial Information Sciences* 38-1/C22: 7–12. <http://dx.doi.org/10.5194/isprsarchives-XXXVIII-1-C22-7-2011>.
4. Konecny, G. 2003. *Geoinformation: Remote Sensing, Photogrammetry and Geographic information system*. Taylor and Francis. 248 p.
5. Kraus, K. 2007. *Photogrammetry: Geometry from Images and Laser Scans*. Berlin: Walter de Gruyter. 459 p.
6. Linder, W. 2009. *Digital Photogrammetry. A practical Course*. Springer-Verlag, Berlin, Heidelberg. 33- 73, 121-131 p.
7. *Manual of Photogrammetry* (Edited by J. Chris McGlone). 2004. American Society for Photogrammetry and Remote Sensing, Maryland, USA. 959-963 p.
8. Neitzel, F.; Klonowski, J. 2011. Mobile Mapping with Low-Cost UAV System, *International Archives of the Photogrammetry, Remote Sensing and Spatial Information Sciences* 38-1/C22: 1–6.

9. **Rock, G.; Ries, J. B.; Udelhoven, T.** 2011. Sensitivity Analysis of UAV-Photogrammetry for Creating Digital Elevation Models (DEM), *International Archives of the Photogrammetry, Remote Sensing and Spatial Information Sciences* 38-1/C22: 1–5.
10. **Rudinskas, D.** 2011. *Bepiločių orlaivių skrydžio parametų matavimų duomenų perdavimo saugos metodikos sukūrimas*: Daktaro disertacija. Vilniaus Gedimino technikos universitetas. Vilnius: Technika. 85 p.
11. **Ruzgienė, B.** 2008. *Fotogrametrija*. Vilnius: Technika. 93-132 p.
12. **Ruzgienė, B.; Aksamitauskas, V. Č.; Daugėla, I.; Prokopimas, Š.; Puodžiukas, V.; Rekus, D.** 2015. UAV photogrammetry for road surface modelling. *The Baltic journal of road and bridge engineering*. Vilnius: Technika. Vol. 10, no. 2, p. 151-158.
13. **Ruzgienė, B.; Berteška, T.; Gečytė, S.; Jakubauskienė, E.; Aksamitauskas, V. Č.** 2015. The surface modelling based on UAV Photogrammetry and qualitative estimation. *Measurement*. Oxford: Elsevier Ltd. Vol. 73, p. 619-627.
14. **Ruzgienė, B.; Gečytė, S.; Jakubauskienė, E.** 2014. Užstatytų teritorijų kartografavimas, naudojant fotogrametrinius duomenis, gautus fotografuojant iš bepiločio skraidymo aparato. *Inžinerinės ir edukacinės technologijos* [Engineering and educational technologies]. Kauno technikos kolegija. Nr.1, p. 69-77.
15. Trimble, *UX5*. Available from Internet: <http://uas.trimble.com/ux5> (9 September 2017).
16. **Sauerbier, M.; Siegrist, E.; Eisenbeiss, H.; Demir, N.** 2011. The Practical Application of UAV-Based Photogrammetry Under Economic Aspects. *Remote Sensing and Spatial Information Sciences*, Volume XXXVIII-1/C22, Zurich, Switzerland. 45–50 p.
17. UAV Systems–Unmanned Aerial Photography. AUVSI. <http://www.uavsystems.com.au/> (2 September 2017).
18. **Watts, A. C.; Ambrosia, V. G.; Hinkey E. A.** 2012. Unmanned Aircraft Systems in Remote Sensing and Scientific. Research: Classification and Considerations of Use. *Remote Sensing* 4(6). 1671-1692 p.

Ukrainian Cadastral Exchange File Evolution Path and its Features

Roman Peresoliak, *Land Management and Cadastre Department, Uzhhorod National University*

Abstract. Ukrainian Land Cadastre has a special place in cadastral ecosystem of the country since Land Cadastre is the primary source of information for other cadastres. Ukrainian Land Cadastre is an implementation of the specific GIS, known as LIS (Land Information Systems). However, such a huge mechanism cannot work without appropriately defined basic components. One of the components is a cadastral exchange file. Thus the definition and quality on the Ukrainian cadastral exchange file becomes very important. This study describes the historical path of the Ukrainian cadastral exchange file, reveals benefits and disadvantages of the cadastral exchange file of the new format based on XML, as well as hidden and unused functionality that potentially could be used in future. To achieve the goal, the following tasks were set: to follow the path of development and formation of the old IN4 format in Ukraine; to define XML functionality; to characterize the cadastral exchange file of a new format based on XML. Given the historical aspects of the development of the Ukrainian cadastral exchange file, the following should be noted: IN4 format is based on INI format; IN4 realizes a simple vector model for describing geometry; a cadastral exchange file should be considered as the file implemented using the cadastral exchange file markup language; the cadastral exchange file implements a topological model; the XML-based cadastral exchange file uses an object-oriented approach to describe complex structured information.

Key words: Cadastral exchange file, XML, IN4, GIS

Introduction

The development of modern land use needs more technological support, and the land register as any large-scale project requires automation of a large part of the manual work. That is a mechanism which will provide the opportunity to view, search, interact with the data in addition to data accumulation. It will have the opportunity to organize network access and control information access policy, the mechanism for generating documentation and much more. The mechanism has been implemented by means of geoinformation systems and technologies (GIS).

An automated system of the state land cadastre of Ukraine could be considered as an analogue of the widely deployed GIS for land management. An important feature of this kind of GIS is the implementation of a large number of automated processes, including registration process of land parcels, their inclusion in the state land cadastre database, the automated formation of paper documents and reports, the generation of cartographic and planned materials, spatial modelling and spatial analysis, the detection of hidden spatial patterns, monitoring of the environment, etc.

Given the specificity of such geographic information systems and their special tools, it is appropriate to classify them as land information systems (LIS). Implementation of the LIS in practice on the territory of Ukraine is functionally expressed in the land cadastre. As it is known, the land cadastre among other cadastres has a special and fundamental place because land cadastre is the primary source and the source of basic information for other cadastres. In particular, the land cadastre is the basis for [23]:

- cadastre of water resources;
- cadastre of natural plant resources;
- cadastre of resources of the animal world;
- cadastre of natural therapeutic resources;
- cadastre of mineral resources, minerals, manifestations, and minerals of man-made deposits;
- cadastre of forest resources [14];
- cadastre of natural areas of the resorts [20];
- cadastre of territories and objects of the natural reserve fund [21];
- municipal cadastre [22];
- cadastre of the anthropogenic emissions and removals of greenhouse gases [24].

However, land cadastre, LIS and GIS, in general, use only the platform for implementation of a variety of tools for solving land management issues. By itself, the tool is not able to solve all diversity of functions assigned to it without the existence and functioning of an ecosystem of technological, normative and methodological levels. In particular, one of such levels can be considered to be the basis of electronic document flow of land cadastre, i.e., cadastral exchange file.

As the cadastral exchange file is important in the cadastral system of Ukraine, consideration of its features and the process of its formation is of crucial importance. This study describes the historical path of the Ukrainian cadastral exchange file and points at benefits and disadvantages of the cadastral exchange file of the new format based on XML, reveals hidden and unused functionality that potentially could be used in future. To achieve the goal, the following tasks were set: to follow the path of development and

formation of the old IN4 format in Ukraine; to define XML functionality; to characterize a cadastral exchange file of new format based on XML.

Methodology of research and materials

IN4 cadastral exchange file format

According to [25], the exchange file is a unified structure of the land cadastre data containing the results of the performed land management activities in electronic form intended to unify the land cadastral data on the land plot or their collection in electronic form and contains: metric, semantic and service information. An important feature of the IN4 format is that it is presented as a text file in ASCII codes using code table 1251 (Code 1251). It is not allowed to use other code pages to create an exchange file.

The use of this code table, also known as Windows-1251 [4], is inherent for Windows family operating systems and can represent encoded characters for Ukrainian, Belarusian, Serbian, Bulgarian and Russian [30]. This feature significantly limits the amount of information entered, as it is possible to insert characters only of the above mentioned languages and Latin characters; all others will be considered incorrect.

The IN4 exchange file consists of structural blocks of land cadastral data [25]:

- cadastral quarter;
- parcel;
- land type;
- cadastral zone;
- cadastral unit substitute.

Structural blocks are clearly associated with spatial layers that environment can generate.

Each structural block of the land cadastre data contains lines with a fixed number of structural fields of metric information (rectangular coordinates in the Gauss-Kruger projection) and semantic (attributive) information of the cadastral unit. Each line (tag) begins with the keyword (descriptor) connected by the symbol "=" (equality sign) with the string containing the fields of land cadastral data. As a delimiter of the line fields and the end of the line, the character "," (comma) is used. The absence of the "," (comma) symbol at the end of the line indicates the completion of the land-cadastral data transfer to the block [25].

The data of the strings of semantic information is limited to the character "" (the quotes are the ASCII character code 034). The data of the lines of metric information are not limited by the "" character (quotes). When the metric information is taken as a delimiter of the whole and fractional part of the number, the symbol "." is used (point). If the semantic information contains a character "" (quotes), for example, in the proper name of the subject of the land relations, then the "/" (slash) is inserted before the

quotes. The "#" (hash) symbol at the beginning of the line converts the string to comment [25] This approach allows to save a set of characters that better describe the data in the file and are ignored by the program that processes the file.

XML basics

XML (Extensible Markup Language) describes a class of data objects called documents, and briefly describes the mechanization of document processing using computer programs. An XML document consists of container elements that are called entities. The markup in the document serves as a description of the document itself and the logical structure. Also, XML provides a mechanism for imposing restrictions on the storage scheme and the logical structure. XML also includes a program module called the XML processor used to read documents, search data, access the structure [2, p. 1].

In general, an XML document contains one or more elements, each of which is marked with an initial and a final tag, or in the case of a blank element, an empty tag. Each element has a type defined by its name, called the "base identifier," and may contain a set of non-mandatory attributes [2, p. 14].

Often it is possible to find the "XML document", "XML technology", "XML document". However, what is actually XML is? At the first level, XML is a protocol for storing and managing information. At the next level, this is a family of technologies that can help to do everything from document execution to data filtering. At the highest level this is the philosophy of information processing, the purpose of which is to ensure the maximum benefit and flexibility of the data by providing them with the purest and structured form [6, p. 13].

It would be nice to remember that single name (XML) contains simultaneously many related values, which often leads to confusion. Regardless the name itself, XML is not a markup language: it is a set of rules for creating a markup languages [6, p. 13].

As mentioned above, XML represents a whole set of technologies that work closely with each other. In the author's opinion, it is the excellent workflow and the number of these technologies that allows you to store XML in the first positions, since it is not the only representative of the markup languages, which can be attributed to JSON Schema [13]. Checking and generating new, simpler documents such as JSON or YAML, is gaining popularity [28], but the most advanced set of technologies in XML tools leaves it at the forefront. According to [31], the tools contained in XML are shown in the Figure 1.

When storing a large amount of data using XML, it is important to pay attention to the exact place that holds among the data models. This question becomes extremely important if we consider XML not as a

mechanism for describing data but as a means of preserving it. This is confirmed by a number of sources [16, 1, 32]. In the author’s opinion, the

consideration of XML really becomes a data storage system, since this interpretation is due to the developed set of technologies that offers XML [1].

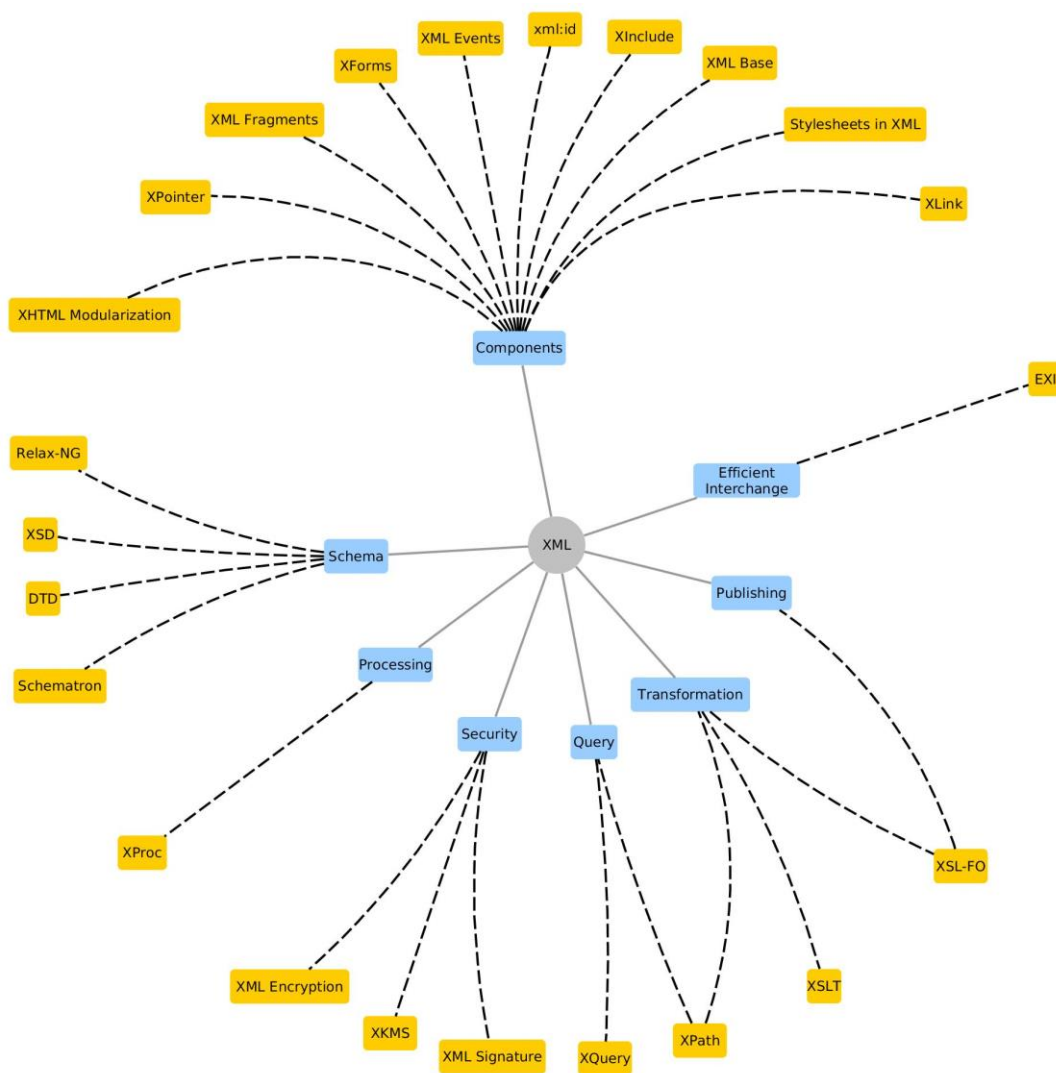


Fig. 1. XML components

Given the use of XML on the territory of Ukraine in the field of cadastre, it, first of all, should be considered as a means of describing the complex structured information, and only then as mechanics of its preservation. In the author’s opinion, this approach justifies the use of just XML, but not other similar technologies.

Discussions and results

IN4 structure features

Given the types of attribute information that can be used to implement this data format, it is worthwhile to elaborate on how data types display

end attributes, that is, the preservation of certain specific information.

IN4 offers the following implementation of attribute data on the basis of numeric and string types:

- numeric
 - simple
- string
 - simple
 - denormalized
 - consistent
 - variational
 - composite

Simple numeric and simple string attributes are the simplest form of data storage:

```
# Area unit
SZ="r a . " ,
# Parcel area value
AS=0.2481
```

Fig. 2. Simple numeric and simple string attributes

The large amount of data stored in IN4 by its very nature is not atomic data, but they are a collection of

data. It is this type of string attributes can be classified as denormalized.

```
# chairman of executive body
GL="Петренко Іван Васильович"
```

Fig. 3. Denormalized string attribute

Figure 3 demonstrates how a group of data that can represent several independent attributes are combined into one. This approach eliminates the flexibility of access to information, and makes a

detailed search complicated. Also, some of the attributes partly adhere to the atomicity of the data but retain them in a clearly defined sequence:

```
# Address structure
AU = "<country code >,<index >, <district>, <region>, <settlement with type >, <street with type >, <building >, <department >, <flat>"
# Address example
AU="804 ,07416 , Київська , Броварський , с . Погреби , вул . Лугова , 12 , - ,1"
```

Fig. 4. Consistent string attributes

The disadvantage of the approach in Figure 4 is the positionality of parts of the attribute field, which makes filling and the presence of a special notation to fill in empty fields ("") complicated. Also, it should

be noted that not all parts of the attribute field observe atomicity. So, for example, a town and a street also contain information about the type of settlement and type of street.

```
# Information about land owners
# Three owners
VP="35%35%30%"
# One owner
VP="35%"
```

Fig. 5. Variational string attributes

The types of attribute string fields that may contain multiple attributes in a row can be attributed to the variational attributes. The feature of this kind

of attributes is that they can contain one mentioning of attribute values or several. Compositional attribute fields can be attributed to the last type of attributes.

```
# Metric information (one point example)
N=1 ,NP="172" ,X=5 5398 80. 30 ,Y=4 2544 68. 52 ,H=125.03 ,MX=0.02 ,MY=0.02 ,MH=0.05
```

Fig. 6. Composite string attributes

That is, the line of metric information is responsible for preserving the spatial description of the object. In spite of the fact that there are several keys at the same time, this record representing the same line in the file is one and indivisible attribute.

Another feature of representing spatial information by IN4 locks is the use of a spaghetti model. This can clearly be metric information of the exchange file:

```
N=1 ,NP="172" ,X=5 5398 80. 30 ,Y=4 2544 68. 52 ,H=125.03 ,MX=0.02 ,MY=0.02 ,MH=0.05
N=2 ,NP="172" ,X=5 5398 80. 30 ,Y=4 2544 68. 52 ,H=125.03 ,MX=0.02 ,MY=0.02 ,MH=0.05
```

Fig. 7. IN4 spaghetti vector model

Historical prerequisites for the formation of IN4

Despite rather narrow specialization of this format and the limited scope of application, which can be attributed to the territory of Ukraine, when applying

exclusively in the field of land cadastre, the format can follow a fairly clear path of development. As it is known [5, p. 272], this format has grown from the most popular Invent Grad system; later it was duly amended and approved for the use of land resources. The format has a simple syntax. With some skills, you can easily create and edit it using simple tools such as Notepad. Today, IN4 was officially abolished on the territory of Ukraine and replaced by the XML format. Nevertheless, the files of this format are found quite often, given the large number of previous activities. IN4 on the territory of Ukraine has operated since May 23, 2003 [25].

It should be noted that up to [27, p. 3, 26, p. 7, 10, p. 88, 12, p. 14] it becomes apparent that IN4 is to some extent based on the GBD format and is sometimes considered as one and with the format [26, p. 7]. The mentioned format contains information about the coordinates of the land and internal economic system. GBD data represent a set of point objects from the [18, p. 175] typed attribute attributes for them. According to [27, c. 20], the GBD file is a character and is created in the form of delimited keywords, where the character “#” converts the file’s record into a comment.

Indeed, the similarity of the formats IN4 and GBD, in terms of preserving geometry, is unprincipled. For the format, for example, the

continuation of the spatial information [12, p. 268] completely corresponds to the format adapted for the territory of Ukraine:

As you can see in Figure 8, the field of information about the GBD format almost completely repeats the form of recording metric information of the IN4 cadastral file. That is, it is possible to clearly state the origins of the IN4 format from the Invent-Grad system and origins of the adapted IN4 format for the land cadastre of Ukraine from GBD format. However, from the mentioned above and considering the name of the IN4 format, it is possible to try to make a deeper analogy of this family of formats (GBD and IN4) with previously existing data formats, namely, the format of the configuration files – INI. The sources of GBD and IN4 formats in the INI format indicate a number of links, namely:

- string is an attribute;
- the attribute is described by the key-value type token, where the separator is the “=” sign;
- attributes can be numeric and string (data limited by pins “”);
- character “,” as a delimiter of several values;
- the possibility of using independent data blocks;
- character as a comment;
- non-fixed formats;
- file encoding;
- other.

```
# point data in GBD
P,N =T12 ,FL=2 ,CD=0 ,LC=5 ,X=64797.60 ,Y=46362.16 ,H=278.7236 ,MX=0.01 ,MY=0.05
# point data in IN4
N=1 ,NP="172" ,X=5 5398 80. 30 ,Y=4 2544 68. 52 ,H=125.03 ,MX=0.02 ,MY=0.02 ,MH=0.05
```

Fig. 8. Geometry data in IN4 and GBD file formats

Obviously, due to the lack of clarity of the INI format and the lack of its specification, [8] variations in its implementations may be somewhat different. This applies to which character will be used as a

comment, or if one wants to use the characters “” as a metric for string attributes, but overall, the syntax remains the same. For the best analogy between INI and IN4 (GDB), it necessary give an example [7]:

```
[ SNAserverAutoTPs ]
BounceTP=bnceprms
TestTP=testprms
[bnceprms]
PathName=c:\sna\wbounce.exe
LocalLU=Eric
```

Fig. 9. INI file example

As it can be seen in Figure 9, the configuration file contains logical blocks (elements in square brackets), similarly as in the IN4 representing the layers. This assumption is supported by the popularity of parser

programs that can read the INI syntax for many programming languages. A part of the test file IN4 when reading a parser is shown in Fig 10.

```
BL,  
DS="1210100000" ,  
SZ="г а . " ,  
SR ,  
SC="0200021" ,  
AD="м . Дніпро , просп . Кірова , 93 , -" ,  
N=1 ,NP="104" ,X=55 744 40.9 2 ,Y=3 3728 97.5 2 ,MX=0,MY=0,
```

Fig. 10. IN4 sample

An error was received because the blocks, which in this case are presented as BL and SR, are not properly formatted, but the file is presented as a file. We receive a complete IN4 file that is designed in accordance with the requirements of INI. However, due to the compositional nature of the metric attributes, it is worth noting that they can be flashed as an INI file, since at the base level it returns all values as the single string attribute. In view of this, in the author's opinion, it is possible to speak about the presence of the INI format in IN4 format. The developed technology is shown in Figure 12. It is also

worth adding that the name of the format may lead to misunderstanding due to the lack of detailed information. In particular, there is the so-called IN5 [18, p. 172] format, which is called the new format of an XML-based cadastral file.

Therefore, in the author's opinion, it is important to note how exactly consider the file extension IN4. Due to the expansion of .info [9, 11] and .inf [17], however, with the need to keep a file association as informational, an unofficial approach was used to replace associative words with numbers. Therefore, IN4 should be pronounced as IN(in)4(four) or info.

```
[BL]  
DS="1210100000" ,  
SZ="г а . " ,  
[SR]  
SC="0200021" ,  
AD="м . Дніпро , просп . Кірова , 93 , -" ,  
N=1 ,NP="104" ,X=55 744 40.9 2 ,Y=3 3728 97.5 2 ,MX=0,MY=0,
```

Fig. 11. Updated IN4 sample

It can also be assumed that the digit at the end of the extension indicates a generation or version of the format, where "IN" indicates the use of the INI format as the base one, and "4" indicates versatility. However, even in this case, the IN4 has not undergone any changes and improvements to the release of the fifth generation since it was replaced by a new implementation that uses XML technology as a base.

However, due to the lack of IN1, IN2, and IN3, the version approach mentioned above seems to be ineffective. Therefore, in the author's opinion, IN4 should be considered as a file containing information or as info(IN4).

Features of the XML-based cadastral exchange file structure

With the introduction of a new cadastral exchange file, based on XML, document filling and the approach to document creation, significant changes have taken place.

By analogy with IN4, here, in addition to preserving the information itself, the logical sections of the information appear and join them into groups. However, it should be noted that the formats are strikingly different in nature, and making any direct analogies, in the author's opinion, are inappropriate.

However, comparing the form of preservation of information made for mechanism format deserves attention. Since, in the author's opinion, the very complex nature of cadastral information has led to a change in technology.

An important feature of the new cadastral exchange file is that it is the same as other XML-based formats, of which you can often refer to the most commonly used ones:

- SVG (Scalable Vector Graphics) [29, c. 2]
- GML (Geography Markup Language) [19, c. 6]
- KML (Keyhole Markup Language) [3, c. 26]
- SLD (Styled Layer Descriptor) [15, c. 6]

It is not just the format of the document but the entire markup language. So by means of analogy one can clearly state that the cadastral file is the result of the generated document executed using the cadastral exchange file markup language.

Since any language that uses XML must have a file schema, that is, a set of rules, then the cadastral exchange file markup language should have it. Consequently, the Digitals software contains a schema file called "IN4XMLSchema.xsd". This file can be considered as a file description of the rules for cadastral exchange file markup language.

As it was described before, XML is a relevant mechanism for describing complex structured

information and for reproducing the object nature of data. Despite the fact that interrelations between data in XML are formed by inserting one node in another, one can assume that in this case the data has a tree-like structure, however, the elements of the tree that are repeated or can be repeated in a constant form, in fact, also transform a set of node trees into objects, because it is necessary to perform a formal description by modulating the document, which will answer the question correctly whether it is executed or not.

It is obvious that describing the entire document by a scheme without its logical division into a subset is not convenient and generally leads to the complexity of supporting such schemes. Therefore, in the author’s opinion, it is necessary to allocate components of the scheme which should be considered as objects. Objects in the author’s interpretation are XML Schema components that can be represented using the XML Schema terminology exclusively by the end-node XML document (xsd:

element), which can consist of both simple (xsd: simpleType) and complex (xsd: complexType) types for describing nested nodes, their attributes, and interrelationships between them. An object is a container for storage of structured information.

This approach, in the author’s opinion, is suitable to work better with documents executed using XML and cadastral files, in particular. This method allows us to assess the level of implementation of the technological potential of the XML object mapping in the cadastral exchange file markup language. However, it should be noted that this approach is implemented in the language of markup cadastral files of the first generation exchange only partially.

Consequently, the problem of structured information cadastral exchange files that are implemented using XML technology is solved by presenting this information in the form of objects.

So, for example, a block of information about the address is implemented as a structure and has the form:

```
<Address>
  <Country></ Country>
  <ZIP></ZIP>
  <Region></ Region>
  < District></ District>
  <Settlement></ Settlement>
  <Street></ Street>
  <Building></ Building>
  <Block></ Block>
  <BuildingUnit></BuildingUnit>
</ Address>
```

Fig. 12. The address presentation of the first generation cadastral exchange file markup language

It is also worth noting that the usual division of information into groups using layers that can be found when generating cadastral exchange file using Digital software is absent in the structure of the cadastral file executed using XML. In contrast, IN4 stores data belonging to the layer consistently. It

should be noted that the vivid example of this is the mechanism of spatial information preservation, since it is a component that more closely distinguishes the process of storing XML data from the approach of storing IN4 data.

```

<MetricInfo>
  <PointInfo>
    <Point>
      <UIDP>1</UIDP>
      <DeterminationMethod>
        <GPS/>
      </DeterminationMethod>
      <PN>--</PN>
      <X>6 4 . 8 0 4</X>
      <Y>5 9 . 9 6 7</Y>
      <MX>1 0 . 0 0</MX>
      <MY>1 0 . 0 0</MY>
      <Description>--</Description>
    </Point>
    ...
  </PointInfo>
</Polyline>
<PI >

```

Fig. 13. Geometry representation of the first generation of cadastral exchange file markup language

As can be seen from the representation of a simple vector model, the deductions in XML are presented. In contrast to the spaghetti model, the topological model is taken. It is important to note that the analogue of the linear-node topology is used here.

The POLYVRT model is based on the fact that "PL" is an analogue of the chain and may contain several points, which in particular is confirmed by the data schema "IN4XMLSchema.xsd":

```
<xsd:element name="P" type="xsd:int" minOccurs="2" maxOccurs="unbounded" default="0" />
```

Fig. 14. Point links of the first generation of cadastral exchange file markup language

The number of elements "P" can vary from a range of 2 to infinity. However, an axial element is only half way to determine the ultimate geometry of the object, since there is no data which particular polyline belong to the object. The above data is included without

restriction in the data group of a particular object, and has the form. The Figure 16 displays the assignment of the previously defined polylines of the object. It is worth noting that this is a realization of the polygonal-linear topology.

```

<Externals>
  <Boundary>
    <Lines>
      <Line>
        <ULID>-1</ULID>
      </Line>
      <Line>
        <ULID>-1</ULID>
      </Line>
    </Lines>
    <Closed>true</Closed>
  </Boundary>
</Externals>

```

Fig. 15. Representation of the objects geometry of the first generation of cadastral exchange file markup language

Conclusions and proposals

During the transition from IN4 to XML, the re-compilation of the information on which the cadastral system in Ukraine works was carried out. In particular, an attempt was made to get closer to the structure of information and its preservation by means of a cadastral file. However, in general, the data structure remained open and required the finalization.

Given the historical aspects of the development of the Ukrainian cadastral exchange file, the following should be noted:

- The IN4 format was based on the INI format;
- IN4 realized a simple vector model for describing geometry;
- XML-based cadastral exchange file should be considered as file implemented using the cadastral exchange file markup language;

- XML-based cadastral exchange file implemented a topological model;
- XML-based cadastral exchange file used an object-oriented approach to describe complex structured information.
- object description of complex structured data requires a major revision;
- the cadastral exchange file markup language needs to be defined as such and fixed in the legal field.

Given the potential for using XML in the implementation of the cadastral exchange file, it is necessary to perform:

References

1. Bourret, Ronald. XML and Databases [online]. 2005. url: <http://www.rpbouret.com/xml/XMLAndDatabases.htm>.
2. Bray, Tim et al. Extensible Markup Language (XML). 1.1 (Second Edition). 2006, p. 45. url: <http://www.w3pdf.com/W3cSpec/XML/2/REC-xml11-20060816.pdf>.
3. Burggraf, David, ed. OGC KML 2.3. 2015, p. 266. url: <http://docs.openeospatial.org/is/12-007r2/12-007r2.html>.
4. Code Page 1251 Windows Cyrillic (Slavic) [online]. url: <https://msdn.microsoft.com/en-us/library/cc195053.aspx>.
5. D., Fedorov. Digitals. Vykorystannya v heodeziyi, kartohrafiyi ta zemleustriy. TOV "Analitika", 2015, p. 354. url: <http://geosystema.net/digitals/book/digitals-book.pdf>.
6. Eryk, Rey. Izuchaem XML. Ed. by Halunov A. Sankt-Peterburh: Symvol-Plyus, 2001. P. 408.
7. Example of WIN.INI Lines for an Invokable TP [online]. url: [https://msdn.microsoft.com/en-us/library/ee251978\(v=bts.10\).aspx](https://msdn.microsoft.com/en-us/library/ee251978(v=bts.10).aspx).
8. Fayly initsializatsiyi .ini [online]. url: <https://uk.wikipedia.org/wiki/.ini>.
9. File Extension INFO [online]. url: <http://file.downloadatoz.com/info-file-extension/>.
10. Heodezychna informatsiyna systema 6. chast II. ukovodstvo polzovatelya, p. 248. url: http://shels.com.ua/download/gis6_doc2.pdf.
11. .INFO File [online]. url: <http://filext.com/file-extension/INFO>.
12. Invent-HRAD v 2.01. url: <http://kadastrua.ru/stati/865-invent-grad.html>.
13. JSON Schema [online]. url: <http://json-schema.org/>.
14. Lisovyy kodeks Ukrainy. Kodeks [online]. 1994. url: <http://zakon2.rada.gov.ua/laws/show/3852-12>.
15. Lupp, Dr. Markus, ed. Styled Layer Descriptor Implementation Specification. 2007, p. 54. url: <http://www.openeospatial.org/standards/sld>.
16. Mertz, David. XML Matters: Putting XML in context with hierarchical, relational, and object-oriented models. 2001, p. 7. url: <https://www.ibm.com/developerworks/library/x-matters8/x-matters8-pdf.pdf>.
17. Overview of INF Files [online]. url: <https://docs.microsoft.com/uk-ua/windows-hardware/drivers/install/overview-of-inf-files>.
18. O.YE., Tolchevska and Konyayev YU.H. ?HIS tekhnolohiyi u zemleustroyi? In: Ekolohichna bezpekata pryrodokorystuvannya (2014) [online], pp. 168–179. url: http://irbis-nbuv.gov.ua/cgi-bin/irbis_nbuv/cgibis_64.exe?C21COM=2&I21DBN=UJRN&P21DBN=UJRN&IMAGE_FILE_DOWNLOAD=1&Image_file_name=PDF/ebpk_2014_14_19.pdf.
19. Portele, Clemens, ed. Geography Markup Language (GML) — Extended schemas and encoding rules. 2012, p. 91. url: <http://www.openeospatial.org/standards/gml>.
20. Pro kurorty. Zakon Ukrainy [online], 2000. url: <http://zakon2.rada.gov.ua/laws/show/2026-14>.
21. Pro pryrodno-zapovidnyy fond Ukrainy. Zakon Ukrainy [online], 1992. url: <http://zakon5.rada.gov.ua/laws/show/2456-12>.
22. Pro rehulyuvannya mistobudivnoyi diyalnosti. Zakon Ukrainy [online]. 2011. url: <http://zakon3.rada.gov.ua/laws/show/3038-17>.
23. Pro zatverdzhennya Polozhennya pro rehionalni kadastry pryrodnykh resursiv. Postanova kabinetu ministriv Ukrainy [online]. 2001. url: <http://zakon2.rada.gov.ua/laws/show/1781-2001-%D0%BF>.
24. Pro zatverdzhennya Poryadku funktsionuvannya natsionalnoyi systemy otsinky antropohennykh vyky-div ta absorbtsiyi pamykovykh haziv, yaki ne rehulyuyutsya Monrealskym protokolom pro rechovyny, shcho ruynuyut ozonovyy shar. Postanova kabinetu ministriv Ukrainy [online]. 2006. url: <http://zakon2.rada.gov.ua/laws/show/554-2006-%C3%90%C2%BF>.
25. Pro zatverdzhennya vymoh do struktury, zmistu ta formatu faylu obminu danymy rezultativ zemlev-poryadnykh robot u elektronnomu vyhyadi na mahnitnykh nosiyakh. Nakaz derzhavnogo komitetu Ukrainy z zemelnykh resursiv (Derzhkomzem Ukrainy) [online]. 2003.
26. Prohramni zasoby dlya roboty z prostorovymy danymy [online]. url: <https://buksis.nethouse.ua/static/doc/0000/0000/0031/31531.kdmks50i30.pdf>.
27. Rukovodstvo polzovatelya TopomapGeodezia 1.2 [online]. url: http://www.geodez-pro.com.ua/topomapegeodezia/topomapegeodezia_ug.doc.
28. RX Schema [online]. url: <http://rx.codesimply.com/>.
29. Scalable Vector Graphics (SVG). 1.1 (Second Edition). 2011, p. 826. url: <https://www.w3.org/TR/SVG11/REC-SVG11-20110816.pdf>.
30. Windows-1251 [online]. url: <https://uk.wikipedia.org/wiki/Windows-1251>.
31. XML technology [online]. url: <https://www.w3.org/standards/xml/>.
32. XML, the New Database Heresy [online]. url: <http://www.25hoursaday.com/weblog/PermaLink.aspx?guid=d28ce1fb-7b27-407d-b1a3-0b9a34831ca1>.

Impact of Various Vegetation Types on Mobile Laser Scanning Elevation Accuracy

Natalja Liba, Kaupo Kokamägi, Ina Järve, *Estonian University of Life Sciences*

Abstract. Geodesy is currently experiencing a rapid and very diverse development of surveying technologies. Therefore it is important to evaluate the suitability of one or another technology in different situations for different tasks. This is especially needed for geodesy companies to make the right investment decisions. One of the innovative measurement technologies is mobile laser scanning, a rapidly evolving method of collecting survey data. It is mainly used for surveying objects such as streets, roads, railways and rivers. The results of mobile laser scanning can be used in everyday geodesy as well as for making three-dimensional models. As the development of other technologies makes it possible to process large amounts of mobile laser scanning data, this measuring method will soon become increasingly more attractive in Estonia. The paper analyses the technology of mobile laser scanning in one specific situation pointing out the dependence of elevation accuracy on the nature of the vegetation. It also analyses the amount of accuracy of mobile laser scanning technology that it is possible to increase by using cross-section profiles. For accuracy assessment, the mobile laser scanning elevation data and control points measured with GNSS device were compared. The study found that the elevation accuracy of mobile laser scanning depends substantially on the density and height of vegetation. Drawing ground profiles increases the accuracy of the final result. The result of RMSE of mobile laser scanning elevation data was 0.70 meters, the result of the RMSE of mobile laser scanning elevation data using drawing ground profile was 0.53 meters. It can be concluded that the most reasonable time for conducting mobile laser scanning would be during the season when vegetation is sparsest.

Keywords: laser scanning; mobile laser scanning; accuracy of elevation data.

Introduction

Laser scanning is a survey method that collects X, Y and Z coordinates from surrounding environment for representing spatial image of a surveyed object. For that specific technology is used. The result from scanning is a point cloud that after processing is combined into the model and bound into the coordinate system. [2] It is possible to make 2D drawings and 3D models, fix objects from environment, make control measurements and so on from point clouds. [8]

Laser scanning is divided into the terrestrial and aerial laser scanning. Terrestrial laser scanning can

also be divided into the static and mobile laser scanning. In the static mode, the scanning is carried out in one fixed stable position on the ground level: on a tripod. Mobile laser scanning is performed on a moving vehicle (a car, a train or a boat). Often, laser scanning systems used on water are treated as a separate scanning thread called a Boat-Based Mobile Mapping System (*BoMMS*) [5]. Aerial laser scanning is carried out by aircraft.

Figure 1 shows different ways of scanning.



Fig. 1. Methods of laser scanning: A) static laser scanning in room on a tripod [16]; B) mobile laser scanning outside from the car [17]; C) aerial laser scanning from an aircraft [15]

Laser scanning was invented in the beginning of the 1960s, but the technology then did not allow to use devices for mapping. In the middle of the 1990s, the technology of direct positioning and the overall development of computer technology enabled to use

laser and scanning systems in topographic mapping. Since then, the laser scanner has been used in geodesy and engineering sciences. [11]

One of the innovative measurement technologies is mobile laser scanning. It is a rapidly evolving way

of collecting survey data. The first mobile laser scanning system began to spread abroad in the late 1990s, and since then the scope and the supporting hardware of the laser has increased [7]. Therefore, the use of mobile laser scanning systems has become increasingly attractive and more common for foreign geodetic companies.

Mobile laser scanning is a new direction for geodetic companies in Estonia also. At the moment, only few companies have their own mobile laser scanners, mostly hardware is borrowed from abroad through different projects [13]. Before using the hardware, it is necessary to investigate its accuracy and effectiveness. Several companies cooperate with the Estonian universities, including the Estonian University of Life Sciences (a Chair of Geomatics) where several graduation theses have been written in this field.

Researchers at the Estonian University of Life Sciences with students studied the accuracy of mobile laser scanning elevation data in forests and open areas. From the results it can be concluded that high-level objects beside the road areas affect the elevation data reached by the mobile laser scanning system. In geodetic works, requiring greater accuracy, additional methods such as denser placement of positioning marks, should be used. [1].

The above described method was investigated in the USA, California, where an experiment was conducted to find out what is the indicative placement for the marks on the road and what is the accuracy of the point cloud according to the placement. The results showed that the standard deviation remains constant after 1,200 meters between marks. It appeared from the 24-hour experiment that the vertical error decreased 51% and more using ground control targets, even at very large target spacing. [10]

In 2016, mobile laser scanning in one of the car parks of Tallinn University of Technology was conducted at various speeds. The point clouds of

mobile laser scanning and static terrestrial laser scanning were compared. It turned out that differences in absolute values did not exceed 15 cm in most cases. [4]

In current research, mobile laser scanning technology is analysed, pointing out the dependence of elevation accuracy on the nature of the vegetation and distance of the measurement. It is also analysed how much it is possible to increase accuracy of mobile laser scanning technology by using cross-section profiles.

Materials and methods

The methodology of the research can be divided as follows:

- Collecting laser scanning data;
- Data processing and additional surveys outside;
- Elevation accuracy assessment by control points;
- Analysis and conclusions.

Collecting laser scanning data

Mobile laser scanning data used in research were collected in the summer of 2015 on the route Tallinn-Tartu (E263) in the section of Põltsamaa-Kärevere. The project was carried out according to the order of Estonian Road Administration and accomplished by an Estonian surveying company OÜ REIB.

For the preparation, the pavement markings, used as control points, were measured with a GNSS device Trimble R8. Measurements were done early in the morning.

The scanning was carried out on June 30, 2015. Collecting scanning data lasted about two hours and about 40 km of road was scanned in that time. Scanning was performed by the continuous measurement method. In this case, the vehicle moved along the trajectory without stopping.

As the vehicle moves along the trajectory, a three-dimensional point cloud draws out from the profiles (Figure 2).

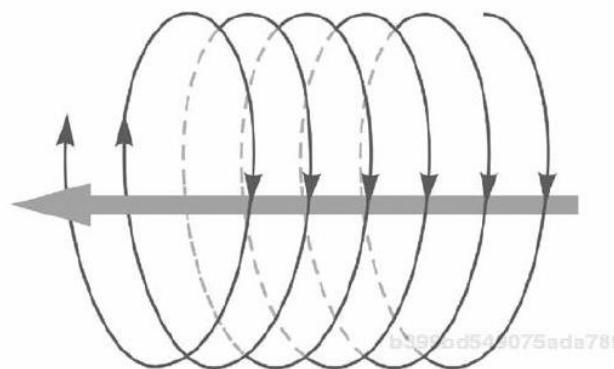


Fig. 2. Mobile laser scanning made by the continuous measurement method: the point cloud is formed by the profiles perpendicular to the direction of travel [14]

The scanning density is directly related to the speed of the vehicle carrying the laser scanner. At higher speed, the point density is lower. To initialize and calibrate the IMU (*Inertial Measurement Unit*) and GNSS devices for mobile laser scanning, the vehicle moved on the road back and forth at a speed of approximately 80 km/h. At that speed the point cloud density, 5 meters from scanner, was 430 points

per square meter (Table 1). Mobile laser scanner system StreetMapper 360 was used for this research. The system has two Riegl VQ250 laser scanners. During the scanning two Ashtech XII GNSS receivers were set up on geodetic reference network points in each end of the road section and data were collected during the whole scanning.

TABLE 1
Average point density of VQ250 laser scanners used for scanning the Põltsamaa-Kärevere section (StreetMapper 360 Specifications)

Speed (km/h)	Average point density per 1 scanner (points per square meter, 5 meters from scanner)				
		25	30	60	80
Point density (pt/m ²)	1375	860	573	430	344

Each measurement produces points in a new coordinate system. For producing a point cloud in general coordinate system, the mobile scanner is

equipped with GNSS receiver and IMU device (Figure 3). In addition, the watches for all sensors must be exactly synchronized. [14]

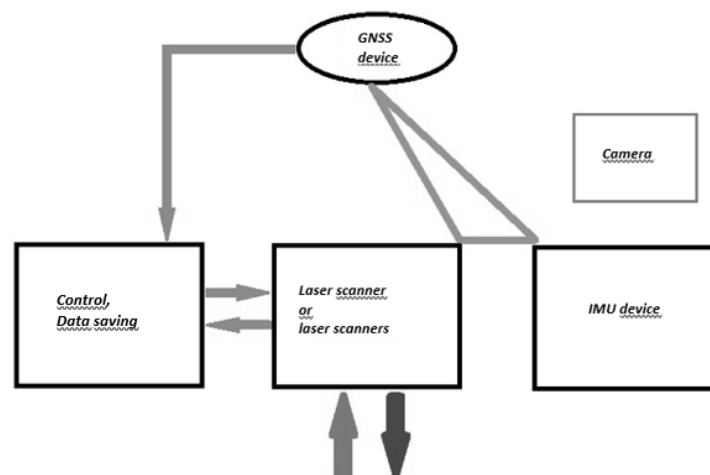


Fig. 3. Mobile and aerial laser scanning system parts on board [14]

Data processing and additional surveys

Data processing and additional surveys took place after receiving scanning data. An important part here is the software which is used to merging overlapping point clouds, connecting point cloud in global coordinate system and removing deviated points from the point cloud [6]. Data processing is done by software AutoCAD LT 2014, AutoCAD Civil 3D 2015 and by Autodesk Recap 2015.

During data processing, the point clouds were classified and corrected. Control points coordinates measured previously and GNSS data were used for that. The point cloud was divided into smaller sections to make the further processing smoother. Then ground profiles were drawn after every 25 meters. This was done for making the ground elevation model (Figure 4).

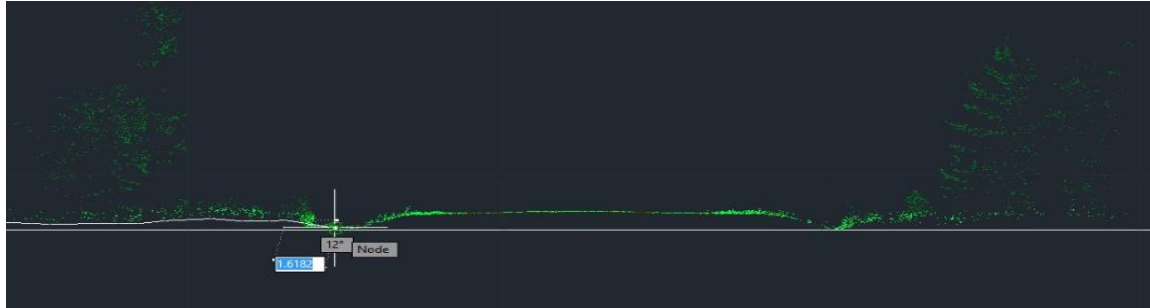


Fig. 4. Drawing ground cross-section profile with AutoCAD

The places without enough information in the point cloud (like road crossing ditches and rivers) were surveyed with total station and GNS devices during additional surveys.

Accuracy assessment of elevation data

An extra road section Kärevere-Põltsamaa with adjacent areas was measured for the research. Three different vegetation polygons formed from the section. In order to study the dependence of elevation accuracy on the nature of vegetation and on the distance of the survey, the mobile laser scanning elevation data were compared to elevation data of GNSS control points. Also, the accuracy of mobile laser scanning elevation data was compared to the accuracy of ground profile elevation data in order to

analyse the level of accuracy of mobile laser scanning technology that it is possible to increase by using cross-section profiles obtained from the point cloud.

Only classified, corrected and block-sectioned point clouds were used in this research.

The characterization of the three chosen polygons:

- Polygon I: a field vegetated with 1 meter high crop. 73 checkpoints were measured (Figure 5);
- Polygon II: a pasture with low and sparse vegetation. 50 checkpoints were measured (Figure 6);
- Polygon III: contained a bushy ditch and a field behind it. 97 checkpoints were measured (Figure 7).

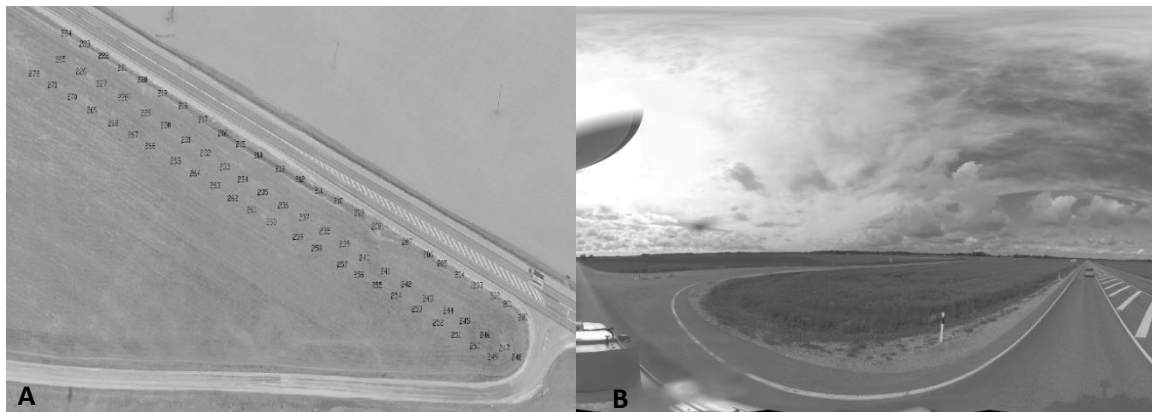


Fig. 5. Polygon I: A) the layout of checkpoints measured with a GNSS device, B) photographed from the mobile scanning system during the scanning

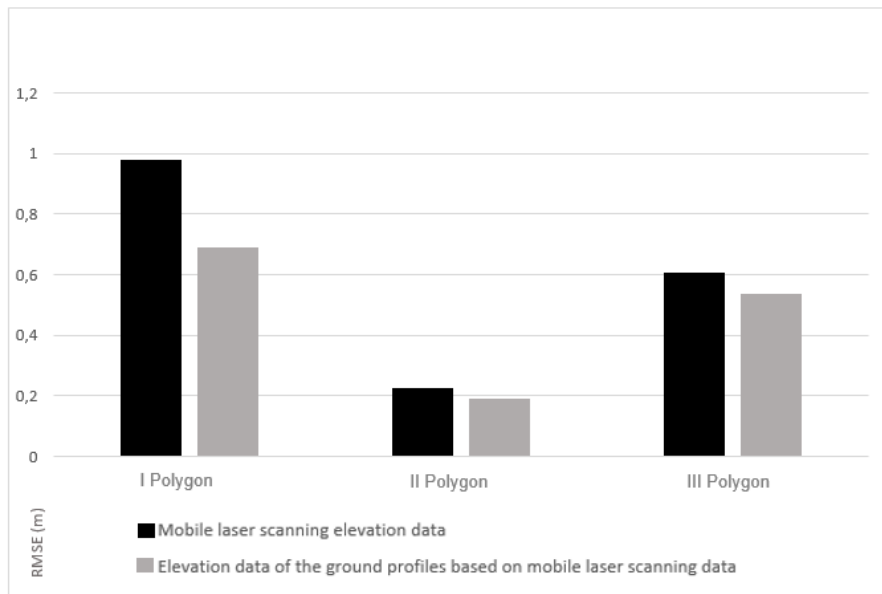


Fig. 8. Comparison of elevation data RMSE's using different measuring methods in Polygons I, II and III

The most accurate elevation data from all three polygons using different measurement method was obtained in Polygon II covered with low vegetation. Surprisingly, the most inaccurate data were in Polygon I covered with crop. In this case the result of the RMSE from mobile laser scanning data was 0.98 m, which was also the approximate height of the crop. As it was very densely populated vegetation, the upper part of the vegetation was probably identified automatically as the ground, which caused the mistake.

As expected, cross-profiles affected mobile laser scanning data to be more accurate. This is possible because the places that are unidentified by laser scanning may be identified by drawing cross-sections (for example, areas behind thick bushes).

The result of the RMSE of the elevation data of three polygons put together was 0.70 meters for mobile laser scanning and 0.53 meters for profiles based on mobile laser scanning. The comparison of the mean accuracy of three sections put together is shown in Figure 9.

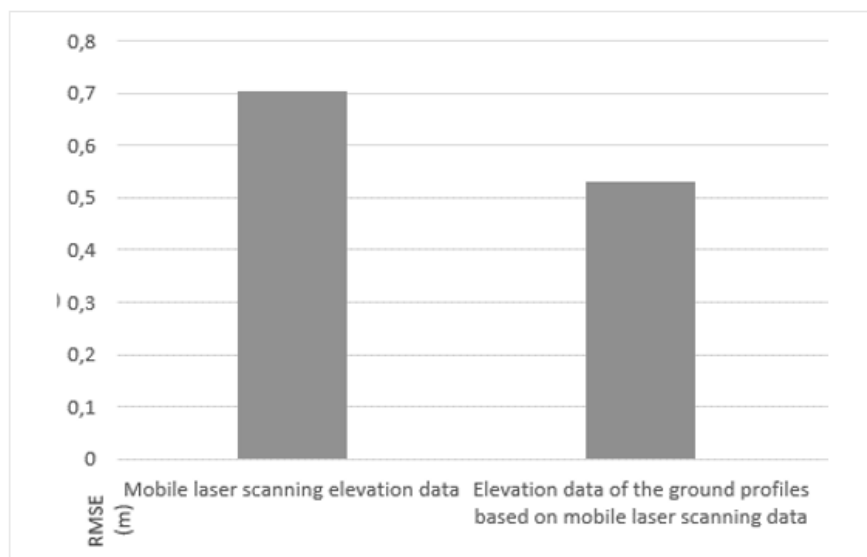


Fig. 9. Comparison of mean elevation data RMSE's of all the polygons using different measuring methods

Results of the research show that the accuracy of mobile laser scanning elevation data depends substantially on the density of vegetation in a scanned area. It can be said that scanning gives more accurate

results at the time when there is less vegetation, in early spring or in late autumn. Also, drawing the cross profiles increases the elevation accuracy of mobile laser scanning data. It was also found that the

further from the mobile scanner the point is, the larger
RMSE results of elevation data become.

References

1. **Annok, G.** *Mobiilse laserskaneerimise kõrguslik täpsus erineva taevaalaotuse korral*, 2017. (Bachelor's thesis). Estonian University of Life Sciences, Institute of forestry and Rural Building. Tartu. 41 p.
2. **Barber, D., Mills, J.** *3D Laser Scanning for Heritage: Advice and guidance to users on laser scanning in archaeology and architecture* [online]. United Kingdom: English Heritage, 2011 (cited 16.08.2016).
3. **Joala, V.** *Laserskaneerimine – suure detailsusega 3D-mõõtmine*. – TeeLeht. 2006. No 2, p. 21-23.
4. **Julge, K., Ellmann, A., Vajakas, T., Kolka, R.** *Initial Tests and Accuracy assessment of a Compact Mobile Laser Scanning System* [online], 2016. Prague, Czech Republic. ISPRS, volume XLI-B1. <https://www.int-arch-photogramm-remote-sens-spatial-inf-sci.net/XLI-B1/633/2016/isprs-archives-XLI-B1-633-2016.pdf>
5. **Kukko, A., Kaartinen, H., Hyypä, J., Chen Y.** *Multiplatform Mobile Laser Scanning: Usability and Performance – Sensors*, 2012. No 12, p. 11712-11733.
6. **Lee, S.Y., Majid, Z., Setan, H.** *3D Data Acquisition for Indoor Assets Using Terrestrial Laser Scanning* [online], 2013 (cited 12.08.2016). Turkey. 6 p. <http://www.isprs-ann-photogramm-remote-sens-spatial-inf-sci.net/II-2-W1/221/2013/isprsannals-II-2-W1-221-2013.pdf>
7. **Puttonen E., Lehtomaki M., Kaartinen H., Zhu L., Kukko A., Jaakkola A.** *Improved Sampling for Terrestrial and Mobile Laser Scanner Point Cloud Data – Remote Sensing*, 2013. No 5, p. 1754-1773.
8. **Pärtna, J.** *Tänapäevastest mõõdistustehnoloogiatest* – TeeLeht. 2016. No 84, p 37-39.
9. **Randjärv, J.** *Geodeesia I*, 1997. Tartu. 399 p.
10. **Ravani B., Yen K., Lasky T.A., Donecker S., Jian Z.** *Application of Mobile Laser Scanning for Lean and Rapid Highway Matenance and Construction* [online], 2015 (cited 23.11.2016). United States of America. 65 p. <http://ahmct.ucdavis.edu/pdf/UCD-ARR-15-08-28-01.pdf>
11. **Shan, J., Toth, C. K.** *Topographic laser ranging and scanning: principles and processing*, 2009. United States of America: CRC Press. 590 p.
12. **Staiger, R.** *Terrestrial Laser Scanning Technology, Systems and Applications*, 2003. Germany. 10 p.
13. **Toompuu, B., Alanurm, K.** *Laserskaneerimise andmete ja tehnoloogia kasutamine Eestis*, 2013. (Bachelor's thesis). Estonian University of Life Sciences, Institute of forestry and Rural Building. Tartu. 85 p.
14. **Vosselman G., Maas H. G.** *Airbone and terrestrial laser scanning*, 2010. Whittles Publishing. 318 p.
15. Informed Infrastructure. <http://informedinfrastructure.com/12620/reality-computing-for-civil-infrastructure> (cited 30.10.2017)
16. Ingeniería y Arquitectura Sinluz. <http://www.sinluz.com/servicios/57-servicios/topografia/escaneado-laser-3d-para-arquitectura> (cited 30.10.2017)
17. Topcon Positioning Systems, Inc. <https://www.topconpositioning.com/utilities> (cited 30.10.2017)

WATER RESOURCES ENGINEERING

DOI: 10.22616/CE.2017.014

Assessment of Improving the Efficiency of Fire Extinguishing by Using Surface Active Agents

Georgij Kiselov, Vladimir Jemeljanov, Janis Ievinsh, *Riga Technical University*

Abstract. Fire causes considerable material damages to the ecology and environment as well as in a number of cases it is accompanied by human victims. No material goods can replace human life, therefore human life and safety always remain in the first place. Since fires potentially can cause a considerable damage, the fire safety and firefighting sphere are permanently developing in the world in order to improve the state of fire safety, reduce the risk of fires, successfully extinguish the fire and minimize the potential consequences. Since successful firefighting is closely associated not only with the level of fire-fighting equipment, extinguishing techniques, manufacturing and construction methods, building constructive solutions, but also to a large extent depends on efficiency of the extinguishing agents, the authors' aim is to study the efficiency improvement of water and its mixtures with surfactants. The article is based on the experiments, which were carried out under laboratory conditions, simulating Class A and B fires. A stationary automatic fire extinguishing system was used as the fire-fighting equipment with a sprinkler-type system, providing firefighting with a sprinkler, feeding extinguishing agents into a hotbed in a fine spray stream. In the practical experiment, foam concentrates of different producers, brands and types were used as surface-active substances and impurities which were added to water in different concentrations and combinations. The concentration of active surfactants in water directly affects fire-extinguishing properties of liquids, i.e., observing the amount of surfactants and water liquids one can achieve the reduction of the amount of water, which allows to reduce material loss connected with using water in fire extinguishing. However, an in-depth study must be carried out to find out how economically profitable is the use of SAA for fire extinguishing.

Keywords: fire extinguishing, efficiency, reaction zone, surface active agents, mixtures.

Introduction

Fire causes considerable material damage to ecology and environment; in a number of cases it is accompanied by human victims. No material goods can replace human life, therefore human life and safety always remain in the first place. Since fires potentially can cause considerable damage, the fire safety and firefighting sphere is permanently developing in the world in order to improve the state of fire safety, reduce the risk of fires, successfully extinguish the fire and minimize the potential consequences. Since successful firefighting is closely associated not only with the level of fire-fighting equipment, extinguishing techniques, manufacturing and construction methods, building constructive solutions, but also it depends on efficiency of the extinguishing agents, the authors' aim is to study the efficiency improvement of water and its mixtures with surfactants in automatic fire extinguishing systems with finely sprayed water by adding the foam agents.

The present work presents a statistical study where the number of fires, their impact on our everyday life, consequences, victims and losses are analysed. The first part of the study describes the fire disposal options from analytical and theoretical point of view, as well as the nature of the combustion process is examined revealing a wide range of

firefighting horizons, showing the directions and techniques for quick and efficient extinguishing of fire, which is practically tested, summarizing the results. The practical part is based on the experiments, which were carried out under laboratory conditions, simulating Class A and B fires. A stationary automatic fire extinguishing system of sprinkler-type was used, providing firefighting with a sprinkler that delivers the extinguishing agent into a hotbed in a fine spray. In the practical experiment, foam concentrates of different producers, brands and types were used as the surface-active substances and admixtures added to the water in different concentrations and combinations. The work studies the regularities of extinguishing agents' admixtures, as well as mixture combination that can conceptually change the automatic fire-extinguishing system design. The firefighting principles have been developed for solid substances fires in open and hard-to-reach areas, considerably reducing the time of firefighting and the amount of required extinguishing agent (water), as well as significantly reducing the negative environmental impact.

Theory of Combustion Heat

To define the most rational techniques of improving fire fighting ability of water, one has to

examine combustion and extinguishing mechanisms. According to the latest views, theory of extinguishing wood and other solid polymer materials is based on the theory of combustion heat. Main regularities are studied in the works of J.Zeldovich, D.Frank-Kamenetsky and others [12]. According to their research, to stop burning of wood or other solid polymer materials means to stop an exothermic reaction that takes place in a thin layer in the combustion zone (reaction zone). Wood, as one of the most wide-spread burning nature materials, burns in two regimes during the fire:

- Homogenous diffusive that defines the spread and development of fire;
- Heterogenous, when charred residues are completely burned.

At the stage of homogenous diffusive burning there takes place pyrolysis of wood, when volatile products are emitted. They mix up with air oxygen of burning zone and make burning mixture. This mixture, burning above wood surface, emits a significant amount of heat energy. Part of this energy comes to the surface of burning material, rising its temperature, intensifying the pyrolysis process and thus speeding up the process of burning until its stabilisation. On average, the parameters of burning material are the following [13]:

- a) Wood surface temperature from 500 - 700 °C;
- b) Thickness of heated layer (until volatile substances emergence temperature from 200 - 500 °C) is about 1 cm;
- c) Speed of combustion from is from 0.008 to 0.01 kg/m² s.

Flame temperature is 1000 - 1200 °C, which creates heat emission on average equal to 225.7 kJ/m²s.

In the reaction zone also combustion products are heated because of emitted heat. Simultaneously with these processes there takes place heat return process. Temperature stabilises in the reaction zone when the speed of heat emission q_1 gets balanced with heat return speed q_2 . Consequently, there is heat balance in the reaction zone, but the temperature of the zone is combustion temperature and heat balance temperature. It is defined that combustion temperature of a substance is not a constant quantity, it varies depending on emitted and returned heat speed proportion. The speed of heat emission in diffusive combustion zone depends on many factors. At constant amount of oxygen in the air and in burning substance, the speed depends on diffusion speed of reactive substances in the reaction zone as well as on the combustion heat and the degree of burning polymer material complete combustion.

In diffusive combustion zone heat emission speed on zone reaction surface unit is the following:

$$q_1 = Qk_s, \quad (1.1)$$

where: k_s – amount of oxygen that reacted in a unit of time on reaction zone surface unit;

Q – reaction heat effect.

Simultaneously with heat emission, in the reaction zone there takes place transfer of heat in convective way into environment and in radiant way from the reaction zone. Heat delivery speed q_2 depends on combustion temperature, gas temperature in the environment and corresponding heat exchange ratios:

$$q_2 = \alpha(T_r - T_c) + \Theta \vartheta(T_r - T_c^4) \quad (1.2)$$

where: α — heat exchange ratio, W/(m²*K);

T_r — combustion temperature, K;

T_c — environment temperature, K;

Θ — reaction zone charring degree (0.20 – 0.85);

ϑ — Stefan —Bolcman constant, 20.5 kJ/(m²*K).

$\sigma = 5.670400(40) \times 10^{-8}$ Wm⁻²K⁻⁴ Bolcman constant

To extinguish burning wood or other solid burning material, it is necessary that heat removal speed would exceed heat emission speed. Then the maximum combustion temperature decrease according to J.Zeldovich research is $\frac{3RT_g^2}{E}$. Then

cooling temperature T_p is:

$$T_p = T_r - \frac{3RT_g^2}{E} \quad (1.3)$$

where: R – universal gas constant; E – activation energy.

Combustion temperature can be made lower than extinguishing temperature by reducing heat emission speed. It can be achieved by various methods, but at least one of the below mentioned conditions should be observed:

- a) to isolate combustion zone from air or reduce oxygen concentration to the level when combustion cannot happen;
- b) to reduce the temperature of burning substances and materials below their flashpoint;
- c) to cool reaction zone below defined cooling temperatures (T_p);
- d) to intensively slow down chemical reaction flames;
- e) to liquidate flames mechanically with the help of strong gas or extinguishing substance jet;
- f) to create conditions for fire blocking.

All fire-extinguishing substances have a combined effect on substance combustion process. But each fire-extinguishing substance has some characteristic dominating feature. Water as fire-extinguishing substance mostly works in three kinds of extinguishing mechanisms: cooling burning materials and reaction zone, dilution of reaction zone with water vapours and isolation of burning material from reaction zone. Extinguishing of burning wood is

now based mostly on its cooling below 200 – 250 °C. Until extinguishing moment burning wood is heated to definite depth, and a surface charcoal layer is formed on it. Its thickness depends on free combustion time of the fire. The temperature of the upper layer can reach 500 - 700 °C [5]. The speed of heat supply to the depth of wood and, consequently, the speed of material combustion depends on surface charcoal layer temperature. So the main task of extinguishing is to reduce the surface charcoal layer temperature to the cooling temperature. Supplying water with a compact or sprinkled jet touches the burning wood surface and forms a thin water layer, which on the one side comes into contact with the charcoal layer, but on the other side contacts heated gas and vapour that are in the combustion zone. That is why water layer simultaneously takes up the heat from wood charcoal (q_d), gas (q_g) and from combustion zone surface (q_2);

$$Q_U = q_d + q_g + q_2, (1.4.)$$

Where: Q_U – heat taken by water during extinguishing process.

Water has high heat capacity and vapour forming heat; it intensively takes heat and forms vapour that dilutes burning substances in the reaction zone. Some very important for fire extinguishing physical water characteristics change at its heating. First of all, it applies to thermal conductivity, which from 1.791×10 W/m.degree at 45 °C reduces until 0.0639×10 W/m.degree at 100 °C, which also changes water heat insulation properties. The most marked changes are in water viscosity depending on the temperature. From the analysis of mentioned changes in water characteristics it can be seen that water with low viscosity quickly drains from burning wood and a large part of it does not participate in extinguishing process. Consequently, water supply intensity and its consumption should be increased that causes certain problems during fire and it leads to the increase in fire extinguishing time and causes bigger material loss [1, 2, 8]. To compare real water consumption with theoretically necessary for extinguishing wood combustion process, we calculate the amount of water necessary for extinguishing 1 m² of burning wood. The water is supplied as compact or spray jets. Dominating mechanism relatively is wood cooling until its decomposition temperature when volatile substances are emitted. Other factors like combustion zone cooling and dilution of burning mixture with water vapours are not taken in consideration.

Then necessary condition for combustion interruption will be:

$$Q_U > Q_K (1.5.)$$

where: Q_U — amount of heat taken by water from burning wood, J.;

Q_K — amount of heat taken by wood from combustion zone, J;

$$Q_u = S_U \delta_U \gamma_U C_U \Delta t_U + S_u \delta_U \gamma_U r (1.6.)$$

where: S_U — water surface area on the material extinguished, m²;

δ_U — thickness of water layer, mm;

γ_U — specific weight of water, kg/m³;

C_U — specific heat capacity of water, J/kg;

Δt_U — difference between boiling temperature and basic temperature of water, which is relatively taken as 20 °C;

r — vapour forming hidden heat, J/kg;

$$Q_K = S_K q_p \tau_p + S_K \delta_K \gamma_K C_K \Delta t_K, (1.7.)$$

where: S_K — burning wood area, m²;

q_p — heat flow from the reaction zone to burning wood surface;

τ_p — burning time (extinguishing), s;

γ_K — specific weight of wood, W;

C_K — heat capacity of wood;

Δt_K — difference between maximum wood heating temperature and temperature to which it is cooled.

All quantities in the equations (1.6. and 1.7.) are known, except δ_U . After relevant modification of the equations 1.5., 1.6. and 1.7. we get:

$$\delta_U = \frac{q_p \tau_p + \delta_K \gamma_K C_K \Delta t_K}{\gamma_U C_U \Delta t_U + \gamma_U r}, (1.8.)$$

Because of extinguishing, heat radiation reduces from maximum to zero. We conditionally accept that the amount of heat taken by wood during extinguishing process is one half from the maximum. Taking into consideration that the temperature of heated wood layer is not homogenous and varies from 700 – 200 °C, we conditionally accept temperature reduction while cooling the heated layer as 250 °C. Then the necessary thickness of water layer at extinguishing time 10 s will be:

$$\delta_U \approx 0.5 \text{ mm}$$

The assumptions introduced significantly simplify the real physical scene of extinguishing process. But the quantitative indicators acquired leave no doubt, as from the set of many extinguishing mechanisms only one, conditionally accepted as dominating, was chosen. While extinguishing, not only the extinguishing mechanism, but also the dilution mechanism with water vapours of the reaction zone is working, as evaporating 1l of water, 1700l of vapour are formed. But only a small part of vapour takes part in zone dilution, as the volume of

the reaction zone is much smaller than the volume of vapour, and water vapour going through it, quickly leave the reaction zone. Water forms only 0.009 mm thick layer on the wood surface. This shortcoming of

water as the means of extinguishing is proved by real specific water consumption for fire extinguishing. It is shown in Table 1.

Specific Water Consumption in Fires [3,5,7.]

TABLE 1

Nr. p.k.	Name of fire object	Fire area, m ²	Total quantity of water consumed, l	Specific water consumption, l/min.
1)	Wooden house	40	2,000	500
2)	Furnishings in a wooden house	20	2,000	100
3)	One-storey wood-working shop, U3 Fireproofness degree	500	25,000	500
4)	One-storey Store for industrial goods U3 Fireproofness degree	40	16,000	400

Slight actual water layer thickness on burning wood surface cannot be a safe insulating layer for heat energy effect from the reaction zone on burning material. Consequently, water flow rapidly down the burning surface, when a water jet is directed to another burning place, hot combustion products and flames from nearby burning wood repeatedly affect the area being extinguished. As a result, the temperature of extinguished area surface rises, combustion products start emitting again and combustion gets renewed. It can be prevented by a longer effect of water on wood and thickening its layer which neutralises the effect of heat factors in the time necessary for extinguishing burning surfaces. Extinguishing practice shows that such an approach is not justified and one has to search for improving the extinguishing capability of water. Due to the fact that the aim of the research is to improve the effectiveness of fire extinguishing, it is necessary to examine and simulate fire combustion and extinguishing processes in a more detailed way, analysing the effect of surface-active agents (further on - SAA) in the process of extinguishing.

The Quantity of Water Mixture Use Ratio

One of the positive characteristics of water is, first of all, its good transportation capacity and cheapness, convenient supply to the combustion zone, accessibility and wide distribution, so it becomes clear why water is the most favourable means of extinguishing. Inspecting all positive and negative characteristics of water closer, the shortcomings of water as means of extinguishing must be noted. High surface tension $\delta = 72.53 \times 10^{-3}$ H/m 20 °C [9, 2], low dynamic viscosity ratio $\eta = 1 \times 10^{-6}$ m²/s, high freezing temperature $t_s = 0$ °C, high electric conductivity 4.41×10^{-8} Ω⁻¹×cm⁻¹ at 18 °C, chemical activity when facing alkali and alkali-earth metals, carbide and others, corrosive effect on metals and other materials

reduces extinguishing effectiveness of water, efficiency ratio and restricts wider use of water.

Due to the fact that water has high surface tension and low dynamic viscosity ratio, it flows down the surfaces very quickly and almost is not absorbed in materials, but the electric conductivity of water does not allow using it without special protective equipment for fire extinguishing systems under voltage. High surface tension and low viscosity is of great importance, as exactly these parameters influence the amount of water consumption and extinguishing time. It is connected with material loss caused by fire, as well as large consumption of funds constructing internal firefighting water supply system with large diameter pipes. That is why it is very important to improve the fire-extinguishing efficiency of water.

To increase the efficiency ratio of water while fire-extinguishing, various types of "quencher" are used in fire extinguishing practice for a long time. The use of quencher reduced the necessary for fire-extinguishing water consumption almost twice due to significant rise in absorption capacity. But further improvement of fire-extinguishing efficiency only with the use of quencher appeared impossible. Therefore, obviously, parallel to improving physical and chemical characteristics of water, water supply technique to the combustion zone, extinguishing tactics and other parameters defining the effect of extinguishing should be improved. But at the moment these hidden reserves for increasing the fire extinguishing efficiency of water with the help of quencher are not implemented. At the moment any research in this direction is not done, because the colour of some materials changes irreversibly, when using quencher, surface-active agents, for fire extinguishing, wood cannot be lacquered further on, interstorey flooring gets soaked much faster [9]. In the authors' opinion, two last fire influencing factors are not significant, but the last one indicates that the

advantages provided by fire extinguishing with modified water using SAA divided into two groups are not fully used.

It is still supplied as previously using a lot of water in excess which drenches interstorey flooring and floods the storeys. To increase the extinguishing efficiency of water, the research on raising water viscosity was done for its greater adhesion to the surfaces extinguished. By raising water viscosity the thickness of water layer on the surface of burning materials grows and its cooling and insulation capacity grows.

The efficiency ratio of all energy systems (further on – ER) has been seriously studied for many years. Such research is being conducted at the moment as well. In our case ER is the water utilization ratio K_i , when extinguishing the fire K_i increase research is connected with its so far low values that complicate the extinguishing process and cause great material loss. K_i must be understood as proportion between the theoretically necessary amount of water V_t for definite fire extinguishing and the actually consumed amount of water V_f . The amount of water necessary for extinguishing open solid combustion materials, including wood, is defined theoretically $K_i = V_t/V_f$. K is a non-dimensional value with multiple dependence that complicates its research. The reasons of these difficulties are both subjective and objective [11]. The factors defining K value can be shown as follows:

1. Efficiency of extinguishing material which depends on physical and chemical characteristics of a substance and the efficiency of its supply to combustion zone K_1 method;
2. Nonsimultaneous supply of fire extinguishing substance to all the fire area (causes of subjective and objective character) K_2 ;
3. Impossibility to supply extinguishing substance to some burning surfaces as there are hidden combustion surfaces K_3 ;
4. Reserve ratio K_4 and others.

The meaning of K_i in fire-fighting practice is essential. The improvement reduces fire extinguishing time, raises extinguishing efficiency of water and its consumption, reduces material loss of all kind, allows to improve the culture and quality of extinguishing, but the main point is that safe work of firefighters in the process of fire-extinguishing is achieved. Processing statistic data on fires proves that K_i is very low and is within 0.0012 to 0.0017. Solving the problem about K_i , we solve also one of the most important questions of fire safety, i.e., the improvement of fire safety efficiency for people and national economy, improving the methods of fire extinguishing at minimum consumption and loss. On the basis of the above mentioned, a crucial role belongs to extinguishing substance to increase extinguishing efficiency, i.e., the efficiency ratio of using this substance which depends both on the

efficiency of extinguishing substance fire extinguishing capacity and other reasons.

The authors in their article describe the research and practical work defining the mixture combinations where SAA are added in mixtures of different composition and manufacturers, increasing the extinguishing properties of water, so the objectives of the research are:

1. to calculate the necessary water specific consumption, extinguishing A and B class simulated fires;
2. to define average statistic K_i value on the basis of the statistic analysis of real fire extinguishing results;
3. to define experimentally V_{ip} values for water in laboratory conditions without and with chemical additives, to define K_i increase limits in fire fighting practice by extinguishing with water and water mixtures;
4. to evaluate the theoretical and practical results obtained to recommend effective extinguishing compositions for practical use in fire fighting in the Republic of Latvia.

Assessment of Fire Extinguishing Efficiency Extinguishing Solid Combustible Materials

The effectiveness of methods and techniques of ensuring fire safety is characterised by composite measures that have an organisational, preventive and technical character, as well as by efficiency of fire extinguishing techniques. To great extent the efficiency of techniques for stopping combustion process depends not only on the type and efficiency of extinguishing substance, but also on the efficiency of supplying technique for these substances to the combustion zone, the determinant direction chosen, effect of weather conditions, the amount of resources at the moment of arrival.

Extinguishing process is of dual character, so it is necessary to define the optimal parameters for fire extinguishing process and objective numeric indicators for its extinguishing efficiency. On the one hand, extinguishing process is a combination of technical, organisational and operatively tactic measures for ensuring a combat action directed at extinguishing and localisation of fire, but, on the other hand, it is the implementation of definite physical processes and phenomena that is subject to objective laws of physics and definite numerical regularities.

Discovering these regularities, defining functional links of these basic parameters and choosing process optimisation parameters allows to describe the set of phenomena numerically that exists during fire extinguishing and choose a favourable combination of these parameters. But this, in its turn, will allow, firstly, to significantly increase the efficiency and quality of fire extinguishing process and, along with it, reduce the danger of fire and the volume of

material loss. Secondly, while extinguishing solid combustible material, it will allow to numerically assess the degree of consistency of numerical values for real fire extinguishing parameters to the optimal value, which in definite conditions can be considered as normative value for this parameter: normative supply intensity for extinguishing substances J_{nep} , J_{pad} , specific consumption of these substances V_{ip} , V_{pad} , and even fire extinguishing normative time T_n .

It is obvious that using such normative parameters, in its turn, would allow easily elaborate the objective numerical indicators for fire extinguishing efficiency, extinguishing solid burning materials and even numerical indicators for extinguishing quality – comparing the numerical value of a definite fire extinguishing efficiency indicator with normative value of this indicator.

As it was noted in the works of previous researchers, knowing the numerical value of the specific consumption for all kinds of combustible substances and materials, you can calculate the consumption of necessary extinguishing substance seconds q_{nep} (l/s), their supply intensity J_{nep} , J_{pad} ($l/m^2 \times s$), specific consumption at a fire extinguishing area unit V_{ip} , (l/m^2) and total stocks of extinguishing substances that are necessary for all the time of fire extinguishing, i.e., all the basic parameters of fire extinguishing process [4]. The specific consumption of extinguishing substances V_{ip} , (l/m^2) and extinguishing time $T_{d\omega}$, (s), the most important parameters of fire extinguishing, can be considered as the main indicators of the fire extinguishing efficiency. These parameters allow to have an objective judgement about real efficiency of ordinary fire extinguishing. Consequently, it possible to elaborate scientific principles for the construction of automatic fire extinguishing systems with optimal parameters, as well as obtain the objective criteria of

fire extinguishing quality and increase the efficiency of fire fighting at objects of national economy [6, 8].

Assessment Methods for Extinguishing Capacity of Surfactants and Water

In the practical part of the article the mixtures of water and surfactants Vacht 2, protein Sthamex AFFF 6%, FP-70; Tridol S6; synthetic Sthamex AFFF 3%, Tridol S3, protein and synthetic foam concentrate mixture Karate MB-5 3% (synthetic) mixture with Sthamex AFFF 6% (protein); Vacht 2 (protein) mixture with Tridol S3 (synthetic), Sthamex AFFF 6% (protein) mixture with Sthamex AFFF 3% (synthetic); Vacht 2 (protein) mixture with Tridol S3 (synthetic); FP-70 (protein) mixture with Tridol S6 (synthetic); efficiency assessment by extinguishing fires of combustible substances and highly inflammable liquids.

Equipment and Materials Used in Practical Study, Description of Experiment Place:

Practical part of the study was implemented at the Faculty of Engineering Economics and Management, Laboratory of Labour and Civil Protection Institute (fire safety research laboratory No. 10) of Riga Technical University. A special space (closed space) is arranged in the laboratory auditorium, which is finished with incombustible materials (hereinafter referred to as specially arranged space).

There is an experimental stationary fire-extinguishing system (automatic fire-extinguishing system), one-directional, connected to a closed tank; the sprinkler Tyco TY-FRB TY-3131 Upright, 5.6 K-Factor of fine sprayer (upward), minimum working pressure 0.07 Mpa; 1 piece.

System capacity estimate was carried out in accordance with technical parameters of automatic fire-extinguishing system (Table 2).

Sprinkler Tyco Ty-Frb Ty-3131(Directed Upwards) Capacity Calculation Table

TABLE 2

Estimate method	Protected area	Water consumption	Required minimal pressure (pump parameters)	Water delivery rate	Minimal flow rate	Number of sprayers
Request	(m^2)	(l/min)	(bar)	($l/min/m^2$)	(l/min)	Unit
	12	60	2.38	0.55	60	1

Upon practical implementation of connection diagram, working pressure in the system was 1.9 MPa, water consumption was estimated proportionally based on data obtained in the program; as a result, output of sprinkler used in practical

experiment was 47.89 l/min or 0.7983 l/min, the results coincided in practical test with minimal relative error [10].

The following mixtures were prepared having a certain concentration: (Table 3)

TABLE 3

Types and Combinations of Mixtures Used in Practical Experiment

Nr.p.k.	Extinguishing substance	Concentration (%)
1.	Water	-
2.	Water	-
3.	Water	-
4.	Water	-
5.	Water	-
6.	STHAMEX®-AFFF 6% (Prot.)	3%
7.	STHAMEX®-AFFF 6% (Prot.)	3%
8.	STHAMEX®-AFFF 6% (Prot.)	2%
9.	Vacht 2 (Prot.)	0.25%
10.	FP-70 (Prot.)	0.50%
11.	STHAMEX®-AFFF 3% (Synth.)	3%
12.	Tridol S3 (Synth.)	0.25%
13.	Tridol S3 (Synth.)	0.25%
14.	Tridol S6 (Synth.)	0.25%
15.	STHAMEX®-AFFF 6% (Prot.)+STHAMEX®-AFFF 3% (Synth.)	3%
16.	Karate MB-5 3% (Synth.)+STHAMEX®-AFFF 6% (Prot.)	2%
17.	Vacht 2 (Prot.)+Tridol S3 (Synth.)	0.50%
18.	FP-70 (Prot.)+Tridol S6 (Synth.)	0.50%
19.	Vacht 2 (Prot.)+Tridol S3 (Synth.)	0.25%

A steel pan with legs wherein solid substance was burnt had been installed in the specially arranged space (hereinafter referred to as specially arranged space) where burning of solid combustible materials was done. The steel pan dimensions: 0.5x0.5x0.1 m, leg height 0.1 m, metal screen with 0.05 mesh is arranged in the pan base. The pan 0.5x0.5x0.05 m wherein solid liquid was burnt was installed under the metal screen. The amount of the wood burnt was 1kg.

The steel pan with legs wherein highly inflammable liquids were burnt was installed in the specially arranged space. The steel pan parameters: Dn 0.6 m, depth 0.25 m. The metal screen with 0.05 mesh is arranged in the pan base. The pan 0.5x0.5x0.05 m, leg height 0.25 m, was installed under the metal screen.

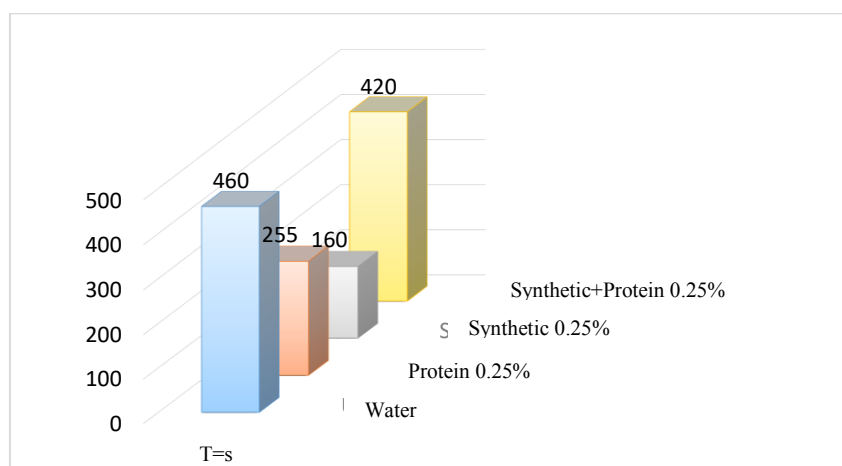


Fig. 1. Class A fire extinguishing time (s) at solution concentration 0.25%

Simulation and extinguishing of class A and B fires were carried out in the experimental part, using a stationary fire-extinguishing system and an upward sprinkler with 5.6 K-Factor as a sprayer. Water and modified water with addition of surface-active agents were delivered for extinguishing. Foam concentrates on protein and synthetic base were used as quenchers. Surfactants were delivered in different concentrations. Mixtures of surfactants, where synthetic and protein-based surfactants were mixed,

were used as well. Water solutions with 0.25% to 3% ratio of surface-active agents were used in the fire extinguishing experiment. The results obtained were analysed and summarized in the table (see Fig.1). The analysis of the obtained results, namely, the fire extinguishing time with the use of 0.25% admixture extinguishing solution, showed that the fire was most rapidly extinguished with the use of synthetic concentrate, the time being 160 seconds (Figure 1).

The analysis of the obtained results, namely, the average fire extinguishing time with the use of 0.25% to 3% admixture extinguishing solution, showed that

the fire was most rapidly extinguished with use of synthetic foam concentrate. Average extinguishing time was 247 seconds (Figure 2).

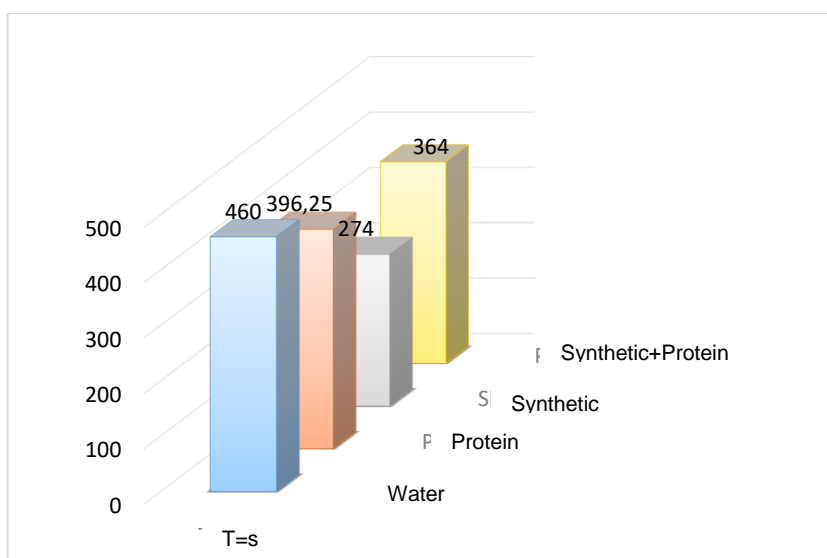


Fig. 2. Class A fire average extinguishing time (s) at solution concentration 0.25 to 3%.

The analysis of the obtained water consumption results with the use of 0.25% admixture extinguishing solution showed that the least extinguishing liquid

amount spent for fire extinguishing was with the use of synthetic foam concentrate. 127 litres of extinguishing solution were used (Table 4).

TABLE 4

The Data Acquired During the Practical Experiment

Nr.	Extinguishing substance	Concentration (%)	Sprinkler productivity (l/s)	Time of free burning Tf (s)	Time of flame extinguishing Tex (s)	Flame burning out time T (s)	Total extinguishing time $\Sigma T = Tf + Tex$ (s)	Sample extinguishing until T°C	Temperature in hotbed T°C	Temperature at open flame disappearing T°C	Amount of water consumed (l)
1.	Water	-	0.798319	180	460		640	50	490	-	367.22674
2.	Water	-	0.798319	180	460		640	50	765	-	367.22674
3.	Water	-	0.798319	180	220	310	400	200	620	445	175.63018
4.	Water	-	0.798319	180	180	300	360	180	820	180	143.69742
5.	Water	-	0.798319	180	170	320	350	200	842	200	135.71423
6.	STHAMEX® -AFFF 6% (Prot.)	3%	0.798319	180	460	-	640	50	760	-	367.22674
7.	STHAMEX® -AFFF 6% (Prot.)	3%	0.798319	180	480	-	660	50	553	-	383.19312
8.	STHAMEX® -AFFF 6% (Prot.)	2%	0.798319	180	390	480	570	200	890	450	311.34441
9.	Vacht 2 (Prot.)	0.25%	0.798319	180	255	350	435	200	670	480	203.571345
10.	FP-70 (Prot.)	0.50%	0.798319	180	280	440	460	50	820	70	223.52932

TABLE 4 CONTINUED

Nr.	Extinguishing substance	Concentration (%)	Sprinkler productivity (l/s)	Time of free burning Tf (s)	Time of flame extinguishing Tex (s)	Flame burning out time T (s)	Total extinguishing time $\Sigma t = T_f + T_{ex}$ (s)	Sample extinguishing until T°C	Temperature in hotbed T°C	Temperature at open flame disappearing T°C	Amount of water consumed (l)
11.	STHAMEX® -AFFF 3% (Synth.)	3%	0.798319	180	360	-	540	50	580	-	287.39484
12.	Tridol S3 (Synth.)	0.25%	0.798319	180	240	410	420	70	720	420	191.59656
13.	Tridol S3 (Synth.)	0.25%	0.798319	180	160	340	340	40	725	40	127.73104
14.	Tridol S6 (Synth.)	0.25%	0.798319	180	330	390	510	200	690	430	263.44527
15.	STHAMEX® -AFFF 6% (Prot.)+STH AMEX®-AFFF 3% (Synth.)	3%	0.798319	180	560	500	740	50	836	-	447.05864
16.	Karate MB-5 3% (Synth.)+STH AMEX®- AFFF 6% (Prot.)	2%	0.798319	180	240	380	420	200	720	360	191.59656
17.	Vacht 2 (Prot.)+Tridol S3 (Synth.)	0.50%	0.798319	180	180	300	360	200	820	400	143.69742
18.	FP-70 (Prot.)+Tridol S6 (Synth.)	0.50%	0.798319	180	420	600	600	50	857	50	335.29398
19.	Vacht 2 (Prot.)+Tridol S3 (Synth.)	0.25%	0.798319	180	420	600	600	30	897	30	335.29398

Conclusions:

1. Concentration of active surfactants in water directly affects fire-extinguishing properties of liquids, i.e., observing the amount of surfactants and water liquids – concentration – one can achieve the reduction of the amount of water, which allows to reduce material loss connected with using water in fire extinguishing.
2. Correct concentration of surfactants and water liquid affect the amount of water used for fire extinguishing and its effect on material values, which allows to reduce material loss caused by water used for fire extinguishing.
3. The use of surfactants and water liquid significantly reduces the temperature in a hotbed, which allows to reduce material loss caused by temperature.
4. The use of surfactants and water liquid significantly reduces not only the temperature in a hotbed, but also reduces smoldering in the combustion area, which allows to reduce material loss caused by temperature.
5. The use of surfactants and water liquid significantly reduces not only the temperature and smoldering in a hotbed, but also reduces smoke in a hotbed, which allows to reduce material loss caused by temperature and the convective smoke flow.
6. The use of surfactants and water liquid significantly reduces water consumption for fire extinguishing purposes, which allows to save drinking water supplies and resources, since fire fighting water supply system is usually combined with the drinking water supply system.
7. Taking into account the amount of water used for extinguishing 1kg of wood and the amount of actually consumed water, we can conclude that an in-depth study must be carried out to find out how

economically profitable is the use of SAA for fire extinguishing.

References

1. **V. Jemeljanovs.** *Ēku iekšējo ugunsdrošības ūdensapgādes sistēmu efektivitātes paaugstināšana. Autoreferāts disertācija inženierzinātņu doktora zinātniskā grāda iegūšanai.* – Rīga: RTU, 1998. – 20 p.
2. **M. Ziemelis** *Promocijas darbs “UGUNS DZĒŠANAS AR ŪDENI EFEKTIVITĀTES PAAUGSTINĀŠANA”* Rīgā 2009., 100 lpp.
3. **World Fire Statistics. Report No.21.** –Center of Fire Statistics of CTIF, 2016. – 62 lpp.
4. **22nd International Scientific Conference, Economics and Management 2017** (ICEM 2017) hosted by Riga Technical University, May 10-12, 2017 Riga, Latvia Vladimirs Jemeljanovs, Georgijs Kiselovs, Jelena Malahova “Improvement of water fire-extinguishing capability by use of foam agents, surfactants and mixtures thereof”.
5. **Мартынов Е.С., Девкин А.П.** *Установки автоматического пожаротушения перегретой воды // Безопасность труда в промышленности., ч.2* – М.: Недра, 1992. – стр. 16.
6. *Исследование новых смачивателей и пенообразователей на основе производственного сырья. Отчет Свердловской ПЖС.* – Свердловск: ПЖС, 1966. – стр. 90.
7. *Исследование влияния добавок на огнегосительные свойства воды. Отчет по теме 2- 86-70 ВНИИПО МВД* – М.: ВНИИПО, 1972. – 64 стр.
8. **Дягилева Л.К., Казаков М.В., Одинец М.В.** *Влияние добавок на огнегосительные свойства воды// Сб. науч. тр. № 12.* – М.: ВНИИПО, 1972. – 80 стр.
9. **Казаков М.В., Демидов П.Г.** *Применение смачивателей для тушения пожаров.* –М.: Стройиздат, 1964. - стр. 54.
10. **Agnis Andžāns, Jānis Čakste, Tomass Larfelds, Līga Ramāna, Mārīte Seile** *VIDĒJĀS VĒRTĪBAS METODE* 218. lpp.
11. **Jemeljanovs A.** *Lieltmolekulāro vielu izmantošana ugunsdzēsības praksē// LR Ugunsdzēsības pārvaldes informatīvais zinātniski tehniskais biļetens, Nr. 5.* – Rīga: Ugunsdzēsības pārvalde, 1993. – 7.- 8. lpp.
12. **Зельдович Я.Б.** *Математическая теория горения и взрыва.* Москва, Наука, 1980.
13. <http://libraryno.ru/7-2-gorenie-drevesiny-teorgorandbax/> Прочее / [Теория горения и взрыва](#) / 7.2. Горение древесины.

ENVIRONMENTAL ENGINEERING

DOI: 10.22616/CE.2017.015

Test Reference Year of Riga, Latvia

Mārtiņš Ruduks, Arturs Lešinskis, *Latvia University of Agriculture*

Abstract. Increasing global demand for energy resources leads to actions that optimize the usage of these resources. To make actual and reliable calculations for energy usage and to be able to determine the optimal heating systems, it is necessary to know the latest climate conditions in the area. One of the methods to determine the climate conditions is to generate a test reference year (TRY) for this area. In this paper the TRY of Riga, the capital city of Latvia, was generated by applying the standard LVS EN ISO 15927-4. To generate TRY, four parameters were used: temperature, relative humidity, cloud coverage and wind velocity. The Latvian Environment Geology and Meteorology Centre (LEGMC) provided the meteorological data used in this research. TRY was generated by analyzing meteorological data for thirty-year period (1984-2013) in Riga. The results were compared with the data from Latvian Building Code LBN 003-15, and it showed a deviation in average temperature values that can be explained by the climate change in this area.

Keywords: test reference year, building energy simulations, climate change

Introduction

There are different possibilities how to determine the latest climate conditions in the particular area. Two most popular methods are test reference year (TRY) and typical meteorological year (TMY). Both methods are similar and are based on Halls et. al. [3] described method with a difference that TMY method uses weighting factors for climate parameter assessment, where TRY uses all parameters at equal base. The use of TRY method is described in LVS EN ISO 15927-4 [5]. Both models consist of 8760-hour measurements of meteorological parameters that correspond with average meteorological parameter values for selected period [10]. Both models have been used in various research [1-3, 7-12]

In Latvia there have been research for TRY creation for Riga [7, 12], but the authors' research for

Riga and their previous research for Liepāja [8] and Aluksne [9] are the first ones that analyses 30 year meteorological data for climate model creation.

Meteorological data provided for the research were gathered from meteorological station in Riga, which is located: latitude 56°57'02.16", longitude 24°06'57.86". It is elevated 6.15 m above the sea level. It is located in the middle part of Latvia (Figure 1). Meteorological data were obtained from Latvian Environment Geology and Meteorology Centre (LEGMC) for 30-year period (1984-2013). LEGMC provides meteorological elements with 3-hour interval; the necessary hourly values were interpolated.



Fig. 1. Illustration of territory of Latvia (Created by authors using border of Latvia [4])

Latvian Building Code LBN 003-15 [6] represents climate conditions in Latvia, but data were generated by analyzing meteorological conditions for the period of 1961-1990. Climate data provided by

LBN 003-15 do not represent the actual climate situation and only monthly average values for temperature and relative humidity are provided, but many detailed building energy simulations for

heating ventilation and air conditioning (HVAC) systems require hourly climate values.

The aim of this research is to generate climate database (TRY) for Riga that would contain more recent hourly climate data that could be used in future research for HVAC devices.

Methodology

In this research, to generate TRY of Riga, LVS EN ISO 15927-4 [5] described method was applied. To generate TRY, four meteorological parameters were taken into account: dry-bulb air temperature, relative humidity, cloud coverage (LVS EN ISO 15927-4 describes to use direct normal irradiance at cloud coverage place, but at this meteorological station there are no data for this parameter, so it was replaced with cloud coverage) and wind speed. The first three parameters are key parameters, but wind speed is secondary parameter.

Meteorological parameter values were provided by the Latvian Environment Geology and Meteorology Centre (LEGMC). LEGMC provided meteorological parameters with 3-hour interval. LVS EN ISO 15927-4 suggests using hourly meteorological parameter values, so the missing values were generated by linear interpolation. TRY creation process requires to analyze at least 10 years of meteorological parameters [5]. In this research 30-year meteorological data were used for the time period 1984-2013.

To be able to compare all 30-year meteorological data equally, 29 February was excluded from this process, therefore TRY consists of 8,760 hourly meteorological parameter values.

The daily mean value was calculated for key parameters p (dry-bulb air temperature, relative humidity and cloud coverage). The cumulative distribution function, $\Phi_{p,m,i}$, of daily means (through 30 years) was calculated for each calendar month m , using equation (1) [5]

$$\Phi_{p,m,i} = \frac{K_i}{N+1} \quad (1)$$

where:

K_i is the rank order of the i -th value of the daily means within that calendar month in the whole data set;

N is the number of days in calendar month.

The cumulative distribution function, $F_{p,y,m,i}$, of the daily means within each calendar month, for each year y , (through 30 years) was calculated using equation (2) [5]

$$F_{p,y,m,i} = \frac{J_i}{n+1} \quad (2)$$

where:

J_i is the rank order of the i -th value of the daily means within that calendar month (that year);

N is the number of days in observed month.

For each calendar month the Finkelstein–Schafer (FS) statistic, $FS_{p,y,m}$, was calculated for each year of the data set using equation (3) [5]

$$FS_{p,y,m} = \sum_{i=1}^n |F_{p,y,m,i} - \Phi_{p,m,i}| \quad (3)$$

Finkelstein–Schafer statistic, $FS_{p,y,m}$, was calculated for key parameters (dry-bulb air temperature, cloud coverage and relative humidity) and each parameter value was ranked in increasing order of $FS_{p,y,m}$ for each calendar month in multiyear record.

For each calendar month, individual months from 30-year record were ranked in order of increasing size of $FS_{p,y,m}$ for all key parameters.

All three separate parameter ranks were added together and ranked in increasing size of total rank number for each calendar month each year. Three months with the lowest total ranking for each calendar month were selected for the second stage (candidate months).

In the second stage, monthly mean values of the wind speed were calculated for all three candidate months for each calendar month. The month that had the closest average wind speed value to the corresponding multi-year calendar month mean was selected as the typical meteorological month (TMM) to be included in the test reference year.

When all twelve TMM were selected to be included in TRY, some adjustments were made – for each climate parameter the last eight hours of each month and the first eight hours of the next month were smoothed to make a smooth transition of values or different TMM. The same adjustment was made for the last eight hours of December and the first eight hours of January to use TRY for repeated simulations [5].

Results and discussion

According to the described methodology, TRY was created for Riga, the capital city of Latvia. The year form which calendar months were included in TRY is shown in Table 1. The results show that two calendar months were selected from 1993 (April and October), and two calendar months were selected from 2008 (January and November), the remaining calendar months were selected from different years. The results show that TMM were selected from a large period and there is no one particular year that has the best match for 30-year average values.

The comparison of the selected calendar months for Riga with Pauls' research results [7] that was

made for the ten-year period (2001 – 2010) shows one calendar month that was selected from the same year, i.e., 2001 (February). Although TRY selection period

is different (30 year over 10 year), February from 2001 is the best match for both periods.

TABLE 1

Selected months for TRY generation [Source: the authors' construction]

Month	Jan	Feb	Mar	Apr	May	Jun
Year selected for TRY	2008	2001	1999	1993	1998	2000
Month	Jul	Aug	Sep	Oct	Nov	Dec
Year selected for TRY	2009	2011	1995	1993	2008	1987

In TMM selection process 30 different months were analyzed; Figure 2 show the cumulative percentage comparison for temperature of December with best (1989) and worst (2006) FS statistics, when the long-term temperature results were compared with the corresponding month temperature. A curve

with triangles represents daily average temperature values from year 1989. This month is included in TRY when all four parameters are taken into account. Temperature values for TRY model reveal high similarity with 30-year average data.

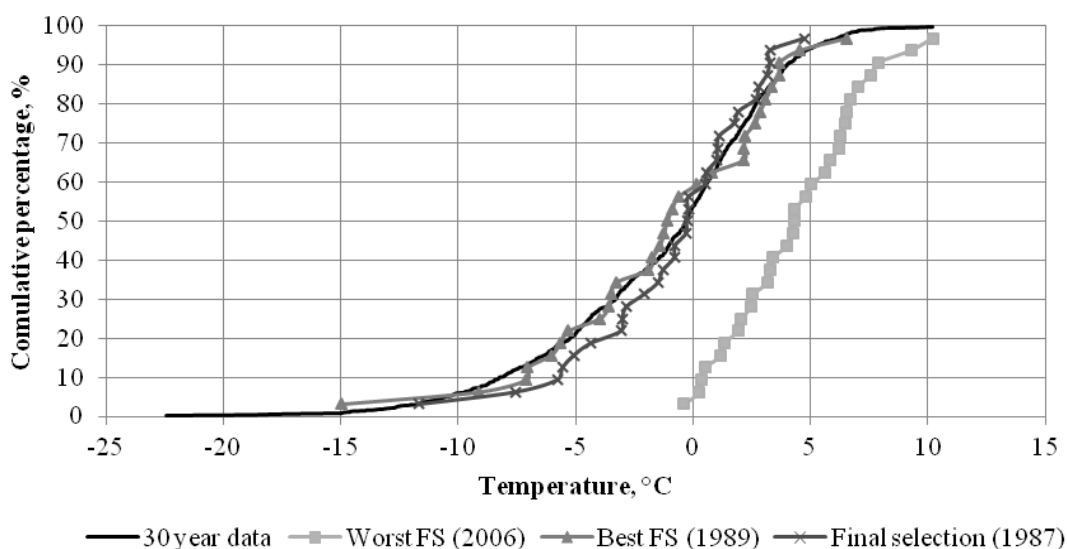


Fig. 2. Comparison of temperature cumulative percentage for December

When all TMM are selected and united, it is possible to compare the average daily temperature values for TRY model with 30-year average data (the results are compared in Figure 3). TRY model values reveal high similarity with 30-year data. There is a difference in the temperature cumulative percentage until 30 % mark, when TRY model shows little higher temperature values, but other values are very similar.

When TRY is created, there are 8,760 hourly values of meteorological elements from January till

December. The air temperature variation over the year period is shown in Figure 4. The maximum value of the air temperature observed in TRY is +30.1 °C, the minimum –18.7 °C and average is 7.5 °C.

When 30-year average air temperature values were compared for the period of 1984-2013 (Figure 5), they showed the increase in air temperature values. The average air temperature has increased from 6.5 °C to 7.9 °C, which is 21.5 % increase in average air temperature value.

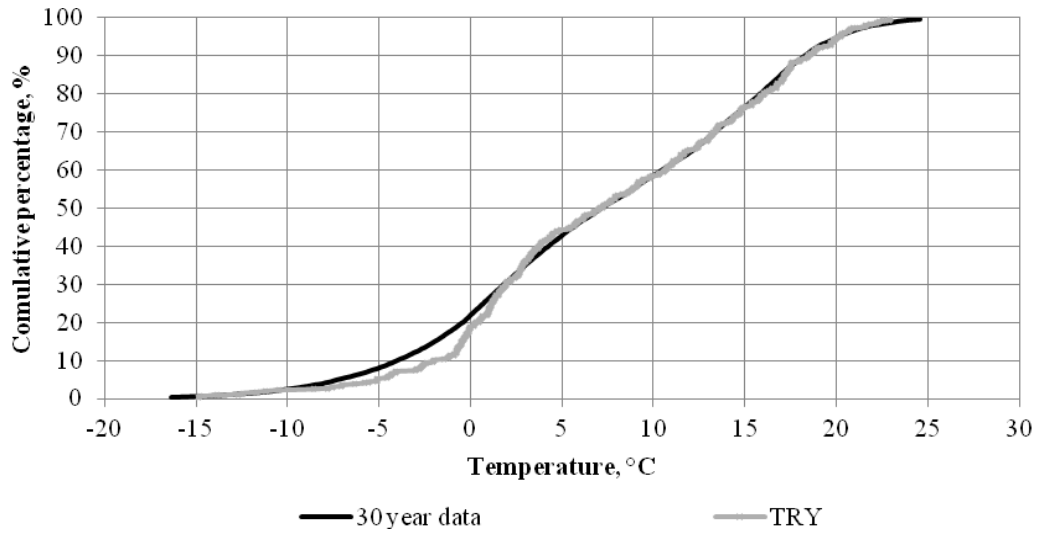


Fig. 3. Comparison of temperature cumulative percentage

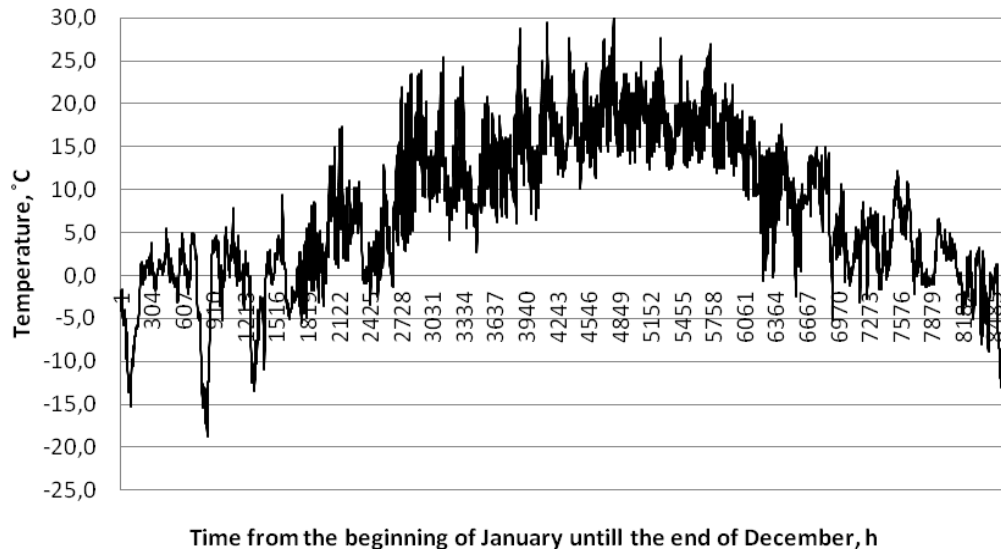


Fig. 4. Temperature variation through TRY

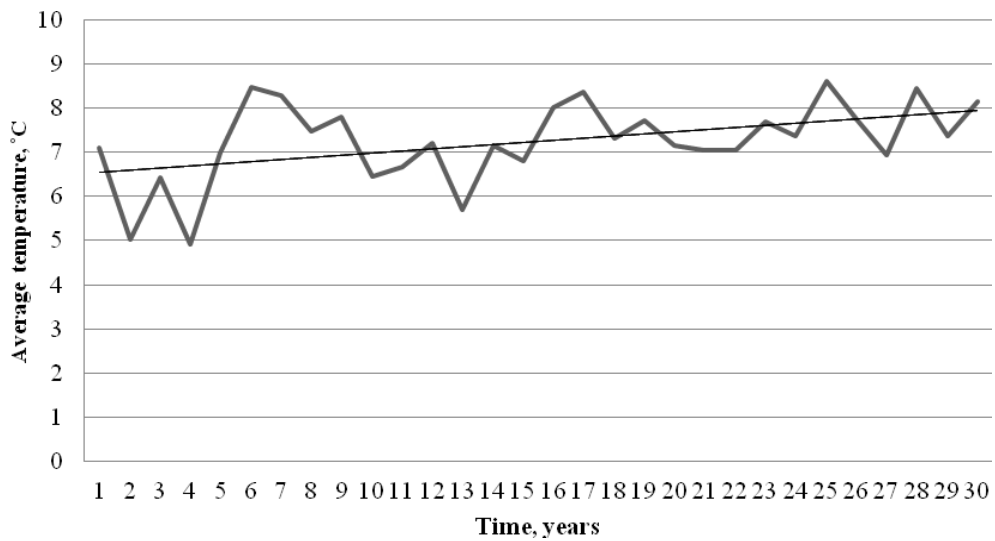


Fig. 5. Average temperature for 30-year period (1984-2013)

TRY average wind speed values reveal high similarity with 30-year average data (Figure 6) with some deviation in values. The largest observed time

difference at 5 m s^{-1} for 170 hours per year, but the total difference for all wind speed values is 851 hour or 9.7 % of all 8,760 hours in a calendar year.

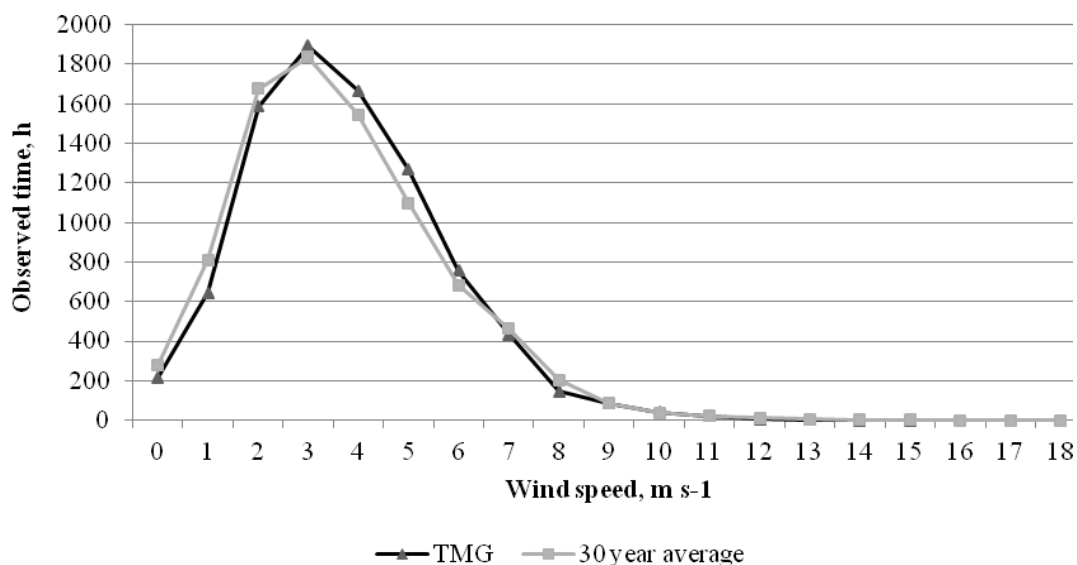


Fig. 6. Comparison of TRY and 30-year average data wind speed distribution

TRY hourly temperature values reveal high similarity with 30-year hourly temperature values, when their air temperature distribution values are compared (Figure 7). The largest observed time difference for TRY and 30-year average air temperature values is 203 hours at $0 \text{ }^{\circ}\text{C}$. The total observed time difference for air temperature

distribution between TRY and 30-year average data values is 1,476 hours or 16.8 % of total year hour values. That is 6.6% increase of the total observed time difference comparing with TRY of Liepaja [8], and 41.4 % increase comparing with TRY of Aluksne [9].

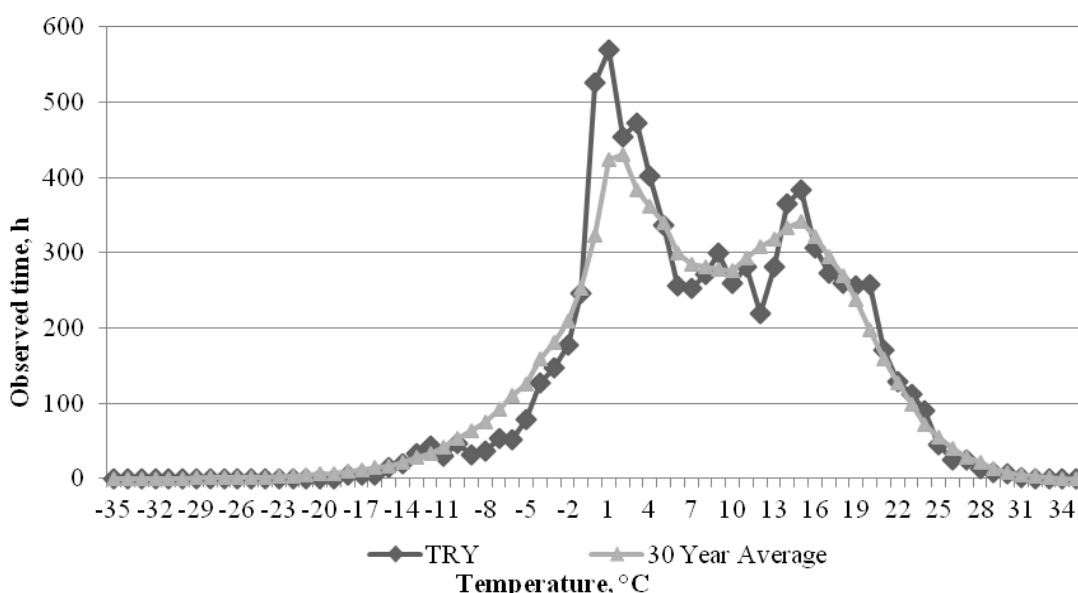


Fig. 7. Comparison of TRY and 30-year average data temperature distribution

A very important result that can be gained from TRY model is temperature and content of a moisture combinations per year. Figure 8 represents how many hours per year each combination can be observed.

The most typical air temperature is $1 \text{ }^{\circ}\text{C}$, it can be observed for 550 hours per year or 6.3 % of all observed air temperature values per year. The most typical content of moisture values is 4 g kg^{-1} , it can be

observed for 1,759 hours per year or 20.1 % of all observed content of moisture values per year. The most typical combination for air temperature and content of moisture is 2 °C and 4 g kg⁻¹, this combination can be observed for 353 hours per year, or 4 % of all possible hourly combinations. Comparing the results with other TRY values, TRY of Riga has the same typical temperature and content of moisture combination as TRY of Liepaja [8], where this combination can be observed for 432 hours

or by 22.3 % more than for TRY of Riga. The TRY of Aluksne has the same most typical content of moisture 4 g kg⁻¹, but the most typical air temperature is by 2 °C lower than TRY of Riga 0 °C, and this combination can be observed for 339 hours.

The results can help to determine what kind of HVAC systems are necessary and how many hours per year each of HVAC systems will be running.

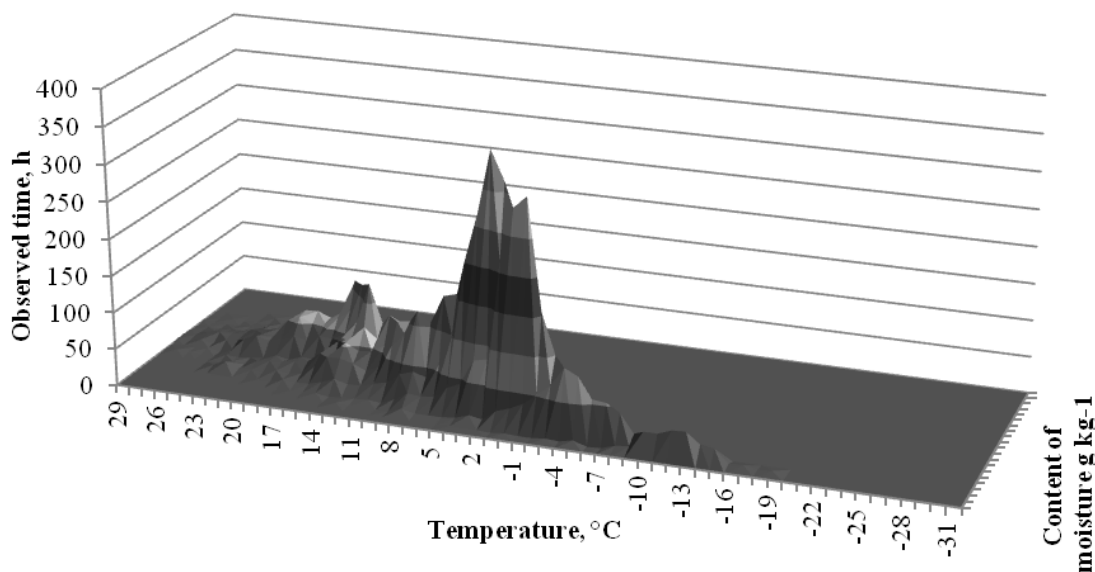


Fig. 8. Temperature and content of moisture combinations for TRY

The highest relative humidity difference in individual months between TRY and 30-year average data is 4 % in February. Average relative humidity

value by TRY and 30-year average data is 78 %, but there is 1 % difference with the LBN 003-15 value (Table 2).

TABLE 2
Comparison of average monthly relative humidity value (%) [Source: the authors' construction]

Month	Jan	Feb	Mar	Apr	May	Jun	Jul	Aug	Sep	Oct	Nov	Dec	Average
30-year average	85	82	77	70	68	72	73	75	80	83	86	87	78
TRY	84	86	76	70	71	69	72	76	77	81	88	88	78
LBN 003-15	85	82	79	73	69	72	76	78	81	83	86	86	79

Average wind speed value by 30-year average data is 3.6 m s⁻¹ and TRY model has the same average wind speed value. The highest wind speed difference

for individual months comparing TRY and 30-year average data is 1 m s⁻¹ in December (Table 3).

TABLE 3
Comparison of average monthly wind speed values (m s⁻¹) [Source: the authors' construction]

Month	Jan	Feb	Mar	Apr	May	Jun	Jul
30-year average	4.2	3.9	3.8	3.5	3.4	3.2	3.1
TRY	4.5	3.9	3.5	3.5	3.4	3.3	2.7
Month	Aug	Sep	Oct	Nov	Dec	Average	
30-year average	3.1	3.4	3.7	4.0	4.1	3.6	
TRY	2.8	3.0	3.7	3.8	5.1	3.6	

The average air temperature value by TRY is 7.5 °C, but for 30-year average data, it is 7.2 °C or 4% decrease. LBN 003-15 average air temperature is 5.7 °C or 20.8% difference with 30-year average data (Table 4). The LBN 003-15 data values have been determined from the period of 1961-1990. Since this period, average air temperature has risen (Figure 5) that can explain the average air temperature difference for LBN 003-15. The largest average air temperature difference is 1.6 °C in January between TRY and 30-year average data for individual months.

LBN 003-15 has the highest number of heating degree-days (HDD) 3,654 comparing with TRY data

3,249. HDD days are calculated at the inside air temperature 18 °C. LBN 003-15 average air temperature in the heating period is 0.0 °C, but for TRY, it is by 0.9 °C higher. LBN 003-15 duration of the heating period is 13 days longer than for TRY, it also has the lowest observed minimal temperature and highest maximum observed air temperature. This tendency is also similar for other TRY models in Latvia [8, 9]. The differences in values can be explained with different time periods for measurements of the values.

TABLE 4

Comparison of average temperature values (°C) [Source: the authors' construction]

Month	Jan	Feb	Mar	Apr	May	Jun	Jul
30-year average	-2.7	-3.1	0.6	6.6	12.2	15.9	18.5
TRY	-1.1	-3.0	2.0	6.4	12.6	15.2	18.8
LBN 003-15	-4.7	-4.3	-0.6	5.1	11.4	15.4	16.9
Month	Aug	Sep	Oct	Nov	Dec	Average	
30-year average	17.5	12.5	7.5	2.3	-1.3	7.2	
TRY	17.9	12.2	6.2	3.5	-0.9	7.5	
LBN 003-15	16.2	11.9	7.2	2.1	-2.3	5.7	

TABLE 5

Climate parameter comparison [Source: the authors' construction]

Parameter	TRY	LBN 003-15
Maximum temperature, °C	30.1	32.2
Minimum temperature, °C	-18.7	-31.0
Duration of heating period, days	190	203
Average air temperature in heating period, °C	0.9	0.0
Number of heating degree days (HDD)	3249	3654

Conclusions

In this research, TRY of Riga was generated based on 30-year meteorological data (1984-2013). The research results show that TRY values reveal high similarity with 30-year average data, but there is a deviation from LBN 003-15 data. The results imply that LBN 003-15 values are not up to date with today's climate situation. The average air temperature has been rising and leading to climate changes. As LBN 003-15 is the only legitimate source for climate parameters and it shows deviation from newer climate parameters, changes should be made in LBN 003-15

climate parameter values to represent more recent climate situation.

TRY provides hourly values of climate parameters that can be used for HVAC system analysis. If LBN 003-15 would be updated with hourly climate parameters, it would be a legitimate source of climate parameters for HVAC system calculations.

Results suggest that future research is necessary to be done for all cities of Latvia that have been included in LBN 003-15, and the results are necessary to be updated in LBN.

References

1. David, M., Adelard, L., Lauret, P., Garde, F. A method to generate Typical Meteorological Years from raw hourly climatic databases. *Building and Environment*, 2010, No. 45, p. 1722–1732.
2. Ebrahimpour, A., Maerefat M. A method for generation of typical meteorological year. *Energy Conversion and Management*, 2010, No 51, p. 410–417.
3. Hall, I.J., Prairie, R.R., Anderson, H.E., Boes, E.C. Generation of a typical meteorological year. *Proceedings of the 1978 Annual Meeting of the American Section of the International Solar Energy Society*, 1987, p.669-671.
4. Latvijas Republika. Kultūra [online 04.11.2017]. http://old.pvg.edu.lv/datori/konkursi/2011_web/Raivis_Pastars/kultura.html (In Latvian).

5. **Latvijas Valsts Standarts** (Latvia State Standard). LVS EN ISO 15927-4. Ēku hidrotermiskie raksturlielumi. Klimatisko raksturlielumu aprēķināšana un izteikšana. 4. daļa: Ikdienas dati apkures un dzesēšanas ikgadējā enerģijas patēriņa novērtēšanai. (Hygrothermal performance of buildings - Calculation and presentation of climatic - Part 4: Hourly data for assessing the annual energy use for heating and cooling), 2005. 5 p.
6. **Ministru kabineta noteikumi Nr. 338**. Noteikumi par Latvijas būvnormatīvu 003-15 “Būvklimatoloģija” (Latvian Building Code 003-15 “Construction climatology”) [online 10.10.2017.]. <http://likumi.lv/ta/id/275013-noteikumi-par-latvijas-buvnormativu-lbn-003-15-buvklimatologija-> (in Latvian).
7. **Pauls, R.** *Klimatoloģiskie dati ēkas enerģijas patēriņa novērtēšanai (Climatic data for assessing building energy consumption)*. Master thesis (in Latvian). Riga: Riga Technical University, 2011. 40 p.
8. **Ruduks, M., Lešinskis, A.** Generation of a Test Reference Year for Liepāja, Latvia. *Proceedings of annual 22nd International Scientific Conference Research for Rural Development 2016*, 2016, Vol. 1, No. 1, p. 175–181.
9. **Ruduks, M., Lešinskis, A.** Generation of a Test Reference Year for Alūksne, Latvia. *Proceedings of the Latvia University of Agriculture*, 2015, Vol. 33, No. 1, p. 46–54.
10. **Skeiker K., Ghani B.A.** Advance software tool for the creation of a typical meteorological year. *Energy Conversion and Management*, 2008, No 49, p. 2581–2587.
11. **Skeiker, K.** Generation of a typical meteorological year for Damascus zone using the Filkenstein–Schafer statistical method. *Energy Conversion and Management*, 2004, Vol. 45, p. 99–112.
12. **Zariņš, M.** *Klimata datu izvēle gaisa kondicionēšanas jaudas aprēķinam (Climate data for air conditioning power calculations)*. Bachelor thesis (in Latvian). Jelgava: Latvia University of Agriculture, 2001. 59 p.

BUILDING AND RENOVATION

DOI: 10.22616/CE.2017.016

Heat Supply Systems of Renovated Residential Buildings

Andris Kreslins, Visvaldis Vrublevskis, Anna Ramata, *Riga Technical University*

Abstract. Since 2010 in Latvia energy efficiency improvement measures in residential buildings have been actively implemented with an aim to reduce heat energy consumption and heating costs in houses. The aim of the study is to find optimal solutions for reducing energy consumption and increasing energy efficiency indicators of heating and domestic hot water systems. In the framework of the study heat consumption analysis of the domestic hot water supply systems in residential buildings was carried out. The results showed that heat energy savings and home energy efficiency theoretically and optimistically predicted by the renovation project after three years of operation of renovated houses were not reached. It was concluded after a thorough analysis that the external enclosing construction insulation reached predicted energy savings. Energy efficiency of the heat supply system was low, thermal energy consumption was higher than expected. Central heating systems are hydraulically unstable because heat in apartments is regulated emotionally, exceeding the regulated operating mode. The domestic hot water supply systems low energy efficiency causes relatively large thermal energy losses in hot water distribution and in circulation pipelines. The project was implemented in 2014; after three heating seasons of operation data monitoring, fixation of project deficiency and correction of solutions were carried out. According to the operation data monitoring, this innovative system is the most functional and energy efficient, corresponding to installed requirements of the project. After the assembly was completed the system was tuned to work in calculation mode and put into operation. During operation while heat consumption regime is changing, the functional efficiency does not change. Apartment heating system heat output is automatically regulated according to the room temperature. Preparation of hot water is provided in every apartment's boiler capacity (in local space heaters) with the combined heating system heat transmission at 70 °C temperature. It provides hot water heating to 60°C close to the final user and prevents the growth of microorganisms in hot water distribution system pipelines of the end user.

Keywords – massiveness, heating, heating season, hot domestic water supply

Introduction

Renovation of buildings

Terminology used in the article

Partial renovation – selectively renovated completely dilapidated engineering systems or building elements whose further qualitative operation is not possible.

Complex renovation – replacement of engineering systems; performance of the renovation or replacement of dilapidated parts of the building, if possible.

Traditional central heating system – unified single-pipe heating system of the whole house with vertical risers functioning in a unified hydraulic and heat-output mode.

Innovative central heating system – unified hydraulic supply system of a house divided into apartment autonomous subsystems, which functions autonomously without affecting the total building functional quality and the hydraulic and heat-output mode.

Massiveness of building elements – the ability of building to accumulate heat.

The aim of the study is to find optimal solutions for reducing energy consumption and increasing energy efficiency indicators of heating and domestic hot water systems. In the framework of the study heat consumption analysis of the domestic hot water

supply systems in residential buildings was carried out.

On the basis of the EU energy policy guidelines and using the EU co-financing, since 2010 in Latvia improvement of existing low energy efficiency (up to 160 – 240 kWh /m² in a heating period) in privatized multi-apartment residential buildings have been actively implemented in order to reduce heat energy costs and heat supply costs for these buildings.

The priority in the projects was given to the renovation of dilapidated external deteriorated constructions and arrangement of building elements along with the renovation of physically and morally, partly or completely dilapidated thermal energy consuming engineering systems of houses: central heating, hot water supply and ventilation systems by performing partial or complex renovation, accordingly.

In the time period from 1960 to 1990 multi-apartment residential buildings were built quickly and cheaply using the existing material base and construction technologies. They belonged to the state and were rented to residents. In the 90s of the previous century, these houses were privatized and apartment renters became apartment owners. House building elements and engineering systems (heating,

ventilation, water supply, and sewerage) were defined as the common ownership of all privatized apartments. Home apartment owners were jointly responsible for the qualitative operation of building elements and engineering systems. Central heating systems such as a traditional single-pipe heating system with vertical risers for water heating systems, with horizontal flow and reverse heat dividing transfer mains were located in the attics and the basement of buildings.

Centralized hot water supply system for water preparation takes place in heating substation, from where it is supplied to the apartments through the recirculation pipe with the circulation pump. The negative side of hot water systems is that there is a waste of hot water.

Ventilation has a natural gravity system. The extract is arranged from the upper area of the room through the vent channels. The inflow is provided through special openings in the window leaf through

ventilations panes, special air supply devices, which were installed in outside walls under the windows. The cold outside air, which flows inside, is heated with increased warmth of heaters from the heating systems. Central heating systems of old apartment buildings have successfully fulfilled their functions, but they have to be changed due to their depreciation.

Results

The study analysed 18 multi-apartment residential houses in different cities of Latvia: Liepaja, Talsi, Stende. Their renovation was carried out in different time periods. Data is collected from non-renovated houses (written in black), insulated houses (written in blue Italic) and fully renovated houses (written in red Bold) according to the heat consumption in kWh/m² in the heating season. Table 1 shows the data of the heat energy consumption of houses.

TABLE 1

Data of the 7 most typical houses for thermal energy consumption.

House No.	heated area, m ²	2009/10	2010/11	2011/12	2012/13	2013/14	2014/15	2015/16	2016/17
1.	1,850	116.3	<i>65.4</i>	55.2	38.5	41.9	38.7	39.1	40.7
2.	3,186	136.5	143.9	117.2	133.6	111.2	51.8	56.8	63.6
3.	3,259	133.9	127.8	125.7	<i>91.4</i>	<i>111.4</i>	66.9	71.7	81.7
4.	1,610	143.6	153.3	62.5	68.4	57.7	59.3	64.3	67.9
5.	1,001	202.1	204.5	189.4	<i>115.3</i>	83.12	79.6	72.1	78.4
6.	967	171.4	170.9	178.7	147.7	67.8	55.2	56.9	62.8
7.	973	169.9	160.1	132.2	159.8	70.97	58.4	56.9	62.9

The actual heat losses of the building at $t_{\text{inside}}=+18^{\circ}\text{C}$ and $t_{\text{outside}}=-20^{\circ}\text{C}$ exceeded the project's previously calculated losses, as a result thermal discomfort was observed during the operation of the building. The improperly operated traditional central heating system was inefficient with high energy consumption and losses. This is partly due to the lack of understanding of the owners of the apartments about the operation of the system.

Depreciation of 50 years old houses which have been functioning insufficiently was close to 100%, so they had to undergo complex renovation. The evaluation of achieved energy efficiency was carried out after 3 years of operation of renovated houses in 2013. Having comprehensively and thoroughly analysed the summarized evaluation results, the conclusion was made that in most cases partially renovated houses have not reached the previously estimated energy efficiency results, corresponding energy saving and economic efficiency. After the analysis it was possible to conclude that the energy saving reached due to the insulation of the external enclosing structure of buildings was in accordance with the predicted results. Heat energy consumption of renovated houses was affected by non-renovated

or partially renovated central heating systems. Their functional quality was unsatisfactory.

Partially renovated or completely renovated traditional central heating system solutions do not radically improve the operation of the system, but makes it more expensive to operate. Efficiently insulated multi-apartment residential building solutions for traditional heating systems are not functional and economically effective in the conditions of Latvian seaside climate [1]. Climate conditions are a determining factor for the quality operation of traditional central heating systems and the economic efficiency.

In order to ensure that the room is at standard or comfortable temperature, traditional central heating system's heat output in renovated non-heated houses is regulated depending on the outdoor temperature and the corresponding loss of house heat.

Thermal conductivity of exterior walls and upper floors of non-heated houses is rationed at 1.0–0.8 W/m²°C. The outdoor temperature fluctuations quickly affect thermal comfort of a house. Automation of heating system's heat output control either raises or lowers circulating heat flow temperature in central heating system accordingly.

Such a method of regulating heat output in non-heated houses with traditional central heating system was recognized as effective [2]. In non-heated and

heated standard houses heat conduction coefficient U-values of building constructions heat transfer is shown in Table 2.

TABLE 2

Heat conduction U-values

Building element	Non-renovated house U, W/m ² *K	Renovated house U, W/m ² *K
Outer wall of facade	1.02	0.29
Covering	0.86	0.19
Floor on soil	0.23	0.2
Door	4.53	2.0
Windows	3.23	1.8

However, such a heat-regulating technique is not economically efficient for insulated houses with high massiveness D [3]. The climate of Latvia is characterized by rapid fluctuations in outdoor temperature during a heating season in early hours and in the evenings, when a range of temperature variation can reach 15 - 20 ° C within 4-6 hours. In late evening hours when the temperature outside drops sharply, efficiently insulated buildings equipped with traditional, partially modernized central heating systems and their heat-regulating automation, increase the heat output of the central heating system that compensates heat loss according to the outside temperature. The massiveness D of efficiently insulated houses, which can continuously recoup the increasing heat loss, maintains normal thermal comfort at home. Houses are "overheated", heat energy consumption increases because people have to ventilate rooms.

In early morning hours, the outside temperature rises rapidly, as the heat loss of buildings decreases, the central heating system practically does not work, because the accumulated heat can be sufficient to maintain thermal comfort. The proper operation of houses' central heating system is ensured by a proper operation of the system.

The massiveness of a building is determined by the potential for accumulation of heat in buildings. It is calculated using the following formulas:

$$D = R \cdot S, \quad (1)$$

where

R – coefficient of thermal resistance of building elements $R_n = \delta_n / \lambda_n$, (m²*K)/W;

S – thermal conductivity or heat absorption coefficient of the external building structure, W/(m²·K). The building absorption coefficient is calculated according to the formula:

$$S_m = 0.27 \sqrt{(\lambda_m \cdot \rho_m \cdot (C_0 + 0.0419 \cdot \omega_0))} \quad (2)$$

where

λ_m - thermal conductivity of the building element material layer, W/(m*K); ρ_m – the volume density of the building element material layer, kg/m³;

C_0 - the specific heat capacity of an absolutely dry ($\omega_0=0\%$) material layer of a building element, kJ/(kg*K); ω_0 – layer weight humidity of building element material, %.

The empirical coefficient of 0.27 is applied in the permanent heating mode following materials and physical properties of the building elements used [4].

If the building structure is multi-layered of different materials, then "S" must be calculated for each layer according to formula 3:

$$D_n = R_1 \cdot S_1 + R_2 \cdot S_2 + \dots + R_n \cdot S_n. \quad (3)$$

Taking into account the building area of each building, the total massiveness of the building was calculated:

$$D_e = \frac{D_1 \cdot F_1 + D_2 \cdot F_2 + \dots + D_n \cdot F_n}{F_1 + F_2 + \dots + F_n}, \quad (4)$$

where

D_1, D_2, \dots, D_n – the massiveness of building construction; F_1, F_2, \dots, F_n – the area of building construction, m².

The massiveness of houses and building elements is determined by 4 levels [5]:

- 1) $D \geq 7$ – high massiveness building;
- 2) $7 > D \geq 4$ – medium massiveness building;
- 3) $4 > D \geq 1.5$ – low massiveness building;
- 4) $D < 1.5$ – building without massiveness.

Using the formulas 1, 2, 3, 4 the massiveness of building elements of residential buildings was calculated. Calculation data for the house No.7 for heat inertia are summarized in Table 3.

TABLE 3

Calculation of massiveness of building elements for the house No.7

Building element	Total massiveness "D" of the building element	Total area of the building element, m ²
Walls	8.86	1,904
Upper floor cover	4.30	973
Windows	5.49	738

$$D_e = \frac{8,86 \cdot 1904 + 4,30 \cdot 973 + 5,49 \cdot 738}{1904 + 973 + 738} = 6,94 \cdot 1,1 = 7,64$$

The coefficient 1.1 refers to the accumulation of heat in premises, increasing the heat inertia. The particular house after the insulation is with a large massiveness $D \geq 7$.

The heating season of an effectively heated building begins when internal heat releases do not compensate for heat losses. As a result, the length of the heating season and the heat consumption of the heating season change. Graph 1 shows the internal heat dissipation of the non-insulated and insulated houses, the heat loss and the duration of the heating period [6]. A heating season begins, when internal heat releases do not compensate for building heat losses. The building's heat losses Q_x at outside normative temperature t_2 are calculated:

$$Q_x = Q - 20(t_1 - t_x) / (t_1 - t_2), \quad (5)$$

where:

Q – Specific heat losses at normative outside temperature t_2 (in Riga -20°C), W/m^2 ; t_1 – building's internal temperature, $^\circ\text{C}$; t_2 – outside normative temperature, $^\circ\text{C}$; t_x – outside temperature for beginning of the heating season, $^\circ\text{C}$.

Heating season begins for internal comfort temperature of apartments, when specific heat losses of building Q_x and specific heat releases are equal to $11 \text{ W}/\text{m}^2$, but the outside temperature is 1.5°C . The graphical calculation of the heating period is shown in Figure 1.

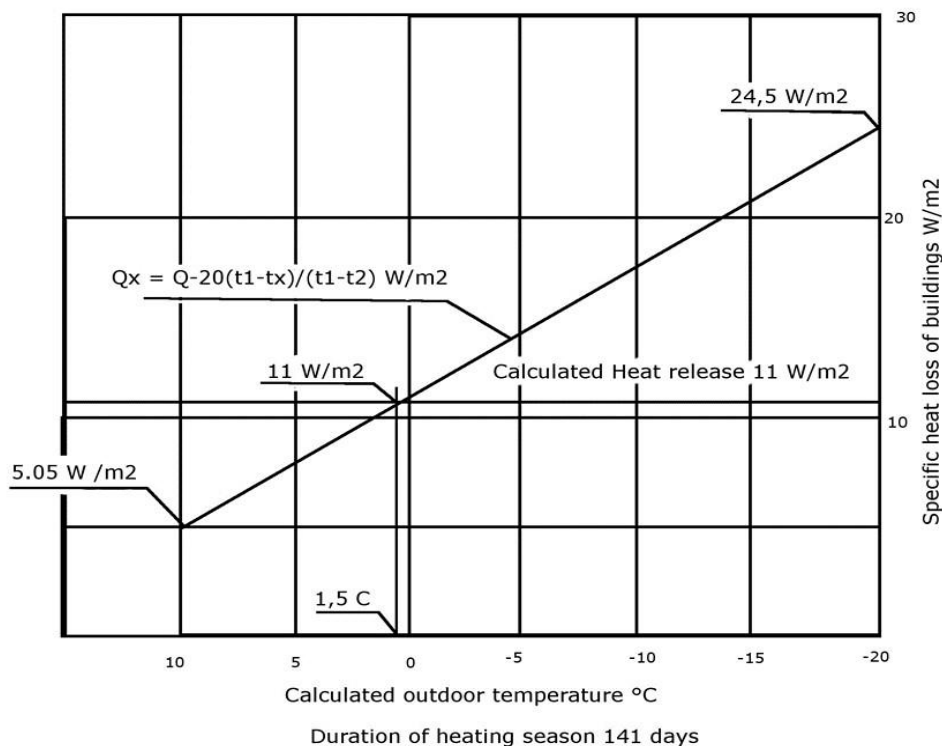


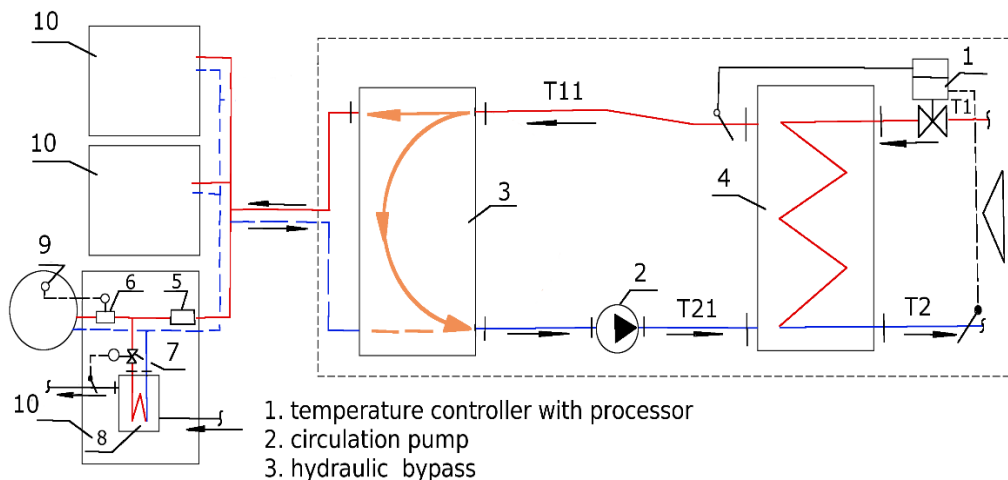
Fig. 1. Calculation of duration of heating season.

The duration of the heating season is determined using the monthly temperature fluctuation schedules for the heating period. Before the heating season the heating system of the house was hydraulically balanced and adjusted, so that all apartments and auxiliary spaces are provided with normative or required thermal comfort. In view of the decrease in outdoor temperature, it was planned in the heating system projects to increase its heat output and raise the temperature in the premises by 2-3 °C above the normative temperature. Such a possibility for the population to regulate the heat supply of heaters themselves created the misbalance of the hydraulic and heat output of all heating systems and reduction of functional efficiency [7].

Insulated houses with a traditional heating system were compared to (heat flow adjustment based on outdoor temperature, centralized preparation of hot water for the whole house at the heat supply control point) the same houses with a

new innovative autonomous heating system with hot water autonomous preparation in apartments. The functional operation of autonomous heating and a hot water system is regulated in the apartments' heating substation.

The functional operation of autonomous heating systems is regulated by indoor normative or required temperature provision and temperature fluctuations in apartments. Temperature sensors are installed in apartments. When fixing the temperature mismatch with the normative one, the command to the thermostatic valve "is given" to stop or restart the heat flow supply to the system. As soon as the temperature in the room meets the standard or falls to the limit, the sensor "gives command" to the thermostat valve to open and the heat flow circulation in the system and the return of heat in the premises restarts [8]. The schematic image of the innovative heating system is shown in Figure 2.



1. temperature controller with processor
2. circulation pump
3. hydraulic bypass
4. heat exchanger
5. hot water consumption heat meter for the apartment
6. thermostatic valve for capacity control of heating system of the apartment
7. regulator for hot domestic water
8. boiler for hot domestic water
9. temperature sensor in the apartment
10. apartment heating system

T1;T2 – heat supply and return from district heating system
 T11;T21 – heat supply and return in the building heating system

Fig. 2. The functional schema of the innovative heating system

The central heating secondary heat supply system of a house operates in low pressure mode up to 3 bars. It is connected to a high pressure centralized heat supply system that is separated by an appropriate heat exchanger.

The duration of the system's shutdown depends on several factors, however, essential is the thermal inertia of the building, ventilation, heat release in the room, insulation through the windows on sunny days and on the south side of the building.

The entire thermal system of the building is regulated quantitatively, but it does not affect the quality of all the apartment heating systems in the house. The hydraulic stability of the house's heating system is provided by a hydraulic bypass in the heat substation of the house. Such systems can only be used in efficiently renovated houses with low heat energy consumption of 60-100 kWh / m² during the heating season [8]. The heat flow supply and reverse temperature of 70°C / 30°C is constant in winter and summer. Such flow of temperature provides low heat

loss from system pipelines. Stable heat flow temperature prepares hot water up to 60°C in heaters directly in an apartment with less heat loss. It provides hot water heating close to the final user and prevents the growth of microorganisms in hot water distribution system pipelines of the end user.

A standard temperature schedule of 80°C / 60°C was used until the reconstruction. It increased the heating area of the heating system and heat output potential in case the outside temperature fell below the calculated temperature. This created an increase in the loss of heat in the house.

An inventory of the heat consumption of an innovative heating system is carried out at the apartment's heating substation, using simple hot water consumption meters with the temperature limit to 70°C. The entire house's heating system's record can be seen in the heating substation.

Conclusions

Since 2010 in Latvia improvement of existing low energy efficiency (up to 160 – 240 kWh/m² in a heating period) in privatized multi-apartment residential buildings has been implemented. After efficient renovation in residential buildings heat energy consumption decreased to 40-100 kWh / m² during the heating season.

In order to improve the energy efficiency of the house heating system, the study was carried out and a new central heating system project was developed. It was implemented in the heating season of 2013/2014. Economic efficiency evaluation was performed after 4 years of operation and monitoring of the new non-traditional heating system.

Energy consumption in the heating season of 4 buildings before renovation, after partly renovation and after complex renovation is shown in Figure 3.

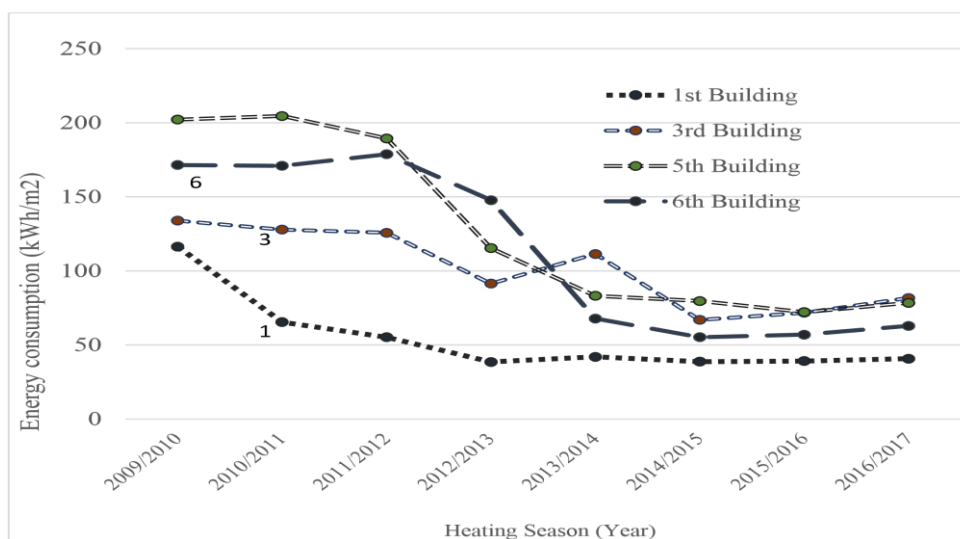


Fig. 3. Energy consumption of buildings, kWh/m² in 8 heating seasons.

After estimating the functional quality of operation and economic efficiency of the given heating innovative system during 3 years of operating data, it is evaluated as functionally and economically efficient compared to the traditional

heating system and can be recommended for renovated, energy-efficient homes in the climatic conditions of Latvia. Heat energy consumption kWh/m² decreased by 60-70%.

References

1. *Latvian Building standard LBN 003-15 "Building climatology"* // www.likumi.lv
2. **Vrublevskis V., Ekmanis J., Zebergs V., Zeltins N.** *Thermal characteristics of new building materials and their effect upon the energy efficiency* // Latvian Journal of Physics and Technical Sciences, vol. 45, 2008, Nr 3, p. 3-13
3. *Latvian Building standard LBN 002-01 "Thermotechnics of building envelopes"* // www.likumi.lv
4. *Building laws and regulations „Construction heat engineering”*. «СТРОИТЕЛЬНАЯ ТЕПЛОТЕХНИКА». СНиП II-3-79*. МОСКВА, Госстрой России, 1998. - Разработаны НИИСФ: Ю.А. Табунчиков, Ю.А. Матросов и др.
5. **Fokin K.F.**, *Construction heat engineering of building envelope*. Moscow, 2006, 256 pp. Фокин К. Ф. Строительная теплотехника ограждающих частей зданий. Moscow, Авок- Пресс, 2006, 256 p.
6. **Kreslins, A., Ramata, A.** *Calculations of Energy Consumption in Ventilation Systems*// Proc. 6th International Green Energy Conference (IGEC-VI). Eskisehir, Turkey, June 5-9, 2011, p.1-6
7. **Vrublevskis V., Zebergs V., Zeltins N., Davis A.** *Methodological problems of evaluation of the building envelopes depending on their thermal inertia and balance temperature* // Proc. 5th International Workshop on Energy and Environment of Residential Buildings and 3rd International Conference on Built Environment and Public Health (EERB-BEPH 2009) May 29-31, 2009, Guilin, Guangxi, China, vol. II, p. 1385 – 1394
8. **Vrublevskis V., Ekmanis J., Zebergs V., Zeltins N.** *Energy efficiency development: the thermal inertia of buildings* // 11th IAEE European Conference "Energy Economy, Policies and Supply security: Surviving in Global economical Crisis" Vilnius, Lithuania, August 25-28, 2010, 11 p.

Hygrothermal Behaviour of the Timber-Framed Sauna with Straw-Bale Walls

Martti-Jaan Miljan, Rain Allikmäe, Andres Jürgenson, Matis Miljan, Jaan Miljan, *Estonian University of Life Sciences*

Abstract. In the autumn of 2016 a timber-framed sauna with straw-bale walls was built for testing hygrothermal properties of walls during permanent usage. The main dimensions of the building's plan were 6.58 x 4.08 m with two rooms on the ground floor: a resting room and a room for washing and wetting (sauna part). The thickness of walls depended on the straw-bale dimensions which were 50 cm. External surfaces of the walls were plastered with the lime plaster. Both clay and lime plasters were used inside to check a better plaster variant for straw. Measuring devices and sensors to determine the temperature and relative moisture content were mounted into walls during construction. The heat flux rate through the wall was measured with a heat flux plate; data were recorded by an Almemo data recorder. Measurements began in December 2016 and ended in April 2017. The heating procedure of the sauna took place once a week. Meanwhile the sauna was heated with electric batteries. The measuring results were interesting. During the heating time the temperature inside the steam room rose to 83 °C, but in the middle of the wall it was 23 °C. At the same time the external temperature was about 0 °C. The data based calculation of thermal transmittance of the wall was $U = 0.15 \text{ W/m}^2\text{K}$ which was a little lower than predicted.

Keywords: construction process of straw-bale walls, thermal conductivity of straw-bale walls, relative moisture content, lime plaster, clay plaster

Introduction

Energy efficiency has been one of the major tasks to be improved in the EU. The aim is to purchase energy efficient buildings in the public sector in the EU countries. Using local natural building materials is a small step towards improvement to have a positive influence on environment. Part of inhabitants prefer to live in houses built from natural materials therefore there is an interested target group. To work out proper construction technique and structure solutions, a lot of tests is needed to be done. One solution of how to save energy is to use straw, which is an agricultural waste product. Straw-bale walls have been in use since the end of 19th century in the USA. A bit later straw was taken into use in Europe [1]. When industrially produced materials became available, the natural materials were forgotten. Then in the 70-80-ies of the 20th century the straw-bale building experienced revival to stay until present [2]. In those days magazines, like *Die Last Straw* and books like *Build It with Bales. A Step-by-Step Guide to Straw-Bale Construction* were published to advertise and introduce natural materials. In Europe the restart of building from straw took place in the 90-ties of the 20th century. The climate in the countries like Germany, England, Sweden, Denmark and so on is humid and certain requirements were established to envelope buildings which should be followed. In England the first straw-bale house was built in 1994, and in Estonia in 2003 [3].

Simultaneously, the investigation of physical-mechanical properties of straw-bale as a building material began. The largest investigation center was founded in Germany under the guidance of Prof.

Minke in Kassel. Material properties like density, thermal conductivity, sorption, air and moisture tightness were investigated from the point of hygrothermal state of a house. Guidelines were published [4, 5] with instructions how to build a straw-bale house. The first tests showed that the thermal conductivity of straw-bale was $\lambda = 0.045 \text{ W/(m K)}$ and the thermal transmittance of the wall with clay rendering of 25 mm outside and inside finish, and straw layer of 500 mm, was $U = 0.11 \text{ W/(m}^2\text{K)}$ [4]. The obtained results lead to a decision to measure hygrothermal properties of different wall structures made of local natural materials. Test elements were built into the window openings of the laboratory of the department of a rural building. One of the tested wall elements was constructed from 500 mm thick straw-bales and rendered with 40 mm clay plaster outside and inside. Calculated thermal transmittance of this test element was $U = 0.182 \text{ W/(m}^2\text{K)}$ [6], but the result from the office with straw bale walls located at Tammistu (in Tartu county) was $U = 0.092 \text{ W/(m}^2\text{K)}$ [7]. Having compared our results to those obtained in Germany we were intrigued to continue this research, and the master thesis was written about constructing the sauna and performing measurements.

Description of construction process

The sauna is located at Palupera, in Valga county. Two rooms, a resting room and a sauna part, are on the ground floor. Places to sleep are meant to be built in the attic, so the whole building is insulated. The plan of the sauna is presented in Figure 1.

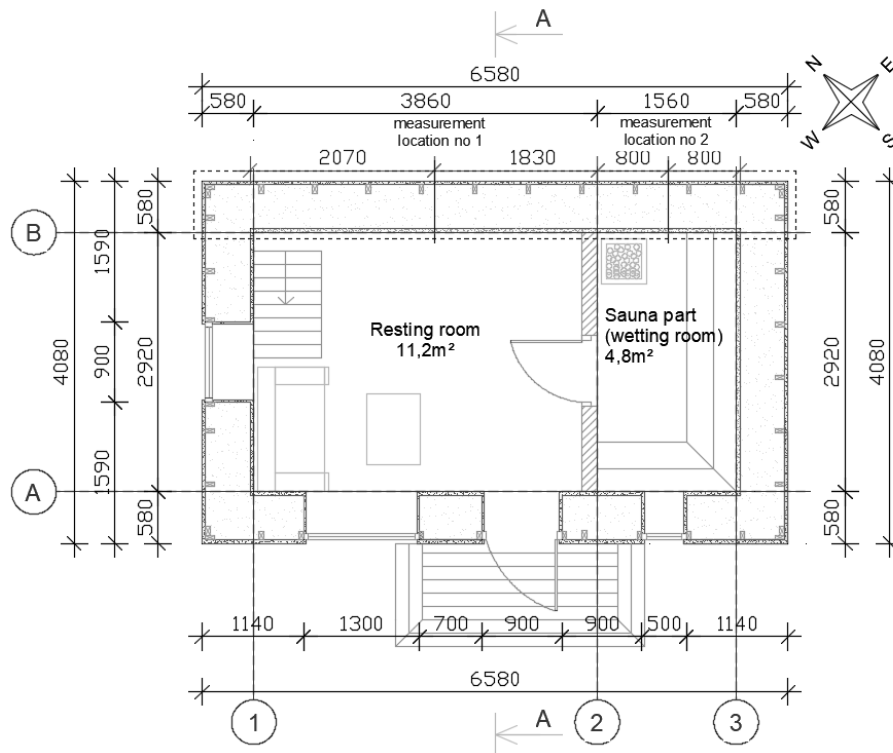


Fig. 1. The plan of the ground floor of the sauna, with indicated Measuring Points 1 and 2 inside the wall

The section A – A of the sauna is presented in Figure 2.

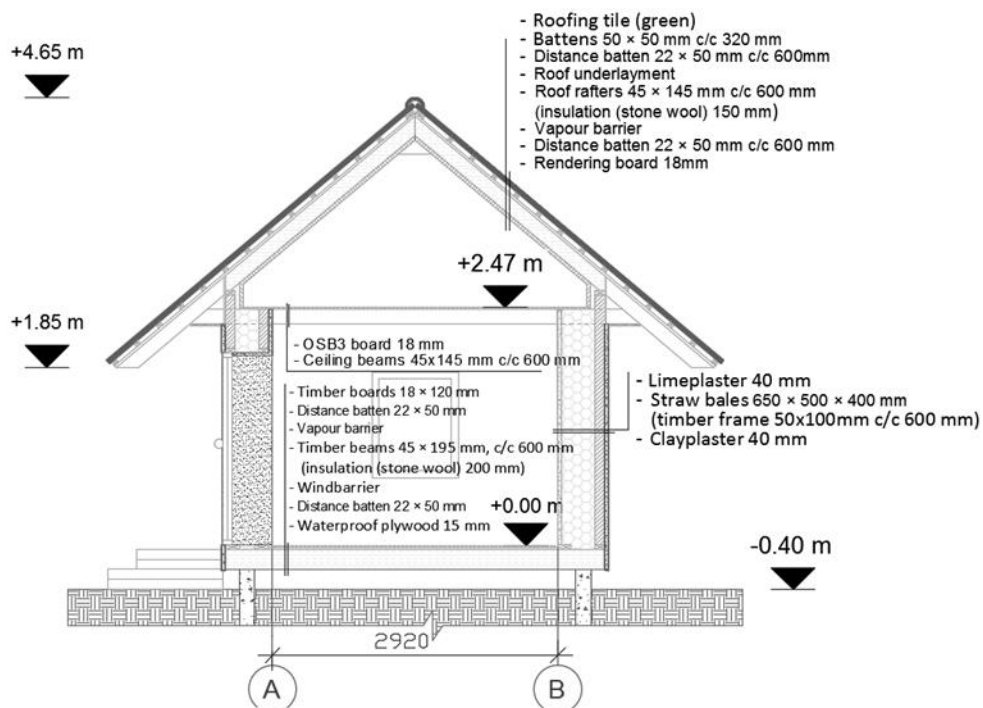


Fig.2. The section A-A of the sauna

Figure 3 shows the timber frame. The step of frame columns is taken considering the mostly used size of straw-bales, which is 500 mm in length.



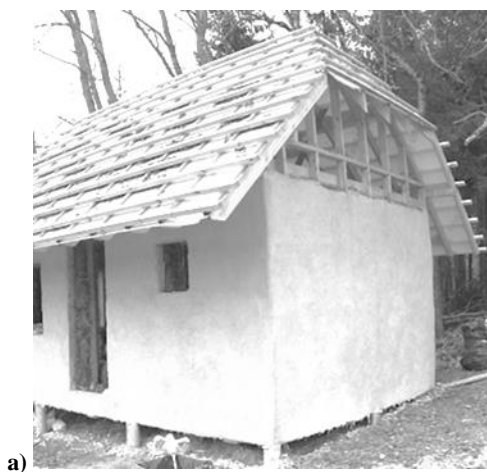
Fig. 3. Timber frame of the sauna is ready



Fig. 4. External appearance of the sauna before rendering

The external wall was done sorting out and applying dense and dry straw-bales. Straw-bales for the lower row of the wall were sorted by size for constructing. To get the wanted height of the wall, six rows of bales were needed. During construction the placed bales were tightened after placing the third and sixth row. The height of bales in the wall decreased by about $\sim 7.5\%$ due to tightening. To fill possible gaps between bales, the loose straw was used and pressed into the gaps. Before rendering the surface of straw-bale wall, it was flattened using a chainsaw. After that the walls were stiffened using diagonal timber laths of 22×100 mm (Fig. 4). The sauna before rendering is presented in Figure 4.

To follow our own experience and information acquired from literature [8], the walls were rendered from outside with lime plaster. Internal surfaces of the wall were rendered with clay in Measuring Point 1 and with lime in Measuring Point 2. Rendering was done manually in four layers, and the average amount of the used render was 15 kg/m^2 per layer. Total thickness of the rendering on the surfaces was ca 40 mm on both sides. The most difficult work was to apply the first layer of render. The external wall rendered with lime plaster is presented in Figure 5a, and the internal wall rendered with clay is presented in Figure 5b.



a)



b)

Fig. 5. Rendered walls: a) external wall and lime plaster; b) internal surface covered with clay plaster.

Aims and methods

The aim of research was to describe the hygrothermal behaviour of straw-bale walls in the sauna conditions when heat and relative moisture content gained their maximum at the certain point for a short time during heating the sauna's electric stove and making steam. Meanwhile the sauna was heated

by electric radiators and the door was left open, so internal temperature at this time was the same in all the house. Measurement sensors were placed as shown in Figure 1: Point 1 in the resting room and Point 2 in the wetting room. The scheme of placement of sensors is presented in Figure 6.

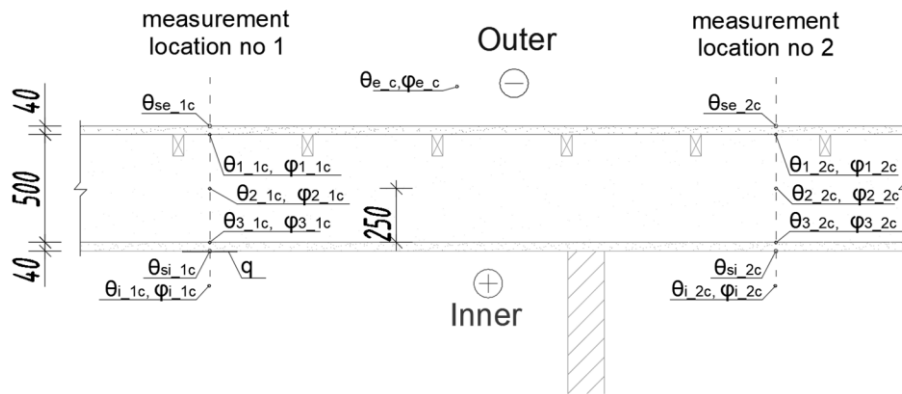


Fig. 6. Placement of sensors in the external wall

The following parameters were measured (a measurement device is given in the brackets):

- q – heat flux rate [W/m^2], (Ahlborn sensors FQA018 CSD);
- θ_e, φ_e – external temperature and RH [$^{\circ}C, RH\%$], (OnSet data logger Hobo U12-011);
- θ_{se} – temperature on the external surface of the wall [$^{\circ}C$], (Ahlborn NiCr-Ni-thermowire T 190-1);
- θ_1, φ_1 – temperature and RH between external surface of straw-bale and lime render [$^{\circ}C, RH\%$], (Ahlborn sensors FHA646R);
- θ_2, φ_2 – temperature and RH in the middle of the straw-bale [$^{\circ}C, RH\%$], (Ahlborn sensors FHA646R);
- θ_3, φ_3 – temperature and RH between the internal layer of the straw-bale and render [$^{\circ}C, RH\%$], (Ahlborn sensors FHA646R);
- θ_{si} – temperature of the internal surface of the wall [$^{\circ}C$], (Ahlborn NiCr-Ni-thermowire T 190-1);
- θ_i, φ_i – internal temperature and RH in the room [$^{\circ}C, RH\%$], (OnSet data logger Hobo U12-011).

Results and discussion

The test period lasted from 29.12.2016 until 23.04.2017. The minimum temperature was measured on 07.01.2017 at 0.00 and it was $-20.9^{\circ}C$, and the maximum temperature was $16.4^{\circ}C$ measured on 10.04.2017 at 17.00. The RH of external air varied

in the range of 31.8-100%. Average temperature in the house was $19.6^{\circ}C$ and average RH was ca 33%. Graphs describing the thermal situation of the wall are presented in Figure 7.

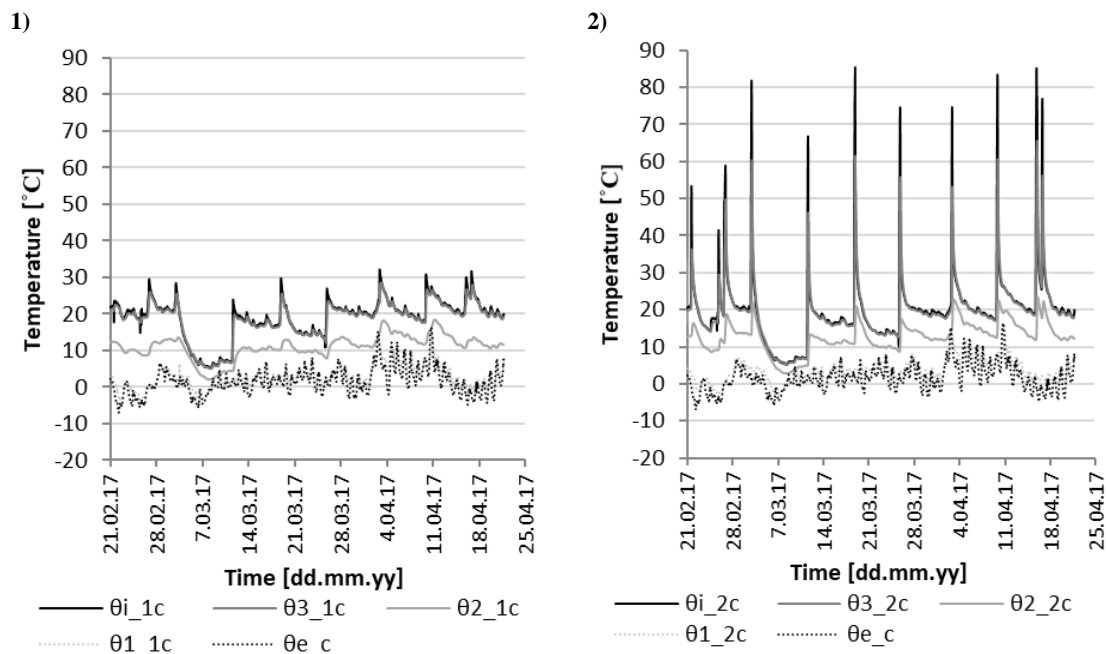


Fig. 7. Temperature changes in Measuring Points 1 and 2 in the period from 21.02.2017 to 21.04.2017

From Figure 7 we can see that lines ($\theta_{i_{1c}}$ and $\theta_{3_{1c}}$ or $\theta_{i_{2c}}$ and $\theta_{3_{2c}}$ lines) characterizing inside temperature and temperature between the inner surface of straw-bale wall and render coincide. In the wetting room the temperature during heating increased on average ~ 60 °C. The temperature in the middle of the straw-bale wall was quite stable, increasing only by about ~ 10 °C. On 15.04.2017 the

temperature in the wetting room was $\theta_{i_{2}} = 85.2$ °C being 23.4 °C at the same time in the middle of the wall. Comparison of graphs in Fig 7 and Fig 8 allows to conclude that when the temperature rises, the RH decreases. In the resting room, where temperature doesn't rise so much as in the wetting room, the RH is higher than in a hotter space.

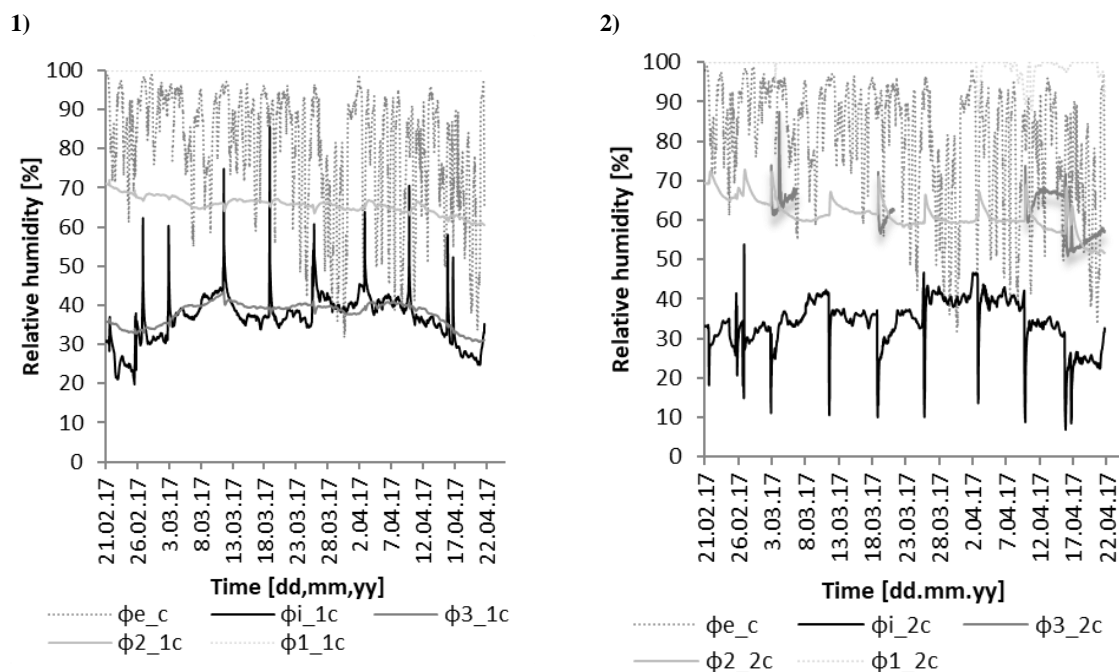


Fig. 8. Relative humidity changes in Measuring Points 1 and 2 in the period from 21.02.2017 to 21.04.2017.

We can see from Figure 8 that if the temperature rises, the RH decreases. This change is especially notable in the steaming room. The RH is more or less stable in the middle of the wall.

During the period 29.12.2016-21.04.2017 the heat flux rate through the wall was measured with heat flux plate "FQA 018 CSI". Thermal transmittance of the wall was calculated using measured results and the Equation 1 given in the Almemo manual [9].

$$U = \frac{q}{\theta_i - \theta_e}, \quad (1)$$

where U – thermal transmittance [$W/(m^2 \cdot K)$];
 q – heat flux rate through the wall [W/m^2];
 θ_i – internal temperature in resting room [°C];
 θ_e – external temperature [°C].

The calculated result $U = 0.15$ $W/(m^2 \cdot K)$, based on the test data, was a little better than the predicted

result, that was $U_c = 0.16$ $W/(m^2 \cdot K)$. The predicted calculation was done using $\lambda = 0.08$ $W/(m \cdot K)$ [10]. According to the regulations of the Government of the Republic of Estonia, Minimum energy performance requirements for the thermal transmittance of the external wall could be 0.12 – 0.22 $W/(m^2 \cdot K)$, so the tested straw-bale wall conforms to the set requirement. [11]. The testing period was still influenced by the construction process. So we predict that in the next heating period the thermal transmittance of the wall should be even lower.

Figure 10 shows that during testing the thermal situation in the wall stabilized. Tops on the graphs are caused by heating. A black line in the middle of the graph presents the moving average of 100 measurements. At the first stage of the measuring period the influence of the moisture content of the render was greater (freshly rendered wall) and external temperatures were lower, therefore the fluctuation of thermal transmittance was notable.

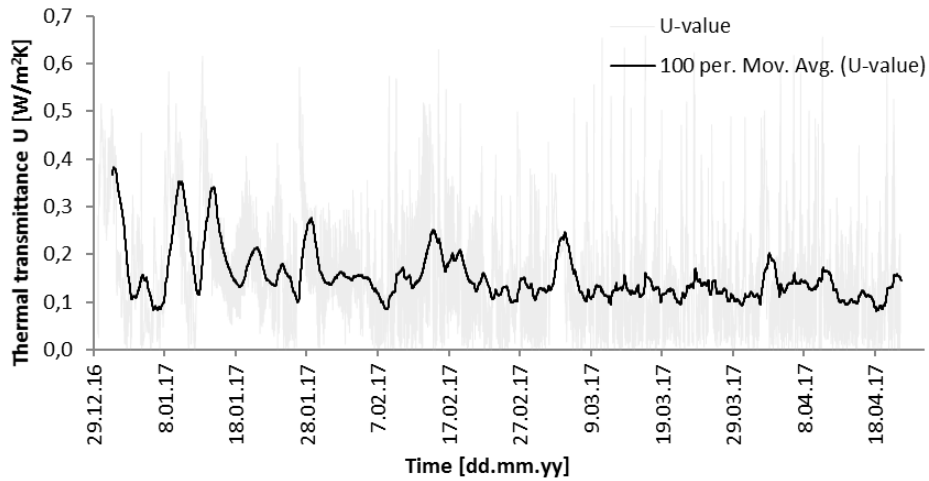


Fig. 9. Thermal transmittance of the wall calculated by test based data in Measuring Point 1 (resting room)

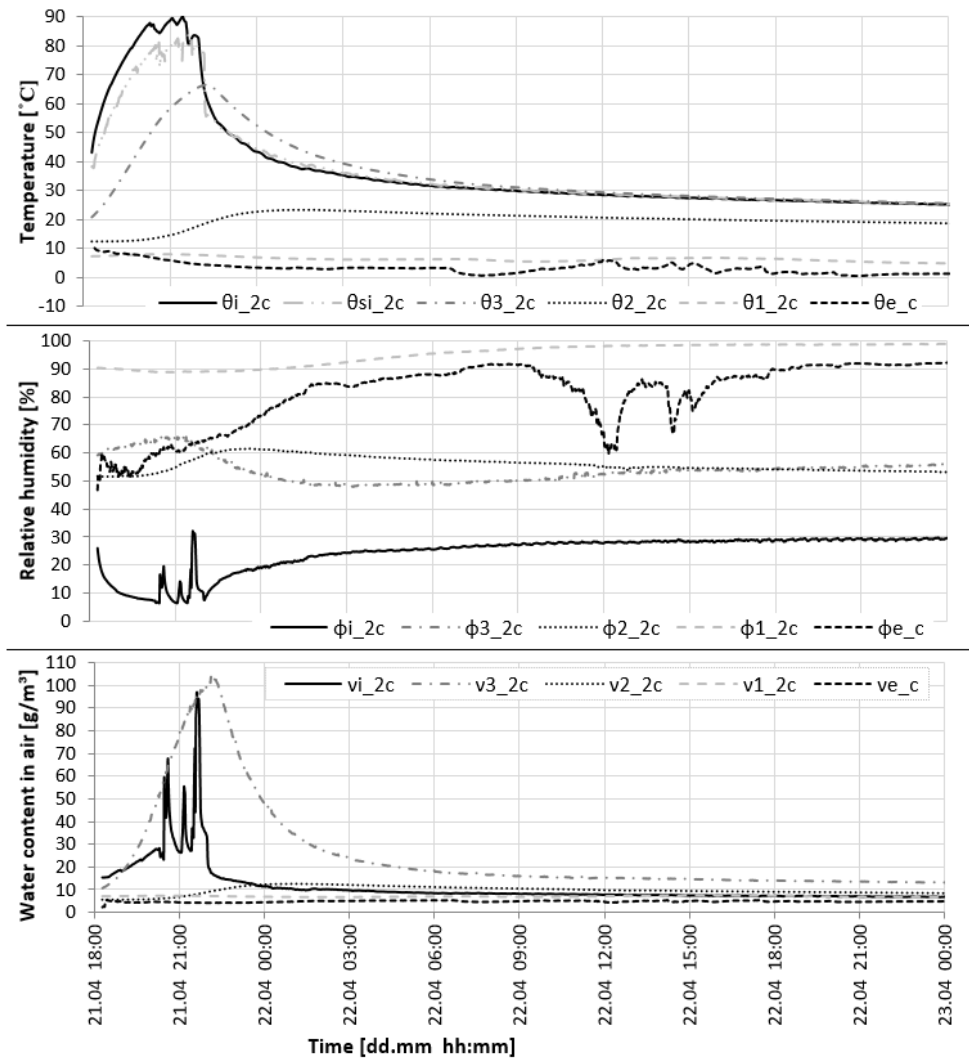


Fig. 10. Short time test in measurements in Point 2 in the time period 21.04.2017-22.04.2017

The short time test was done in the wetting room (Fig. 10) to figure out if the water vapor condensates between the inner surface of straw-bales and a

rendering layer. The room was heated with an electric sauna stove until the temperature in the room was above 80 °C. Then the steaming test began.

Approximately 2.5 liters of water was used in four portions to make steam in the space of 11 m³. The results were the following: internal temperature at the height of 1.55 m from floor was $\theta_{1,2} = 90.1 \pm 0.35$ °C, and below the ceiling it was 100.0 ± 0.35 °C, the temperature on the inner surface of the clay plaster was 83.5 ± 1.5 °C, the temperature between the internal surface of the straw-bale and clay plaster was 66.5 ± 0.1 °C, at the same time the temperature in the middle of the straw-bale was only 23.3 ± 0.1 °C and the temperature between the straw-bale external surface and lime plaster didn't change. During steaming the water content in the wetting room's air rose from $v_{1,2} = 5.59$ g/m³ to $v_{1,2} = 97$ g/m³. The RH in the beginning of the test was 32.6 ± 2.0 % and it decreased to 6.5 %. The measuring results show that condensation didn't take place. The rapid decreasing of temperature after the test was caused by the fact that the window was open and the room was ventilated. After eight hours the situation in the sauna was normal.

Conclusions

The tests show that the use of straw-bales for construction of external walls is conceivable in the climate conditions of Estonia and in such a complicated building as a sauna. Thermal transmittance of the wall built from straw-bales with

the thickness of 500 mm and rendered with clay and lime plaster conforms to the requirements set in the minimum requirements for energy performance in Estonia. Thermal transmittance of the wall was $U = 0.15$ W/(m²·K). The most distressful zone during the long-term test was located between the straw-bale external surface and an outer rendering layer. But the graph in Figure 10 shows that heating and steaming didn't influence the situation in the rooms longer than for 8 hours. On the basis of the test results we conclude that measurements should go on. The authors are continuing measurements in the sauna because in the next testing period the building will not be heated continually but only during the use. Before using the sauna, the building is heated to be comfortable and after using sauna the rooms are ventilated for some hours. The aim is to solve out what will happen inside the wall between the inner clay render layer and straw-bale. This point is hygrothermally critical. No washing happened in the sauna room, only wetting.

Acknowledgement

This article was supported by the Estonian Center of Excellence in Zero Energy and Resource Efficient Smart Buildings and Districts, ZEBE, (2014-2020) funded by the European Regional Development Fund

References

1. **Amazon Nails**, Information guide to straw bale building: for self builders and the construction industry, Todmorden in United Kingdom: Amazon Nails, 2001. 78 p.
2. **Myhrman, M., MacDonald, S. O.**, Build it with Bales (Version Two), A Step-by-Step Guide to Straw-Bale Construction, 1997. 151p.
3. **Minke, G., Mahlke, F.**, Der Strohhallenbau. Ein Konstruktionshandbuch. Staufen bei Freiburg: Ökobuch, , 2004. 141 p.
4. **Kõresaar, P.**, EAL Uudised, Soomaal kerkib Eesti esimene põhupakimaja <http://www.arhliit.ee/uudised/2633/>, 04.08.2003 [30.11.2017]
5. **Minke, G., Krick, B.**, Handbuch Strohhallenbau: Grundlagen, Konstruktionen, Beispiele. 2. neu bearbeitete und erweiterte Auflage. Staufen bei Freiburg: Ökobuch, 2009. 141 p.
6. **Miljan, M.-J., Miljan, M., Miljan, J.**, Thermal conductivity of walls insulated with natural materials, 4th International Scientific Conference CIVIL ENGINEERING '13: Proceedings Part I, Jelgava, 2013. p 175-179.
7. **Miljan, M., Miljan, J.**, Thermal transmittance and the embodied energy of timber frame lightweight walls insulated with straw and reed, 2nd International Conference on Innovative Materials, Structures and Technologies. Riga, Latvia: IOP Publishing Ltd, Article No 012076. (IOP Conference Series-Materials Science and Engineering; 96), 2015.
8. **Lacinski, P. Bergeron, M.**, Serious Straw Bale: A Home Construction Guide for all Climates, Chelsea Green Publishing Company, 2000. 371 p.
9. **ALMEMO Manual**. 9. Edition, 2011.
10. **Costes, J.-P., Evrard, A, Biot, B., Keutgen G., Daras, A., Dubois, S., Lebeau, F., Courard, L.**, Thermal Con-ductivity of Straw Bales: Full Size Measurements Considering the Direction of the Heat Flow. Buildings 2017, 7, 11
11. Minimum requirements for energy performance, The State Gazette I, 28.02.2017, 2, §12 (4) the Government of the Republic of Estonia, 2017.